In Silico Investigations into Human Ventricular Pro-arrhythmic Mechanisms Combined with *In Vivo* and *In Vitro* Experiments

Xin Zhou

Kellogg College



Computational Cardiovascular Science Group
Department of Computer Science
University of Oxford

Trinity Term 2016

This thesis is submitted to the Department of Computer Science, University of Oxford, for the degree of Doctor of Philosophy. This thesis is entirely my own work, and, except where otherwise indicated, describes my own research.

Xin Zhou Doctor of Philosophy

Kellogg College Trinity Term 2016

In Silico Investigations into Human Ventricular Pro-arrhythmic Mechanisms Combined with *In Vivo* and *In Vitro* Experiments

Abstract

Sudden cardiac death (SCD) is one of the largest causes of natural mortality throughout the world. SCD can be triggered through ventricular arrhythmias due to many pathological conditions, including coronary artery diseases, arrhythmogenic cardiomyopathies and genetic mutations of ionic channel proteins. Although considerable research has been conducted to study proarrhythmic mechanisms, most studies were in animal models due to ethical limitations in human cardiac research. Therefore, more research is needed to investigate the proarrhythmic ionic mechanisms in human.

In this thesis, we use biophysically-detailed models of human cardiac electrophysiology to explore the ionic mechanisms underlying several proarrhythmic conditions. A first study is to use traditional modeling approach to explore the effect of ionic remodelling in human epicardial border zone (EBZ) cells post myocardial infarction by introducing the analogous remodelling observed in canine. Sensitivity analysis of the human EBZ models leads to our interest in developing new techniques to include general variability into human cardiac electrophysiology research.

Therefore, a novel methodology to include the effect of *in vivo* cardiac variability in human electrophysiology is developed in this study by constructing a population of models calibrated using *in vivo* human data. The experimentally-calibrated population of human ventricular cell models is then applied to investigate the proarrhythmic ionic mechanisms underlying cardiac alternans, and to test the effects of potential anti-arrhythmic drug therapies on alternans. We then explore the interaction between cardiac variability and a mutation of slow delayed rectifier potassium channel. Our simulation results reveal the complex interactions between different ionic components in the integrated electrophysiological system, highlighting the importance of cardiac variability in the development of proarrhythmic conditions.

This thesis is dedicated to my parents.

谨以此文献给我的父亲周振寰先生和母亲张玢玢女士。

Acknowledgements

First of all, I would like to thank my supervisors sincerely, Prof. Blanca Rodriguez, Dr Alfonso Bueno-Orovio, and Prof. Kevin Burrage, for being excellent supervisors and best friends. Without their supervision and support throughout the whole course of my DPhil, I would not have enjoyed my study so much. I want to thank Blanca for her remarkable wisdom in shaping the direction of this work, and for her enormous effort in the development of my academic skills. I would like to thank Alfonso for devoting so much time for me and helping me to rigorously cope with numerous difficulties in my work. I would like to thank Kevin for his invaluable input and his wise suggestions on the mathematical methodology related to this work. In addition, I want to thank my friends and colleagues in the computational biology group for their help and precious suggestions to improve my work.

The work of my thesis was built on the integration of experimental data and mathematical modelling. Here I want to acknowledge my experimental collaborators. I would like to thank Dr Michele Orini, Dr Ben Hanson, Dr Martin Hayward, Professor Peter Taggart, and Dr Pier Lambiase from the Heart Hospital and University College London for providing the invaluable *in vivo* human data for my work. I would like to thank Dr Stephen Harmer and Professor Andy Tinker from the William Harvey Heart Centre for providing all the data from patch clamp experiments, as well as broadening my electrophysiological knowledge.

I would like to thank System Biology Doctoral Training Centre for their training and career support. One year's systemic training modules helped me transfer from 'biology' to 'systems biology' area. I would also like to acknowledge China Scholarship Council for funding my DPhil research.

Last but not least, I would like to thank my family and friends. I want to thank Zhe for always accompanying me through the happiness and sorrow. I want to thank my remarkable parents for their love and support. I must thank my dear mother for her always understanding me and encouraging me to pursue my dreams. I must thank my dear father for all his faith on me and his irreplaceable encouragement during my growth. His tutorship on math and science during my childhood inspired my interest and passion on scientific research. Finally, I want to thank all my family and friends for their help and support.

Publications

Below is a list of publications related to the work described in this thesis:

Xin Zhou, A. Bueno−Orovio, M. Orini, B. Hanson, M. Hayward, P. Taggart, P.D. Lambiase, K. Burrage and B. Rodriguez, *In vivo* and *in silico* investigation into human ventricular action potential alternans and the role of sarcolemmal currents and calcium dynamics. In *Circ Res*, 2016; 118: 266-278. doi: 10.1161/CIRCRESAHA.115.307836

Xin Zhou, Stephen Harmer, Alfonso Bueno-Orovio, Kevin Burrage, Andrew Tinker, Blanca Rodriguez, How Can a Gain-of-Function Mutation in KCNQ1 Lead to Action Potential Prolongation? In *Heart Rhythm*, 2016; 13(5) S545.

Xin Zhou, A. Bueno−Orovio, M. Orini, B. Hanson, M. Hayward, P. Taggart, P.D. Lambiase, K. Burrage and B. Rodriguez, Comparison of the effects of different ionic interventions on the inhibition of human cardiac alternans. In preparation.

Anna Muszkiewicz, Oliver J Britton, Philip Gemmell, Elisa Passini, Carlos Sanchez, **Xin Zhou**, Annamaria Carusi, T Alexander Quinn, Kevin Burrage, Alfonso Bueno-Orovio, Blanca Rodriguez. Variability in Cardiac Electrophysiology: Using Experimentally-Calibrated Populations of Models to Move Beyond the Single Virtual Physiological Human Paradigm. In *Progress in Biophysics and Molecular Biology*, 2016; 120(1-3):115-27. doi: 10.1016/j.pbiomolbio.2015.12.002.

Blanca Rodriguez, Annamaria Carusi, Najah Abi-Gerges, Rina Ariga, Oliver Britton, Gil Bub, Alfonso Bueno-Orovio, Rebecca A.B.Burton, Valentina Carapella, Louie Cardone-Noott, Matthew J Daniels, Mark R. Davies, Sara Dutta, Andre Ghetti, Vicente Grau, Stephen Harmer, Ivan Kopljar, Pier Lambiase, Hua Rong Lu, Aurore Lyon, Ana Minchole, Anna Muszkiewicz, Julien Oster, Michelangelo Paci, Elisa Passini, Stefano Severi, Peter Taggart, Andy Tinker, Jean-Pierre Valentin, Andras Varro, Mikael Wallman, **Xin Zhou**. Human-based approaches to pharmacology and cardiology: An interdisciplinary and intersectorial workshop. In *Europace*, 2015; doi:10.1093/europace/euv320.

Xin Zhou, A. Bueno−Orovio, M. Orini, B. Hanson, M. Hayward, P. Taggart, P.D. Lambiase, K. Burrage and B. Rodriguez, hERG determines alternating behavior at fast pacing by modulating action potential morphology and sarcolemmal Ca^{2+} balance. In *Heart Rhythm*, 2014; 11(5) S167.

Xin Zhou, A. Bueno−Orovio, M. Orini, B. Hanson, M. Hayward, P. Taggart, P.D. Lambiase, K. Burrage and B. Rodriguez, Population of human ventricular cell models calibrated with *in vivo* measurements unravels ionic mechanisms of cardiac alternans. In *Computing in Cardiology Conference (CinC)*, 2013; Pages 855−858.

Prizes

Microsoft Research Project Award, Systems Biology Doctoral Training Centre, Oxford

Conferences and Presentations

- Heart Rhythm – San Francisco, USA, May 2016.
- Innovations in Cardiology – Fermo, Italy, October 2015
- Computational Cardiovascular Science Workshop: Computational Technologies in Biomedicine and Pharmacology, – Oxford, UK, September 2014.
- The 38th European Working Group on Cardiac Cellular Electrophysiology – Maastricht, Netherlands, September 2014.
- Heart Rhythm – San Francisco, USA, May 2014.
- Computing in Cardiology – Zaragoza, Spain, September 2013.
- Computational Cardiovascular Science Workshop: Computer Science meets Cardiology, – Oxford, UK, September 2013.
- The 36th European Working Group on Cardiac Cellular Electrophysiology – Nantes, France, September 2012.

Contents

1 Introduction 1
1.1 Motivation 1
1.2 Thesis goals 4
1.3 Thesis outline 6
2 Literature review on cardiac electrophysiology 11
2.1 Basic cardiac electrophysiology 11
2.1.1 The basic function and structure of the heart 11
2.1.2 The electrophysiology of cardiomyocytes 13
2.2 Important experimental techniques in cardiac electrophysiology research 18
2.2.1 Voltage clamp and patch clamp techniques 18
2.2.2 *In vivo* measurement of whole heart electrophysiology 20
2.3 The variability in cardiac myocytes 23
2.3.1 Circadian rhythm regulates ionic channel gene transcription 24
2.3.2 Sustained heart rate change affects ion channel expression 24
2.3.3 Exposure to drugs affects ionic channel expression 25
2.3.4 Diseases alter ionic channel expression 25
2.3.5 Sympathetic neural stimulation regulates ionic channel activity 25
2.4 Several proarrhythmic conditions 27
2.4.1 Effects of myocardial infarction 27
2.4.2 Cardiac alternans 28
2.4.3 Long-QT syndrome 32
2.5 Introduction to anti-arrhythmic drug therapy 33
2.5.1 Classification of anti-arrhythmic drugs 33
2.5.2 The clinical use of anti-arrhythmic drugs 35
2.6 Difference between animal and human cardiac electrophysiology 36
2.7 Summary 39
3 Literature review on the modelling of cardiac electrophysiology 41
3.1 Basic formulations underlying the electrophysiological modelling of cardiomyocytes 41
3.1.1 The Hodgkin-Huxley formulation for ionic currents 41
3.1.2 The Markov chain formulation for ion channel behaviour 44
3.2 Development of cardiac cellular models 46
3.3 Latest human ventricular cell models 47
3.4 Comparison between animal and human ventricular cell models 49
3.4.1 General structure 49
3.4.2 Initial conditions and basic settings 50
3.4.3 Major differences in currents 51
3.5 Modelling of diseased cardiomyocytes 53
3.6 Modelling of pharmacological drug effects 55
3.7 Modelling of variability in cardiac electrophysiology 55
3.7.1 Cell-specific modelling 56
3.7.2 Sensitivity analysis 57

3.7.3 Experimentally-calibrated population of models 58
3.8 Summary 62
4 Post-myocardial infarction ionic remodelling and hERG block prolong the action potential and facilitate alternans in a human ventricular model of the epicardial border zone 64
4.1 Introduction 64
4.2 Methods 66
4.2.1 Development of an electrophysiological model for human EBZ 66
4.2.2 Sensitivity analysis 69
4.2.3 Simulation protocols 69
4.2.4 Model implementation and data analysis 69
4.3 Results 70
4.3.1 Action potentials in canine EBZ models 70
4.3.2 Action potentials in human EBZ models 71
4.3.3 Development of alternans in human EBZ models 73
4.3.4 Sensitivity to EBZ remodelling 74
4.3.5 Modulation of EBZ-remodelling under pharmacological I_{Kr} block 76
4.4 Discussion 80
5 Construction of a population of human ventricular cell electrophysiology models based on *in vivo* measurements 84
5.1 Introduction 84
5.2 Methods 86
5.2.1 *In vivo* data acquisition 86
5.2.2 Population of models 88
5.2.3 Parameters varied in the population of models 89
5.2.4 Latin hypercube sampling 89
5.2.5 Simulation protocol 90
5.2.6 Biomarker calculation 90
5.2.7 Partial correlation analysis 91
5.3 Results 91
5.3.1 Construction of the initial population of models 91
5.3.2 Calibration of the population of models 91
5.3.3 Calibration results 95
5.4 Discussion and conclusions 99
6 Mechanisms underlying different rate dependent alternans types in human ventricular models 102
6.1 Introduction 102
6.2 Methods 105
6.2.1 Definition of alternans 105
6.2.2 Sarcoplasmic reticulum calcium balance 105
6.2.3 Sarcolemmal calcium balance 105
6.2.4 Action potential clamp simulation 106
6.2.5 I_{CaL} kinetics variation analysis 106
6.2.6 Statistical analysis 106

6.3 Results 106
6.3.1 Key currents related to the generation of alternans 106
6.3.2 Two types of alternans are observed in both *in vivo* and *in silico* data 109
6.3.3 APD alternans in the human ventricular models initiate following the loss of SR calcium content balance 110
6.3.4 Strong I_{NaCa} and fluctuations in SCB result in APD alternans in both Eye-type and Fork-type human models, and strong I_{CaL} restores SCB suppressing APD alternans at fast pacing rates for Eye-type models. 114
6.3.5 Ionic mechanisms of APD alternans in human ventricular myocytes. 116
6.3.6 I_{CaL} kinetics variation can affect alternans by regulating SCB and SRCB 120
6.3.7 I_{Na} and I_{Kr} can affect alternans by regulating I_{NaCa} activity 121
6.4 Discussion and conclusions 124
6.4.1 Fluctuations in SR Ca^{2+} content as a primary cause of APD alternans in human ventricular cardiomyocytes 125
6.4.2 Sarcolemmal calcium balance translates Ca^{2+} fluctuations into APD alternans in human ventricular cardiomyocytes 127
6.4.3 Limitations 128
7 Effects of current interventions on the stability of different types of alternans models 130
7.1 Introduction 130
7.2 Methods 132
7.3 Results 132
7.3.1 Comparison between the effects of different current interventions 132
7.3.2 Effects of I_{CaL} inhibition 135
7.3.3 Effects of I_{NaCa} inhibition 137
7.3.4 Effects of J_{up} enhancement 139
7.4 Discussion and conclusions 141
8 Computational investigation of pro-arrhythmic mechanisms of LQT1 mutations in human ventricular cardiomyocytes 145
8.1 Introduction 145
8.2 Methods 147
8.2.1 Clinical identification of I_{Ks} mutations 147
8.2.2 I_{Ks} mutants expression system for patch clamp experiments 147
8.2.3 Patch clamp protocol 148
8.2.4 Biomarker calculation 148
8.2.5 Parameters related to mutations 149
8.2.6 Preprocessing of CHO patch clamp data 150
8.2.7 Multi-start least square fitting 151
8.3 Results 151
8.3.1 Patch clamp current traces of WT I_{Ks} and LQT1 mutants 151
8.3.2 The analysis of the KCNQ1 G229D mutation patch clamp biomarkers

.....154
8.3.3 Modification of WT ORd I_{Ks} model to fit WT and G229D mutated I_{Ks} patch clamp data 157
8.3.4 Generation of the population of KCNQ1 G229D mutated human ventricular cell models.....162
8.3.5 Effects of KCNQ1 G229D mutation in the population of models....163
8.4 Discussion and conclusions 171
9 Conclusions and discussions.....176
9.1 Summary 176
9.2 Key contributions and main findings.....180
9.3 Future directions 181
9.3.1 Incorporating post-MI EBZ information from human.....181
9.3.2 Variation of current conductances based on experimental data 182
9.3.3 Ryanodine receptor refractoriness and calcium alternans in human cardiomyocytes 183
9.3.4 Repolarisation reserve and β-adrenergic stimulation.....183
9.3.5 Risk stratification for different subgroups and individuals.....184
9.3.6 The effects of tissue coupling 185
9.4 Conclusions.....186
References.....189

List of Figures

Figure 2.1: Diagram of the structural anatomy for a human heart. 12
Figure 2.2: Schematic illustrations for the five phases in action potential, indicating the key currents contributing to individual phases. 14
Figure 2.3: The restitution of APDs with the change of pacing CLs in human ventricular tissue and model.. 18

Figure 3.1: Conformation transitions of four voltage sensors in I_{Ks} channel based on the two-stage activation theory.. 46
Figure 3.2: Schematic diagram of human and canine models. 51

Figure 4.1: Transfer of EBZ electrical remodelling from canine to human AP model. 66
Figure 4.2: Action potential, individual currents and S1S2 restitution curve of the canine ventricular cell model. 71
Figure 4.3: Action potential and main ionic currents for the two versions of the human EBZ model. 73
Figure 4.4: APD alternans in human EBZ models. 74
Figure 4.5: Sensitivity of human EBZ models to the extent of EBZ-remodelling. 76
Figure 4.6: Effect of I_{Kr} block on human EBZ models.. 77
Figure 4.7: Alternans in human EBZ models after I_{Kr} block. 79

Figure 5.1: *In vivo* recordings of the activation recovery interval (ARI) used for calibration of the population of human ventricular models. 88
Figure 5.2: Analyzing *in vivo* ARI data and using skewed normal distribution to select 95% of data coverage thresholds. 92
Figure 5.3: Representative models excluded during the calibration process by Filters 2-6. 94
Figure 5.4: Calibration results from the initial population. 96
Figure 5.5: The distribution of 11 parameter scaling factors in the accepted population of models. 97
Figure 5.6: Evolution of accepted conductance scaling factors through calibration. 98
Figure 5.7: Partial correlation coefficients (PCC) between action potential biomarkers and current conductance parameters under CL=350ms. 99

Figure 6.1: Key currents related to alternans. 108
Figure 6.2: Types of APD alternans *in vivo* and *in silico*.. 110
Figure 6.3: SR Ca^{2+} cycling properties and fluctuations in alternans models.. 112
Figure 6.4: Action potential clamp simulations.. 113
Figure 6.5: Sarcolemmal Ca^{2+} balance (SCB) in alternans models.. 115

Figure 6.6: Rate dependency of I_{CaL} magnitude, CaT magnitude, J_{up} magnitude and J_{rel} magnitude.....116
Figure 6.7: Ionic mechanisms resulting in APD alternans in human *in silico* ventricular cardiomyocytes.. 119
Figure 6.8: Effects of varying I_{CaL} kinetics on the Eye-type and Fork-type models with biggest alternans magnitudes.....121
Figure 6.9: Sodium currents fluctuation analysis between long/short alternating beats in a representative model of cardiac alternans.. 123
Figure 6.10: Effects of I_{Kr} modulation in the original ORd model.....124

Figure 7.1: Effects of different current interventions on alternans models.....134
Figure 7.2: Suppression of APD alternans by I_{CaL} inhibition.....136
Figure 7.3: Effects of I_{CaL} down-regulation on AP and CaT. 137
Figure 7.4: Suppression of APD alternans by I_{NaCa} inhibition.. 138
Figure 7.5: Effects of I_{NaCa} down-regulation on AP and CaT.....139
Figure 7.6: Suppression of APD alternans by increasing J_{up}.. 140
Figure 7.7: Effects of enhancing J_{up} on AP and CaT.....141

Figure 8.1: Patch clamp protocol and biomarkers calculation.. 149
Figure 8.2: Linear correlation between WT patch clamp data (CD) and ORd model output (CD) after using the same patch clamp protocol. 151
Figure 8.3: Representative traces of the currents produced by the LQT1 mutations G229D, D242N, G325R, R518P and Y662X.....153
Figure 8.4: Comparison between I_{Ks} current biomarkers of WT, Single and DN G229D mutations from patch clamp experiments. 156
Figure 8.5: Multi-start best fitting results for KCNQ1 G229D DN mutation patch clamp biomarkers. 158
Figure 8.6: Multi-start best fitting results for KCNQ1 G229D Single mutation patch clamp biomarkers. 159
Figure 8.7: Comparison of I_{Ks} patch clamp traces between model (μA/μF) and experiments. 160
Figure 8.8: Effects of KCNQ1 G229D mutation on the baseline ORd model..161
Figure 8.9: Different G229D Single mutation fittings produced similar APD shortening.....161
Figure 8.10: Effects of KCNQ1 G229D mutations on APD in the experimentally-calibrated population of human epicardial ventricular cell models. 162
Figure 8.11: Effects of KCNQ1 G229D DN mutation on APD in the population, comparing with WT.....163
Figure 8.12: Comparison of the WT biomarkers between the Not Sensitive group and Sensitive group. 164
Figure 8.13: Comparison of current conductance scaling factors between the Not Sensitive and Sensitive groups.....165
Figure 8.14: Partial correlation analysis of models' response in APD to the

introduction of KCNQ1 G229D mutation. 166
Figure 8.15: The response of APD_{90} to KCNQ1 G229D mutation was related to the baseline level of G_{CaL}, G_{Kr} and G_{Ks}. $\Delta APD = APD_{G229D_DNmutation} - APD_{WT}$. 166
Figure 8.16: Effects of KCNQ1 G229D mutation on different ionic currents in representative models displaying (A) APD prolongation and (B) APD shortening, at CL=1000ms. 167
Figure 8.17: The subtle balance between I_{Kr} decrease and I_{Ks} increase after KCNQ1 G229D mutation regulates APD. 170

List of Tables

Table 3.1: Parameters of the two models (Na^+, K^+, Cl^- Ca^{2+} (mM)).....52
Table 3.2: Currents included in the two models.....52
Table 3.3: Ion channel conductances and permeabilities 53

Table 4.1: Modifications from healthy canine model to EBZ canine model. 67
Table 4.2: Modifications to the permeabilities and conductances in the human EBZ model. 68
Table 4.3: Modifications to the relative shifts and time constants in the human EBZ model. 68

Table 5.1: Patients' information in the study 87
Table 5.2: Biomarker calculation algorithm 91

Table 7.1: Comparison of the medians of six current conductances and permeabilities between Normal, Eye-type alternans, Fork-type alternans and CaT alternans, relative to Normal models.....133

Nonstandard Abbreviations and Acronyms

AP (action potential)
APA (action potential amplitude)
APD (action potential duration)
ARI (activation recovery interval)
AVR (aortic valve replacement)
CABG (coronary artery bypass grafting)
Ca_{JSR} (JSR calcium level)
CaMKII (Ca^{2+}/calmodulin-dependent protein kinase II)
cAMP (second messenger cyclic AMP)
CaT (calcium transient)
CaTD (calcium transient duration)
CaT_{max} (systolic Ca^{2+} level)
CaT_{min} (diastolic Ca^{2+} level)
CD (current density)
CDF (cumulative distribution function)
CHO (Chinese hamster ovary)
CICR (calcium induced calcium release)
CL (cycle length)
C-loop (cytoplasmic loop of transmabrane protein)
DI (diastolic interval)
DSS (deactivation steady state)
DT (depolarisation time)
EBZ (epicardial border zone)
ECG (electrocardiogram)
EGM (electrogram)
G_{CaL} (Ca^{2+} channel permeability)
G_{K1} (K1 channel conductance)
G_{Kr} (Kr channel conductance)
G_{Ks} (Ks channel conductance)
G_{Na} (fast Na^{+} channel conductance)
G_{NaCa} (Na^{+}/Ca^{2+} exchanger conductance)
G_{NaK} (Na^{+}/K^{+} pump activity)
G_{NaL} (late Na^{+} channel conductance)
G_{to} (transient outward potassium channel conductance)
HRd model (Hund-Rudy dynamic model)
I_{CaL} (L-type Ca^{2+} current)
I_{Cab} (background Ca^{2+} current)
ICD (internal cardioverter defibrillator)
I_{Kr} (rapid delayed rectifier K^{+} current)

I_{Ks} (slow delayed rectifier K^+ current)
I_{K1} (inward rectifier K^+ current)
I_{Kur} (ultra-rapid activating delayed rectifier K^+ channel)
I_{Na} (fast Na^+ current)
I_{NaCa} (Na^+/Ca^{2+} exchanger current)
I_{NaK} (Na^+/K^+ pump current)
I_{NaL} (late Na^+ current)
I_{pCa} (sarcolemmal calcium pump current)
I_{to} (transient outward potassium current)
J_{rel} (Ca^{2+} release flux)
JSR (junctional sarcoplasmic reticulum)
J_{up} (Ca^{2+} re-uptake flux)
LHS (Latin hypercube sampling)
LQTS (long QT syndrome)
LVEF (low left ventricular ejection fraction)
MAP (monophasic action potential)
MC (monte carlo)
MI (myocardial infarction)
MYO (bulk myoplasm)
NSR (network sarcoplasmic reticulum)
NZ (normal zone)
ORd model (O'Hara-Rudy dynamic model)
P_{Ca} (Ca^{2+} channel permeability, referred to as G_{CaL} in this study)
PCC (partial correlation coefficients)
PDF (probability distribution function)
P_{Jrel} (Ca^{2+} release permeability via ryanodine receptors to myoplasm)
P_{Jup} (Ca^{2+} uptake permeability via SERCA from the myoplasm)
PKA (protein kinase A)
PTCD (peak tail current density)
QTc (corrected QT interval)
RMP (resting membrane potential)
RT (repolarisation time)
RyR (ryanodine receptor)
SCB (sarcolemmal calcium balance)
SCD (sudden cardiac death)
SERCA (sarco/endoplasmic reticulum Ca^{2+}-ATPase)
SR (sarcoplasmic reticulum)
SRCB (sarcoplasmic reticulum calcium balance)
SS (subspace)
SSA (steady state of activation)
UPD (upstroke duration)
UT (upstroke time)
V_m (membrane voltage)
V_{max} (peak upstroke voltage)

Chapter 1

Introduction

1.1 Motivation

Sudden cardiac death (SCD) is one of the leading causes of death throughout the world. In Europe and North America, about 50 to 100 unexpected cardiac deaths occur per 100000 people per year. For adults older than 35 years, the incidence is 1 per 1000 population, and for those younger than 35 years, the ratio is about 1 per 100000 (John *et al*., 2012). For unclear reasons, the proportion of patients with pulseless electrical activity or asystole has increased over the past twenty years (Teodorescu *et al*., 2010). Overall, less than 5% of people with an out-of-hospital cardiac arrest can survive (Fishman et al., 2010; John et al., 2012; Nichol et al., 2008). Some of the victims have structural heart disease, such as coronary artery disease. Unfortunately, the underlying disease of SCD victims is often unrecognized before death, so that sudden death is the first manifestation of heart disease (Fishman et al., 2010; John et al., 2012).

SCD is often triggered by cardiac arrhythmias under conditions of metabolic stress or chronotropic stimulations. The initiation of arrhythmias can be due to many different sources, such as hypertrophic and arrhythmogenic cardiomyopathies, coronary artery malformations and genetic arrhythmic syndromes (John *et al*., 2012). About half of these events are related to ventricular tachycardia or ventricular fibrillation (John *et al*., 2012), therefore the severity of ventricular dysfunction is often the most important risk marker (Fishman *et al*., 2010).

Considerable research has been conducted to study the mechanisms underlying ventricular arrhythmias. One of the important sources of ventricular arrhythmias comes from the tissue remodelling and heterogeneity associated with post myocardial infarction (MI). The overall risk of arrhythmic death was higher in post myocardial infarction patients (Yap *et al*., 2005). Although many efforts have been focused on the stratification of ventricular arrhythmias after myocardial infarction, currently no optimal strategy for risk stratification exists (Goldberger *et al*., 2011).

In addition to structural dysfunction and remodelling after coronary artery diseases, ventricular arrhythmias can also arise from electrophysiological abnormalities. Stable beat to beat fluctuations between subsequent cardiac action potentials (APs), which are called alternans, are an important indicator of arrhythmias. Patients with cardiac alternans are at increased risk for ventricular arrhythmias (Rosenbaum *et al*., 1994). Subtle electrical alternans on the electrocardiogram have been proposed as a noninvasive marker of vulnerability to ventricular arrhythmias (Rosenbaum *et al*., 1994). Considerable research has been conducted to study the mechanisms underlying cardiac alternans, but the exact mechanisms are still under debate: alternation of sarcolemmal currents and fluctuation of calcium regulatory system are both suggested to be related to alternans initiation. As the generation of the cardiac action potential involves the combination and interaction of multiple ion channels and proteins, it is difficult to understand cardiac alternans by isolated alternations of independent ionic currents. In addition, most of previous studies on alternans were conducted on animal species (Cutler et al., 2009; Díaz et al., 2004; Picht et al., 2006; Wang et al., 2014), and therefore the mechanisms underlying cardiac alternans in human need to be further investigated to ensure translation to patients.

Genetic channelopathies can also introduce disruptions of ion channel function, which can lead to the initiation of ventricular arrhythmias and SCD. Examples of these genetic cardiac abnormalities include the long QT syndrome (LQTS), the short

QT syndrome or the Brugada syndrome, among others. Most of the mutations are uncommon, and the penetrance of a mutation usually varies according to the conditions of different individuals. Even within a same family, a same mutation can cause frequent arrhythmias in one individual, but can be asymptomatic in another (John *et al*., 2012). This suggests that in order to improve the risk stratification of cardiac arrhythmias for individual patients, the inter-subject variability in cardiac electrophysiological systems needs to be considered.

To achieve a thorough investigation of the interaction between multiple ionic currents in the cardiac system and to improve the risk stratification of ventricular arrhythmias, systems biology methods are needed. The combination of mathematical approaches, computational models and experimental observations can provide new perspectives to understanding and treating these cardiac diseases.

Since the development of the first cardiac model five decades ago (Noble, 1962), the use of mathematical models and computational simulations has provided important insights into cardiac electrophysiological research. With the development of experimental techniques, cardiac models can simulate and predict many phenomena at the cell and tissue level. The use of cardiac models can also provide experimentalists additional insights, and refine and generate new hypothesis. Moreover, modelling approaches can be used in the assessment of potential therapeutic methods, which are always expensive and sometimes almost impossible to test experimentally, even more in patients due to inherent ethical limitations.

Biophysically detailed models of cardiac electrophysiology are normally developed based on averaged experimental data of a certain type of cardiac cell from a specific species (if available). Therefore, a standard cardiac cell model may be close to the average behaviour of the isolated cells used in the experiments. However, variability exists between cardiac cells within a same species, for example in terms of ion channel density and ionic currents.

One approach to model the effect of cardiac variability is to introduce a certain degree of variation to the strength of individual currents in a cardiac cell (Romero et al., 2009; Sobie, 2009). By varying the conductance or permeability parameter of multiple currents simultaneously around their baseline values, the complex interaction between variability in different currents can be explored systematically. One recent approach to model cardiac variability is to construct a population of models based on a standard model, and then calibrate the population with experimental data. The methodology to construct experimentally-calibrated population of models was first proposed by (Britton *et al*., 2013) for rabbit Purkinje cells. Similar investigations need to be applied to explore the effect of cardiac variability in humans.

The fundamental hypothesis underlying this thesis is that the combination of *in vivo* and *in vitro* human experimental data and *in silico* modelling can allow us to construct a platform to investigate the effect of variability in the generation of human pro-arrhythmic conditions. In addition, the complex interaction between different currents can be better explored after introducing cardiac variability as reported experimentally compared with traditional methods.

1.2 Thesis goals

The main aim of this thesis is to develop and use mathematical models of human ventricular cell electrophysiology informed by experimental recordings to investigate pro-arrhythmic ionic mechanisms and to provide novel insights that may guide the development of anti-arrhythmic drug therapies. In this process, variability in ionic properties is considered and explored using experimentally calibrated population of models.

At the first stage of the research, we aim to explore the pro-arrhythmic effect of post myocardial infarction remodelling in a human ventricular cell model. To achieve this goal, we initially use a traditional modelling approach, which involves a sensitivity analysis based on a single set of parameters. Due to the lack of human experimental data in post myocardial infarction, a remodelling analogous to that in canine electrophysiology is introduced into a human ventricular cardiomyocyte model, given the similarities in electrophysiology between both species. The development of cardiac alternans is observed after introducing the post infarction remodelling of current conductances. Further remodelling of current kinetics increases the sensitivity of the human model to pacing rates, but does not fundamentally alter the post infarction properties. These results suggest that current conductances play a more crucial role than kinetics in determining the pro-arrhythmic characteristics.

At the next stage of the research we aim to investigate pro-arrhythmic mechanisms, especially mechanisms of cardiac alternans, in human ventricular cells under a broader electrophysiological range. The effect of variability in current densities can be included by introducing random combinations of current conductance variations. A population of human ventricular cell models is constructed and calibrated based on human *in vivo/in vitro* data. The development of this framework provides a platform for the investigation of human pro-arrhythmic mechanisms that includes the variability observed in human.

The ionic mechanisms underlying the development of cardiac alternans and their rate dependence are then investigated using this framework of a population of human ventricular cell models. The interactions between multiple ionic currents and fluxes are explored using this population-based approach, to unravel the complex ionic mechanisms underlying alternans generation. The effects of different potential therapeutic interventions under human physiological conditions are also investigated taking into account the aforesaid variations in current conductances and permeabilities.

At the third stage, we aim to explore the effects of low penetrance genetic channelopathies. By probing formulations of mutated channel action into a population of human ventricular cell models, the interaction between the mutated ionic current and other relevant components in cardiac myocytes are studied, so that the mechanisms underlying the low penetrance of gene mutation carriers can be explored within the existence of variability.

The specific goals of the thesis are as follows:

1. To construct and to explore the characteristics of a human ventricular cell model representative of the post myocardial infarction epicardial border zone (EBZ), and to investigate the remodelling effect of current conductance and current kinetics.
2. To calibrate a population of human epicardial cardiomyocytes models using *in vivo* human electrophysiological measurements.
3. To investigate the mechanisms of alternans generation in the human ventricular cell model population, and to explore the effects of different ion channel interventions on alternans generation.
4. To modify the standard healthy I_{Ks} model into a I_{Ks} mutation model by fitting KCNQ1 G229D mutated I_{Ks} patch clamp data, and to explore the effects of KCNQ1 G229D mutation on repolarisation by inserting the KCNQ1 G229D mutated I_{Ks} model into the population of human ventricular cell models.

1.3 Thesis outline

Chapter 2 provides a literature review of relevant cardiac electrophysiology knowledge. We firstly introduce basic concepts in cardiac electrophysiology such as the basic structure and function of the heart, and the electrophysiological

characteristics of cardiomyocytes. Then we introduce important electrophysiological techniques used in wet lab experiments and in the clinic, such as patch clamp and *in vivo* electrograms. The mechanisms affecting the cardiac variability will be reviewed, such as circadian rhythms, drug exposure, and sympathetic neural stimulation. Then we introduce several proarrhythmic conditions that are relevant to this thesis, namely myocardial infarction, cardiac alternans and LQT syndrome. A discussion on antiarrhythmic drug therapy is then introduced, and inter-species comparison between human and animals is included at the end.

Chapter 3 is an introduction to mathematical modelling in cardiac electrophysiology. The basic concepts and formulations underlying cardiomyocyte electrophysiological modelling are firstly introduced. Then we review the development of cardiac cellular models, and compare the latest human ventricular cell models. We then use one example of a human ventricular and a canine ventricular cell model to illustrate inter-species similarities and differences in cardiac electrophysiological modelling. Following this we briefly introduce the modelling of diseased conditions and drug effects in cardiomyocytes. Finally, techniques for the modelling of variability in cardiac electrophysiology are introduced and discussed.

Chapter 4 achieves the first goal in this thesis. Given that canine heart is generally considered to be the best model of human heart compared to other species (Gönczi *et al*., 2012), we generate a human model of a post infarction epicardial border zone cell by introducing analogous electrical remodelling to that experimentally characterized in canine electrophysiology, and sensitivity analysis is applied to the human epicardial border zone cell model to account for possible inter-species differences. We observe the prolongation of action potential duration and the generation of cardiac alternans after the ionic remodelling. We also report that the application of drug block to the rapid delayed rectifier potassium current can further increase the dispersion between the normal zone (NZ) cell and the epicardial border zone cell, which facilitates the development of alternans. In this chapter, we also find

that the remodelling of current conductances is sufficient to induce the proarrhythmic characteristics of the epicardial border zone cell, and additional remodelling to current kinetics only affects the threshold pacing cycle length for alternans generation.

Chapter 5 presents the construction and calibration process for the population of human epicardial ventricular cell models based on *in vivo* human electrophysiological recordings. In order to reproduce the cardiac variability observed in the *in vivo* human data, one parameter set in a single model is insufficient. Instead, we base our analysis on a population of models of human ventricular electrophysiology utilizing the O'Hara- Rudy dynamic model (ORd model) (O'Hara *et al*., 2011). According to the results of Chapter 4, the variations to current conductances are sufficient to account for the proarrhythmic effects. Therefore, we choose to introduce variability in current conductances in the population of models, without initially altering ionic current kinetics. To exclude unphysiological models in the initial population, different electrophysiology filters are used to select the models that are within the physiological envelope observed in the experiment data. The fundamental filter in this calibration process is the human *in vivo* activation recovery intervals (ARI), as measured in patients undergoing coronary artery bypass graft (CABG) or aortic valve replacement (AVR). The selected models after the calibration process are then analyzed to explore the mechanisms of the generation of alternans.

Chapter 6 will present the mechanisms underlying different types of alternans using the population of human ventricular cell models developed in Chapter 5. After comparing normal models and those exhibiting alternans, six ionic currents and fluxes are found to be related to the generation of alternans. Two types of action potential duration (APD) alternans are defined based on the shape of their restitution curves: some of the alternans disappear at fast pacing rates while others remain stable. The two types of alternans are also observed in the *in vivo* ARI data. The

ionic current mechanisms for the initiation and maintenance of alternans are investigated in the alternans models, and the role of the currents and fluxes involved in the alternating process are identified and used to explain the generation of alternans. The disappearance of alternans in some models under short cycle lengths (CLs) can also be explained by the rate dependence of the underlying ionic currents. A strong correlation between the net change of intracellular calcium amount and the amplitude of alternans is discovered.

Chapter 7 presents a simulation study on pharmacological drug action on the alternans models. Based on the simulation results in Chapter 6, the pharmacological interventions on six currents or ionic fluxes are explored: the fast sodium current (I_{Na}), the L-type calcium current (I_{CaL}), the rapid delayed rectifier potassium current (I_{Kr}) and sodium calcium exchanger current (I_{NaCa}), the calcium release through ryanodine receptor (J_{rel}) and the calcium re-uptake to sarcoplasmic reticulum (J_{up}). Decreasing I_{CaL} or I_{NaCa} and increasing J_{up} are identified to be the most effective interventions in alternans suppression. The effects of these three interventions are then further simulated and compared. The inhibition of I_{NaCa} is found to be the most promising and feasible anti-arrhythmic target among the three.

Chapter 8 will present the effect of a genetic mutation of I_{Ks} in the population of models. G229D mutation of KCNQ1 protein is discovered in patients to be related to LQTS; however, it is also reported to be able to shorten APD and induce atria fibrillation (Hasegawa *et al*., 2014). The kinetic parameters of the O'Hara *et al* I_{Ks} model (O'Hara *et al*., 2011) are modified to fit the patch clamp data from G229D mutated I_{Ks} channels. The G229D mutated I_{Ks} model is subsequently inserted into the population of human ventricular cell models constructed in Chapter 5, to explore the ionic interaction between this KCNQ1 G229D mutation and the variation of multiple currents.

Chapter 9 will summarise simulation results, discuss the contributions of the work,

list future work arising from the present investigations, and present the conclusions for this thesis.

Chapter 2

Literature review on cardiac electrophysiology

2.1 Basic cardiac electrophysiology

2.1.1 The basic function and structure of the heart

The heart is the central organ of the circulatory system, which functions as a pump to provide continuous blood supply to the whole body. The normal function of the heart enables the oxygen and nutrients in the blood to be supplied to different parts of body, and also facilitates the removal of the metabolic waste.

In humans, the heart is located in the middle and slightly left of the chest. As shown in Figure 2.1, the anatomical structure of the human heart can be divided into four chambers: the left and right atria and the left and right ventricles. When the heart beats, the blood with low oxygen levels and high carbon dioxide levels from the superior and inferior vena cavae enters the right atrium, passes the right ventricle, and is then pumped via the pulmonary artery from the right ventricle into the lungs where oxygen is received and carbon dioxide is released from the blood. The blood high in oxygen returns to the left atrium via the pulmonary vein, and then enters the left ventricle where it is pumped through the aorta to the whole body.

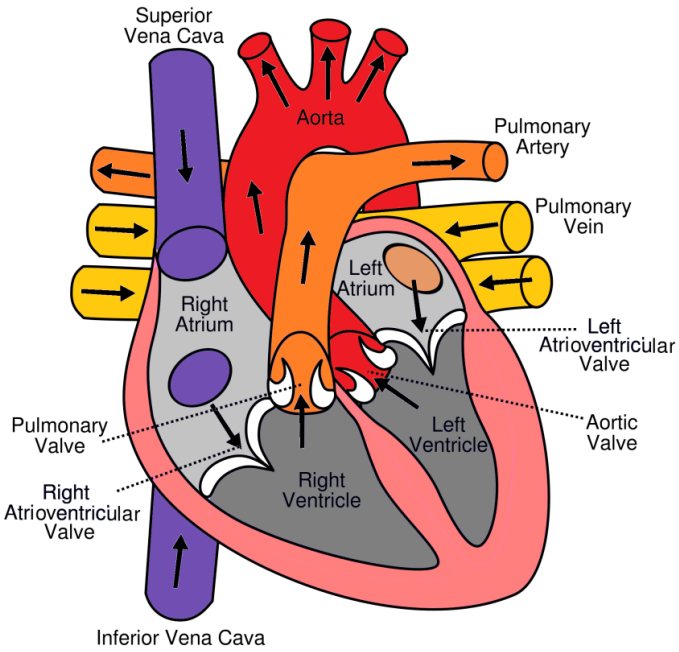


Figure 2.1: Diagram of the structural anatomy for a human heart.
The black solid arrows indicate the direction of blood flow. This is adapted from https://en.wikipedia.org/wiki/Heart .

The normal pumping of the blood is due to the contraction of the cardiac chamber walls. The cardiac muscle tissue that comprises the wall of these chambers is known as the myocardium. The inner layer of myocardium is called the endocardium, while the outer layer is known as the epicardium. The myocardium mainly consists of cardiac muscle cells, known as cardiomyocytes or cardiac myocytes. These cardiomyocytes are long and tubular in shape, and organized into sheets and fibres through the coupling of the connective protein complex known as gap junctions. The coupling enables very fast intercellular signal propagation and the synchronized behavior of these cells, and can therefore maximize the force of each beat and increase the efficiency of blood pumping.

The initial signal for the contraction of the whole heart comes from pacemaker cells of the sinoatrial node located on the wall of the right atrium, and the normal rhythm of the signal is known as the sinus rhythm. Once an electric signal is generated from the sinoatrial node, it will be conducted to other parts of the heart through a specialized cardiac conduction system. As the electric impulses pass the

cardiomyocytes, the electrophysiological activity of the cells leads to their contraction and relaxation.

2.1.2 The electrophysiology of cardiomyocytes

The electrophysiological activity of the cardiomyocytes involves three main types of membrane proteins: ion channels, ion exchangers and ion pumps. The intracellular space of cardiomyocytes always contains a much higher concentration of potassium ions (K^+) and a much lower concentration of sodium ions (Na^+) than the extracellular space due to the continuous activity of Na^+/K^+ pump driven by ATPase. Due to the transmembrane ion gradient, there is a potential difference across the cell membrane, known as the transmembrane potential, or membrane potential. The normal membrane potential of a cardiac myocyte at rest is always negative, and for a human cardiomyocyte, this resting potential is around -80mV; while for pacemaker cells in the sinoatrial node, this potential is between -50mV to -60mV.

2.1.2.1 The gating of ion channels

The ionic channels of cardiomyocytes are a type of transmembrane proteins that selectively allow the movement of one type of ions. Many ionic channels are regulated by the change of membrane voltage (Vm), and are also known as voltage-gated ion channels. When the cardiomyocyte is at rest, most of the ion channels are closed, and there is no current through these channels. If the cell receives an electric impulse and the membrane potential is increased to a certain threshold, the conformation of the voltage-gated ion channels will switch to its open state, leading to the influx or efflux of a certain type of ions.

Apart from the voltage-gated mechanism, the activity of ion channels can also be affected by transmembrane ion gradients. For example, the increase in intracellular calcium concentration can lead to the inactivation of L-type Ca^{2+} channels.

2.1.2.2 The action potential of cardiomyocytes

The cardiac action potential is a process that after receiving an electric impulse, the transmenbrane potential of cardiac cells rapidly increases and then gradually falls back to the resting level. In this process, different types of ion channels, exchangers and pumps on the cell membrane successively activate and inactivate, contributing to the influx and efflux of Na^+, K^+, calcium (Ca^{2+}) and chlorine ions (Cl^-), *etc*. Although the shape of the cardiac AP varies between different species and different types of cardiomyocytes, the whole course of AP can be divided into five phases as shown in Figure 2.2.

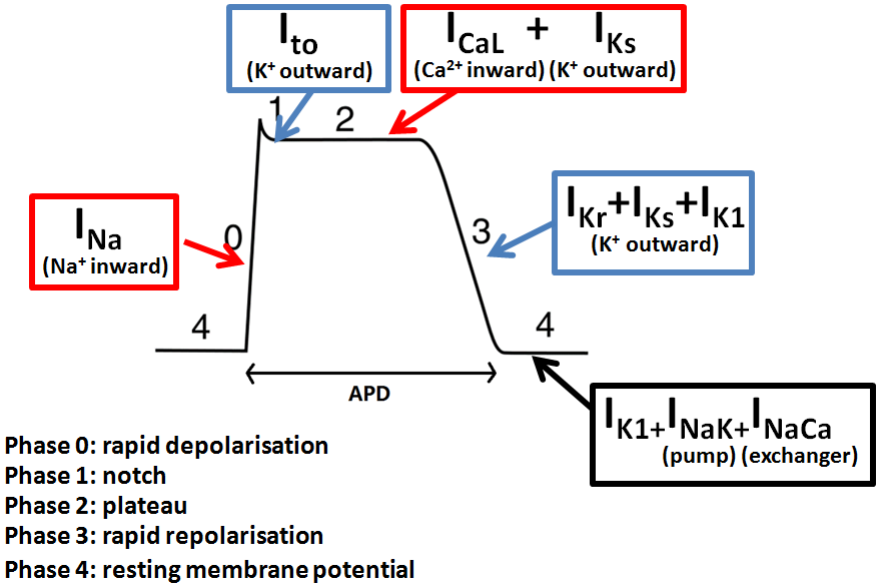


Figure 2.2: Schematic illustrations for the five phases in action potential, indicating the key currents contributing to individual phases. This is adapted from https://en.wikipedia.org/wiki/Action_potential .

Phase 0 is the rapid upstroke phase. At the beginning of this phase, the cell senses the electric stimuli from its neighbouring cell, and the transmembrane potential rapidly rises to a positive value. This process is also called as depolarisation, and in cardiomyocytes, it is mainly caused by the very fast inward sodium current (I_{Na}).

Phase 1 is the transient repolarisation phase (the 'notch'). In this phase, the fast sodium channel is inactivated, and the outward K^+ movement carried by the transient

outward potassium current (I_{to} or I_{to1}) contributes to the transient net outward current.

Phase 2 is the plateau phase of AP. During this phase, the membrane potential is maintained as a plateau by a balance between an outward potassium current through the slow delayed rectifier potassium channels (I_{Ks}) and an inward calcium current (I_{CaL}) caused by the activation of L-type calcium ion channels.

Phase 3 is the repolarisation phase. The L-type Ca^{2+} channel is inactivated in this phase, while the slow delayed rectifier (I_{Ks}) K^+ channel is still open. Meanwhile, the potassium current through rapid delayed rectifier K^+ channels (I_{Kr}) and the inward rectifier K^+ current (I_{K1}) also contribute to the decrease of transmembrane potential. This process is known as repolarisation.

Phase 4 is the resting membrane potential (RMP). At the end of phase 3, the membrane potential gets close to the resting potential, and the I_{Ks} and I_{Kr} channel close, but I_{K1} remains to be active throughout phase 4. Currents through the Na^+/K^+ pump (I_{NaK}) continue to be responsible for the maintenance of the resting potential.

The depolarising Na^+ and Ca^{2+} currents and the repolarising K^+ currents lead to the change of intracellular ion concentrations during the AP. The homeostasis of intracellular ions before and after the AP is maintained through the activity of pumps and exchangers, such as the Na^+/Ca^{2+} exchanger current (I_{NaCa}) and I_{NaK}. The Na^+/Ca^{2+} exchanger has two working modes: the forward mode and the reverse mode. At the beginning of the AP, when Na^+ enters the cell through I_{Na}, the Na^+/Ca^{2+} exchanger works in the reverse mode to remove three sodium ions from the cell and exchange for one calcium ion; therefore in the reverse mode, the net I_{NaCa} is an outward repolarisation current. During most of the time of the AP, the Na^+/Ca^{2+} exchanger works in the forward mode producing a depolarisation net current to exclude one calcium ion from the cell and exchange for three sodium ions. To

maintain the membrane potential, the I_{NaK} pumps three sodium ions against the transmembrane sodium ion gradient to exchange for two potassium ions. Apart from the I_{NaCa}, calcium ions can also be exported from the cell through the sarcolemmal calcium pump current (IpCa). The combination balance between all sarcolemmal currents on the membrane contributes to the maintenance of intracellular ion homeostasis.

2.1.2.3 Excitation-contraction coupling in cardiomyocytes

Calcium ions are the link between electric excitation and mechanical contraction of cardiomyocytes. A large amount of calcium is stored in a type of specialized smooth endoplasmic reticulum named as the sarcoplasmic reticulum (SR). On the membrane of the SR, there is a specialized type of calcium release channels known as ryanodine receptors (RyR). The RyR calcium release can be induced by the increase of local calcium concentration caused by calcium influx during APs. Therefore, the activation of I_{CaL} can initiate a large calcium release from the SR, leading to the contraction of cardiomyocytes. This positive feedback process is also known as calcium-induced calcium release (CICR) (Fabiato, 1983).

As the SR calcium level is depleted by CICR, the RyRs close and calcium release stops. During the resting time of the AP, the released SR calcium can be mostly taken back by the sarco/endoplasmic Ca-ATPase (SERCA), which is located on the SR membrane, and some can also be excluded from the cell through the Na^+/Ca^{2+} exchanger. The decline of intracellular calcium level leads to the relaxation of the cardiomyocytes.

2.1.2.4 Refractory period and refractoriness

Under normal conditions, the cardiomyocytes respond to electric stimuli originated from pacemaker cells by generating APs. Once an AP starts, there will be a period of time that a cardiac cell cannot initiate another AP. This duration is referred to as the refractory period, and it is usually shorter than the whole action potential duration.

The refractory period can help to protect the cardiomyocytes, so that only after most ion concentrations and channel states are back to their resting level, can a new AP be generated.

The refractory period of the AP is mainly due to the refractoriness of the fast sodium channel. The refractoriness of other ionic channels, such as the L-type calcium channel and RyR, can also affect the normal electrophysiological activity of cardiomyocytes (Fox et al., 2002; Shkryl et al., 2012).

2.1.2.5 Rate dependence of the action potential

The shortening of the AP is essential for the normal functioning of the heart at fast pacing rates. The APD becomes shorter under shorter cycle lengths, allowing for enough long diastolic intervals to enable the recovery of ion channels and the relaxation of the myocardium. This functional property of the AP is known as rate-dependent APD adaptation. The relationship between the change of cycle length (CL) /diastolic interval (DI) and APD is also known as restitution (Figure 2.3). The rate dependence of APD mainly depends on ion channel kinetics, such as I_{CaL}, I_{Kr} and I_{Ks} (Hund and Rudy, 2004; Viswanathan et al., 1999) . The rate dependence of the intracellular calcium subsystem can be regulated by the Ca^{2+}/calmodulin-dependent protein kinase II (CaMKII) regulatory pathway (Hund and Rudy, 2004).

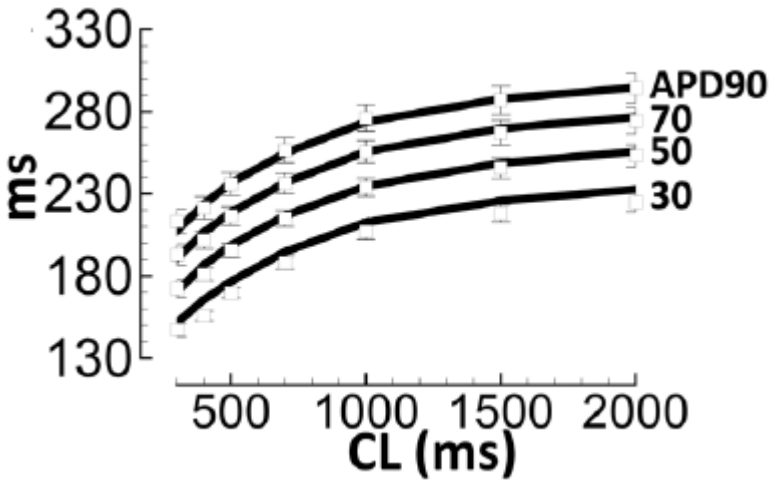


Figure 2.3: The restitution of APDs with the change of pacing CLs in human ventricular tissue and model. White squares are experimental results at 37 degrees, and solid lines are simulation results from ORd model (O'Hara *et al*., 2011).

2.2 Important experimental techniques in cardiac electrophysiology research

In the previous section, we have given a brief introduction to the basic functioning of the heart and also to the basic electrophysiological activity of cardiomyocytes. In this section, we now describe two experimental techniques directly related to this thesis. There are a wide range of other experimental techniques used in cardiac electrophysiology research, such as microelectrode recordings, used to record the membrane potential of a cardiomyocyte, or optical mapping, for the dynamic analysis of membrane potential and intracellular calcium at tissue level.

2.2.1 Voltage clamp and patch clamp techniques

The voltage-clamp technique was firstly designed by Cole and Marmont in 1949 (Verkhratsky *et al*., 2006), and then almost immediately applied by Hodgkin and Huxley (Hodgkin and Huxley, 1952a, 1952b, 1952c, 1952d) to the study of membrane excitability (Verkhratsky *et al*., 2006). During voltage clamp experiments,

an excitable cell is attached to one electrode that records the membrane voltage, and is also attached to another electrode that injects current into the cell to hold the membrane voltage at a predetermined level (the holding potential). The two electrodes can be combined into one single electrode that records and also injects current. The amount of current needed to maintain the membrane voltage can be the opposite measure of current through the membrane under this holding potential. Therefore, by changing the holding potential, the cell response under different membrane potentials can be measured.

In 1976, Neher and Sakmann refined the voltage clamp and developed the patch clamp technique (Neher and Sakmann, 1976). In patch clamping, instead of a traditional electrode, a glass micropipette that contains a recording electrode is used in the experiment. The diameter of the pipette is usually in the micrometer range, therefore a small enclosed membrane surface area enables the measurement of current through single or multiple ionic channels (Sakmann and Neher, 1984). Before the patch clamp recording, the pipette is pressed on the cell, and suction is applied to obtain a high resistance seal (GΩ) with a patch of cell membrane. Then the membrane voltage can be clamped to a certain level, and the current injected to maintain the holding potential is opposite in sign and with equal amplitude with the current through channels on the patch of membrane.

There are several variations of patch clamp techniques. For cell-attached patch, the pipette is sealed onto the membrane, which enables the recording of currents through channels on the patch of membrane enclosed by the pipette. For inside-out patch, outside-out patch, more suction is applied, and the membrane patch is detached from the whole cell. These three patch clamping variations allow for the study of individual ion channels on the patch of membrane. For whole-cell patch, more suction is applied to rupture the membrane patch, but the pipette is sealed with the entire cell membrane, accessing the intracellular space. Therefore, the whole-cell patch can study the electrophysiological behaviour of the entire cell, rather than

single ion channels.

The development of patch clamp techniques is an important milestone in the history of cardiac electrophysiology research. The key properties of the important ion channels cannot be revealed without the patch clamping to individual channels. Furthermore, patch clamp techniques provide important data for the development of cardiac models. The characterization and validation of gating kinetics of individual currents in cardiac models rely on the experimental data of these channels under different holding potentials in the patch clamping process.

2.2.2 *In vivo* measurement of whole heart electrophysiology

Although patch clamp techniques can provide substantial experimental data on different ionic channels, an aggressive cell isolation procedure is required. Therefore, patch clamp experiments cannot provide electrophysiological information for the *in vivo* condition. Thus, the acquisition of basic electrophysiological data in the intact heart, especially from human hearts, is necessary for the study of human cardiac electrophysiology (Taggart *et al*., 2014).

In 1959, Hoffman *et al.* discovered in rabbit hearts that by opposing a suction electrode to myocardium, the entire process of local action potential of the cardiomyocytes can be detected (Hoffman *et al*., 1959). Cardiac catheters were then developed and introduced to the human heart to obtain *in vivo* APD (Olsson *et al*., 1971). This provides a direct link between basic and clinical cardiac electrophysiological study. Since then, more techniques have been developed to measure normal and diseased cardiac electrophysiological processes during clinical procedures.

2.2.2.1 Monophasic action potentials

Monophasic action potentials (MAPs) are extracellularly recorded electrical waveforms that can reproduce the repolarisation process of APs with high reliability (Franz, 1999). It is an important technique to bridge the gap between laboratory electrophysiology and *in vivo* human conditions (Taggart *et al*., 2014).

The application of the MAP technique needs two electrodes: one electrode presses against the myocardium to inactivate the site, whereas the other electrode functions normally near the site. As validated *in vitro* by comparing with transmembrane microelectrode recordings, the potential difference between the two electrodes of MAP follows the shape of the APs of the region (Franz *et al*., 1986), and can therefore be used in the investigation of *in vivo* APs.

Early MAP recordings used one suction catheter onto the endocardium (Olsson *et al*., 1971), while later MAPs mostly used a Franz bipolar electrode configuration (Franz et al., 1986; Moore and Franz, 2007). MAPs can be recorded from the endocardium (through cardiac catheterisation) and epicardium (through cardiac surgery) of *in situ* beating human hearts, and therefore represent an extremely valuable source of electrophysiological data (Franz, 1999). The normal range of APDs, the dynamics of APD rate adaptation and restitution, the relationship between APD and refractoriness, and the effects of drugs can be obtained through endocardial or epicardial MAPs (Taggart *et al*., 2014).

2.2.2.2 The electrograms and the activation-recovery interval

An electrogram (EGM) is a representation of the time course of the potential difference between two sites during the cardiac cycle (Taggart *et al*., 2014). Unlike the MAP technique, the EGM does not need the inactivation of a region to obtain *in vivo* recordings. The shape of EGM signals does not resemble action potentials like the MAP technique, and is more similar to electrocardiograms (ECGs): a QRS complex in EGM reflects depolarisation and a T wave represents repolarisation.

There are several types of electrograms. In bipolar EGMs, the difference between the potential of two close sites is measured, while in unipolar configuration, the EGM is measured as the potential difference between an exploring site and an indifferent site which is far from the exploring site and without electrophysiological activity. Thus, the bipolar EGMs only provide local fast electrical dynamics, and therefore are often used to study the propagation of activation wavefronts. Although the unipolar EGMs are less sensitive to the propagation direction, the repolarisation dynamics can only be reliably estimated using unipolar EGM (Taggart *et al*., 2014).

The activation-recovery interval (ARI) calculated from EGMs has been shown as an *in vivo* estimation of APD (Coronel et al., 2006; Haws and Lux, 1990; Potse et al., 2009; Yue et al., 2004). ARIs are usually calculated as the interval between the activation time, estimated as the instant with maximum downward slope during depolarisation (dV/dt_{min}), and recovery time, estimated as the instant of maximum upward slope during repolarisation (dV/dt_{max}) (Potse et al., 2009; Steinhaus, 1989; Taggart et al., 2014; Wyatt, 1980) (Steinhaus, 1989).

2.2.2.3 The multi-electrode mapping

In order to understand the spatial dispersion of electrophysiological properties at different parts of an in situ beating heart, the technique of multielectrode mapping was developed in animal models, and then extended to humans. Initially, small epicardial multielectrode plaques with 25 electrodes were developed for the study of transverse and longitudinal conduction velocity (Taggart *et al*., 2014). Then a multielectrode sock with 127 electrodes was developed for the cardiac electrophysiology study in large animals (Nash *et al*., 2003), and epicardial socks with 256 electrodes were adapted for patients undergoing cardiac surgery (Nash *et al*., 2006). The development of the multielectrode sock enables the recording of unipolar EGMs over the entire human ventricles, and can therefore provide unique *in vivo* data for human whole heart electrophysiology.

2.3 The variability in cardiac myocytes

Along with the development of electrophysiological experimental techniques, variability between cardiomyocytes was observed in animal cardiomyocytes (Szentandrássy *et al*., 2015). A considerable degree of inter- and intra-subject variability in APD can also be observed in ventricular cardiomyocytes from human hearts (Glukhov et al., 2012, 2010; Lou et al., 2011).

The multiple ionic currents that contribute to the cardiac APs are controlled by the transmenbrane ion channels. Therefore, the major cause of the variability between individual APs is expected to be related to the activity of ionic channels. Within the same species, the structure, function and characteristics of one type of ion channel is expected to be consistent between individual cells, when there is no genetic mutation to alter the protein structure or function. However, the density of a type of ionic channel can vary between individual cells, producing the cell-to-cell variability in APs.

One example to illustrate the effect of ion channel density on AP variability is the transmural heterogeneity that exists in the myocardium. It has been reported in human and animal cardiomyocytes that the expression level of many ion channel proteins are different between endocardium and epicardium (Boukens et al., 2015; Gaborit et al., 2007; Näbauer et al., 1996; Soltysinska et al., 2009; Szabó et al., 2005), which results in the difference in the morphology and duration of APs between epicardium and endocardium.

Even from a same layer or a same region of the myocardium, substantial cell-to-cell variability in APs between individual myocytes can still be observed (Feng et al., 1998; Glukhov et al., 2012, 2010; Lou et al., 2011; Péréon et al., 2000). The generation of cell-to-cell variability can be due to the difference in the expression level of ion channel proteins. Many different factors, including circadian rhythms,

sustained heart rate change, drug effects and the development of disease, can also affect the expression of these channels.

2.3.1 Circadian rhythm regulates ionic channel gene transcription

Circadian rhythm refers to the biological process in living organisms that oscillate within a cycle of roughly 24 hours (Jeyaraj *et al*., 2012). The circadian rhythm has been found to be able to affect the density of ionic current by regulating ion channel protein expression during a cycle of 24 hours. For instance, Jeyaraj *et al.* showed in mice that the expression of α-subunit for the transient outward potassium current Kv4.2 (encoded by Kcnd2) and the regulatory β-subunit, KChIP2 exhibited endogenous circadian rhythm (Jeyaraj *et al*., 2012). In addition, a clock-dependent oscillator Klf15 can regulate the circadian rhythmicity of KChIP2 transcription. Yamashita *et al*. also found in rat that Kv4.2 and Kv1.5 (subunit of ultra-rapid activating delayed rectifier K^+ channel (I_{Kur})) gene showed significant circadian variation in their transcripts. Apart from protein transcription, recent studies have identified that the cardiomyocyte's circadian clock influences multiple myocardial processes, such as metabolism, growth and repair (Durgan and Young, 2010). In humans, circadian rhythm has been found to have significant effect on the onset of acute myocardial infarction and sudden cardiac death (Muller et al., 1987, 1985).

2.3.2 Sustained heart rate change affects ion channel expression

Sustained heart rate abnormalities have been shown to regulate ion channel expression levels. Tsuji *et al.* found in rabbit hearts that after bradypacing (slower than normal pacing) or tachypacing (faster than normal pacing) for three weeks, the I_{Ks} expression level was decreased. I_{Kr} activity was also reduced after bradypacing (Tsuji *et al*., 2006). Another experiment conducted in dogs showed that after tachypacing of 3Hz for 24 hours, the mRNA level of L-type calcium channel protein

was significantly decreased (Qi *et al*., 2008).

2.3.3 Exposure to drugs affects ionic channel expression

Chronic exposure to ion channel blockers has been found to alter ion channel expression, although the underlying mechanism is still not understood. Xiao *et al*. reported in canine ventricular myocytes that sustained exposure to I_{Kr} blocker can lead to the compensatory increase in the expression of I_{Ks} channel proteins (Xiao *et al*., 2008). The long term treatment of amiodarone, a type of anti-arrhythmic drug that blocks multiple channels, has been reported to alter the gene expression level of sodium, potassium and calcium channel subunits (Le Bouter *et al*., 2004).

2.3.4 Diseases alter ionic channel expression

Many diseases have been found to be associated with the expression of ion channels. For instance, heart failure is a pathological condition when the heart is unable to pump sufficient blood to meet the needs of the whole body. Soltysinska *et al*. compared the mRNA level profile in human hearts with or without heart failure, and they found the genes encoding I_{K1}, I_{Ks}, and I_{NaCa} were up-regulated in heart failure, while the genes encoding I_{to}, SERCA were down-regulated in the failing hearts. In addition, the transmural gradient in ion channel expression was also altered in failing hearts (Soltysinska *et al*., 2009).

2.3.5 Sympathetic neural stimulation regulates ionic channel activity

In addition to the above mechanisms that can regulate the expression level of ion channel proteins in cardiomyocytes, the densitiy of ionic currents can also be regulated by sympathetic stimulation through β-adrenergic receptors. The binding of

an agonist to β-adrenergic receptor can lead to the activation of Gs protein, the increase of second messenger cyclic AMP (cAMP), and the consequent activation of protein kinase A (PKA) (Taggart *et al*., 2011). The activation of PKA can then lead to the phosphorylation of a variety of ion channels and the increase of the corresponding sarcolemmal currents, such as I_{Na} (Wang *et al*., 2009), I_{CaL} (Ganesan *et al*., 2006), I_{Ks} (Marx *et al*., 2002) and I_{NaCa} (Perchenet *et al*., 2000). The increase of I_{CaL} results in the prolongation of the AP plateau, and the enhancement of I_{Ks} accelerates repolarisation and contributes to a shorter APD. Therefore β-adrenergic stimulation can affect the morphology of APs through the regulation of sarcolemmal current densities.

In addition, β-adrenergic stimulation also participates in the regulation of the intracellular Ca^{2+} handling process. PKA can phosphorylate phospholamban to increase Ca^{2+} re-uptake through SERCA (Ramirez-Correa and Murphy, 2007), and also phosphorylate RyRs to enhance Ca^{2+} release (Shan *et al*., 2010). The β-adrenergic stimulation can accelerate Ca^{2+} release and re-uptake and therefore further affect sarcolemmal calcium density through the regulation of the intracellular Ca^{2+} level.

From the studies above, we can see that the ionic current density can vary due to a number of factors: circardian rhythm, sustained heart rate change, drug exposure, and disease development can affect current density by regulating ion channel expression levels; while neural stimulation can change current density through the regulation of ion channel activity. All these factors can contribute to AP variability by affecting the variation of current densities.

Although the density of a current can be measured experimentally in an isolated cardiomyocyte using voltage clamp technique, the aggressive cell isolation procedure can damage the cell membrane and result in a decrease in numbers of ion channels (Yue *et al*., 1996). Therefore, the natural variation ranges of current

densities are difficult to measure accurately. However, as an important component in cardiac electrophysiological system, the variability between cardiomyocytes should be included in cardiac research since it can have a significant effect on the proarrhythmic behaviour of cardiomyocytes.

2.4 Several proarrhythmic conditions

The variation of the electrophysiological properties of cardiomyocytes can be a source for the development of proarrhythmic conditions. Here we introduce three types of proarrhythmic conditions that are related to the work of this thesis.

2.4.1 Effects of myocardial infarction

Myocardial infarction (MI) is directly linked to coronary disease, which includes the narrowing or blockage of the coronary arteries. The lack of oxygen and nutrients in cardiac cells caused by coronary disease can lead to cardiac tissue infarction or tissue death (necrosis) in the heart. As a result of MI, the balance and synchronization between cardiac cells is destroyed, and electrophysiological and structural remodellings are induced in the surviving normal zone (NZ) and epicardial border zone (EBZ). These ionic remodellings can further increase the inhomogeneity in post-MI tissue and promote the generation of cardiac alternans (Chou *et al*., 2007).

The EBZ is a thin rim of surviving epicardial tissue that borders the infarcted region. It is sometimes referred to as the gray zone, and has been characterised as a heterogeneous mix of viable tissue and necrotic scar (Arevalo *et al*., 2013). The electrophysiological characteristics of this region are different from those of the NZ, and this dispersion in tissue electrophysiology may lead to the initiation and maintenance of potentially lethal arrhythmias. In the human heart, it has been observed that the contractility is impaired in the EBZ (Wenk *et al*., 2012). Research

studies in canine and rabbit hearts have also shown that conduction delays in this region are sufficient to cause pathological phenomena such as re-entrant tachycardia (Arevalo et al., 2013; Kramer et al., 1985; Nassif et al., 1993).

A number of studies have characterised the remodelling of ion channels in the post-infarction EBZ cells in animal models (often in canine hearts). The magnitudes of many currents contributing to the cardiac AP are decreased in EBZ myocytes, such as the fast Na^+ current (I_{Na}), the L-type Ca^{2+} current (I_{CaL}), K^+ currents (I_{K1}, I_{Kr}, I_{Ks}, I_{to1}) and the Cl^- current (I_{to2}). The kinetics of the I_{Na} current has also been observed to be leftward shifted (Decker and Rudy, 2010). The overall effect of EBZ current remodelling leads to APD prolongation, the absence of phase I notch (due to loss of I_{to1}) and the increase of AP triangulation (due to the reduction in I_{K1}), as observed experimentally in canine hearts (Lue and Boyden, 1992).

In addition to the alterations on EBZ electrophysiology, MI can also affect the cellular coupling of the post-MI cardiac tissue. In the canine EBZ, the expression level of connexin45 is reduced after infarction. In addition, connexin45 in the EBZ tends to relocalise from the intercalated disks to non disk lateral membranes (Macia *et al*., 2011). This lateralization is associated with loss of gap junctional coupling between myocytes, which may lead to conduction block and re-entrant arrhythmias (Macia *et al*., 2011).

2.4.2 Cardiac alternans

Cardiac alternans are repetitive beat-to-beat fluctuations between subsequent APs, and have been regarded as an important risk factor for the genesis of ventricular arrhythmias and fibrillation in a wide range of pathophysiological conditions (Merchant and Armoundas, 2012). It has been found that cardiac alternans can be produced in failing and post-MI hearts as well as in some normal hearts under

conditions of metabolic stress and chronotropic stimulations (Merchant and Armoundas, 2012).

2.4.2.1 Cardiac alternans can be triggered due to short diastolic intervals

Cardiac alternans can be triggered at fast pacing rates, and are known to be promoted by conditions resulting in prolonged APD due to fluctuations of ion channel availability. Theoretical studies have shown that a short diastolic interval (DI) of one beat can result in partial recovery from inactivation of the sodium and calcium channels in the next beat, leading to beat-to-beat instabilities in ion channel availability and APDs (Clancy and Sato, 2013; Fox *et al*., 2002; Qu *et al*., 2010). A steep APD restitution curve for short DIs has been associated with repolarisation alternans in canine experiments and theoretical studies (Clancy and Sato, 2013; Koller *et al*., 1998; Qu *et al*., 2010), and importantly in human *in vivo* studies (Koller *et al*., 2005). However, alternans have also been observed clinically on the flat portion of the APD restitution curve (Narayan *et al*., 2007), indicating that steep APD restitution is not the only mechanism resulting in alternans.

2.4.2.2 Calcium-driven or Voltage-driven

The exact mechanisms of alternans initiation at the ionic level are still not clear. Two major hypotheses have been developed to explain the generation of alternans in cardiac myocytes.

According to the first hypothesis, changes in sarcolemmal currents such as K^+ and Ca^{2+} currents, lead to the changes in AP morphology, which then result in the beat-to-beat fluctuations of cytosolic calcium concentration (Merchant and Armoundas, 2012). Modulation to sarcolemmal K^+ and Ca^{2+} currents has been found to have a significant effect on the stability of Ca^{2+} cycling and the generation of stable alternans (Merchant and Armoundas, 2012). Moreover, a number of sarcolemmal currents such as I_{to}, I_{CaL} and I_{Kr} can also exhibit alternating type activity (Merchant and Armoundas, 2012). Some other transmembrane proteins such as the

Na^+/Ca^{2+} exchanger and the Na^+/K^+ pump may also play a role in the generation and maintenance of the alternans.

The other hypothesis, however, suggests that alternation in intracellular calcium concentration is the primary event that then leads to the changes in AP morphology and the initiation of stable alternans (Merchant and Armoundas, 2012). Intracellular calcium storage plays a crucial role in the maintenance of normal myocyte physiological activity. The amount of calcium releases from the SR to initiate contraction must match the amount of calcium reclaimed from the cytoplasm. Under this hypothesis, cardiac alternans occur when the heart rate exceeds the capability of cardiac myocyte to cycle calcium. According to this hypothesis, alternans generation may also initiate from anywhere in the multistep calcium cycling process, such as the recovery of RyRs and SERCA from inactivation, triggering of SR Ca^{2+} release and uptake, redistribution of intra-SR Ca^{2+} and transportation of cytosolic Ca^{2+} (Merchant and Armoundas, 2012).

Recently, more experimental data tends to support the interpretation that the perturbation in the intracellular calcium transport cycling is the fundamental event in the generation of alternans (Merchant and Armoundas, 2012). The latest results in rabbit myocytes showed that calcium alternans can be observed with or without alternations in APD, indicating that the primary mechanism underlying alternans resides in calcium fluctuation, and APD alternans are likely to be the secondary effects of calcium signaling disturbance (Kanaporis and Blatter, 2014).

2.4.2.3 SR calcium fluctuation or RyR refractoriness

A large number of studies have related a variety of Ca^{2+} dynamics properties to Ca^{2+} alternans. From these studies, two major mechanisms were raised to be the first critical factor in the generation calcium alternans: fluctuations of SR calcium content, and RyR refractoriness.

The balance between SR calcium release and re-uptake is crucial for sustainable normal APs; once the balance is disrupted, the level of SR calcium may fluctuate. Díaz *et al.* reported in rat ventricular myocytes that the beat-to-beat fluctuations in SR Ca^{2+} content are sufficient to produce alternans (Díaz *et al*., 2004). Consistent with this finding, Cutler *et al.* also found that SERCA2a over-expression in intact rabbit hearts can significantly increase the resistance to APD alternans and reduce alternans-mediated ventricular arrhythmias (Cutler *et al*., 2009).

On the other hand, Picht *et al.* found that although SR calcium fluctuations in rabbit myocytes were crucial for the generation of calcium alternans, they were not always required (Picht *et al*., 2006). About 50% of their rabbit myocytes exhibited SR calcium fluctuations, and another 20% of the myocytes displayed stable calcium alternans without fluctuations in SR calcium level (Picht *et al*., 2006). A recent study in intact rabbit hearts also showed that alternans in calcium release from RyR can be initiated by RyR refractoriness, rather than by the SR calcium level (Wang *et al*., 2014).

A simulation study using rabbit ventricular myocytes model compared the role of these two mechanisms in calcium alternans initiation, and their results showed that the inactivation and activation rates of RyR can determine the relative weights of the two mechanisms in alternans initiation (Alvarez-Lacalle *et al*., 2013). As both of the mechanisms were only investigated in animals, they need to be further studied in human cardiomyocytes.

2.4.2.4 Cardiac alternans at the tissue level

Cardiac alternans at the tissue level can be a dangerous precursor of ventricular arrhythmias. If alternans in all areas of the tissue are in phase with the alternans at the stimulus site, alternans are classified as concordant. Otherwise; if there are areas of the tissue alternating out of phase with the stimulus site, the alternans are classified as discordant (Watanabe *et al*., 2001). Compared with concordant alternans,

discordant alternans are potentially more dangerous as they can produce larger alternans in electrocardiograms (Watanabe *et al*., 2001).

It has been found in mice hearts that the calcium alternans among neighbouring cells are predominantly concordant, probably due to the electric coupling (Hammer *et al*., 2015). The intercellular electric coupling between myocytes can inhibit alternans, but also allow alternans to be more stable once established (Hammer *et al*., 2015).

2.4.3 Long-QT syndrome

Long-QT Syndrome (LQTS) is a type of cardiac phenotype that is often related to syncope and sudden cardiac death (Moss and Robinson, 2002). It is frequently caused by inherited genetic mutations (inherited form of LQTS) or medical treatment (acquired form of LQTS). The QT interval is the interval encompassing the Q wave and the T wave in the electrocardiogram (ECG). The prolongation of the QT interval on an ECG reflects the delay of repolarisation in myocytes, and can induce arrhythmias through the ion channel variability and transmural dispersion of repolarisation (Abrams and Macrae, 2014).

Genetic analysis first identified the mutation of the I_{Ks} channel component KCNQ1 as the basis for LQT type 1 (LQT1). Then the mutations of the I_{Kr} channel component hERG and the mutations of the sodium channel protein SCN5A were recognized as the genetic mechanisms for LQT2 and LQT3, respectively. Nowadays, 12 genes have been found to be related to inherited LQTS, and about 70% of LQTS patients have at least one of these gene mutations (Priori *et al*., 2003).

The prevalence of inherited LQT is recently suggested to be around 1:2000-2500 through a genetic analysis among white infants (Schwartz *et al*., 2009). LQT1 is the most common type of LQTS, and in this type of mutation, the outward I_{Ks} current is

reduced leading to a delayed repolarisation and prolonged QT interval.

Although genetic mutation is highly connected to LQTS, the penetrance of those mutation carriers is only about 25% (Priori *et al*., 1999). The low penetrance of LQTS mutation carriers suggests the complex interaction between multiple components in cardiac electrophysiological system: for example, the potassium currents can compensate each other when a mutation exists in one type of potassium channel.

In addition, there is a significant overlap in corrected QT interval (QTc) values between undiseased patients and LQTS gene mutation carriers who have no or only borderline QT prolongations (Taggart *et al*., 2007). Clinical treatment, such as the use of I_{Kr} blockers (also known as hERG blockers), can lead to greater QT prolongation and often unmasks otherwise quiescent LQTS, increasing the risk of lethal arrhythmias (Abrams and Macrae, 2014). Therefore, to improve the clinical treatment and management for LQTS, it is crucial to investigate the interaction between LQTS gene mutations and other ionic currents in human cardiomyocytes.

2.5 Introduction to anti-arrhythmic drug therapy

In the previous two sections, we have introduced different factors that can affect the variability between cardiomyocytes, and reviewed some basic knowledge of important proarrhythmic conditions. In this section, we will introduce several important anti-arrhythmic drugs used in the clinic.

2.5.1 Classification of anti-arrhythmic drugs

Anti-arrhythmic drugs have been available for over 100 years, and for more than a quarter of a century, anti-arrhythmic drugs have been classified based on their

mechanisms of action according to a well-known classification system developed by Vaughan Williams (Vaughan Williams, 1970).

According to the Vaughan Williams classification, the class I anti-arrhythmic drugs are sodium channel blockers, and they can reduce phase 0 peak of action potentials and also decrease the conduction velocity (Kowey PR, 1998). Class Ia drugs have intermediate kinetics, can also block potassium channels, and therefore lead to prolongation of APD. Examples of Class Ia drug include quinidine, procainamide and disopyramide. Class Ib drugs, such as lidocaine, mexilitine and tocainide, have fast kinetics, but can only produce modest inhibition on the sodium channels. Class Ic blockers have slow kinetics, and they can significantly slow down conduction velocity, but have little effect on repolarisation. Examples of Class Ic drugs include flecainide and propafenone.

Class II anti-arrhythmic drugs are β-adrenergic receptor blockers, and they block the effect of sympathetic activity, and slow down sinus rhythm without significantly changing APD. This type of drugs includes propanolol, nadolol, acebutolol, atenolol, bisoprolol.

Class III drugs block the outward potassium currents, thus prolonging repolarisation and APD. This type of anti-arrhythmic drugs contains sotalol, dofetilite, and amiodarone.

Class IV anti-arrhythmic drugs are calcium channel blockers, mainly including verapamil and diltiazem. They can inhibit phase 2 (plateau) of the AP, and reduce the contractility of the cardiomyocytes.

Other anti-arrhythmic agents that work by unknown or other mechanisms are classified as Class V, such as digoxin that inhibits Na^+/K^+ pump, and adenosine that modulates many signalling processes.

Despite the common classification mentioned above, each drug has a unique pharmacological profile. Although most of the anti-arrhythmic drugs have a relatively narrow therapeutic index, some of these drugs have more than one action (Kowey PR, 1998). For example, quinidine is classified as a Class Ia, and it also has potassium channel blocker activity; sotalol has Class II and Class III properties, and can block β-adrenergic receptor and potassium channels. Some drugs such as amiodarone and dronedarone can affect a broad range of channels including sodium, calcium, and multiple potassium channels (Zimetbaum, 2012).

2.5.2 The clinical use of anti-arrhythmic drugs

Antiarrhythmic drug therapies are widely used in the clinic. For instance, propanolol has been used in the treatment of sinus tachycardia (faster sinus rhythm than normal) due to their properties of inhibiting β-adrenergic receptors (Kowey PR, 1998). A number of drugs, such as lidocaine, procainamide, amiodarone, propafenone, flecainide and sotalol have been used in the prevention or treatment of ventricular tachycardia (Kowey PR, 1998). As a β-adrenergic receptor and Class III potassium channel blocker, sotalol has minimal non-cardiovascular side effects, and therefore has a high rate of utilization in the United States (26% of annual prescriptions) (Zimetbaum, 2012). Amiodarone, although not approved by the Food and Drug Administration for atrial fibrillation, is the most commonly used anti-arrhythmic drug for the disease, accounting for 45% of annual drug prescriptions (Zimetbaum, 2012).

The correct use of anti-arrhythmic drugs can help to reduce the onset of arrhythmias and prolong the lifespan of patients; however, when misprescribed by selecting an inappropriate drug or dosage, the effect can be inadequate for the control of arrhythmias, or even proarrhythmic (Kowey PR, 1998). For example, flecainide and

propafenone are recommended for the management of atria fibrillation patients without structural heart disease (Zimetbaum, 2012). But for people with prior myocardial infarction and reduced left ventricular function, the use of flecainide and propafenone can lead to a higher risk of ventricular arrhythmias (Echt *et al*., 1991). Anti-arrhythmic drug therapy in elderly people also brings additional risks. Although most recommendations of common anti-arrhythmic therapies still apply for this age group, lower doses are usually required due to reduced renal and hepatic functions (Kowey PR, 1998). Although the extent of aging remodelling on ion channel expression in human cardiomyocytes is still unknown, voltage clamp measurements have suggested the regulatory effect of aging on current densities during developmental process (Crumb et al., 1995; Mansourati and Le Grand, 1993). Elderly people have been found to be more sensitive and susceptible for sotalol and amiodarone, both of which have Class II and Class III activity (Kowey PR, 1998).

Therefore, the safe management of anti-arrhythmic drugs on different patients requires a better understanding of the complex interaction between drugs and multiple ion channels. In this process, the variability caused by aging and different disease conditions should be considered.

2.6 Difference between animal and human cardiac electrophysiology

The motivation underlying many biological researches is to improve the understanding of human diseases. However, most of the experimental studies on pathological conditions are conducted in animals due to ethical limitations and difficulties in obtaining human samples. Therefore, it is possible that the physiological mechanisms are not consistent between human and animals due to inter-species differences. In this section, we review recent experimental results from cardiac electrophysiological research where important differences between animals

and human were found. These findings justified our choice of a human-based study in this thesis.

One of the major differences between human and animal cardiac electrophysiology is the difference in heart rate. The slower heart rates in human hearts correspond to longer APDs in cardiomyocytes, and therefore the contribution of individual currents to the action potential varies substantially between species.

It has been found that there are important species-specific differences in potassium currents and arrhythmia susceptibility. Zicha *et al.* quantified the expression of voltage-gated potassium channel subunit in rabbits, guinea pigs, and humans (Zicha *et al*., 2003). The levels of Kv1.4, Kv4.2, and Kv4.3 mRNA were present in humans but extremely low in guinea pigs; while the minimal potassium channel subunit (minK) mRNA and protein levels in guinea pigs were threefold and twofold greater than in humans, and 20-fold greater than rabbits. The mRNA and protein level of KvLQT1 were the greatest in humans, with the protein expression level 2-fold and 7-fold larger than in rabbits and guinea pigs, respectively. These important inter-species differences in the expression of cardiac potassium channel subunits can therefore explain 1) the lack of I_{to} and phase 1 notch in guinea pig; 2) the small I_{Ks} in rabbits caused by low minK expression; 3) and the large I_{Ks} in guinea pigs related to strong minK expression (Zicha *et al*., 2003).

Canine heart is generally considered to be the best model of the human heart in terms of its electrophysiological properties (Gönczi *et al*., 2012). Similar AP morphology and distribution pattern of ionic current densities were found between human and canine ventricular myocardium (Szabó et al., 2005; Szentadrassy et al., 2005). However, there are electrophysiological differences between dogs and humans.

For instance, Akar *et al.* reported that despite the expression of the homologous subunit proteins as in humans, the function of I_{to} is distinct in dogs. Slower current

decay, faster recovery from inactivation and a depolarizing shift of steady-state inactivation were detected in the I_{to} of human than in dogs (Akar *et al*., 2004). For human I_{to}, the recovery from inactivation exhibited a monoexponential time course, whereas in dogs, it followed a biexponential kinetics (Akar *et al*., 2004). In addition, the pharmacological sensitivity to flecainide was higher in human I_{to} compared to dogs. These data suggest that the variation in the electrophysiological and pharmacological properties between human and dog I_{to} may come from the difference in protein structure or post-translational modification (Akar *et al*., 2004).

A recent study by (Norbert Jost et al., 2013) compared the repolarisation reserve between human and canine. Selective I_{Kr} block led to a 3-fold larger increase of APD in human than in canine, while selective I_{K1} block increased APD more in canine than in human. Ionic measurements in isolated cardiomyocytes showed that I_{K1} and I_{Ks} densities were 3- and 4.5-fold larger in dogs, and I_{to} were about 30% smaller in human. In addition, lower Kir2.1 (I_{K1} ion channel subunit) and minK (I_{Ks} accessory subunit), and higher KvLQT1 (I_{Ks} α-subunit) protein expression were identified in human *versus* canine cardiomyocytes. I_{K1} and I_{Ks} inhibition further facilitated the APD prolongation effect of I_{Kr} block more in dogs than in human. These results demonstrated the species-specific repolarisation reserve provided by potassium currents.

Apart from the inter-species difference in potassium currents, L-type Ca^{2+} current is also related to the interspecies differences in APs. Linz *et al.* conducted a study on isolated ventricular myocytes from guinea pigs, rats and rabbits to compare the activation and inactivation of L-type Ca^{2+} channel during APs (Linz and Meyer, 2000). Their results showed that the species-specific AP shape and Ca^{2+} influx strongly influenced the amplitude of I_{CaL} and the inactivation of the channel. Therefore, it is very plausible that there exist significant inter-species differences between the human and animal L-type Ca^{2+} current.

At the tissue level, the differences between human and animal hearts become even more complicated, since the size of the heart also affects the initiation of arrhythmias. Some experimental evidence has shown that sustained ventricular fibrillation is uncommon in small animals and in human infants (Coronel *et al*., 1997), which agrees with the theoretical concept of a minimum size required to sustain multiple wavelet re-entry (Janse and Wit, 1989).

Panfilov further investigated the relationship between heart size and reentry using computational models, and the simulation results showed that rather than actual heart size (D), the effective size of the heart (L) is the main determinant of reentry (Panfilov, 2006). L was defined as the ratio between D and the wavelength (λ) that is the product between refractory period and conduction velocity. These results showed there are differences in effective size between different species, therefore, it is not always possible to accurately simulate human cardiac disease in animal models (Coronel *et al*., 1997).

2.7 Summary

In this chapter, we began by introducing the basic structure and function of the heart, and then described the basic electrophysiology of cardiomyocytes. Following these, we introduced the key *in vitro* and *in vivo* experimental techniques related to this study. Then we demonstrated that the variability observed in cardiac ionic current densities can come from multiple sources. Several proarrhythmic conditions that are relevant to this thesis were reviewed, such as myocardial infarction, cardiac alternans and LQT syndrome. Finally we briefly introduced the current antiarrhythmic drug therapies and discussed the inter-species electrophysiological differences between human and animals.

In summary, this chapter demonstrated the complexity and variability in

cardiomyocyte electrophysiology. In addition, this review highlights the need to address the significant difference between experimental animal and human electrophysiology. Therefore, computational models of human cardiomyocyte electrophysiology can be used to fill in the gap in this area.

Chapter 3

Literature review on the modelling of cardiac electrophysiology

3.1 Basic formulations underlying the electrophysiological modelling of cardiomyocytes

3.1.1 The Hodgkin-Huxley formulation for ionic currents

In 1952, Hodgkin and Huxley published a series of papers to explain the ionic mechanisms underlying the AP of the isolated squid giant axon, and the Hodgkin-Huxley model became the first mathematical model of an AP (Hodgkin and Huxley, 1952a, 1952a, 1952c, 1952d). Although originally developed for a neuronal AP, its modelling framework has been successfully and widely applied to simulate the behaviour of cardiac APs.

Due to its bilipid nature, the cell membrane is treated in the Hodgkin-Huxley model as a capacitor, and the change of membrane voltage (V_m) is the formulated as:

$$\frac{dV_m}{dt} = -\frac{1}{Cm} \times I_{ion}, \tag{3.1}$$

where C_m is the membrane capacitance, and I_{ion} is the total transmembrane current, including currents through channels, exchangers and pumps. In this formulation, V_m is assumed to be the same at the whole membrane, and there is no external stimulation. When a stimulus current (I_{stim}) is injected into the cell, the equation will become:

$$\frac{dV_m}{dt} = -\frac{1}{Cm} \times (I_{ion} + I_{stim}). \quad (3.2)$$

In these two equations, the I_{ion} is negative if positive ions enter the cell (inward current), leading to the positive dV_m/dt and the depolarisation of V_m. On the other hand, if positive ions exit the cell (outward current), I_{ion} is positive, resulting in negative dV_m/dt and the repolarisation of V_m. The external stimulus current I_{stim} is normally negative.

I_{ion} is the total balance of all the sarcolemmal inward and outward currents during the AP. The dynamic interplay of these currents determines the shape, time course and the duration of the AP. The basic representation of each of the individual sarcolemmal current (I_i) that constitutes the total I_{ion} is given by the following equation:

$$I_i = g_i \times (V_m - E_i), \quad (3.3)$$

where (V_m -E_i) is the driving force of the current, E_i is the reverse potential (also known as Nernst potential or equilibrium potential), and g_i is the conductance or the permeability of the ion channel. E_i reflects the transmembrane ion gradient, and can be formulated using the equation:

$$E_i = \frac{R \times T}{z \times F} \times \ln \frac{[C_{in}]}{[C_{out}]}, \quad (3.4)$$

where R is the universal gas constant, T is the absolute temperature in Kelvin, z is the valency of the ion (for example, +1 for Na^+ and +2 for Ca^{2+}), F is the Faraday constant, and $[C_{in}]$ and $[C_{out}]$ are the intracellular and extracellular concentrations of the ion, respectively. The reverse potential is the potential required for the net flow of a type of ion across the membrane to be zero. When V_m equals the reverse potential, the inward and outward ion fluxes are the same, and a change of V_m on either side of the equilibrium reverses the overall direction of ion flow.

The conductance of an ion channel (g_i) changes with V_m and the time course of the AP, and can also be affected by ionic concentrations. In the Hodgkin-Huxley formulation, the time course of g_i is represented using the voltage and time

dependent behaviours of different 'gates'. For each type of ion channel, there will be a set of ordinary differential equations governing the activation, deactivation, inactivation and recovery from inactivation of the gates. Each gate has one open state and one closed state.

If we take the sodium current (I_{Na}) as an example, which is generally modelled with three activation gates and one inactivation gate, the conductance can be represented as:

$$g_{Na} = G_{Na} \times m1 \times m2 \times m3 \times h. \quad (3.5)$$

Here G_{Na} is a constant that represents the maximum conductance of the I_{Na} current, and it can be regarded as the product of the number of this type of ion channels on the cell membrane and the maximum conductance of one single ion channel of this type. The variables m1, m2 and m3 represent the open probability of the three activation gates, respectively, and h represents the open probability of the inactivation gate. Given the three activation gates are independent and identical, then the above equation can be simplified as:

$$g_{Na} = G_{Na} \times m^3 \times h. \quad (3.6)$$

The values of m and h vary between 0 (closed) and 1(open), and they are governed by ordinary differential equations using the form (using the m gate as an example):

$$\frac{dm}{dt} = \alpha(V_m) \times (1 - m) - \beta(V_m) \times m. \quad (3.7)$$

Here, α and β are voltage-dependent transition rates from closed to open, and from open to closed, respectively, whereas m and (1-m) represent open and closed probabilities of the gate, respectively. The expressions of these voltage-dependent equations can be determined using patch clamp recordings of the current.

Therefore, the full Hodgkin-Huxley equation for I_{Na} can be expressed as:

$$I_{Na} = G_{Na} \times m^3 \times h \times (V_m - E_{Na}). \quad (3.8)$$

By fitting the above formula with the patch clamp experimental data for all ionic

currents, the I_{ion} term in equation 3.1 can be computed as the sum of all the currents, and the overall behaviour of V_m can be calculated by solving a system of ordinary differential equations. For contemporary models of cardiomyocytes, additional information, such as the calcium diffusion between different intracellular compartments, needs to be integrated into the system.

3.1.2 The Markov chain formulation for ion channel behaviour

In the Hodgkin-Huxley formulation, the I_{ion} term in equation 3.1 describes the macroscopic current through the membrane. Since it was developed, the Hodgkin-Huxley formulation has inspired the improvement of cardiac models for decades (Noble *et al*., 2012). However, the gating parameters do not correspond to specific characteristics of ion channel kinetics. When Hodgkin and Huxley published their formulation of an AP, the structural properties of ion channel proteins were not yet known. With the development of electrophysiology and structural biology knowledge, it is obvious that the Hodgkin-Huxley formulation is limited in describing the specific properties of ion channel structure dynamics. A new formulation is hence needed in order to represent the specific state transitions of ion channel proteins.

Markovian models of ion channels have been developed in recent years to meet these demands. A Markov chain describes the random processes in which the probability of transition from one state to another only depends on the current state, and the history of previous states has no effect on the transition. In a Markov model of an ion channel, the probability of various kinetics states is represented by a function of time and V_m, and the full formulation of current I_i can be written in a similar form as the Hodgkin-Huxley formulation:

$$I_i = g_{i_single} \times P(O) \times N \times (V_m - E_i). \quad (3.9)$$

In this equation, g_{i_single} is the conductance of a single ion channel, P (O) is the probability for a single channel to open, N is the number of ion channels, and (V_m -E_i)

is the driving force of the current.

The probability of a single ion channel residing in its open state can be formulated depending on the structure of the protein, such as the number of transmembrane subunits. For the simplest case when the channel has only one single subunit that can be open or closed, the following equations can be used to describe the transition of states:

$$\frac{dC}{dt} = -\alpha(V_m) \times C + \beta(V_m) \times O, \tag{3.10}$$

$$\frac{dO}{dt} = \alpha \times C(V_m) - \beta(V_m) \times O, \tag{3.11}$$

where C and O are the probabilities for the subunit to be closed or open, and α and β are voltage-dependent transition rates between the two states. Additional properties, such as the transition rates of multiple subunits, can be added to the system to describe the characteristics of the ion channel kinetics.

For instance, the slow delayed rectifying K^+ current (I_{Ks}) channel contains four KCNQ1 α-subunits (H. Chen et al., 2003), and on each of the KCNQ1 subunit, there is a voltage sensor (S4 domain). To explain the activation delay of I_{Ks}, a two-stage voltage-dependent activation model was proposed and supported by experimental evidence (Silverman et al., 2003; Zagotta et al., 1994). Each of the four voltage sensors can have three states: closed, intermediate and active. Only when all four voltage sensors are active can the channel open. All possible combination states of the four voltage sensors are shown in Figure 3.1A, where α, β, γ and δ are the voltage-dependent transition rates from closed to intermediate, from intermediate to closed, from intermediate to active and from active to intermediate, respectively. There are 15 possible combinations during the whole two-state transitions, and a Markov formulation can be used to describe the process (Figure 3.1B).

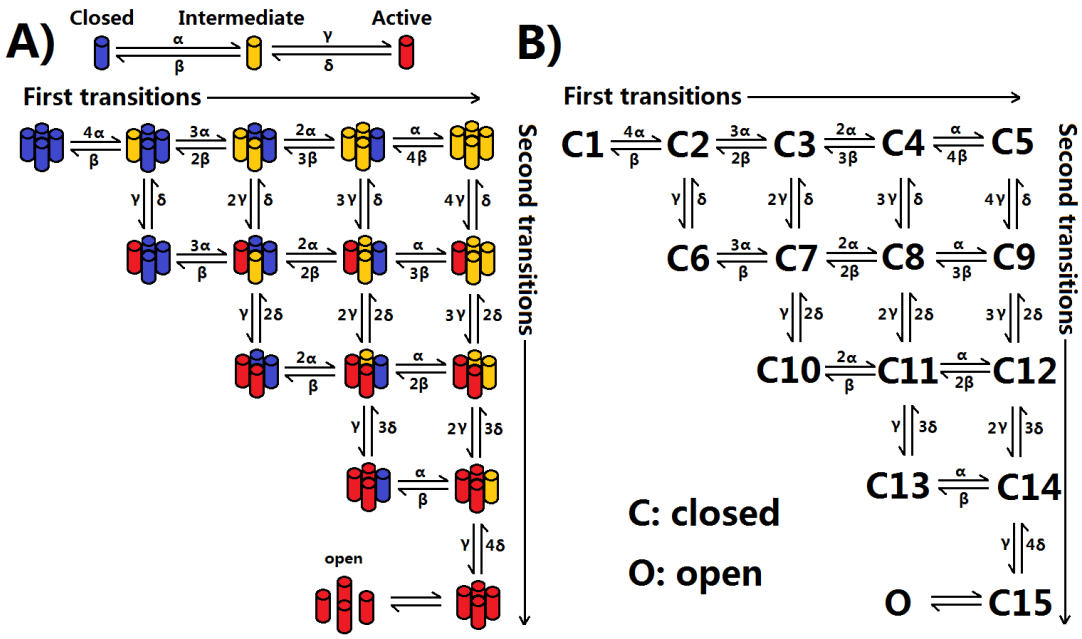


Figure 3.1: Conformation transitions of four voltage sensors in I_{Ks} channel based on the two-stage activation theory. This figure is adapted from (Rudy, 2006; Silva and Rudy, 2005). A) all possible transition states of I_{Ks} voltage sensors. B) the Markov states corresponding to all the conformation states.

3.2 Development of cardiac cellular models

The first mathematical model of a cardiac cell was published by Professor Denis Noble in 1962 (Noble, 1962). The Hodgkin & Huxley's formulation (Hodgkin and Huxley, 1952d) was modified to describe the APs of Purkinje fibres based on measurements from sheep and dog hearts. The first model of a ventricular cell was later developed in 1977 by Beeler and Reuter (Beeler and Reuter, 1977). At this stage, only a fast sodium current I_{Na}, a slower inward calcium current I_S and two outward potassium currents I_{K1} and Ix1 had been incorporated into the system, following the electrophysiological knowledge at that time.

In 1985 the DiFrancesco-Noble model of Purkinje fibres (DiFrancesco and Noble, 1985) brought ion exchangers and pumps together with intracellular calcium release from the SR into a model of cardiac cellular electrophysiology. Then in the 1990s, with the development of single-channel experimental techniques, Luo and Rudy

incorporated more recent experimental findings, further developing the ion regulation previously introduced in DiFrancesco-Noble model (Luo and Rudy, 1994a, 1994b). The L-type calcium current I_{CaL} was added to replace the slow inward current I_S.

Through their development over several decades, cardiac cell models have become highly sophisticated and have benefited from the interaction between experimental and computational investigations (Noble, 2002). Models for all the main types of cardiac myocytes have been developed, and in many cases several models of the same cell type exist (Noble, 2002). Nevertheless, most ionic currents included in these mathematical models are similar regardless of species and cell types: Na^+ currents (I_{Na}, both fast and late components), K^+ currents (I_{to}, I_{Kr}, I_{Ks}, I_{K1}), L-type Ca^{2+} current (I_{CaL}), and in the later models a Cl^- current is also considered (Carro et al., 2011; Grandi et al., 2010). The contributions of ion pumps and exchangers such as the Na^+/K^- pump and the Na^+/Ca^{2+} exchanger, as well as ionic fluxes between different intracellular subspaces, are also included in these models.

3.3 Latest human ventricular cell models

The first mathematical model of a human ventricular cell was published by (Priebe and Beuckelmann, 1998). Since then, several models for human ventricular cardiomyocytes have been developed (Bernus et al., 2002; Bueno-Orovio et al., 2008; Fink et al., 2008; Iyer et al., 2004; Seemann et al., 2003; ten Tusscher et al., 2004; Ten Tusscher and Panfilov, 2006; ten Tusscher and Panfilov, 2006).

Four main biophysically detailed mathematical models have been developed for human ventricular cellular electrophysiology in the past decade: the ten Tusscher-Panfilov model (2006), the Grandi *et al.* model (2010), the Carro *et al.* model (2011) and the O'Hara *et al.* model (2011) (Carro et al., 2011; Grandi et al.,

2010; O'Hara et al., 2011; ten Tusscher and Panfilov, 2006).

Ten Tusscher and Panfilov developed a new version of their previous human ventricular model (ten Tusscher *et al*., 2004) based on newer experimental restitution data. In this model, they incorporated a more detailed description of intracellular calcium cycling by considering the calcium induced calcium release (CICR) of the SR, used a Markov model to mimic the activity of RyRs, applied both fast and slow voltage inactivation processes to the description of the L-type calcium current, and introduced a modified formulation of their I_{Ks} current.

In 2010, Grandi *et al.* developed another human ventricular model following on from the ten Tusscher model (Grandi *et al*., 2010). This model was based on the framework of their rabbit ventricular myocyte model (Shannon *et al*., 2004), adapted to replicate new experimental data of potassium currents, APD restitution and intracellular calcium and sodium rate dependence from human ventricular myocytes. The improvements in this model include better calcium handling and a better model performance under blockades of several potassium currents.

Carro *et al.* introduced in 2011 further improvements in the Grandi *et al*. model (Carro et al., 2011; Grandi et al., 2010). Two ionic currents (I_{CaL} and I_{K1}) were considerably reformulated and a few other currents were also optimised. S1S2 restitution and APD rate adaptation dynamics were significantly improved in this new model, as well as model performance under hyperkalemic conditions.

Finally the O'Hara-Rudy *et al*. model was developed in 2011 (O'Hara *et al*., 2011). Electrophysiological data and additional mRNA measurements from over 100 human hearts obtained in Professor Varró's laboratory in Szeged were used in the model validation over the entire physiological frequency range. The accuracy of APD rate dependence in the O'Hara-Rudy model is substantially increased than in the Ten Tusscher or Grandi *et al.* models. Some major currents such as I_{CaL}, I_{to}, and I_{NaCa}

were improved by incorporating new experimental data. A late Na^+ current was also incorporated in this model, and therefore the O'Hara *et al.* model is so far the most comprehensive and thoroughly validated model of human ventricular electrophysiology.

3.4 Comparison between animal and human ventricular cell models

As discussed in Chapter 2, there are significant inter-species variations between animal and human cardiac electrophysiology. Therefore the computational cardiac models developed based on human and animal experimental data show substantial differences. As an example, here we use a recent human model of ventricular cell electrophysiology (O'Hara *et al*., 2011) and a canine ventricular cell model (Decker *et al*., 2009) developed by the same group to compare the similarity and difference between human and canine ventricular cell models.

3.4.1 General structure

In the human non-diseased model developed by O'Hara *et al*. (short for ORd model), four major compartments were included: 1) bulk myoplasm (MYO), 2) junctional sarcoplasmic reticulum (JSR), 3) network sarcoplasmic reticulum (NSR), and 4) subspace (SS), representing the space near the T-tubules (Figure 3.2A) (O'Hara *et al*., 2011). 15 ion channels or pumps/exchangers were included in the ORd model, and the additional targets of Ca^{2+}/Calmodulin-dependent protein kinese II (CaMKII) were incorporated based on new findings.

The canine non-diseased canine model published by Decker *et al.* (Decker *et al*., 2009) included some updated formulation of I_{to}, I_{Ks}, I_{CaL} and I_{NaK} based on Hund *et al.* (Hund and Rudy, 2004) (short for HRd model, Figure 3.2B). The Decker *et al.*

model also contains 1) myoplasm, 2) junctional sarcoplasmic reticulum (JSR), 3) network sarcoplasmic reticulum (NSR), and 4) subspace (SS). 16 different ionic currents were described in the HRD model, and the CaMKII system was also included.

3.4.2 Initial conditions and basic settings

Most of the basic initial concentrations and cellular settings for Na^+ and K^+ currents were found to be similar in the human (ORd) and canine (HRd) ventricular cell AP models (Table 3.1), but significant Ca^{2+} concentration differences were found between the two models. The initial intracellular Ca^{2+} concentration in the canine model is almost 100 times higher than in the human model.

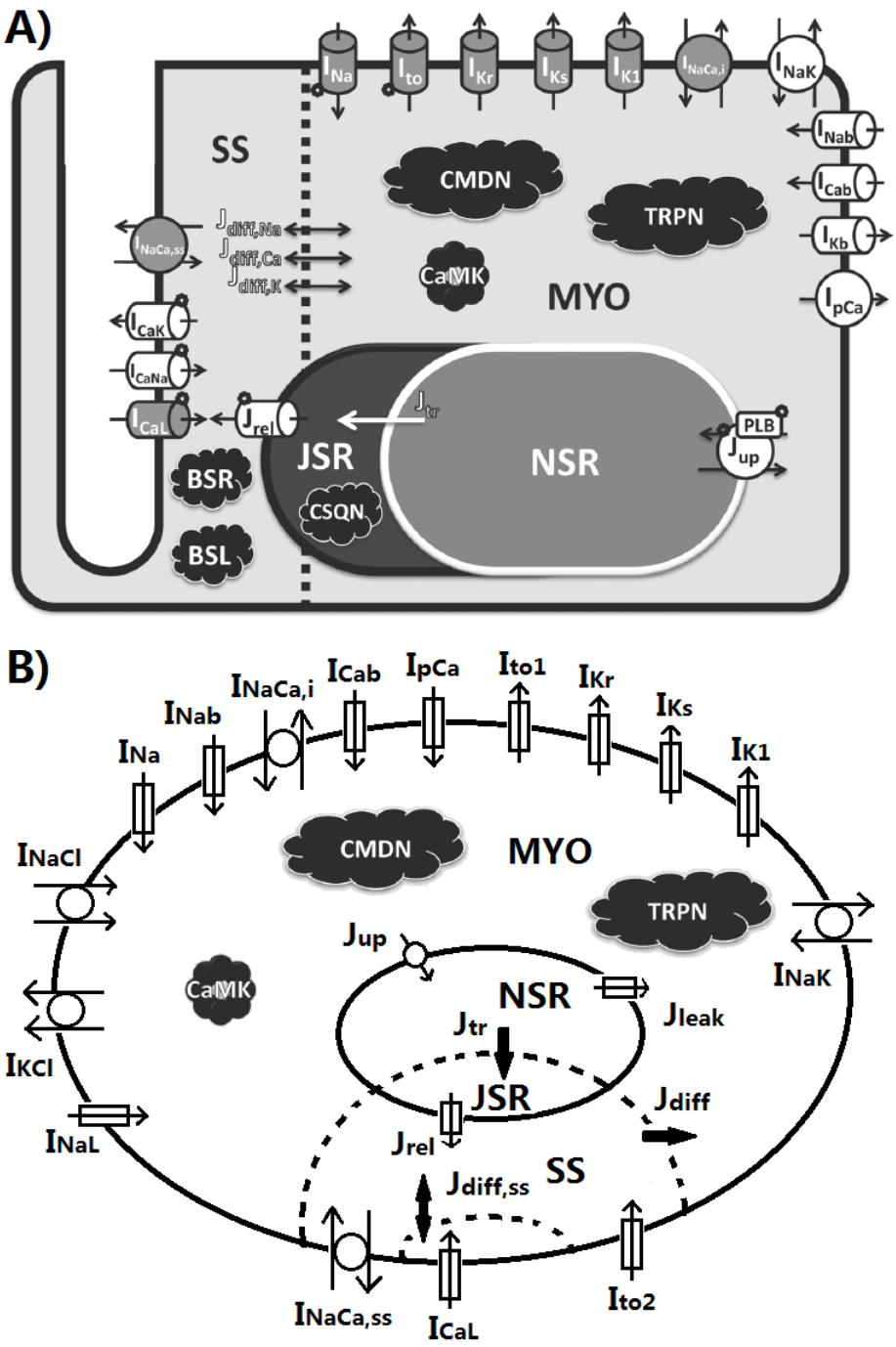


Figure 3.2: Schematic diagram of human and canine models. A) Schematic diagram of human undiseased model from (O'Hara *et al*., 2011). B) Schematic diagram of canine model adapted from (Decker and Rudy, 2010).

3.4.3 Major differences in currents

The most significant difference between both models lies in their specific description of transmembrane ionic currents and intracellular Ca^{2+} dynamics. The biggest differences between the two models include an absence of Cl^- current in the healthy

ORd human model, which also incorporates some background ionic currents through calcium channels compared to the HRd canine model (Table 3.2). The magnitude of ion channel conductances and permeabilities in canine and human models are also usually distinct (Table 3.3). Another different aspect is that rather than just containing voltage dependent inactivation, the ORd human model also includes calcium dependent inactivation for I_{CaL}.

	Na_o	Na_i	Na_ss	K_o	K_i	K_ss	Cl_o	Cl_i	Cl_ss
HRd	140	6.935	6.93	5.4	145	~	**100**	**20.26**	**20.26**
ORd	140	7	7	5.4	145	**145**	~	~	~

	Ca_o	Ca_i	Ca_ss	Ca_JSR	Ca_NSR	Ca_ssCaL
HRd	1.8	**0.0134**	**0.024**	**6.994**	**1.159**	**0.025**
ORd	1.8	**1.0e-4**	**1.0e-4**	**1.2**	**1.2**	~

Table 3.1: Parameters of the two models (Na^+, K^+, Cl^- Ca^{2+} (mM))
(Differences are highlighted in bold, and ~ means data not available)

	INa	INaL	INaK	INab	INaCa_i	INaCa_ss	ICaNa
HRd	Y	Y	Y	Y	Y	Y	**N**
ORd	Y	Y	Y	Y	Y	Y	**Y**

	ICaL	ICab	IpCa	INaCa_i	INaCa_ss	Jrel	Jup	Jtr
HRd	Y	Y	Y	Y	Y	Y	Y	Y
ORd	Y	Y	Y	Y	Y	Y	Y	Y

	IKr	IKs	IK1	Ito1	INaK	IKp	IKb	ICaK	Ito2	IClb
HRd	Y	Y	Y	Y	Y	**Y**	**N**	**N**	**Y**	**Y**
ORd	Y	Y	Y	Y	Y	**N**	**Y**	**Y**	**N**	**N**

Table 3.2: Currents included in the two models
(Y: included; N: not included, differences are highlighted in bold)

	GNa (ms/μF)	GNaL (ms/μF)	PNab (cm/s)	PCa (cm/s)	Pcab (ms/μF)
HRd	9.075	6.5e-3	3.2e-9	1.5552e-4	19.95e-8
ORd	75	7.5e-3	0.375e-9	1e-4	2.5e-8
	GKr (ms/μF)	GKs (ms/μF)	GK1 (ms/μF)	GKb (ms/μF)	GKp (ms/μF)
HRd	0.0138542	0.0826	0.5	~	2.76e-3
ORd	0.046	0.0034	0.1908	0.003	~

	GpCa (ms/μF)	Gto1 (ms/μF)	KmCaMK (mM)	KmPCa (mM)	GClb (ms/μF)	PCl (cm/s)	PNaK (μA/μF)	GNaCa (μA/μF)
HRd	0.0575	0.4975	0.15	5e-4	2.25e-4	9e-7	1.4	~
ORd	0.0005	0.02	0.15	5e-4	~	~	30	0.0008

Table 3.3: Ion channel conductances and permeabilities
(Differences are highlighted in bold, and ~ means data not available)

From the above example, it is clear that despite the similar structure in human and animal cardiac models, the inter-species variations in cardiac electrophysiology can lead to distinct current parameter settings in each species. Therefore, the development of human cardiac cell models enables more accurate simulations of human cardiac conditions than animal models.

3.5 Modelling of diseased cardiomyocytes

The first big step in the electrophysiological modelling of cardiomyocytes is to reproduce the normal APs observed in undiseased cells. However, one of the biggest advantages of cardiac modelling is to simulate the electrophysiological properties in diseased conditions. By investigating the complex interplay of different ionic currents, potential anti-arrhythmic strategies can be proposed and tested.

Genetic defects in ion channel proteins can be incorporated into electrophysiological modelling through the change of equation parameters and/or formulation structure. The Hodgkin-Huxley formulation can be used to fit the experimental data of ion

channel mutations as in (Hasegawa *et al*., 2014), and reproduce the phenotype of the mutated channels. Although the traditional Hodgkin-Huxley formulation is very powerful in modelling the macroscopic current behaviour, it is sometimes insufficient in reproducing the discrete states of the mutated channels, and Markov models can be very useful in these cases.

For example, Clancy and Rudy simulated the effects of ΔKPQ mutation in the SCN5a gene that affected the normal function of the sodium channel (Clancy and Rudy, 1999). The original Markovian chain for the wild type channel was reformulated to produce faster activation and the increased rate of recovery from inactivation. The remodelling of the sodium channel can reproduce the dispersed channel re-opening and a late component of I_{Na} (Clancy and Rudy, 1999). After integrating the mutated I_{Na} channel into a ventricular cell model, the mutation model can reproduce longer APD and the development of early after depolarisation observed in experiments. Therefore, appropriate modifications of ion channel formulations allow for the investigation of arrhythmogenic consequences of ion channel genetic mutations.

Apart from ion channel genetic mutations, cardiac modelling can also be used to simulate other pathological conditions, such as the behaviour of the epicardial border zone after myocardial infarction. Based on experimental data from multiple sources, Decker *et al*. developed a model for the canine epicardial border zone. By introducing the remodelling in current conductances and steady state inactivation, the new model predicted the abnormal prolongation of APD and the potential conduction block at fast pacing rates (Decker and Rudy, 2010).

Therefore, mathematical modelling can be a very useful tool in the investigation of pathological cardiac conditions, and can also facilitate the research of anti-arrhythmic strategies.

3.6 Modelling of pharmacological drug effects

Many drugs fail in clinical trials due to their serious side effects on cardiac electrophysiological function (Brennan *et al*., 2009). The adverse effects from diverse pharmacological drug groups and their interaction with cardiac electrophysiology can increase the risk of potentially life threatening arrhythmias (Brennan *et al*., 2009). Computational modelling of cardiac electrophysiology can provide additional insights into the exploration of proarrhythmic mechanisms, and can therefore function as a powerful tool for the investigation of drug effects in cardiac electrophysiology.

There are several approaches to model the interaction between drug molecules and ionic channels, including simple pore block, voltage and state-dependent binding and allosteric effect. Although voltage and state-dependent binding and allosteric effect involve more detailed dose-dependent electrophysiological and conformational changes, more experimental data is needed to parameterize the complex Markov states. On the other hand, the simple pore block that requires less data is more commonly used in simulation studies.

During a simple pore block, the magnitude of ionic current is restricted by the continuous block of the drug to the ion channel (Brennan *et al*., 2009). Given the dose–response relationship between a drug ligand and its ion channel receptor, the effect of the drug block can be modeled by simply applying scaling factors to adjust the overall current density as in (Britton et al., 2013; O'Hara et al., 2011; Passini et al., n.d.).

3.7 Modelling of variability in cardiac electrophysiology

Variability and uncertainty exist in almost all biological processes. In cardiac

electrophysiology, variability in the physiological activity of myocytes and interactions between different levels of cardiac tissue can all lead to the generation of various physiological conditions. Cardiac alternans, for example, is a special type of beat-to-beat intra-subject cardiac variability. Inter-subject variability, such as the divergent responses of patients to a same type of clinical intervention, is also a very important aspect of cardiac variability. Studies of inter-subject and intra-subject variability are therefore necessary in order to understand the generation of pathological conditions and to test the effects of pharmacological treatments.

Mathematical modelling may represent a very powerful tool in the study of cardiac variability, since it allows dissecting mechanisms arising through the complex interactions between various ionic currents by introducing variability to multiple model parameters simultaneously. Over the last years, a number of *in silico* studies have been conducted to explore the effects of cardiac variability.

3.7.1 Cell-specific modelling

One technique used in the modelling of cardiac variability is cell-specific modelling. The model parameters were varied to fit the transmembrane potential during APs for individual cells (Davies *et al*., 2012). A genetic algorithm can be applied in the cell-specific fitting to generate a set of parameter for a single cardiomyocyte (Groenendaal et al., 2015; Syed et al., 2005). In this genetic algorithm, an initial population of parameter sets is randomly generated based on the original values. The optimization process proceeds in generations: by crossover (parameter swapping), mutation (introducing variation) and selection (discarding the ones with poor performance), the best parameter set with minimum errors can be found.

To accurately reproduce the electrophysiological behaviour of one cardiomyocyte, complex electrophysiological experimental protocols are usually needed to

determine the parameter set that is the best fit. However, these complex protocols are not commonly used in most electrophysiology laboratories. In addition, due to the complexity of experiments and the fragility of the cells, usually only one type of electrophysiological data, such as the AP traces, can be generated and used for the fitting.

3.7.2 Sensitivity analysis

Sensitivity analysis is one commonly used method to investigate the effect of variability in models. Romero *et al.* explored the effect of introducing ±15% and ±30% modifications to one key model parameter at a time in the ten Tusscher model of human ventricular electrophysiology (Romero *et al*., 2009). Sensitivity analysis was conducted to quantify the contribution of each key parameter to APD, AP triangulation, AP rate dependence, and intracellular ion concentrations. In a recent work of Sobie *et al.*, they performed a multivariable sensitivity analysis by varying multiple parameters at the same time. Partial least squares regression was applied to quantify the relationship between the change in a single parameter to some model simulation outputs such as APD, resting membrane potential and peak value of transmembrane potential. The overall variations of these outputs were usually the combination results of multiple parameter variances (Cummins et al., 2014; Devenyi and Sobie, 2015; Sarkar et al., 2012; Sobie, 2009; Sobie and Sarkar, 2011; Yang and Clancy, 2012).

Similar methods can also be applied to study diseased conditions. Walmsley *et al.* created two populations of human cardiac models based on the O'Hara *et al*. human ventricular model, representing undiseased cells and cells in failing hearts (Walmsley *et al*., 2013). Within the two populations, models share the same equations representing identical ionic kinetics but different combination of multiple conductance parameters. Experimental differences at ion channel protein expression

between failing and non-failing hearts were introduced into the two populations of models by increasing or decreasing specific conductance parameter values. Linear regression analysis was also performed to reveal the contribution of individual currents to APD properties and alternans generation in normal *versus* failing hearts.

Although the sensitivity analysis approach can introduce variability in many ionic currents and can be a very useful tool to study the complex interaction between different components of the myocytes, the variation ranges of the parameters are usually relatively narrow due to the lack of a reasonable variation range supported by experiments.

3.7.3 Experimentally-calibrated population of models

A recently developed strategy for studying cardiac variability is the use of experimentally-calibrated populations of models. Within the population, models share the same equations representing identical ionic current kinetics but different conductance values (Zhou *et al*., 2013). As a further development of the sensitivity analysis, a population of models can be generated based on the random variation and combination of multiple current conductances, and then calibrated with experimental data to select the models whose behaviours are within physiological range. This new step of calibration allows for a larger initial variation of the parameters, and therefore the experimentally-calibrated population of models can be used to investigate boarder physiological ranges. In neuroscience studies, similar approaches have previously been used to select a population of neuronal models that are generated using random parameters and are able to reproduce the electrophysiological response of experiments.

Experimentally-calibrated population of models in cardiac research was proposed by Britton *et al*. In this study, a population of rabbit Purkinje cells was generated and

calibrated with experimental recordings. 213 out of 10000 models were accepted after the calibration process and most of the parameter values in these accepted models covered a wide range: in some cases up to ±100% of the original values. The calibrated population of models also quantitatively predicted and explained the APD prolongation caused by pharmacological potassium channel blockage (Britton *et al*., 2013).

Comparing with sensitivity analysis and cell-specific modelling, the experimentally-calibrated population of models approach can generate a group of models mimicking the output of a population of myocytes under routine experimental protocols. No special electrophysiological protocols are needed to generate suitable data for model fitting.

The generation and analysis of an experimentally-calibrated population of models can be divided into four main steps: 1) selection of the original model based on the research question; 2) parameter sampling to introduce variation to the original model; 3) simulation and calibration of the population of models; and 4) analysis of the experimentally-calibrated population of models.

3.7.3.1 Selection of the original model

The selection of the original baseline model should be based on the research question and the underlying hypothesis. The complexity of the models should be considered, and if several models of a same type of cell exist, the major differences between these models should be compared before determining the most suitable model for the research question.

For example, and as aforementioned, several models for human ventricle or ventricular cells have been developed since 1998 (Bernus et al., 2002; Bueno-Orovio et al., 2008; Carro et al., 2011; Fink et al., 2008; Grandi et al., 2010; Iyer et al., 2004; Marder and Taylor, 2011; O'Hara et al., 2011; Priebe and Beuckelmann, 1998;

Seemann et al., 2003; ten Tusscher et al., 2004; Ten Tusscher and Panfilov, 2006; ten Tusscher and Panfilov, 2006). The currents or framework in some models were adopted based on animal models due to the lack of human ionic current data (Grandi et al., 2010; Priebe and Beuckelmann, 1998), and some of the currents in the Iyer *et al.* model were based on data from recombinant human ion channels (Iyer *et al*., 2004). Some of the models are relatively simple and suitable for tissue simulation (Bueno-Orovio et al., 2008; ten Tusscher et al., 2004), while some other models contain more recent electrophysiological data from human cardiomyocytes and are more suitable for the study of ionic mechanisms at cellular level (O'Hara *et al*., 2011).

3.7.3.2 Parameter sampling

To extend the original model into an initial population of models, the standard parameters need to be varied based on a sampling method. There are many different approaches for sampling parameters. Monte Carlo (MC) methods are one of the most popular sampling algorithms used in computational studies. A MC based study performs multiple simulations using random or pseudo-random numbers to sample from a probability distribution (Marino *et al*., 2008). For each parameter, sampling is based on a probability density function (PDF), such as a uniform or normal distribution, depending on a prior knowledge. If a value of a parameter is expected or observed from experiments beforehand, a normal distribution will be a good choice. Otherwise, a uniform distribution would be a natural choice.

Latin hypercube sampling (LHS) is a type of MC based sampling method and was introduced by Mckay *et al*. in 1979 (McKay *et al*., 1979). LHS allows an efficient and un-biased generation of parameter sets over large numbers of parameters (McKay *et al*., 1979). In those cases where the simulation variations of many parameters are considered, the calculation for every possible combination of parameters would be computationally unfeasible. The LHS method assumes that for each parameter, the sampling processes are independent. For example, if the number

of parameters that are considered is K, and the number of samples that will be generated is N, the sampling range of each parameter is divided into N regions and only one value is selected within each region. The N values of a parameter are paired randomly with the N values of another parameter, and in this way, a matrix size of N*K is generated as a population of parameter sets. Thus, LHS does not depend on the dimension of the parameter space. This LHS sampling method has the advantages of sampling across the whole parameter range with the minimum computational cost, and yielding a number of samples being independent of the number of input parameters. However, the disadvantage of LHS is that the parameter space is not sampled completely for a given resolution.

3.7.3.3 Simulation and calibration of the initial population of models

Once the parameter sets for the initial population of models are generated, the next step is to simulate the population of models using these new parameter sets. The simulation protocols are determined by the type of experimental data that is going to be used to calibrate the models. For example, if patch clamp data is going to be used in the calibration, the candidate models should be simulated using the same experimental protocol: identical testing potential steps, values and durations should be applied to the models.

Then the experimental data can be used to select the models whose simulation outputs are within the physiological range. In this process, the distribution of the experimental data should be considered, which means that the extreme values in the experimental raw data should be excluded and the physiological threshold should be determined based on the behaviours of the majority data points. If multiple calibration filters are available, the calibrated population of models can be a better estimation of the research target.

3.7.3.4 Analysis of the calibrated population of models

The electrophysiological characteristics of the experimentally-calibrated population

of models can then be analysed. One way to understand the dynamics of the population of models is to visualise the distribution of the accepted parameters. Scatter plots can be used to analyse the correlation between pairs of parameters, and histograms are useful to visualise the distribution of the parameters across the whole sampling range. If multiple parameters are varied at the same time, the multi-dimensional visualisation can be very difficult, and statistical analysis can prove useful in the investigations. For example, regression analysis and partial correlation analysis have been previously used in the analysis of relationships between model parameters and AP biomarkers (Britton et al., 2013; Walmsley et al., 2013).

Another way to understand the behaviour of the calibrated models is to analyse the standard biomarkers of the cardiac AP. The standard AP biomarkers that are used throughout this thesis are as follows: APDs (at three repolarisation levels: APD_{30}, APD_{80}, APD_{90}), APD_{tri} (triangulation), CaTD (calcium transient duration), UPD (upstroke duration), peak upstroke voltage (V_{max}), RMP (resting membrane potential), APA (action potential amplitude), CaT_{max} (systolic Ca^{2+} level), CaT_{min} (diastolic Ca^{2+} level) and DI (diastolic interval). The detailed calculation approaches for the biomarkers are included in Chapter 5.

3.8 Summary

In this chapter, we began by describing the basic formulations in cardiomyocyte electrophysiological modelling. Then we briefly introduced the development of cardiac cellular models and compared the latest four human ventricular cell models. A canine ventricular and a latest human ventricular cell model were then compared to illustrate the inter-species similarities and differences in modelling. Following this we concisely reviewed the modeling approach under diseased conditions and the effects of drug block. The different modeling techniques to capture cardiac

variability were then described and discussed.

To conclude, we have demonstrated in this chapter that since the publication of the first mathematical model of a cardiac cell five decades ago, considerable research have contributed to the development of cardiac models. Now the cardiac models can simulate and predict many phenomena, including diseased conditions, drug effects and cardiac variability observed in experiments.

Chapter 4

Post-myocardial infarction ionic remodelling and hERG block prolong the action potential and facilitate alternans in a human ventricular model of the epicardial border zone

4.1 Introduction

As introduced in chapter 1.1, SCD is the most common cause of death in the UK, where over 100,000 people die from SCD every year. Around 80% of these patients suffer from coronary heart disease, such as the narrowing or blockage of the coronary arteries. The lack of oxygen and nutrients in cardiac cells caused by the blockage can lead to cardiac tissue infarction that refers to the tissue death (necrosis) in the heart. Therefore, the balance and synchronization between cardiac cells is destroyed, leading to physiological alternations to the ionic currents in the surviving tissues. A spatio-temporal dispersion also arises in cardiac conductivity and refractoriness, which may trigger arrhythmias and SCD. Infarction and arrhythmic risk have been investigated in a number of studies, but most of these have been conducted in animals rather than in human; therefore, the mechanisms of human infarction and arrhythmic risk are still not fully understood, and the translation from research to clinical conditions is compromised.

Both electrical therapy such as implantation of internal cardioverter defibrillators

(ICDs) and pharmacological therapy are applied in the clinic against arrhythmias (Aziz *et al*., 2010). ICDs are often implanted in patients whose hearts exhibit compromised contraction (low left ventricular ejection fraction (LVEF)); however, a large number of patients with a higher LVEF are also reported as being victims of SCD. Anti-arrhythmic drugs are more commonly used in the clinical treatment of atrial and ventricular arrhythmias, sometimes combined with ICD (Beadle et al., 2010; Davies et al., 2012). The efficacy of most of these drugs is limited because of their potential lethal cardiotoxicity effects (Fletcher et al., 2011; Valentin et al., 2009). For instance, Class III drugs such as flecainide and propafenone can lead to increased mortality in patients with myocardial infarction (Echt *et al*., 1991). These undesirable drug side effects that cause dangerous changes in heart rhythm are one of the major factors leading to the withdrawal of otherwise promising candidates. Unfortunately, many of the toxic drug side effects fail to show up in animal tests due to inter-species differences in physiology. Early clinical trials in human are normally conducted on a limited number of candidates for limited periods and may not be able to detect adverse effects. Therefore, using computational human models may largely improve the efficiency of evaluating new drugs.

Our goal is to develop a mathematical model of the EBZ of the infarcted human heart for drug safety and efficacy evaluation. The EBZ is a thin rim of surviving epicardial tissue that surrounds the infarcted region. The electrophysiological characteristics of this region are different from those of the NZ, and this dispersion in tissue electrophysiology may lead to the initiation and maintenance of potentially lethal arrhythmias (Arevalo et al., 2013; El-Sherif et al., 1977; Estner et al., 2011). A number of studies have characterized the remodelling of ion channels in the EBZ 3-5 days postinfarction in canine experiments and models (Aggarwal et al., 1997; Aggarwal and Boyden, 1995; Baba et al., 2005; Decker and Rudy, 2010; Dun et al., 2004; Dun and Boyden, 2005; Jiang et al., 2000; Lue and Boyden, 1992; Pu and Boyden, 1997). Due to the similar AP morphology and similar distribution pattern of ionic current densities between human and canine ventricular myocardium (Szabó et

al., 2005; Szentadrassy et al., 2005), our hypothesis here is that the EBZ remodelling observed in canine can be extrapolated to mimic the similar phenomena in human ventricles. Our aim is to depict the main features of EBZ by applying these changes to a mathematical description of the human NZ electrophysiology. We aim to evaluate the key features reported in EBZ physiology studies, such as the prolongation of APs and the alternation of refractoriness. We also aim to evaluate the effect of anti-arrhythmic drugs in post myocardial infarction tissue.

4.2 Methods

4.2.1 Development of an electrophysiological model for human EBZ

The non-diseased versions of the human (ORd) and canine (HRd) epicardial AP models were compared as an initial step of our investigations. Details of the comparison results are included in Chapter 3.4. As shown in Figure 4.1, our goal is to introduce the MI-induced electrical remodelling of several important ionic currents in the EBZ to the healthy human model, in a similar way in which a healthy canine model has been previously modified into an EBZ canine model (Decker et al., 2009; Decker and Rudy, 2010).

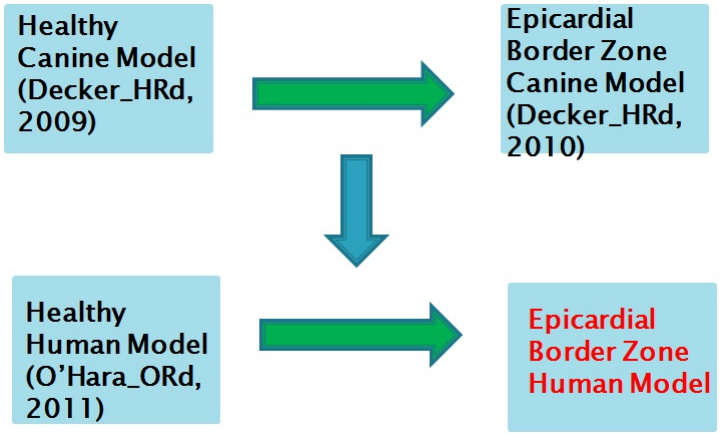


Figure 4.1: Transfer of EBZ electrical remodelling from canine to human AP model.

The healthy HRd canine model was modified by Decker *et al.* to incorporate the electrical remodelling of the EBZ (Aggarwal et al., 1997; Aggarwal and Boyden, 1995; Jiang et al., 2000; Lue and Boyden, 1992; Maltsev et al., 2008a, 2008b, 1998; Maltsev and Undrovinas, 2006; Pinto and Boyden, 1999; Zaza et al., 2008; Zygmunt et al., 2001). In this process, they decreased the density of the fast Na^+ current I_{Na}, L-type Ca^{2+} current I_{CaL}, K^+ currents I_{K1}, I_{Kr}, I_{Ks}, I_{to1} and Cl^- (I_{to2}) current I_{to2} by reducing their conductances and permeabilities based on reported canine EBZ data, as shown in Table 4.1 (Decker and Rudy, 2010). They also shifted the I_{Na} steady state inactication (9mv) (Lue and Boyden, 1992), introduced a rightward shift in the I-V relationship for I_{CaL} (Jiang *et al*., 2000), and accelerated the voltage dependent I_{CaL} inactivation and I_{Kr} activation (Aggarwal and Boyden, 1995; Jiang et al., 2000).

INa	GNa (ms/μF)	Voltage shift (mV)
NZ	9.075	2
EBZ	7.71375	-7

ICaL	PCa (cm/s)	ACTss shift (mV)	τ VDIss (ms)
NZ	1.5552e-4	13.56	30.553
EBZ	1.187e-4	17.5	15

IKr	GKr (ms/μF)	τXr (/(ms*mV))
NZ	0.0138542	0.0006
EBZ	0.009698	0.001

IKs	GKs (ms/μF)	IK1	GK1 (ms/μF)
NZ	0.0826	NZ	0.5
EBZ	0.01652	EBZ	0.15

Ito1	Gto1 (ms/μF)	Ito2	PCl (cm/s)
NZ	0.4975	NZ	9e-7
EBZ	0.04975	EBZ	7.767e-7

Table 4.1: Modifications from healthy canine model to EBZ canine model.

(Voltage shift: relative shift in I_{Na} steady state inactivation;

ACTss shift: Shift in I_{CaL} activation parameter;

τVDIss: Minimal I_{CaL} inactivation time constant parameter;

τXr: I_{Kr} activation time constant parameter)

Based on these modifications in the canine EBZ model, two different versions of the human EBZ were generated to isolate the effects of reduced ion-channel conductances/ permeabilities from those arising from distinct activation/inactivation current kinetics. In the first version of the human EBZ, we introduced the same ratio of reduction in all of the above mentioned conductances and permeabilities in the ORd human model (Table 4.2), except for I_{to2} which is not included in the undiseased human epicardial model. After this, a second version of the human EBZ model was generated, also including the aforementioned changes in current kinetics (Table 4.3). Since the formulation of time constants in the two models are different, instead of using the same parameters than in the canine EBZ model, we modified their overall value by multiplying by the corresponding experimentally reported acceleration ratios for I_{CaL} and I_{Kr} kinetics (Aggarwal and Boyden, 1995; Jiang et al., 2000). Introducing the -9 mV shift in I_{Na} inactivation in the canine Decker *et al.* model brings its voltage of I_{Na} half inactivation from -64.5 mV (NZ) to -73.53 mV (EBZ). However, the voltage of I_{Na} half inactivation in the human O'Hara *et al.* model is -82.9 mV (NZ), which is quite close to the model's resting membrane potential (-87.8 mV). For this reason, we decided to only apply a -4 mV shift in I_{Na} inactivation (hence shifted to -86.9 mV), to avoid an almost complete inactivation of I_{Na} at resting potentials in the EBZ version of the human model.

	INa	ICaL	IK1	IKr	IKs	Ito1
Original Ratio	7.71375/ 9.075	1.187/ 1.5552	0.15/0.5	0.009698/ 0.138542	0.01652/ 0.0826	0.04975 /0.4975

Table 4.2: Modifications to the permeabilities and conductances in the human EBZ model.
(Used in version 1 and 2)

	Voltage shift	ACTss shift	ICaL time constant change	IKr time constant change
Shift Value or Change Ratio	-4 mv	3.94 mv	0.76(fast), 0.65(slow)	0.6

Table 4.3: Modifications to the relative shifts and time constants in the human EBZ model.
(Used in version 2 only)

4.2.2 Sensitivity analysis

Sensitivity analysis was also considered in order to account for possible inter-species differences in EBZ remodelling. For both two versions of the human EBZ models, all the remodelling ratios were varied between ± 20% of their default values at the same time.

4.2.3 Simulation protocols

Two different stimulation protocols were used to investigate the rate dependence characteristics of the two human EBZ models. The first protocol was steady state rate dependence: for each pacing cycle length (CL), pacing was performed until the cell reached steady state (300 beats).

The second protocol investigated was S1S2 restitution: a single cell is paced at a long cycle length (S1=1000 ms) for 300 beats until reaching steady state, then introducing an extra stimulus at a different coupling interval (S2 cycle lengths).

4.2.4 Model implementation and data analysis

Human EBZ models, stimulation protocols and data analysis were implemented using the MATLAB programming language. APD was calculated as the difference between repolarisation and activation times. Activation time was computed as the time of maximum transmembrane upstroke velocity, whereas repolarisation was estimated as the time that the transmembrane voltage repolarized to 90% of the AP amplitude (APD_{90}). For S1S2 restitution, APD was calculated at 90% repolarisation for the S2 beats, and a restitution curve was generated by plotting APD_{90} against diastolic interval (DI) (where $DI=CL-APD_{90}$).

4.3 Results

4.3.1 Action potentials in canine EBZ models

Figure 4.2A shows steady-state APs for the normal (NZ) and EBZ in the canine HRd model. As previously reported, the EBZ AP showed a lack of phase I notch and APD prolongation when compared to the NZ. In terms of the individual currents underlying the canine EBZ model, there was a reduction of I_{Na}, I_{CaL}, I_{to1} and I_{to2} magnitude. I_{K1} and I_{Ks} were also reduced and shifted to the AP end. Some of these phenomena were more obvious at fast pacing rate (CL=300ms) (Figure 4.2B). The S1S2 restitution curves in Figure 2C showed that the APD_{90} of the EBZ model was considerably longer than in the NZ model for all the S2 CLs considered. At short diastolic intervals APD restitution in the EBZ model also remained relatively constant instead of monotonically decreasing when compared to the NZ (Figure 4.2C). We also found that at very fast pacing rate (CL=250ms), the canine EBZ model showed a beat-to-beat alternation of long and short APDs (Figure 4.2D).

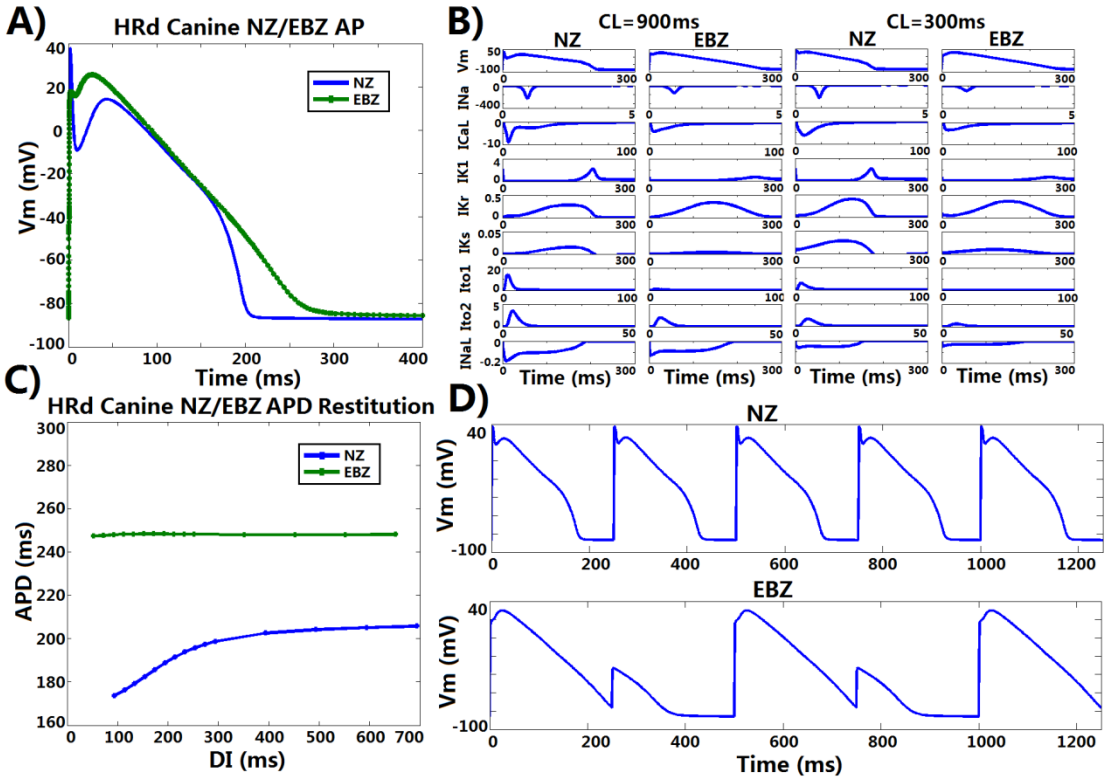


Figure 4.2: Action potential, individual currents and S1S2 restitution curve of the canine ventricular cell model. A) Steady state AP traces for CL=1000ms, Ko=5.4mM; B) Individual currents (μA/μF) for the canine EBZ model; C) S1S2 restitution of the canine EBZ model (S1=1000ms); D) Alternans of canine EBZ steady- state APs at CL=250ms.

4.3.2 Action potentials in human EBZ models

As detailed in Methods, two versions of the human EBZ model were generated by mimicking the modifications in the canine EBZ. In version 1, we only included modifications to the conductances/permeabilities of I_{Na}, I_{CaL}, I_{Kr}, I_{K1}, I_{Ks} and I_{to1}. In version 2, we also introduced the relative shift to I_{Na} voltage dependent currents inactivation observed in experiments (Lue and Boyden, 1992), a faster voltage dependent inactivation of I_{CaL} (Aggarwal and Boyden, 1995), a rightward shift in I_{CaL} I-V relationship and a faster I_{Kr} activation (Jiang *et al*., 2000).

Figure 4.3A showed the steady-state AP morphology of both versions of the single cell human EBZ models and the NZ model. APs of EBZ were markedly longer

compared to NZ, also showing a lack of phase I notch in both cases (Figure 4.3A). However, opposed to the canine model, AP amplitudes remained practically unaffected by the effects of EBZ remodelling, probably due to different relative current densities between the canine and the human model.

In the first version of the human EBZ model, the magnitude of I_{Na}, I_{CaL}, I_{K1}, I_{Ks} and I_{to1} are reduced, in agreement with the canine EBZ model (Figure 4.3B). For the second version of the human EBZ model, most currents displayed similar dynamics than in version 1 with the exception of I_{CaL} (Figure 4.3B). At long CLs, the I_{CaL} current in EBZ model version 2 is larger than in the NZ model, as a result of introducing a rightward shift in its I-V relationship and a faster voltage dependent inactivation. Compared with the NZ model, the current peaks of I_{K1}, I_{Kr} were shifted to the right in both EBZ models (Figure 4.3B, 4^{th} and 5^{th} rows), due to the slower AP in EBZ cell and voltage-dependent regulation.

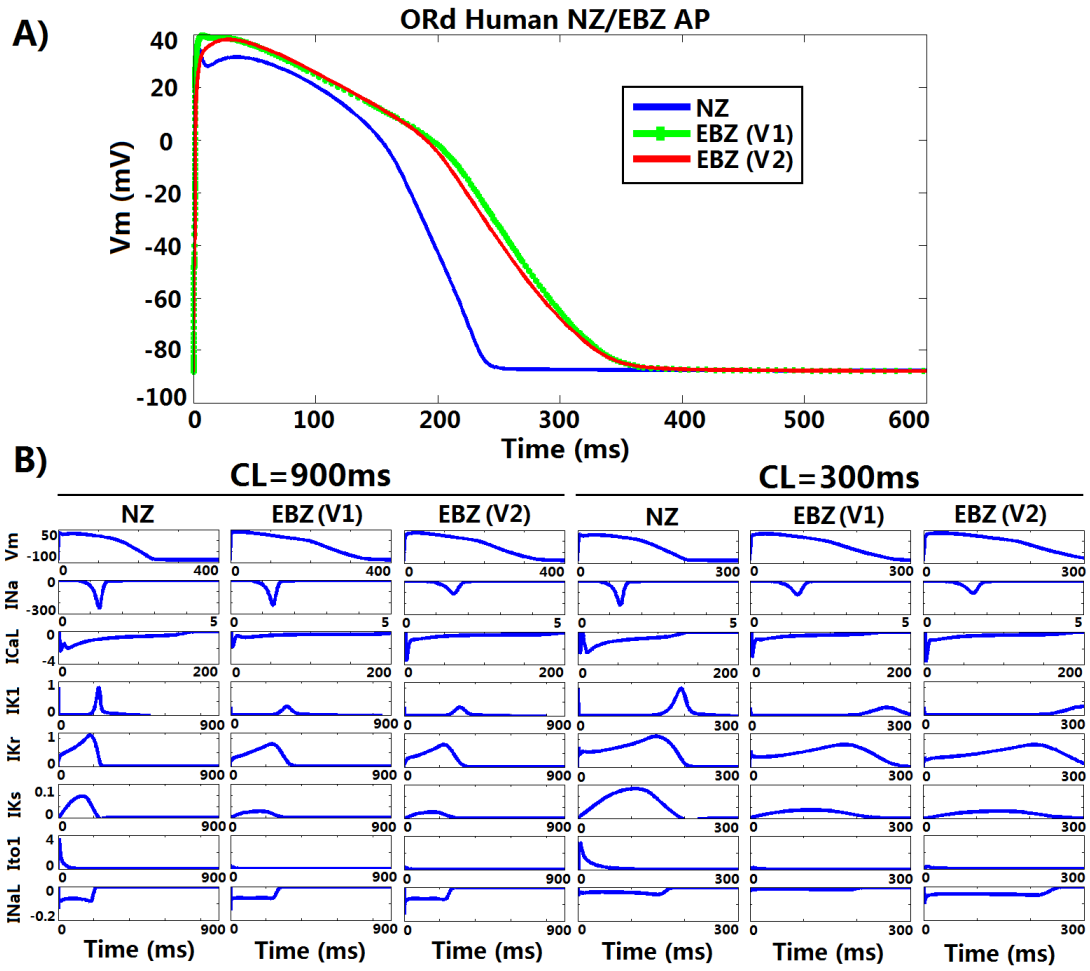


Figure 4.3: Action potential and main ionic currents for the two versions of the human EBZ model. A) Steady-state AP traces of human EBZ models (versions 1 and 2, respectively); B) Main ionic currents (μA/μF) in the human EBZ models (versions 1 and 2, respectively).

4.3.3 Development of alternans in human EBZ models

Figure 4.4A showed that both EBZ models show beat-to-beat APD alternans at fast pacing rates, as we also found in the canine EBZ model at CL=250ms (Figure 4.2D). In the EBZ model considering only remodeling in ionic conductances (V1), the threshold CL for alternans was 280 ms. For the EBZ model with remodeling in both ionic conductances and kinetics (V2), the threshold alternans CL was 320 ms (Figure 4.4 A). As shown in Figure 4.4 B, when CL=300 ms, only the EBZ model version 2 exhibits alternans. For both EBZ models, the beat-to-beat APD differences between

two alternans states were around 200ms.

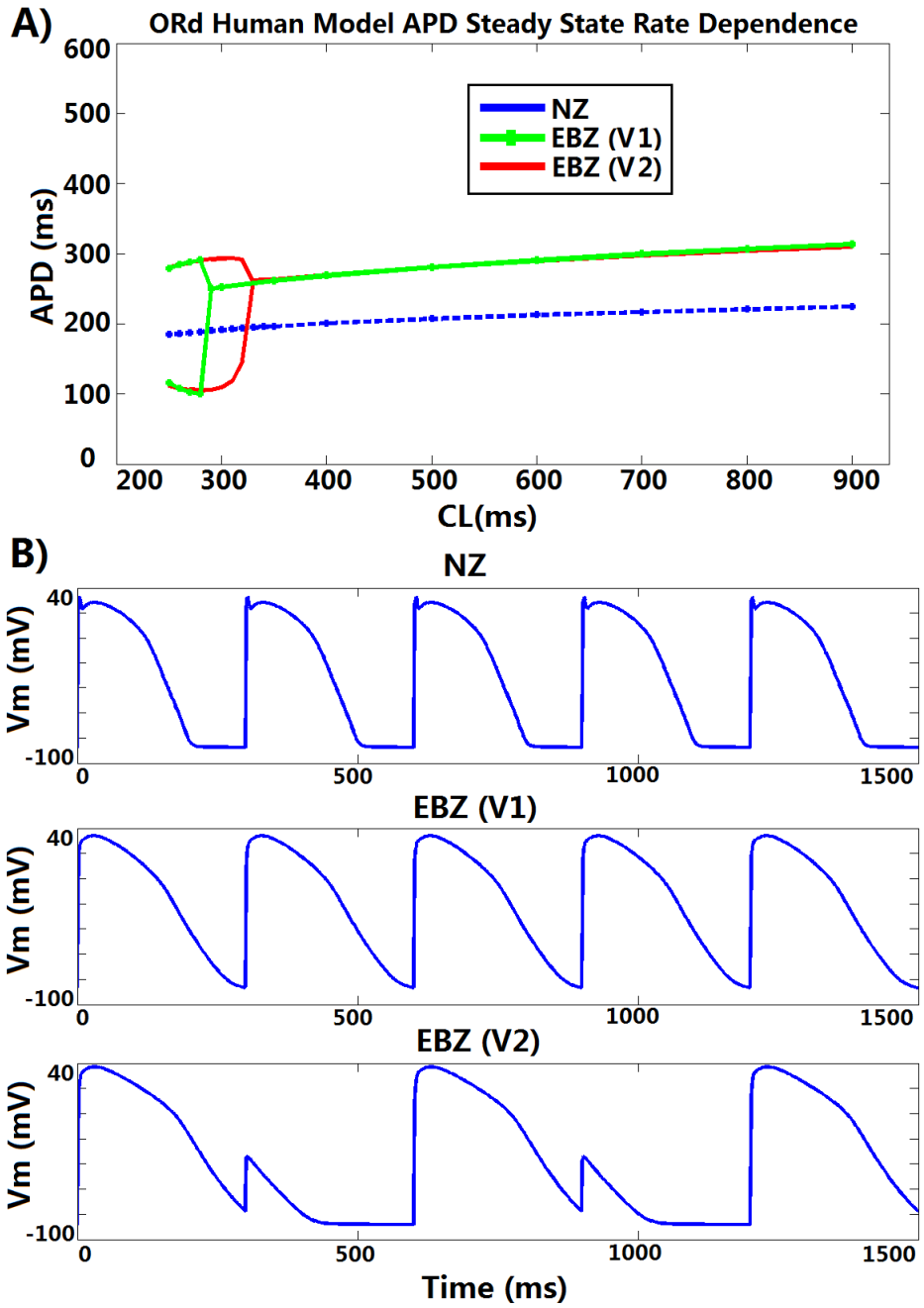


Figure 4.4: APD alternans in human EBZ models. A) Steady-state rate dependence of EBZ models (version1 and 2, respectively); B) Steady-state time series of five consecutive beats (CL=300ms) for NZ and the two EBZ models.

4.3.4 Sensitivity to EBZ remodelling

Figure 4.5 showed the dispersion between human EBZ and NZ under sensitivity

analysis. In the two human EBZ models, APD alternans still occurred under ±20% modifications of the default values of EBZ-induced electrical remodelling. These modifications can affect the CL threshold for alternans generation.

In EBZ model version 1, the original CL threshold of 280ms for APD alternans was altered to 260ms and 320ms after -20% and +20% changes based on the original EBZ-induced remodelling, respectively (Figure 4.5A). Moreover, if we compare the APD difference between NZ and EBZ, introducing a +20% of all the original change led to an enlargement of these APD differences (Figure 4.5A). These results showed that the more EBZ remodelling we introduced into the model, the easier it was for the EBZ model to generate alternans, and the larger the dispersion between NZ and EBZ became.

Equivalently, in the EBZ model version 2, the original CL threshold of 320ms for APD alternans was altered to 280ms and 390ms after -20% and +20% changes based on the original EBZ-induced remodelling, respectively (Figure 4.5B). In fact, APD differences between NZ and EBZ became more dependent on the extent of the modification we introduce to the model (Figure 4.5B).

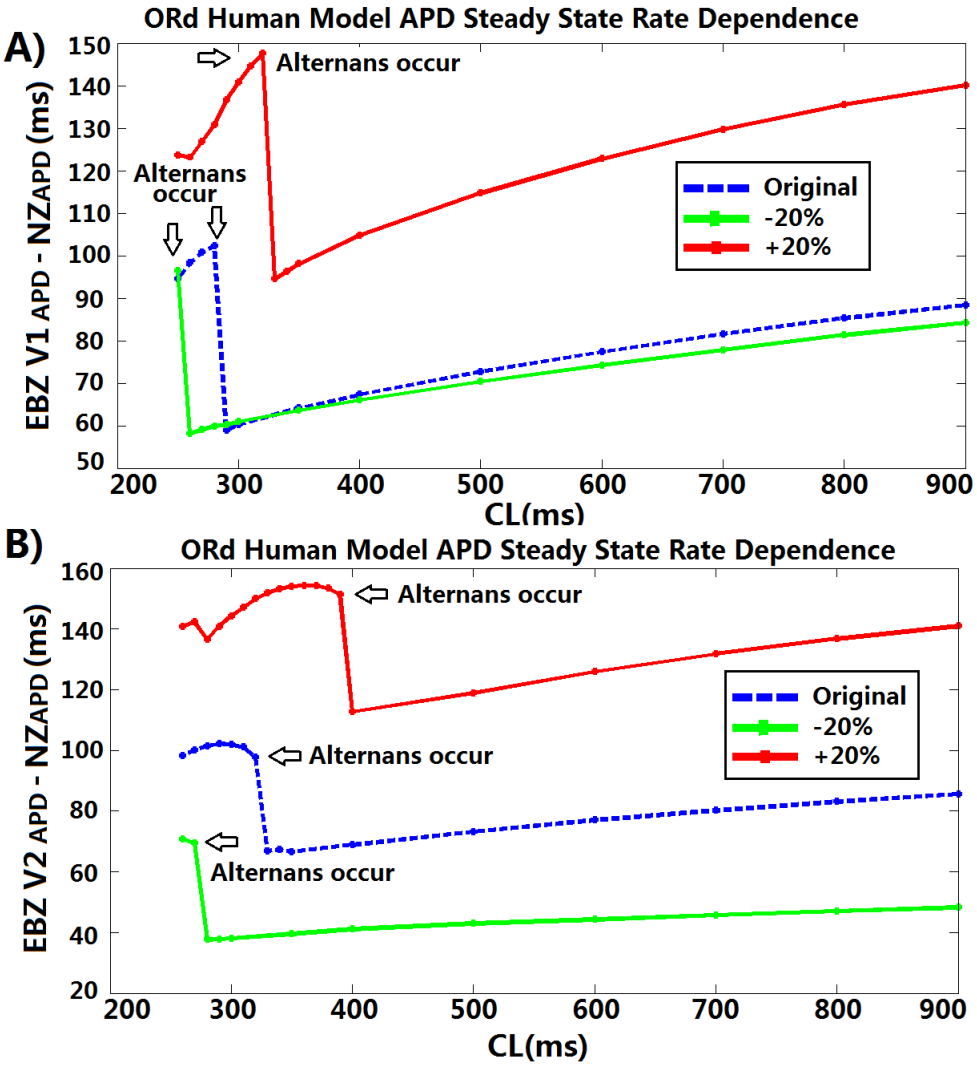


Figure 4.5: Sensitivity of human EBZ models to the extent of EBZ-remodelling. A,B) APD differences (ΔAPD) between NZ and EBZ in the three EBZ models (control and ±20% EBZ remodelling) for EBZ models version 1 and 2, respectively.

4.3.5 Modulation of EBZ-remodelling under pharmacological I_{Kr} block

The rapidly activating potassium current I_{Kr} is crucial to the repolarisation of the AP. The reduction of I_{Kr} often contributes to APD prolongation, thus increasing tissue refractoriness. Different I_{Kr} blockers have been approved to treat atrial and ventricular arrhythmias, including fibrillation. Anti-arrhythmic drugs exhibit limited efficacy in post-MI patients, and the mechanisms underlying the pharmacological

modulation of NZ/EBZ heterogeneities remain unknown. Therefore, we explored the effect of using I_{Kr} blockers in our human EBZ models.

As shown in Figure 4.6A, 50% I_{Kr} block would increase the APD in both the NZ and EBZ models, and also enlarged APD differences between NZ and EBZ (Figure 4.6B).

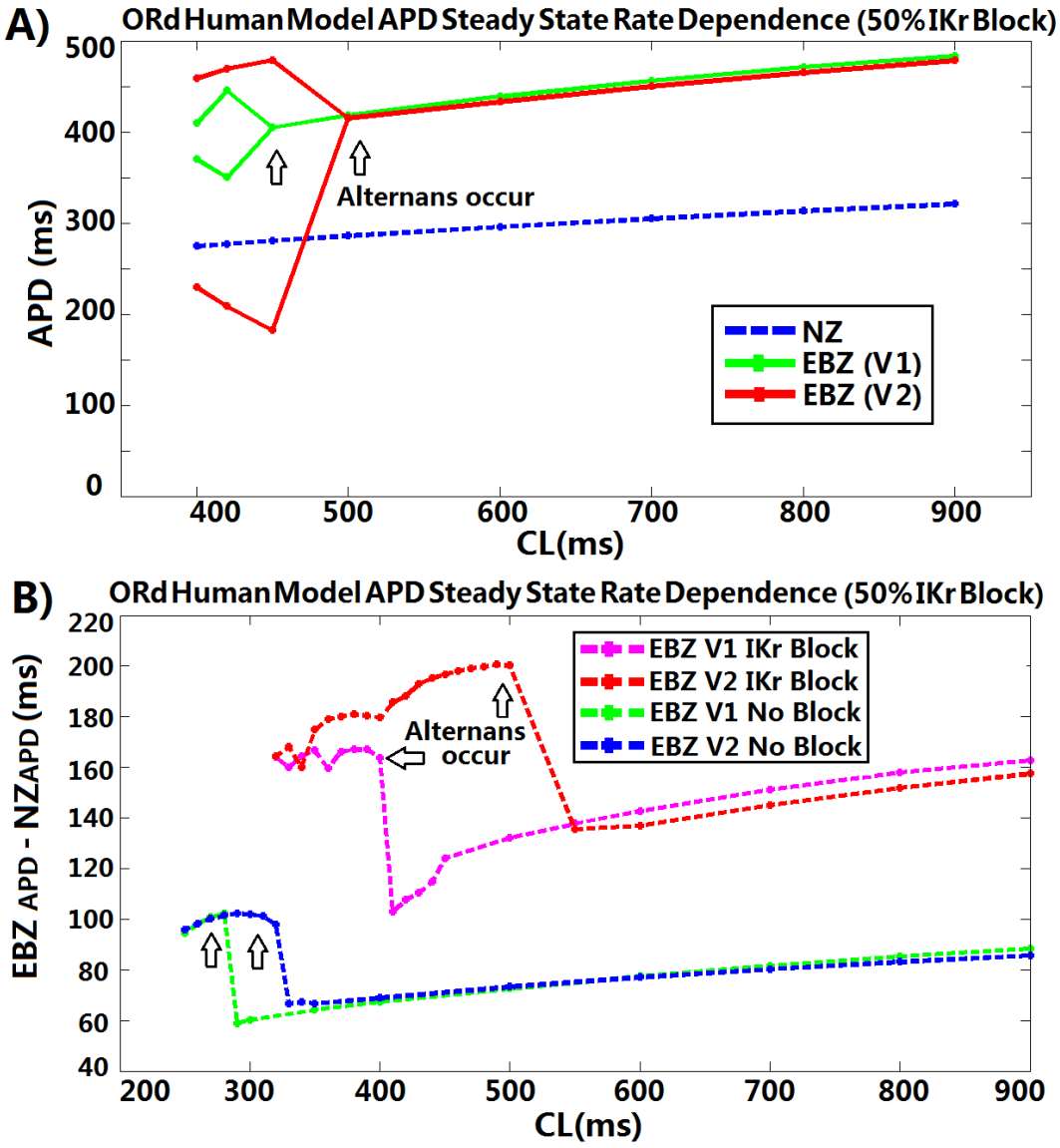


Figure 4.6: Effect of I_{Kr} block on human EBZ models. A) Steady-state rate dependence of NZ and two EBZ models with 50% I_{Kr} block; B) APD differences (ΔAPD) between NZ and EBZ in both EBZ models with or without 50% I_{Kr} block.

Figure 4.7 showed multiple bifurcation states observed in the human EBZ models under conditions of I_{Kr} block. Figure 4.7A demonstrated that at CL=380ms, the EBZ

model version 1 displayed alternans made up by 4 beats (Figure 4.7A, middle panel), while the alternans of EBZ model version 2 contained 3 beats (Figure 4.7A, lower panel). Figure 4.7B showed that when the pacing CL was decreased to 350ms, EBZ model version 1 generated alternans of 5 beats (Figure 4.7B, middle panel), and EBZ model version 2 still had alternans of 3 beats (Figure 4.7B, lower panel).

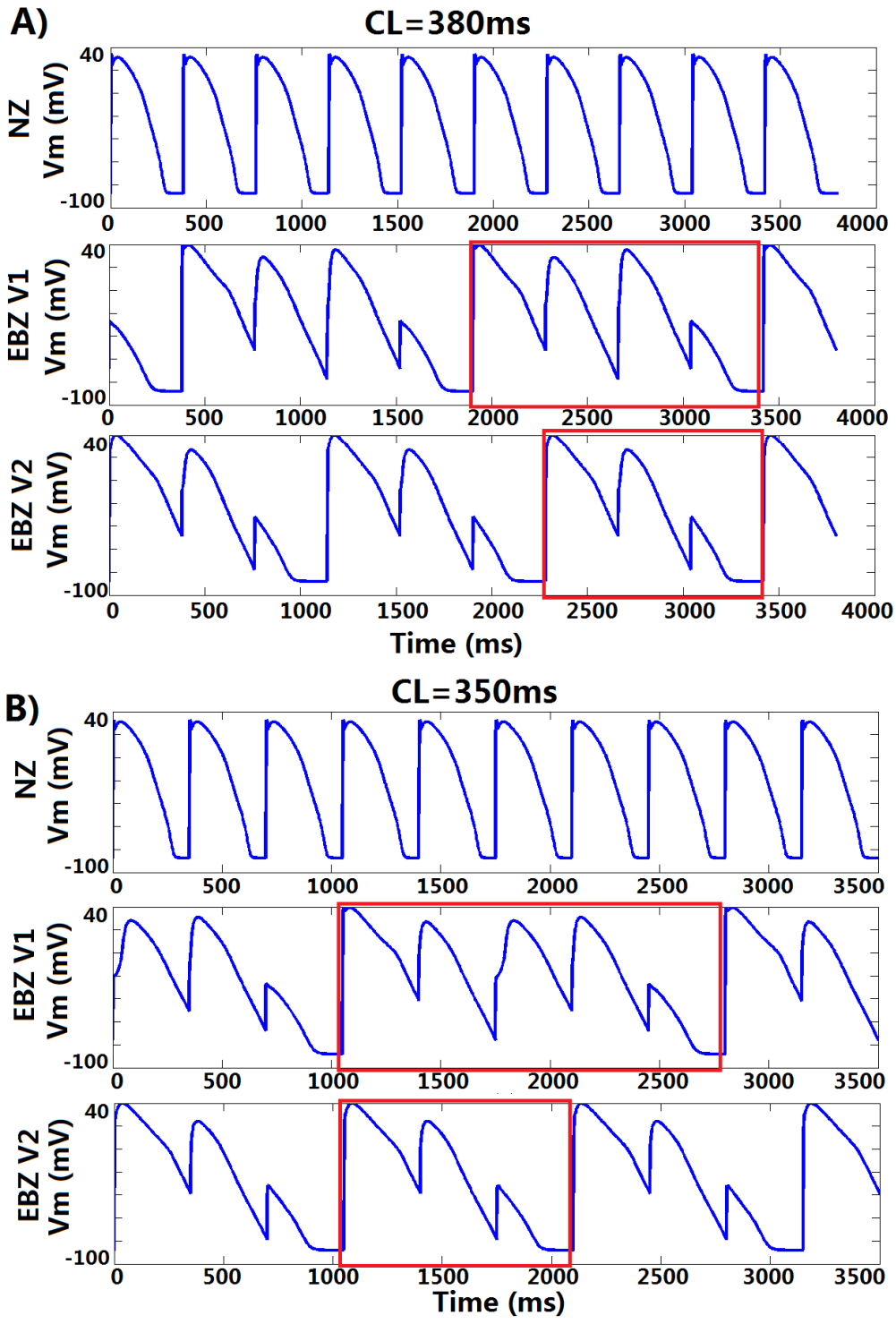


Figure 4.7: Alternans in human EBZ models after I_{Kr} block. A) Ten beats AP comparison between NZ, EBZ version 1, and EBZ version 2 with 50% I_{Kr} block, at CL=380ms; B) Ten beats AP comparison between NZ, EBZ version 1, and EBZ version 2 with 50% I_{Kr} block, at CL=350ms.

Detailed analysis on EBZ model version 1 showed that when CL =400ms, the 50% I_{Kr} block on the model generated alternans made up by two states. For CL between

390ms and 360ms, a cycle of alternans contained 4 beats. When CL was decreased to the range between 350ms and 320ms, the steady state was formed by a total cycle of 5 beats.

Similarly for the EBZ model version 2, the two states alternans occurred in the range of CLs between 490ms and 390ms under 50% I_{Kr} block. When the CL was between 380ms and 330ms, alternans were made up of 3 states, and if CL was further decreased to 320ms, the alternans could become a cycle of 5 states.

These different patterns of alternans may lead to more complex patterns of spatio-temporal dispersion in cardiac tissue, thus increasing the likelihood of initiation and maintenance of ventricular arrhythmias after myocardial infarction.

4.4 Discussion

In the present study we investigate the effect of electrophysiological remodeling in the epicardial border zone of myocardial infarction using a human ventricular cell model (O'Hara *et al*., 2011). EBZ remodelling of ionic currents was introduced into the human model, based on previously reported modifications of healthy canine to EBZ canine models (Decker et al., 2009; Decker and Rudy, 2010). The main assumption was that the similarities between canine and human ventricular electrophysiology support the extrapolation of canine recordings in the EBZ to human. This assumption would need to be tested with additional studies in human, which we hope our new theoretical findings may be able to help design. We investigated the separate contribution of remodeling in ionic current conductances and in the kinetics in the electrophysiological abnormalities in the EBZ by generating two versions of human EBZ models: the first one only included relative changes to conductances and permeabilities to the ion channels; whereas the second one also considered relative changes in the kinetics of activation and inactivation of

several currents (relative voltage dependent inactivation/activation shifts to I_{Na} and I_{CaL}, faster inactivation for I_{CaL}, and faster activation for I_{Kr}). As already indicated, all the above mentioned contributions of EBZ remodelling are based on previously reported experimental data (Aggarwal et al., 1997; Aggarwal and Boyden, 1995; Jiang et al., 2000; Lue and Boyden, 1992; Pinto and Boyden, 1999).

The two resulting versions of human EBZ models shared the same basic electrophysiological properties, and were also consistent with canine simulations. The steady-state AP of the two models was both prolonged compared to NZ, also showed an absence of a phase I notch due to the loss of I_{to1}, and a loss of AP triangulation caused by the reduction in I_{K1}. A detailed analysis of individual ionic currents in our human EBZ models revealed similar rate dependence characteristics than in the canine EBZ model.

Interestingly, alternans occurred in both models at fast pacing rates, which is consistent with the clinical observations in human that post-MI hearts tend to have more significant T-wave alternans (Ren et al., 2011). Alternans are often associated with heart disease, and can be important for the initiation of ventricular arrhythmia (Abe et al., 1989). The heterogeneity in heart tissue caused by this dispersion in refractoriness can seriously compromise the synchronization in cardiac tissue and affect the normal function of heart, potentially leading to arrhythmias and SCD.

The development of alternans was consistently observed in the two versions of the human EBZ, pointing to APD prolongation induced by electrical remodelling as the main mechanism underlying alternans in the EBZ. The remodelling of current magnitudes was sufficient to introduce similar APD prolongation and alternans development, which suggested the more important role of current conductances and permeabilities in proarrhythmic conditions. However, alternans occurred at longer CLs with the presence of remodelling in ionic kinetics (280ms in version 1 vs 320ms in version 2), which meant that current kinetics could affect the sensitivity of the

EBZ model to changes in CLs.

Sensitivity analysis was also considered in order to account for possible inter-species differences in EBZ remodelling. Basic characteristics of both models remained unaltered under changes of +20% in the extent of EBZ-induced remodelling, but the models became more sensitive to the development of alternans at longer cycle lengths. A larger extent of EBZ-induced remodelling also enlarged APD differences between NZ and EBZ.

I_{Kr} potassium channel blockers are often regarded as potential antiarrhythmic agents due to their prolongation effect on APD. However, safety concerns have also been raised by clinical trials such as (Echt *et al*., 1991) . We explored the effect of 50% I_{Kr} block in our two human EBZ models. Simulation results indicated that 50% of I_{Kr} block prolonged the APD in both NZ and EBZ, and in addition it would also enlarge APD differences between both types of tissue. Moreover, multiple bifurcations were present in the EBZ models at fast pacing rates under hERG block conditions, with the EBZ models displaying alternans series made up by 3 to 5 beats instead of just having two alternans states. These complex patterns of alternans were also observed experimentally in Guinea pigs under hERG blocker E-4031 (Fossa et al., 2004). This would definitely enhance beat-to-beat dispersion of repolarisation at the whole heart level, facilitating the possible generation of proarrhythmic substrates for the development of arrhythmias.

Study Limitations

The methodology used to build the human EBZ model is based on prior knowledge on the canine EBZ. We tried to circumvent these limitations by performing a sensitivity analysis on the extent of EBZ remodelling. However, there could be some inter-species differences between the human EBZ and canine EBZ, since as seen in Table 3.3, the conductances and permeabilities of some ion channels in human are sometimes several times larger or smaller than in canine. Moreover, no Cl^- currents

are included in the healthy human model formulation, so changes in Cl^- currents were not included into our human EBZ models. The human NZ model also includes calcium dependent inactivation. In order to improve our human EBZ models to better replicate the physiology, additional human data would be needed to validate our human EBZ models. Consistent results obtained through sensitivity analysis also suggested that instead of having an individual set of parameters for a single model, a population of parameter sets could be developed based on human data to introduce more flexibility into the model. This also would be meaningful for addressing heterogeneous tissue modelling in the future.

Conclusions

A number of research studies have been conducted to address the mathematical modelling of the EBZ, but the majority of these investigations have been performed in canine models. We derived two mathematical models of the human EBZ from a newly published undiseased human ventricular cell model (O'Hara *et al*., 2011). In general, both EBZ models displayed a similar overall behavior of AP as the canine EBZ models. It was found in our human EBZ models that the prolongation of APD can induce the development of alternans that is crucial for the spatio-temporal dispersion and the emergence of arrhythmias. Pharmacological hERG block (as following administration of class III anti-arrhythmic compounds) also led to a further enlargement of the refractoriness dispersion between human NZ and EBZ, with human EBZ models being more prone to the development of alternans and displaying more intriguing alternans dynamics.

Our study in the modelling of the human EBZ constitutes a first step in the iteration between computational, experimental and clinical work. It might help us to understand the physiological mechanisms of human arrhythmias after myocardial infarction, guide clinical and experimental research in the electrophysiological examination of post-infarcted patients, and help to improve the efficiency of drug screening in safety pharmacology to develop new therapies against cardiac disease.

Chapter 5

Construction of a population of human ventricular cell electrophysiology models based on *in vivo* measurements

5.1 Introduction

In the Chapter 4, we described how modelling can be used to simulate the pathological conditions of EBZ cells after myocardial infarction. By introducing a similar remodelling of current conductances as that observed in canine experiments, the healthy human single cell model can be modified to predict similar behaviour of the human EBZ cell as in canine experiments. The need to include sensitivity analysis led to our increasing interest in developing new techniques to include general variability into investigations of human cardiac electrophysiology.

As introduced and discussed in Section 2.3, cardiac electrophysiological variability can come from multiple sources, including the cell-to-cell difference in protein expression level of ionic channels and pumps/exchangers (Pueyo *et al*., 2011) and the sympathetic neural regulation (Taggart *et al*., 2011). One common assumption is that variability in ionic densities is likely to be the main factor modulating physiological variability rather than differences in the kinetics of ionic transporters that depend on protein structure (Groenendaal *et al*., 2015).

Mathematical modelling represents a very powerful tool in the study of cardiac variability. As reviewed in Section 3.7, different modelling approaches such as cell-specific modeling, sensitivity analysis and experimentally-calibrated population of models can be used to explore the effects of cardiac variability. The method of experimentally-calibrated population of models was firstly proposed by (Britton *et al*., 2013). In this approach, a population of models that shares same current formulations but different baseline current conductances or permeabilities can be generated and constrained using experimental data. Compared with traditional sensitivity analysis, experimentally-calibrated population of models allows for a larger initial variation of the parameters. Unlike cell-specific modeling that sometime needs complex electrophysiological experimental protocols, experimentally-calibrated population of models only requires routine experimental data, which increases its flexibility in applications.

In this chapter, we aim to develop a technique that can incorporate the effects of *in vivo* variability in human electrophysiology. Unlike animal experiments, the protocols of *in vivo* human experiments are largely constrained to ensure the safety of patients. Therefore, the experimentally-calibrated population of models is a very appropriate method to integrate human *in vivo* variability.

Here, we generated a population of models using the ORd model (O'Hara *et al*., 2011), and then calibrated them based on human data obtained from the London Heart Hospital. This constitutes the first population of human ventricular cell models calibrated with *in vivo* human measurements. Further analysis shows that this population of models covers a wide sampling range for most ionic parameters, and the combination of such parameters can explain the variation of AP biomarkers. Therefore, this population of models can be a good platform to explore the effects of variability in human ventricular cell electrophysiology.

5.2 Methods

5.2.1 *In vivo* data acquisition

41 patients without myocardial infarction (9 female, 32 male, see Table 1) were studied prior to aortic valve replacement (AVR, n=10) and/or coronary artery bypass graft (CABG, n=35) in the Heart Hospital. The subjects were selected at random from the waiting list without specific selection criteria. The study, according to the principles expressed in the Declaration of Helsinki, was approved by the local Hospital Ethics Committee, and written informed consent was obtained from all patients before the study.

Patient	**Sex**	**Age**	**Surgery**
1	M	49	CABGx3
2	M	79	CABG
3	M	49	CABGx2
4	M	74	CABGx3
5	M	62	AVR
6	M	60	CABGx3
7	M	31	AVR
8	M	73	CABGx2
9	M	44	CABGx3
10	F	56	CABGx3
11	F	75	AVR
12	M	49	CABGx2
13	F	66	CABG
14	F	70	AVR
15	F	80	CABG
16	M	71	AVR
17	M	51	CABG
18	M	57	CABG
19	M	47	CABG
20	F	63	CABG
21	F	78	CABG
22	M	78	CABG
23	M	77	CABG

24	M	73	CABG
25	M	62	AVR
26	M	75	AVR+ CABG
27	M	55	CABGx3
28	M	73	AVR+ CABG
29	M	82	AVR+CABG
30	M	44	CABGx3
31	M	54	CABGx2
32	M	54	CABG
33	M	84	AVR+CABG
34	M	73	CABG
35	F	73	CABG
36	M	67	CABG
37	M	33	CABG
38	M	81	CABG
39	F	55	CABG
40	M	59	CABG
41	M	47	CABG
Mean		63	
Median		63	
Std		13.8	

Table 5.1: Patients' information in the study

AVR: aortic valve replacement; CABG: coronary artery bypass grafting.

During cardiac surgery, a multielectrode sock (as described in Section 2.2.2) was fitted over the epicardium of both ventricles, and unipolar electrograms were recorded from 240 electrodes. Ventricular pacing was established over a range of 6 cycle lengths (CLs), from 600ms to 350ms, in steps of 50ms.

Activation recovery intervals (ARIs), an *in vivo* surrogate of APD, (Bueno-Orovio et al., 2012; Coronel et al., 2006; Potse et al., 2009; Yue et al., 2004) were calculated from the epicardial electrograms as the interval between the minimum derivative during depolarisation and the maximum derivative during repolarisation (Figure 5.1A), using custom-written routines in MATLAB (MathWorks, Natick, MA). This part of the analysis was completed by our collaborators in the Heart Hospital and University College London. *In vivo* ARIs at the different CLs presented rate

dependence and variability (Figure 5.1B), and both normal and alternans sites were observed in these patients (Figure 5.1 C-D). ARIs were used to constrain APD_{90} as the first filter in this calibration process. Any parameter sets that generated a model with non-physiological APD_{90} at any pacing CLs were excluded from the population.

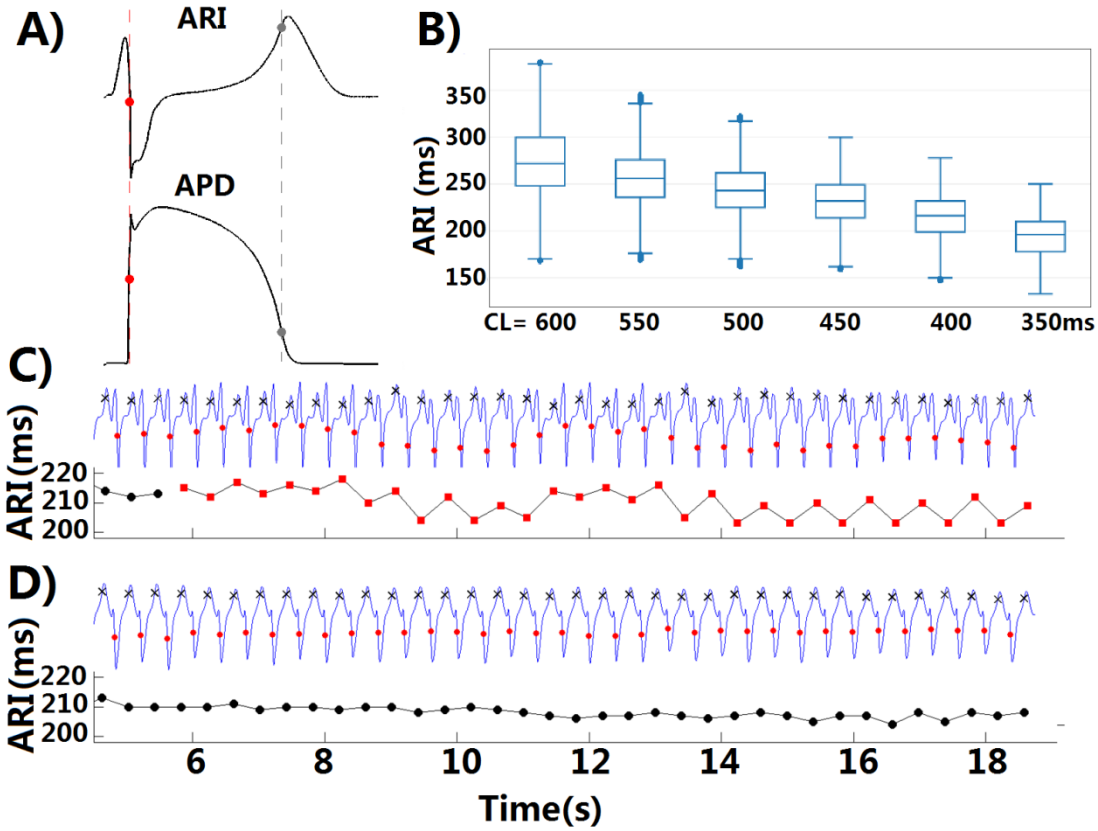


Figure 5.1: *In vivo* recordings of the activation recovery interval (ARI) used for calibration of the population of human ventricular models. A) ARI as an *in vivo* surrogate of APD. Red dots represent activation and depolarisation times, whereas grey dots represent recovery and repolarisation times (adapted from (Potse *et al.*, 2009)). B) Rate dependence and variability in *in vivo* ARIs aggregated from the different patients as a function of decreasing pacing cycle length. C) Unipolar electrograms and corresponding sequence of ARIs from an alternans-susceptible site. D) Unipolar electrograms and corresponding sequence of ARIs from an alternans-resistant site. Dots and crosses on the electrograms represent activation and recovery times, respectively.

5.2.2 Population of models

We build our analysis on a population of models of human ventricular

electrophysiology based on the ORd model (O'Hara *et al*., 2011). Within this population, cell models share the same equations representing ionic current kinetics but different conductance values (Britton et al., 2013; Walmsley et al., 2013).

5.2.3 Parameters varied in the population of models

A population of models was constructed based on the sampling of the following 11 key parameters, previously suggested to be key for mechanisms of cardiac arrhythmias (Merchant and Armoundas, 2012): G_{Na} (fast Na^+ channel conductance), P_{Ca} (Ca^{2+} channel permeability, referred to as G_{CaL} in this study), G_{Ks} (Ks channel conductance), G_{K1} (K1 channel conductance), G_{Kr} (Kr channel conductance), G_{to} (transient outward potassium channel conductance), G_{NaL} (late Na^+ channel conductance), G_{NaCa} (Na^+/Ca^{2+} exchanger conductance), G_{NaK} (Na^+/K^+ pump activity), P_{Jrel} (Ca^{2+} release permeability via ryanodine receptors to the cytoplasm, as a new scaling factor for J_{rel}) and P_{Jup} (Ca^{2+} uptake permeability via SERCA from the cytoplasm, as a new scaling factor for J_{up}).

5.2.4 Latin hypercube sampling

Considering every possible combination of parameter values is computationally intractable due to the complexity of cardiac cell models and the large number of parameters. Latin Hypercube Sampling (McKay *et al*., 1979) was used in this study to generate scaling factors uniformly distributed between 0 and 2, representing ±100% variations with respect baseline model parameters. Original model parameters in the ORd model were then multiplied by these scaling factors to generate an initial population of ionic models.

5.2.5 Simulation protocol

All numerical simulations were performed using the open source simulation software Chaste (Pitt-Francis *et al*., 2009) on a 512 core cluster Intel processors at the Oxford Supercomputing Centre. In order to mimic the *in vivo* experiment protocol, cell models were stimulated for 1000 paces at each of the following cycle lengths (CLs) in a step protocol: 600, 550, 500, 450, 400 and 350ms.

5.2.6 Biomarker calculation

The following biomarkers were calculated when the population of models reached their steady states under all 6 CLs:

Biomarker	**Calculation method**
RMP (resting membrane potential)	Minimum membrane voltage
V_{max} (upstroke voltage)	Maximum membrane voltage
APA (action potential amplitude)	V_{max}-RMP
Upstroke potential	RMP +APA*90%
Transmembrane threshold (repolarisation level 30, 80 or 90)	RMP+APA*(100-repolarisation level)%
UT (upstroke time)	Time when membrane voltage rises to Upstroke potential
DT (depolarisation time)	Time when membrane voltage rises to Transmembrane threshold
RT (repolarisation time)	Time when membrane voltage falls back to Transmembrane threshold
UPD (upstroke duration biomarker)	UT-DT (90% repolarisation)
APD (with repolarisation level 30, 80 or 90)	RT-DT

APD_{tri} (triangulation biomarker)	APD_{30}/APD_{80}
CaT_{min} (minimum calcium transient)	Minimum value of intracellular Ca^{2+} transient (CaT) concentration
CaT_{max} (maximum calcium transient)	Maximum intracellular Ca^{2+} transient concentration
CaTD (with repolarisation level 30 or 80)	Similarly as APD, but based on Ca^{2+}

Table 5.2: Biomarker calculation algorithm

5.2.7 Partial correlation analysis

Partial correlation was used to determine the relationship between biomarkers and parameters (Britton et al., 2013; Marino et al., 2008).

5.3 Results

5.3.1 Construction of the initial population of models

10000 initial models were constructed by varying the above 11 parameters between ±100% (scaling factors varied from 0 to 2), and each of the 10000 models were simulated for 1000 beats under the above mentioned 6 CLs.

5.3.2 Calibration of the population of models

After generating the 10000 initial models using LHS, a calibration process is needed so that all non-physiological models in the initial population can be excluded. Six different filters were used in this process. All the biomarkers from the last two beats of the initial 10000 models under all 6 CLs must pass all the following filters in order to be accepted in the final population.

5.3.2.1 Filter 1: *in vivo* ARI value ranges selection by fitting skewed normal distribution

The most important filter in the calibration process was the ARI data from 41 patients. In order to exclude the effects of extreme values and to avoid possible biased results, 90% or 95% of the total ARI ranges from patients was selected to be the physiological ranges. Since the ARI data from all patients were not normally distributed and the distribution of the data tended to be skewed at short CLs (Figure 5.2, left), skewed normal distributions were used to fit the *in vivo* data and to calculate the range that would exclude the upper 2.5% and lower 2.5% of all the data, in order to get the 95% physiological range. The curves of the probability distribution function (PDF) and the cumulative distribution function (CDF) of the fitted skewed normal distribution are shown in Figure 5.2. Similarly, if we consider 90% of all the ARI values, the range between the upper 5% and lower 5% thresholds will be considered as physiological.

After the selection of Filter 1, five additional filters were used to exclude non-physiological models. Depending on the method of selecting the physiological APD range in Filter 1, two groups of results were gained: Fitting Skewed Normal Distribution 95% (Sk95) and Fitting Skewed Normal Distribution 90% (Sk90).

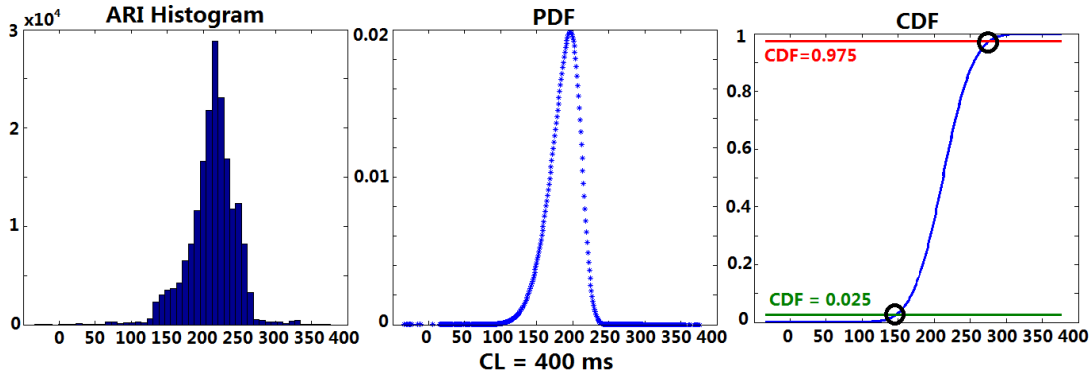


Figure 5.2: Analyzing *in vivo* ARI data and using skewed normal distribution to select 95% of data coverage thresholds. Left: histogram of the ARIs (ms) from all patients when CL=400ms; middle: PDF based on the original data; right: CDF and thresholds selection (cross points in the black circles).

5.3.2.2 Filter 2: normal restitution curve

Filter 2 accepted those models exhibiting monotonic APD restitution curves until alternans occurrence. Models with fluctuations in APD restitution were excluded (Figure 5.3A).

5.3.2.3 Filter 3: normal resting membrane potential values

Filter 3 accepted models that had physiological resting membrane potentials (from -100mV to -64mV). The thresholds were computed as the mean ± 2SD of the experimental data published by Li *et al.* (Li *et al*., 2004), representing a 95% confidence interval of the physiological range of RMP values from human myocytes. An example of models excluded after application of Filter 3 is shown in Figure 5.3B.

5.3.2.4 Filter 4: normal upstroke values

Filter 4 accepted models with peak membrane potential greater than 0mV, and models with weak depolarisation upstroke were excluded. The thresholds used in this filter were calculated and estimated using a small group of 100 models generated using the LHS method. An example of Filter 4 excluded models is shown in Figure 5.3C.

5.3.2 5: Filter 5: normal upstroke durations

Filter 5 accepted models that had physiological upstroke duration (<10 ms), rejecting models with delayed depolarisation. The thresholds used in this filter were calculated and estimated using a small group of 100 models, generated using the LHS method. An example of Filter 5 excluded models is shown in Figure 5.3D.

5.3.2.6: Filter 6: normal resting Ca^{2+} levels

Finally, Filter 6 accepted models that had physiological diastolic cytosolic Ca^{2+} concentrations (from 21nM to 285nM). The thresholds were computed as the mean ± 2SD of the experimental data published by Piacentino *et al.* (Piacentino *et al*., 2003),

representing a 95% confidence interval of the physiological range of diastolic Ca^{2+} levels in human myocytes. An example of Filter 6 excluded models is shown in Figure 5.3E.

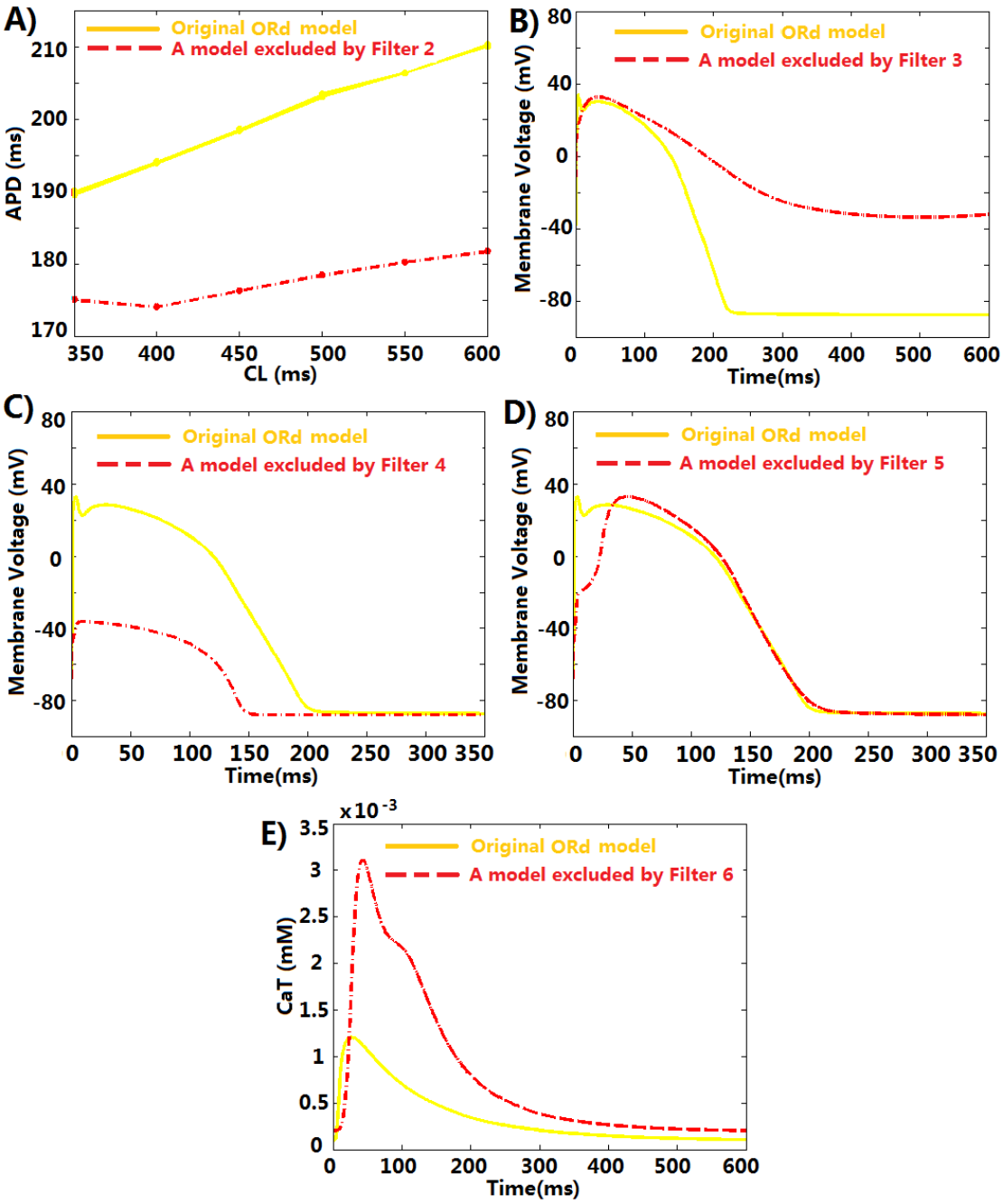


Figure 5.3: Representative models excluded during the calibration process by Filters 2-6.

5.3.3 Calibration results

5.3.3.1 Number of accepted models during the calibration process

Figure 5.4A showed the number of models remained in the population during the calibration process. As the initial population of models went through the 6 filters, the number of accepted physiological models decreased (Figure 5.4A). It is clear that Filter 1 (physiological APD_{90} range) was the most selective filter among the six of them. Despite the fact that different selection levels were used in Filter 1, using 90% (Sk90) or 95% (Sk95) of the ARI values had similar trends. Compared to using 90% of the ARI values, the 95% interval can provide more combinations and interactions for variability. Therefore Sk95 calibration results were used in the further analysis.

5.3.3.2 The action potentials of the accepted models

After calibration, more than 75% of the 10000 initial models were excluded (Figure 5.4A). Compared to the initial population, the accepted models had relatively similar AP morphologies (Figure 5.4B) and those models exhibiting weak upstroke, early after depolarisations, repolarisation failure or extreme APD values were excluded in further analysis.

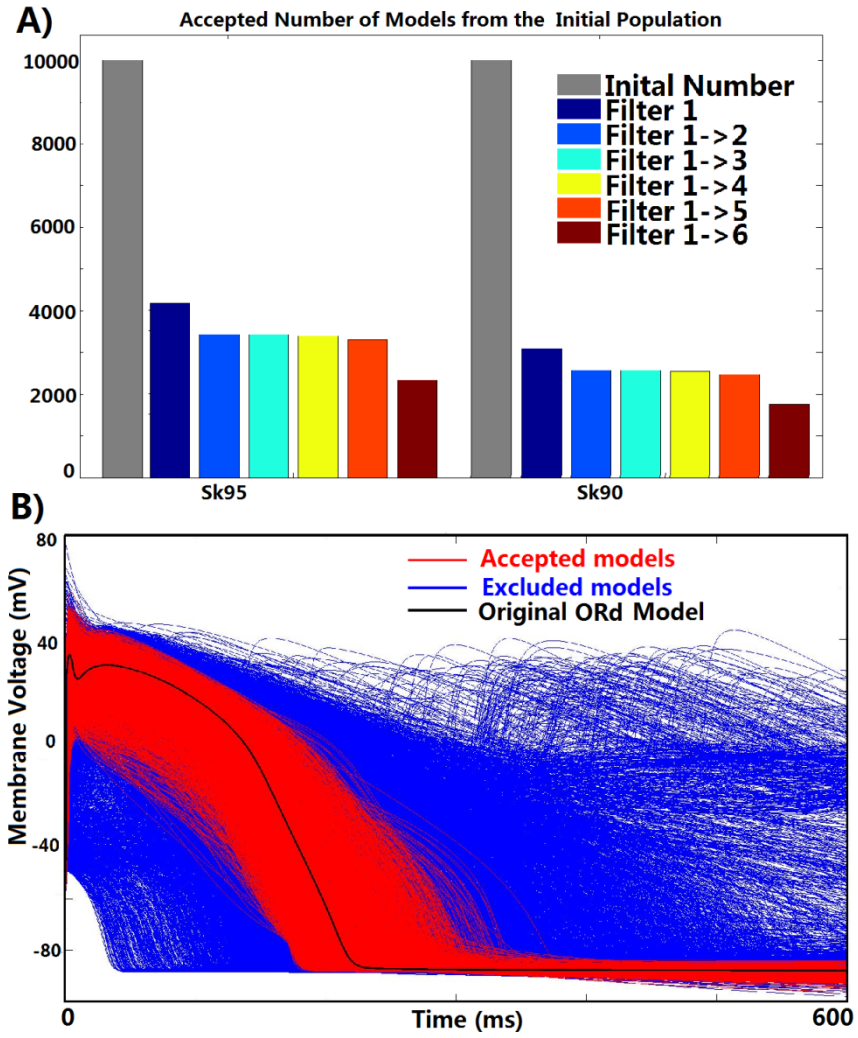


Figure 5.4: Calibration results from the initial population. A) number of accepted models in 2 types of calibrations using 6 filters; B) action potentials of accepted, excluded and original models for CL=600ms.

5.3.3.3 The distribution of the accepted parameters

Despite the similar shape of APs between accepted models, many of their underlying ionic parameters covered a broad sampling range. The distribution of some accepted parameters tended to be skewed, such as G_{CaL}, G_{NaCa}, G_{NaK} and P_{Jup}, and the distribution of G_{Kr} was bell-shaped (Figure 5.5). Small values in G_{Na} were completely excluded after the calibration, which indicated the irreplaceable role of the fast sodium current in the AP upstroke (Figure 5.5). For other current conductanes such as G_{NaL}, G_{to}, G_{Ks}, very small values can be accepted after the calibration steps, which suggested the complex compensation effects between

different currents and possible highly variable expression of these ion channels within myocytes.

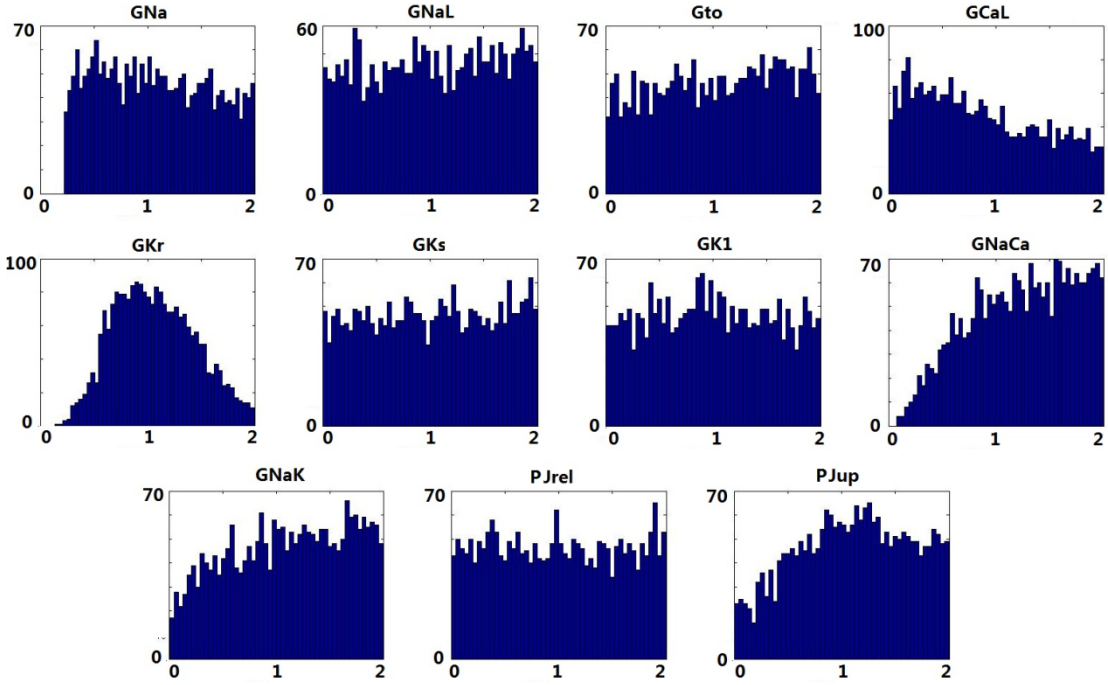


Figure 5.5: The distribution of 11 parameter scaling factors in the accepted population of models.

The different distributions of the accepted parameters were determined by the calibration filters. Filter 1 mainly targeted the shape of G_{Kr}, and Filter 4 and Filter 5 targeted the G_{Na}. Filter 2 and especially Filter 6 constrained the shape of many Ca^{2+} related currents (Figure 5.6).

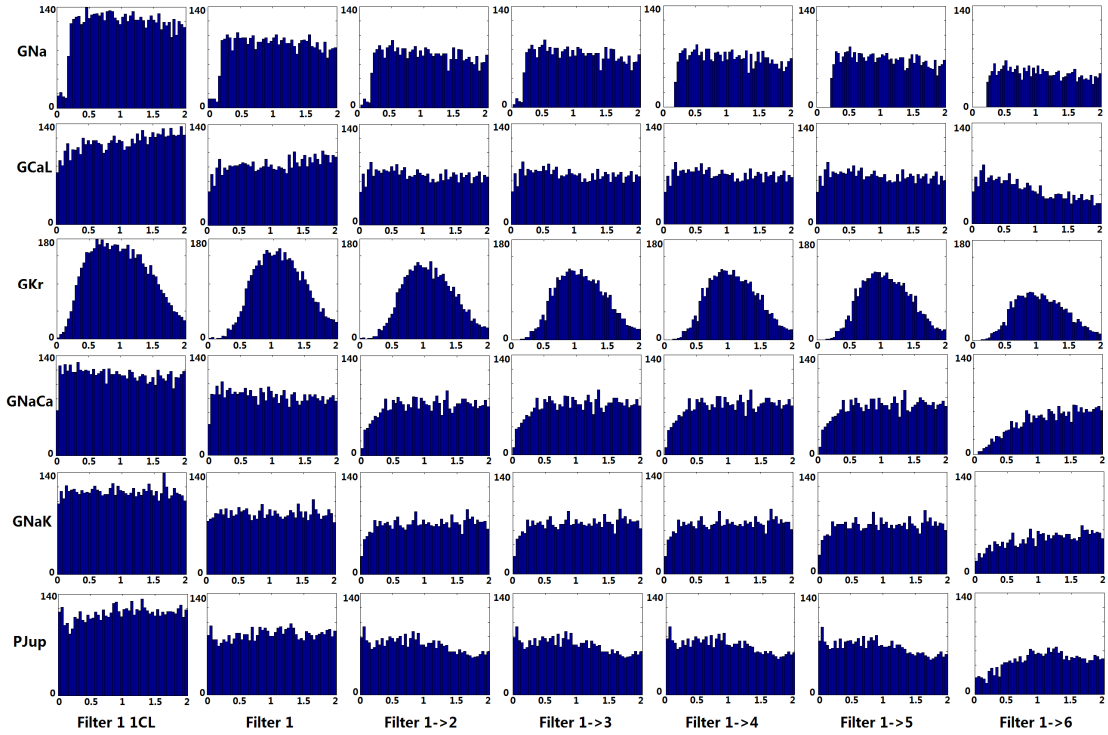


Figure 5.6: Evolution of accepted conductance scaling factors through calibration. The distributions of the accepted ionic parameters were determined by the calibration filters. Filter 1 mainly targeted the shape of G_{Kr}, whilst Filters 4 and 5 targeted G_{Na}. Filter 2 and especially Filter 6 constrained the shape of many Ca^{2+} related currents.

Filter 1 1CL: calibration results using only the physiological APD_{90} range at a CL of 600ms.

Filter 1: calibration results after using Filter 1 at all available CLs.

Filter 1→2: calibration results after using the first 2 calibration filters.

Filter 1→3: calibration results after using the first 3 calibration filters.

Filter 1→4: calibration results after using the first 4 calibration filters.

Filter 1→5: calibration results after using the first 5 calibration filters.

Filter 1→6: final calibration result (all filters considered).

5.3.3.4 Contribution of the ionic currents to action potential biomarkers

We also examined the correlation between individual parameters and different AP biomarkers, which are often the result of the nonlinear interaction of several currents.

The results were in agreement with established knowledge on the role of specific ionic currents on human electrophysiology: (i) big AP upstroke (Vmax and UPD) was related to large G_{Na}, whereas AP amplitude (APA) was also affected by G_{CaL}, G_{NaK} and smaller G_{to}; (ii) the resting membrane potential (RMP) was mainly determined by G_{K1} and G_{NaK}; (iii) higher cytosolic Ca^{2+} transient levels (CaTmax, CaTmin) were related to larger G_{CaL} and smaller G_{NaCa} and G_{NaK}; (iv) shorter Ca^{2+} transient duration (CaTD) was related to large G_{CaL} and P_{Jup}; (v) AP triangulation (APD_{tri}) was mainly determined by G_{CaL}; (vi) APD was positively correlated with G_{CaL} and negatively correlated with G_{Kr}, G_{Na} and G_{K1} (Figure 5.7).

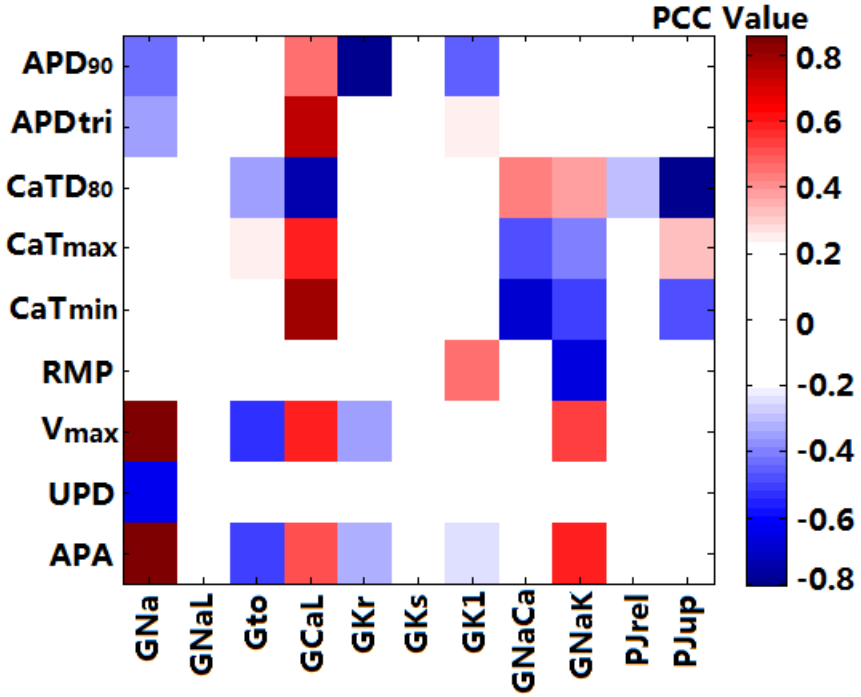


Figure 5.7: Partial correlation coefficients (PCC) between action potential biomarkers and current conductance parameters under CL=350ms.

5.4 Discussion and conclusions

In this study, an experimentally-calibrated population of human ventricular electrophysiology models was built based on the ORd model and *in vivo* epicardial ARI values obtained in patients. Less than 25% of the models were accepted after the calibration steps to mimic the large variability between more than 8000 *in vivo*

epicardial sites, and the percentage of accepted models can vary if a different baseline model is used. The main novelty and contributions of the population of human ventricular cell models are as follows:

1) It is the first biophysically-detailed population of human ventricular cell models that captures the variability of *in vivo* human recordings.
2) It represents a new technique to bridge the gap between human *in vivo* electrophysiological variability and mathematical modeling. In this study, the ARI data from AVR and CABG patients were used in the calibration, and similar method can be applied to patients with different pathological conditions to incorporate the corresponding cardiac variability. In addition, risk stratification of different patient groups can be achieved by generating subpopulation of models for a specific group.
3) This population-based approach provides a good platform for further analysis of normal and pathological conditions, as it includes many combinations and interactions of different sarcolemmal currents and intracellular ionic fluxes. Different from a single model approach, the population of models also allows for feasible statistical analysis to reduce the possibility of biased random results.

In the next chapters, we aim to use this population of human ventricular cell models of electrophysiology to investigate the ionic mechanisms underlying diseased conditions. As illustrated in Figure 5.1, cardiac alternans were also observed in the AVR and CABG patients without myocardial infarction. Therefore, our next step is to explore the ionic mechanisms underlying cardiac alternans within the population of models. In Chapter 6, the models displaying normal AP and alternans will be separated and compared, and ionic currents in the alternans models will be further investigated. Then we aim to explore the effects of potential ionic interventions on the inhibition of alternans in Chapter 7. Following this, the complexity of the electrophysiological system will be further increased by introducing the effect of genetic mutated ion channels. The interaction between genetic mutation of I_{Ks}

channel and cardiac variability of multiple current densities will be investigated in Chapter 8.

Chapter 6

Mechanisms underlying different rate dependent alternans types in human ventricular models

6.1 Introduction

In the previous chapter, we constructed a population of models of human ventricular cardiomyocyte electrophysiology, and then calibrated the population of models based on human *in vivo* ARI data. As illustrated in Figure 5.1, alternans in ARIs were detected on the epicardium of ventricles in the patients at fast pacing rates.

Cardiac alternans are stable beat-to-beat oscillations between subsequent APs, and are considered as an important risk factor for arrhythmogenesis (Armoundas *et al*., 2005, 2002; Merchant and Armoundas, 2012). The mechanisms underlying alternans have been the focus of extensive investigations to unravel their causes, modulators and implications for arrhythmias, such as ventricular and atrial fibrillation (Merchant and Armoundas, 2012). However, the majority of previous studies have been conducted on animal species including rat, rabbit, cat and dog, and therefore translation to human is compromised by inter-species differences in electrophysiology and calcium handling.

Cardiac alternans at fast pacing rates are known to be promoted by APD

prolongation and steep restitution, which involves beat-to-beat fluctuations in sarcolemmal ionic current availability (Clancy and Sato, 2013; Fox *et al*., 2002; Qu *et al*., 2010). However, APD alternans have also been observed clinically in the absence of APD prolongation and without a steep APD restitution curve (Narayan *et al*., 2007). The new paradigm based on animal studies is now supporting that APD alternans may be caused by fluctuations in calcium handling processes in individual myocytes (Cutler and Rosenbaum, 2009; Goldhaber *et al*., 2005; Merchant and Armoundas, 2012; Pruvot *et al*., 2004).

Important issues on APD alternans mechanisms still remain unresolved particularly in human. Firstly, the disturbances in the Ca^{2+} regulatory system responsible for calcium and APD alternans are likely to be multifactorial and modulated by a combination of Ca^{2+} transport processes. The most likely mechanisms point towards Ca^{2+} alternans caused by fluctuations in sarcoplasmic reticulum (SR) Ca^{2+} content (a rat experimental study) (Díaz *et al*., 2004) and/or refractoriness in ryanodine receptors (rabbit isolated cells and whole-heart experimental studies) (Picht et al., 2006; Wang et al., 2014), with modulating factors also including the strength of Ca^{2+} re-uptake through sarcoplasmic reticulum Ca^{2+} ATPase pump (SERCA) (guinea pig experimental study) (Cutler et al., 2009; Kanaporis and Blatter, 2014). The mechanisms in human ventricular myocytes are however unknown.

Secondly, the key mechanisms translating Ca^{2+} alternans to APD alternans in human ventricular myocytes still need to be identified. A large calcium transient would have opposite effects on the L-type calcium current (I_{CaL}) (through its calcium-dependent inactivation) and the sodium/calcium exchanger (I_{NaCa}) (through the potentiation of its forward mode). Therefore, the relative effect of intracellular calcium on both currents could determine whether a large calcium transient results in long or short APD. The balance between I_{CaL} and I_{NaCa} during repolarisation may differ in human ventricular cardiomyocytes with respect to other species, and cell-to-cell differences in conductances and permeabilities may modulate their role in APD alternans.

A key challenge in resolving these issues is the interpretation of findings from different animal species and cell types, and also obtained using different experimental conditions and interventions that, by aiming to segregate individual components, perturb the cellular system as a whole, depriving it of the integral phenomenon, as discussed by Valdivia (Valdivia, 2015). Furthermore, even careful studies performed with consistent cell types and experimental conditions exhibit differences both in the manifestation of cardiac alternans and their potential underlying mechanisms (Picht *et al*., 2006). Species differences and cell-to-cell variability in sarcolemmal conductances and permeabilities determine repolarisation differences in a dynamic process modulated by internal and external factors (such as neuronal stimulation and circadian rhythms) (Groenendaal et al., 2015; Jeyaraj et al., 2012; Taggart et al., 2011), which is also likely to determine cell-to-cell differences in the frequency in APD alternans generation.

Our aim in this study is to characterise *in vivo* and *in silico* APD alternans and to investigate the role of variability in ionic conductances and permeabilities in determining differences in APD alternans generation in human ventricular myocytes using *in silico* models. We hypothesize that in human ventricular cardiomyocytes, cell-to-cell variability in I_{CaL} and I_{NaCa} could explain the different types of APD alternans generation identified in *in vivo* recordings. We first characterise *in vivo* human APD alternans properties using electrophysiological recordings acquired for 6 stimulation frequencies at 240 sites of the epicardium of 41 human ventricles. In order to investigate the ionic mechanisms underlying human cell-to-cell differences in the occurrence and type of APD alternans, the population of human ventricular cell models constructed and calibrated in Chapter 5 is used in the investigation.

6.2 Methods

In order to take into account the natural variability in human cardiac electrophysiology, we used the population of human ventricular cell models generated and calibrated in the previous chapter. The accepted population of models were paced for 1000 beats under 6 CLs to reach steady state.

6.2.1 Definition of alternans

The occurrence of APD and CaTD alternans was defined as a difference greater than 5ms between the APD_{80}s (or $CaTD_{80}$s) of the last two APs at each pacing CL.

6.2.2 Sarcoplasmic reticulum calcium balance

A new property, called the sarcoplasmic reticulum calcium balance (SRCB), is defined and calculated as the overall Ca^{2+} flux through the SR:

$$\mathrm{SRCB} = \int (\mathrm{Jup} * \mathrm{Vcell_NSR} - \mathrm{Jrel} * \mathrm{Vcell_JSR})\, \mathrm{dt}$$

Here, SRCB>0 represents more SR Ca^{2+} re-uptake than release during a given pacing cycle, while SRCB<0 represents more Ca^{2+} release than re-uptake. SRCB magnitudes are represented as the absolute values of SRCB.

6.2.3 Sarcolemmal calcium balance

Another new property, called the sarcolemmal calcium balance (SCB), is defined and calculated as the overall Ca^{2+} flux through the cell membrane:

$$\mathrm{SCB} = \int [-(\mathrm{ICaL} + \mathrm{IpCa} + \mathrm{ICab}) + 2 * \mathrm{INaCa}]\, \mathrm{dt}$$

Here, SCB>0 represents more sarcolemmal Ca^{2+} inflow than outflow during a given pacing cycle, while SCB<0 represents more Ca^{2+} outflow than inflow. SCB

magnitudes are represented as the absolute values of SCB.

6.2.4 Action potential clamp simulation

For each single model displaying alternans, two protocols were generated from its steady state: two consecutive long beats (L+L) or two consecutive short beats (S+S). The simulation started from the end of the 1000^{th} beat, and then either the L+L protocol or the S+S protocol was applied.

6.2.5 I_{CaL} kinetics variation analysis

I_{CaL} activation time constant τ_d, inactivation time constant τ_f and recovery from Ca^{2+} dependent inactivation time constant τ_j were decreased (×50% or 75%) or increased (×125% or 150%) in the representative models, and models were still paced for 1000 beats to reach steady state.

6.2.6 Statistical analysis

Statistical analysis was performed using MATLAB. The Mann-Witney U test was used to determine the statistical differences in parameters and biomarkers. Pearson correlation was used to calculate the correlations.

6.3 Results

6.3.1 Key currents related to the generation of alternans

All the accepted models in the experimentally-calibrated population were divided into two groups (normal and alternans) depending on alternans occurrence. The nine

electrophysiological biomarkers described in Chapter 5 were also compared between normal models and alternans models (Figure 6.1A). There was no significant difference in the APDs between the normal group and the alternans group. APD triangulation (APD_{tri}) tended to be larger in the alternans group, which suggested that the shape of APs may play a role in alternans generation. APA and V_{max} were lower in the alternans group, and UPD was also found to be longer in the alternans group, which implied a role for the fast sodium current. Although CaTD was longer, CaT_{max} was found to be significantly smaller in the alternans group, which indicated the important role of Ca^{2+} dynamics in the generation of alternans.

Both normal and alternans group parameters were distributed across a broad sampling range (Figure 6.1B). G_{Na} and P_{Jup} were significantly smaller in the alternans group, whereas G_{CaL}, G_{Kr}, G_{NaCa} and P_{Jrel} were significantly larger in the alternans group compared to the normal subpopulation. Reduced I_{Na} conductance was consistent with lower APA, V_{max} and longer UPD in the alternans models, while stronger I_{CaL} corresponded to larger APD_{tri} values in the alternans group. In addition, stronger I_{NaCa} may also contribute to the smaller CaT level in the alternans models. These differences between normal and alternans parameters were independent on the 90 or 95% confident intervals in the ARI calibration process (Figure 6.1 C, D). Especially, G_{Na}, G_{NaCa}, P_{Jrel} and P_{Jup} were always significantly different between the normal and alternans groups (Figure 6.1D).

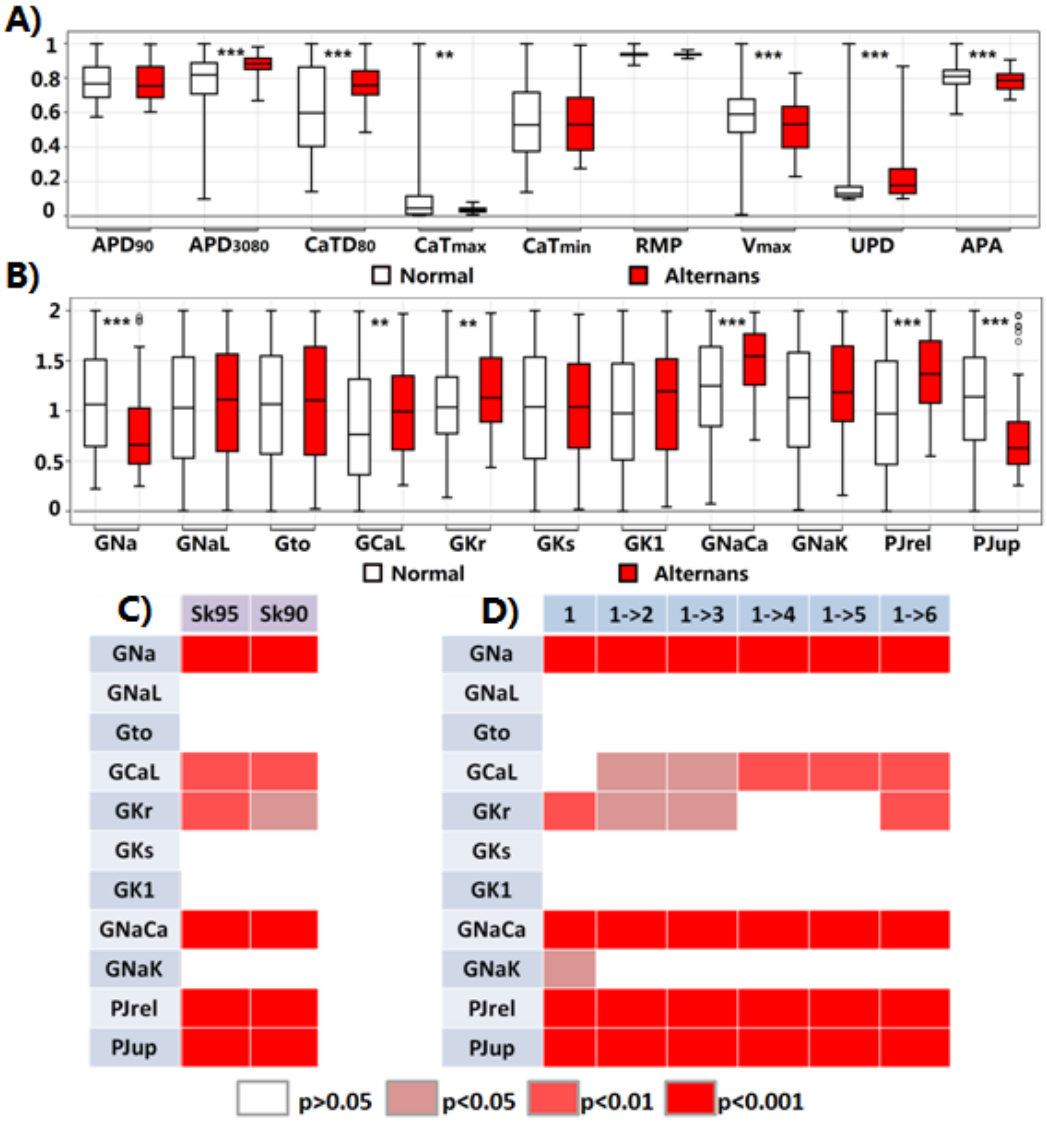


Figure 6.1: Key currents related to alternans. A) Comparison of the action potential biomarkers between normal and alternans models for CL=350ms. Vertical axis represents normalised biomarkers with respect to their maximum values; B) Comparison of conductance parameters between normal and alternans models. Vertical axis shows the scale of parameters: 0, 1 and 2, respectively representing -100%, 100% and +100% variations with respect baseline (*: $p<0.05$; **: $p<0.01$; ***: $p<0.001$); C) Parameters related to alternans when 90% or 95% confidence intervals of all ARI data were used in the calibration process; D) Parameters related to alternans during the calibration process after using 95% confidence intervals of ARI data in the first filter.

6.3.2 Two types of alternans are observed in both *in vivo* and *in silico* data

The analysis of APD alternans *in silico* and *in vivo* revealed similar patterns, and in both cases, two types were identified as illustrated in Figure 6.2A. Eye-type APD alternans were characterised by the disappearance of APD alternans at increasingly fast pacing rates (closed restitution bifurcation), whereas Fork-type APD alternans models displayed stable alternans at increasingly fast frequencies. 14 human models and 2012 *in vivo* events displayed Eye-type restitution, and 47 models and 2344 *in vivo* events were Fork-type for the frequencies tested both *in silico* and *in vivo*. The incidence of *in silico* alternans and *in vivo* alternans were not comparable since the population of models captured the overall variability observed *in vivo*, and there is no one-to-one correspondence between one model and one cell. *In silico*, we were able to increase frequency to confirm that most Fork-type restitution curves (44 out of 47) remained open when the pacing CLs were further decreased to 200ms. In addition, 26 models displayed calcium alternans with APD alternans smaller than 5ms in amplitude, named as CaT alternans models hereafter.

Both *in silico* and *in vivo*, APD alternans initiation started at longer CL in Eye-type alternans than in Fork-type alternans (median CL for APD alternans initiation: 550ms and 500ms *in vivo*, 475ms and 350ms *in silico*, respectively; with statistical differences $p<0.001$). Furthermore, both types of alternans occurred at similar diastolic interval (DI) and APD values than those exhibited by Normal models (Figure 6.2B), which further supports the independence of APD alternans from APD or DI values. The fact that similar patterns of alternans are observed both *in silico* and *in vivo* recordings confers credibility to mechanistic investigations using the population of *in silico* human cardiomyocyte models.

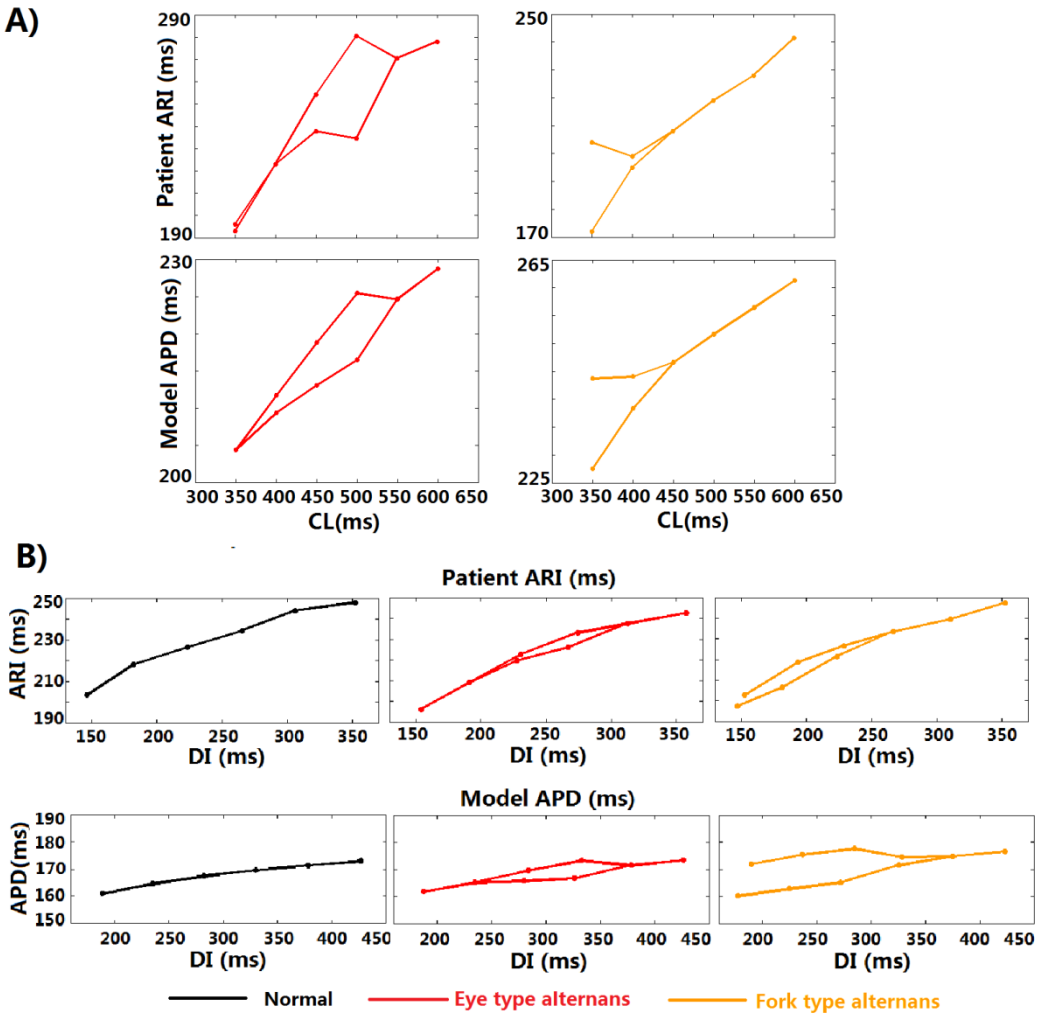


Figure 6.2: Types of APD alternans *in vivo* and *in silico*. A) Representative restitution curves of APD (ARI) *versus* CL exhibiting Eye-type and Fork-type alternans *in vivo* (upper panels) and *in silico* (lower panels) data. B) Representative restitution curves of APD (ARI) *versus* DI exhibiting normal condition, Eye-type and Fork-type alternans *in vivo* (upper panels) and *in silico* (lower panels) data.

6.3.3 APD alternans in the human ventricular models initiate following the loss of SR calcium content balance

As shown in Figure 6.3A-B, both Eye-type and Fork-type alternans models displayed larger SR Ca^{2+} release (P_{Jrel}) and smaller Ca^{2+} uptake (P_{Jup}) permeabilities than Normal models. Based on these data, we hypothesise that APD alternans initiation in the *in silico* human cardiomyocytes would be caused by fluctuations in

junctional SR (JSR) calcium content due to the inability of SERCA (J_{up}) to balance RyR Ca^{2+} release (J_{rel}) at fast frequencies. If found in the human models, the mechanisms would be consistent with previous measurements in rat and rabbit isolated cardiomyocytes (Díaz et al., 2004; Picht et al., 2006).

For all Alternans models, the SR calcium balance (SRCB) was calculated as the integral of calcium ions uptaken by SERCA (J_{up}) minus those released by RyR (J_{rel}) over each beat at each CL. For both Eye-type and Fork-type models, SRCB magnitude displays beat-to-beat fluctuations during APD alternans, with two consecutive beats leading to similar SRCB magnitudes but of different sign (Figure 6.3C). Figure 6.3D shows the magnitude of SRCB for one short APD beat for each CL for Eye-type and Fork-type alternans models. For the CLs leading to APD alternans, the SRCB magnitude increases above zero for both Eye and Fork-type alternans models (Figure 6.3D), and its magnitude strongly correlated with the APD alternans magnitude (correlation coefficient ranging 0.86-0.96 for all CLs).

The primary role of oscillations in calcium dynamics in generating APD alternans was confirmed by conducting simulated AP clamp experiments. We imposed the AP clamp of two identical long beats (L+L) and two identical short beats (S+S) to the Eye-type and Fork-type alternans models displaying the biggest alternans amplitudes (Figure 6.4). In the absence of APD alternans (imposed by the AP clamp), the Ca^{2+} alternans still persisted, which supported the conclusion that the oscillations of SR Ca^{2+} content existed independently of APD alternans. Therefore, our results support that APD alternans in the human models initiate due to the fluctuations in SR calcium content, which are then transferred to the membrane potential as APD alternans.

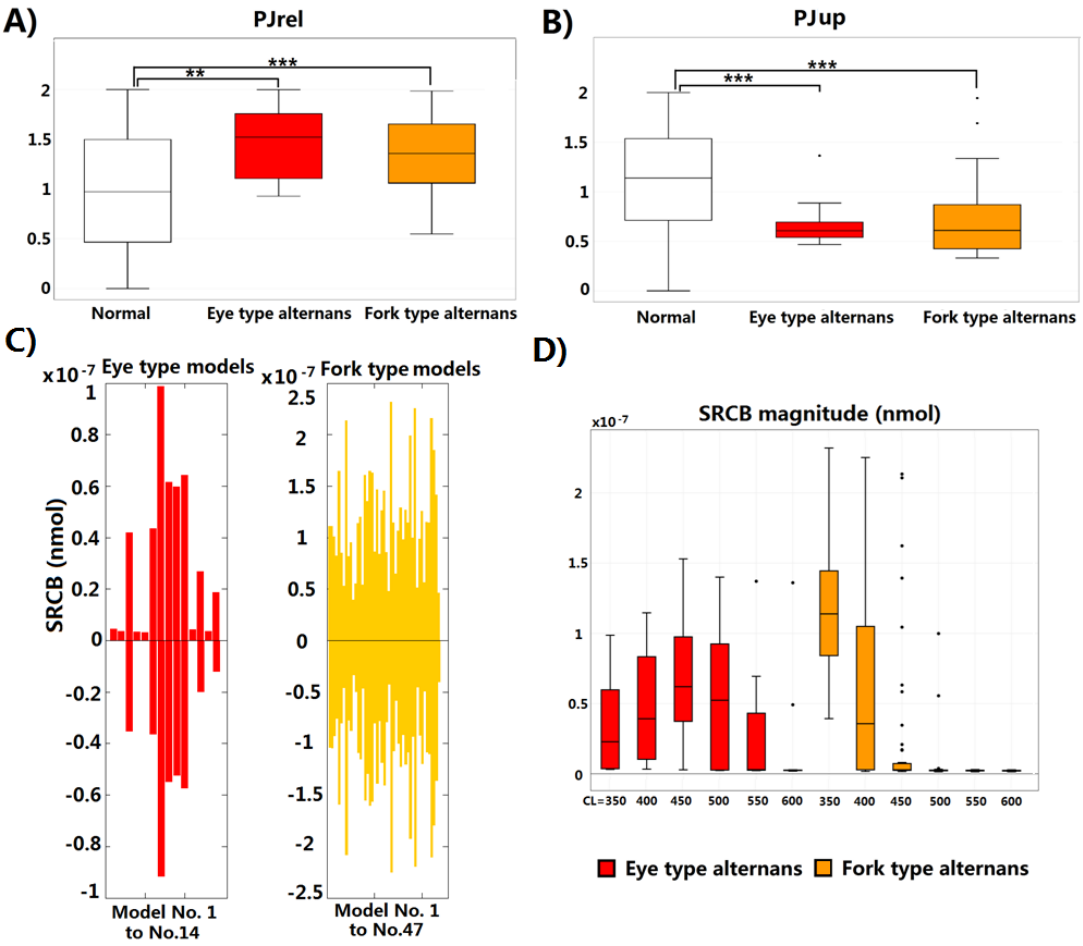


Figure 6.3: SR Ca^{2+} cycling properties and fluctuations in alternans models. Comparison of RyR release (P_{Jrel}, A) and SERCA uptake (P_{Jup}, B) in normal, Eye-type, and Fork-type alternans models. The vertical axis shows parameters scaling. Symbols indicate statistical significance levels (*: $p<0.05$; **: $p<0.01$; ***: $p<0.001$). C) Sarcoplasmic reticulum Ca^{2+} balance (SRCB) of the final two alternating beats in all APD alternans models (CL=350ms). The SRCB in long and short beats compensates for each other (same magnitudes with opposite signs). D) SRCB magnitudes for Eye-type and Fork-type alternans under all considered CLs.

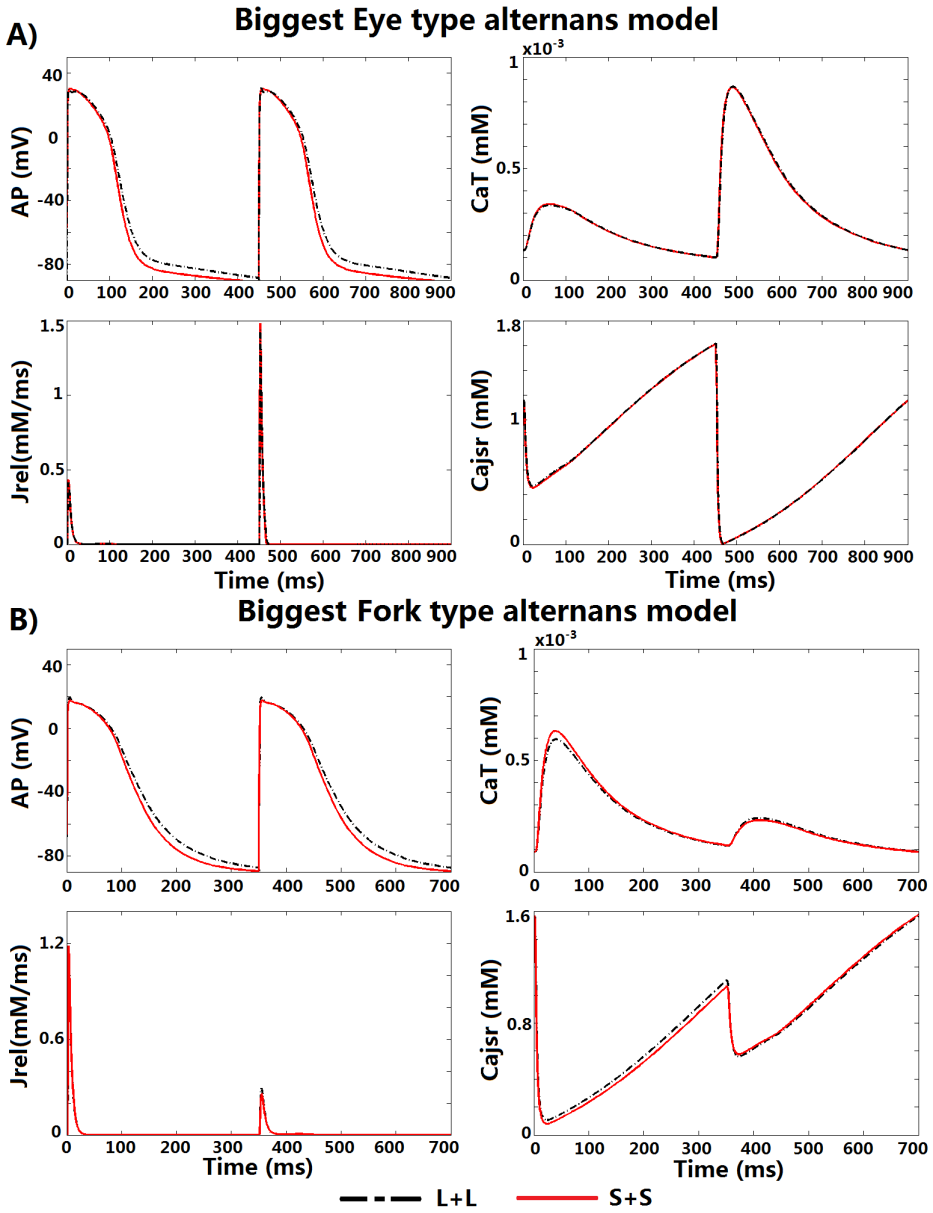


Figure 6.4: Action potential clamp simulations. Two identical long beats (L+L) or two identical short beats (S+S) were applied to Eye-type (A) and Fork-type (B) alternans representive models with biggest alternans amplitude.

6.3.4 Strong I_{NaCa} and fluctuations in SCB result in APD alternans in both Eye-type and Fork-type human models, and strong I_{CaL} restores SCB suppressing APD alternans at fast pacing rates for Eye-type models.

The mechanisms underlying the translation from calcium alternans to APD alternans were then investigated by further examining ionic differences between Normal and Alternans models. As shown in Figure 6.5A-B, the analysis of the *in silico* population reveals that the conductance of I_{NaCa} was significantly larger in both Eye-type and Fork-type models than in Normal models, whereas the I_{CaL} conductance was larger in Eye-type models compared to its similar magnitude in Fork-type and Normal models. A stronger I_{NaCa} in the human models could be expected to maximise the gain from calcium fluctuations to APD alternans, similar to findings in guinea pig myocytes (Wan *et al*., 2012). We therefore hypothesised that SRCB fluctuations would destabilise the intracellular calcium balance, which then propagated to the membrane potential in the form of APD alternans through a strong I_{NaCa} in Eye-type and Fork-type models.

For both Eye-type and Fork-type alternans models, Figure 6.5C showed the sarcolemmal Ca^{2+} balance (SCB) that was quantified as the integration of all the sarcolemmal calcium currents over one beat for each CL. Similar to SRCB, SCB magnitudes of the two alternating beats were practically equal but with different signs, which indicated that the overall calcium amount during the two beats was balanced (Figure 6.5D). As for SRCB, a strong correlation was found between the magnitudes of SCB and APD alternans in Fork and Eye-type alternans (correlation coefficient from 0.80 to 0.95).

The larger G_{CaL} in the Eye-type models resulted in stronger I_{CaL} and also larger CaT values than in Fork-type models, particularly for short CL <400ms (Figure 6.6). This led to the enhancement of SERCA at fast frequencies, which allowed for restoring SRCB and suppressing SR content fluctuations at fast pacing rates for Eye-type models.

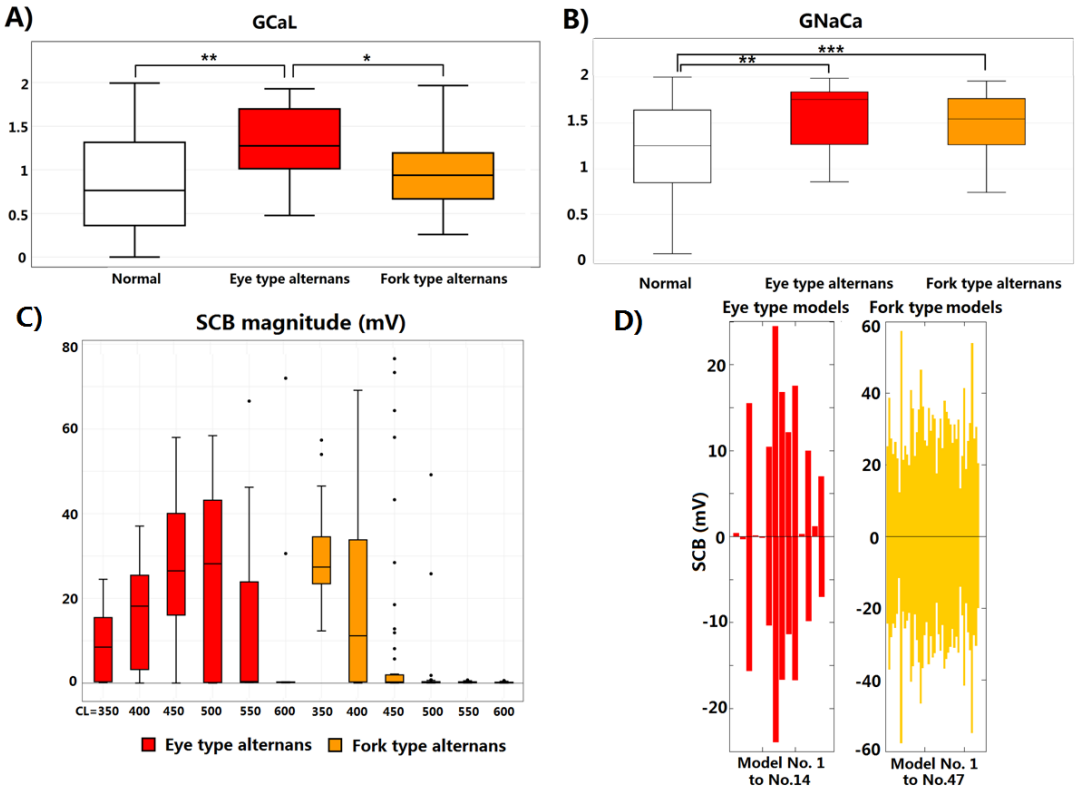


Figure 6.5: Sarcolemmal Ca^{2+} balance (SCB) in alternans models. Comparison of L-type Ca^{2+} channel conductance (G_{CaL}, A) and Na^{+}/Ca^{2+} exchanger conductance (G_{NaCa}, B) in normal, Eye-type and Fork-type alternans models. C) Sarcolemmal calcium balance (SCB) magnitudes for Eye-type and Fork-type alternans under all considered CLs. D) SCB of the final two alternating beats in all APD alternans models (CL=350ms). The SCB in long and short beats compensates for each other (same magnitudes with opposite signs).

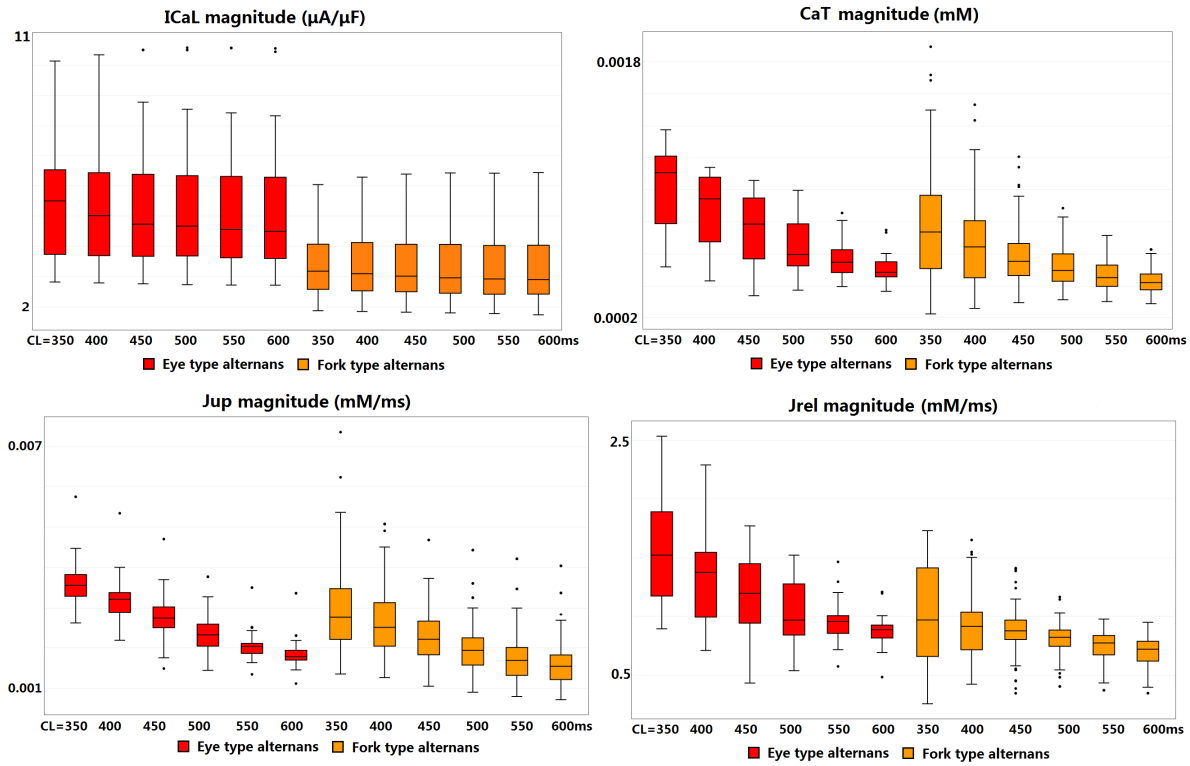


Figure 6.6: Rate dependency of I_{CaL} magnitude, CaT magnitude, J_{up} magnitude and J_{rel} magnitude.

6.3.5 Ionic mechanisms of APD alternans in human ventricular myocytes.

Figure 6.7 illustrated the network of events explaining alternans generation in the human ventricular myocytes. Figure 6.7A showed the time course of the transmembrane potential, JSR calcium level (Ca_{JSR}), J_{rel}, J_{up}, intracellular CaT, and sarcolemmal calcium currents for two consecutive beats for a representative Eye-type model for a long CL with no alternans (CL=600ms, left column), for a fast CL resulting in alternans (CL=500ms, middle column), and for a faster CL with no alternans (CL= 350ms, right column). Figure 6.7B provided a schematic representation of the ionic mechanisms involved, summarising the ionic mechanisms for long *versus* short APD beats.

Beat to beat fluctuations in the magnitude of all properties were only observed in the

central panels of Figure 6.7A, as fast and slow pacing rates lead to alternans disappearance in the Eye- type model (left and right columns, respectively). During the long APD beat (blue dashed lines, first row), Ca_{JSR} (second row) reached a low level following SR release (third row), and then it progressively recovered due to SR re-uptake (fourth row). However, the next beat started before the Ca_{JSR} levels reached its initial value and this resulted in a lower Ca_{JSR} level at the start of the next beat (second row, compare red solid and blue dashed lines). The consequence for the next beat was a lower J_{rel} (third row, red solid lines), leading to a higher minimum Ca_{JSR} value (second row). The reuptake gradually recovered Ca_{JSR} content, which in this beat reached a higher level at the end than at the start of the beat (red solid line, second row). The next beat would therefore start with higher Ca_{JSR} as in the blue dashed line, continuing the oscillations in Ca_{JSR} and SRCB as identified in Figure 6.3.

The beat-to-beat fluctuation in J_{rel} led to intracellular CaT level oscillations (Figure 6.7A, fifth row, middle column), which further resulted in the alternation of calcium related sarcolemmal currents such as I_{CaL} (sixth row, middle column) and I_{NaCa} (seventh row, middle column). For the beat with a higher initial Ca_{JSR} level and stronger J_{rel} (dashed blue lines), the amplitude of CaT was also higher. The fluctuation in intracellular Ca^{2+} content did not affect the I_{CaL} amplitude, in agreement with a number of studies showing peak I_{CaL} was unchanged during alternans (Díaz et al., 2004; Merchant and Armoundas, 2012; Picht et al., 2006). However, it led to a faster calcium induced inactivation of I_{CaL} (sixth row), therefore reducing the overall inward current. However, this was overridden by the calcium induced potentiation of the forward-mode activity of I_{NaCa} (seventh row, middle column), which implied an increased inward current, and resulted in longer APD (first row). I_{NaCa} was therefore the main electrogenic mechanism driving APD alternans in the human ventricular models.

The third column in Figure 6.7A illustrated the mechanisms underlying the

disappearance of Ca_{JSR} fluctuations at faster CL for Eye-type models. As the CL was further decreased (third column), Ca^{2+} concentration increased due to the well-known Ca^{2+} accumulation at fast pacing rates, as reproduced by the models (fifth row). Increased Ca^{2+} levels enhanced SR reuptake (fourth row) and speed up the recovery of Ca_{JSR} levels (second row) enabling for Ca_{JSR} levels to reach their initial values at the end of each beat. Therefore, fluctuations in Ca_{JSR} levels disappeared at fast pacing rates as a result of rate dependent calcium accumulation. Eye-type models displayed stronger I_{CaL} conductances than Normal and Fork-type models, and this also resulted in larger intracellular calcium levels at fast pacing rates (Figure 6.6). This was the reason why APD alternans were suppressed at fast pacing rates in Eye-type models.

Our simulations also explained the mechanisms underlying the occurrence of CaT alternans without significant APD alternans (< 5ms) in the 26 CaT alternans models. Calcium fluctuations were due to the same mechanisms as in the Eye-type and the Fork-type APD alternans models but the magnitude of the oscillations in SRCB was smaller and did not result in significant APD alternans due to a modest G_{NaCa} similar to that in the Normal models.

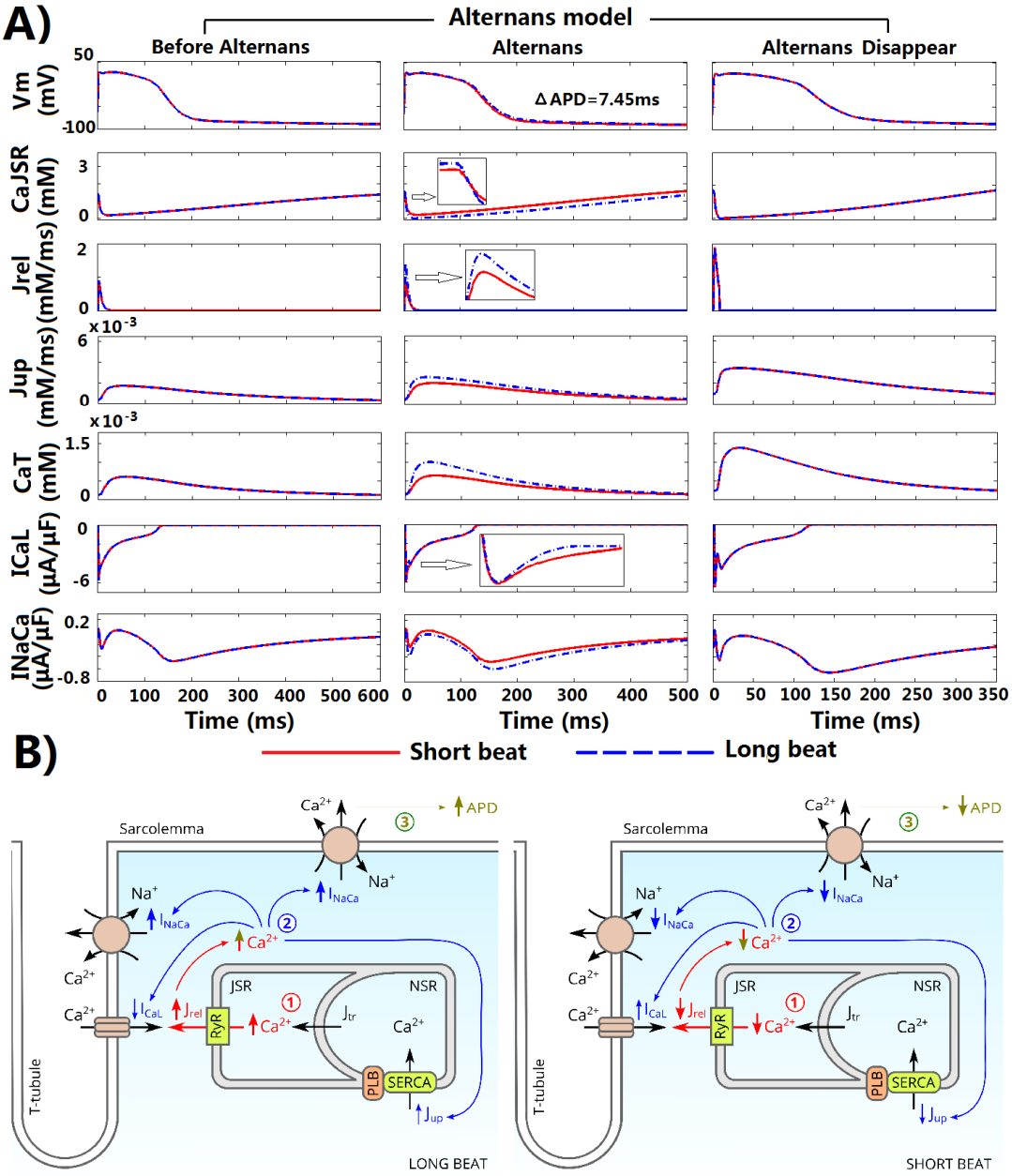


Figure 6.7: Ionic mechanisms resulting in APD alternans in human *in silico* ventricular cardiomyocytes. A) From top to bottom, transmembrane potential (Vm), Ca^{2+} concentration in JSR (Ca_{JSR}), Ca^{2+} release via RyR (J_{rel}), Ca^{2+} re-uptake via SERCA (J_{up}), intracellular Ca^{2+} transient (CaT), L-type Ca^{2+} current (I_{CaL}) and Na^{+}/Ca^{2+} exchanger current (I_{NaCa}) in a representative Eye-type model before the generation of alternans (CL=600ms, left column), during alternans (CL = 500ms, middle column) and alternans disappearance (CL=350ms, right column). B) Schematic diagram illustrating the network of events explaining APD alterans for long and short beats: In (1), larger/smaller Ca_{JSR} levels at the start of the beat, results in larger/smaller J_{rel} and intracellular Ca^{2+} levels (2), leading to (3) increase/decrease in inward current through the I_{NaCa} forward mode, and a smaller decrease/increase in inward current through I_{CaL} calcium induced inactivation.

6.3.6 I_{CaL} kinetics variation can affect alternans by regulating SCB and SRCB

Given the role of I_{CaL} in modulating SCB and its importance in alternans generation, we investigated the effects of variations in I_{CaL} kinetics in modulating APD alternans and the sarcolemmal and SR calcium balances. Simulations were conducted for varying I_{CaL} activation, inactivation and recovery from Ca^{2+} dependent inactivation time constants in representative models, including the Eye-type and Fork-type models displaying the largest APD alternans. In this new set of simulations we also considered the original ORd model and the two models in the Normal population exhibiting the longest and shortest APD values, respectively. Variations in kinetics time constants of ±50% were considered to investigate theoretical mechanisms rather than representing specific pathological situations.

Alternations of I_{CaL} kinetics did not produce alternans in any of the Normal models considered. However, as shown in Figure 6.8, in both the Eye-type and Fork-type alternans models, variations particularly in I_{CaL} inactivation kinetics modulate the propensity of alternans generation. In all cases, APD alternans magnitude was still very strongly correlated with SCB and SRCB (R^2> 0.96), further supporting the mechanisms unraveled in the previous sections. For the Eye-type model, slower I_{CaL} inactivation kinetics (increase in τ_f and τ_j) decreased APD alternans because it increased an already strong I_{CaL}, leading to further Ca^{2+} accumulation and increased SERCA activity, therefore stabilising SRCB and SCB (Figure 6.8 A, C). For the Fork-type model however, the biggest effect was seen for fast inactivation (decrease in τ_f and τ_j) that decreased APD alternans by decreasing I_{CaL} and consequently J_{rel}, making it easier for SERCA to stabilise SRCB (Figure 6.8 B, D). The I_{CaL} conductance is therefore key to determinine the effect of its inactivation kinetics in alternans generation, as it modulates the balance between the effect of I_{CaL} on both

J_{rel} and the intracellular Ca^{2+} content, both of which are frequency dependent.

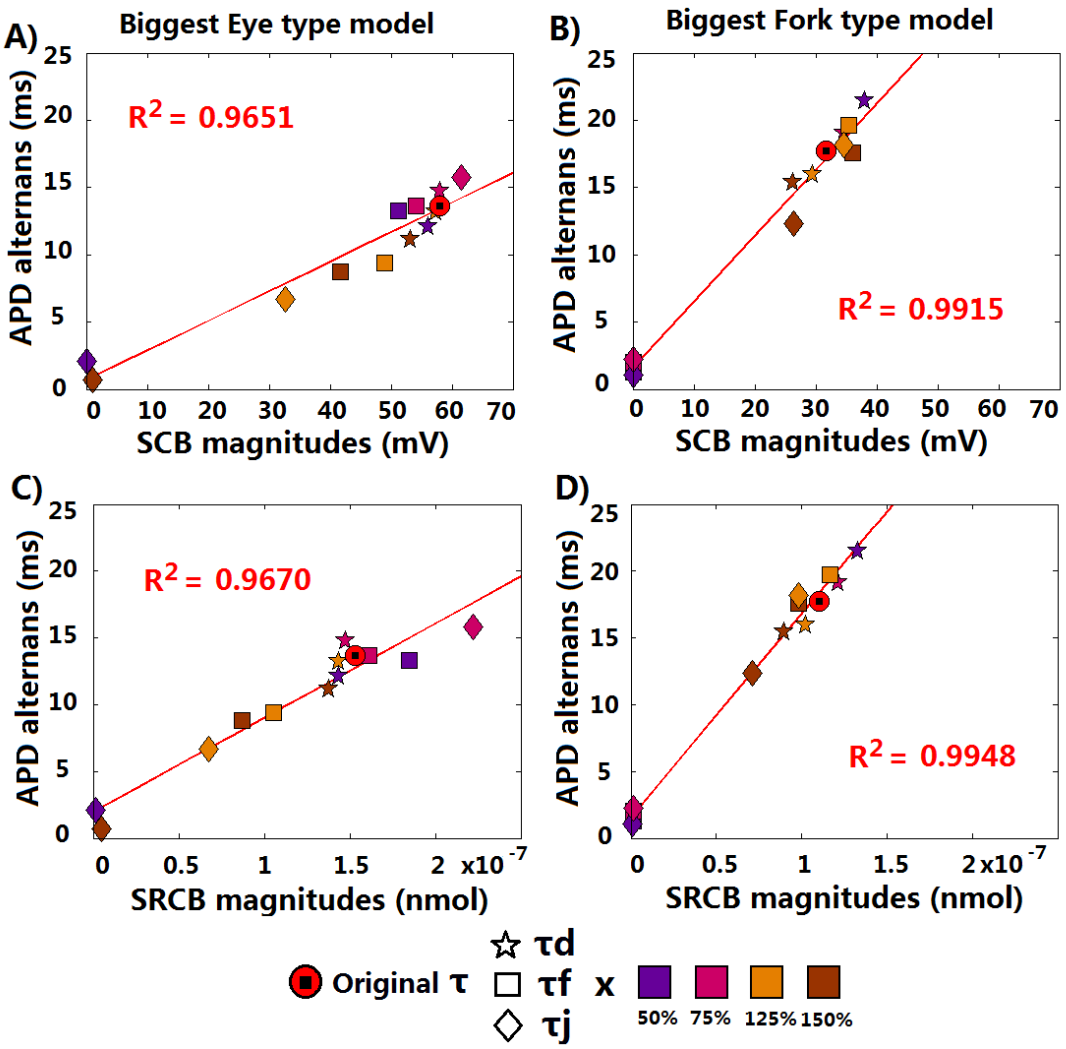


Figure 6.8: Effects of varying I_{CaL} kinetics on the Eye-type and Fork-type models with biggest alternans magnitudes. Correlation between APD alternans magnitudes and SCB magnitudes in the Eye-type model with biggest alternans (A) and the Fork-type model with biggest alternans (B). Correlation between SRCB magnitudes and APD alternans magnitudes in the biggest Eye -type model (C) and the biggest Fork-type model (D). Stars, squares and diamonds represent the variation of I_{CaL} activation (τ_d), inactivation (τ_f) and recovery from Ca^{2+} dependent inactivation (τ_j) time constants, respectively. Colours represent changes in time constants magnitude. The red circle with a square inside represents the original kinetics.

6.3.7 I_{Na} and I_{Kr} can affect alternans by regulating I_{NaCa} activity

The above analysis identified that the balance between calcium release from SR (J_{rel})

and calcium re-uptake to SR (J_{up}) played crucial roles in the initiation of calcium fluctuation, and I_{CaL} and I_{NaCa} can significantly affect the translation from calcium alternans to APD alternans through the modulation of the membrane SCB. Apart from the four currents and fluxes analyzed above, the conductance of I_{Na} (G_{Na}) was also found to be significantly weaker in the Alternans models compared to the Normal group (Figure 6.1B). The effect of I_{Na} on calcium fluctuation in cardiomyocytes can be related to its relationship with I_{NaCa}. For instance, during the alternation of APD and I_{NaCa} (Figure 6.9A-B), we also observed the fluctuation of intracellular Na^+ (Figure 6.9C) together with the alternation of peak I_{Na} magnitude (Figure 6.9D). The stronger I_{NaCa} forward-mode activity during the longer beat (Figure 6.9B, blue dashed line) led to a higher intracellular Na^+ concentration at the end of AP (Figure 6.9C, end of blue dashed curve), which resulted in a smaller I_{Na} peak for the next shorter beat (Figure 6.9D, red solid curve). Similarly, the weaker I_{NaCa} during the shorter beat (Figure 6.9B, red solid curve) corresponded to smaller intracellular Na^+ concentration (Figure 6.9C, red solid curve) and a bigger I_{Na} peak for the longer beat (Figure 6.9D, blue dashed curve). Therefore, I_{Na} could take part in the alternation process through the regulation of Na^+. If I_{Na} is weak, the intracellular Na^+ concentration will be smaller, which can promote the augmentation of forward-mode I_{NaCa}, facilitating calcium extrusion and alternans development.

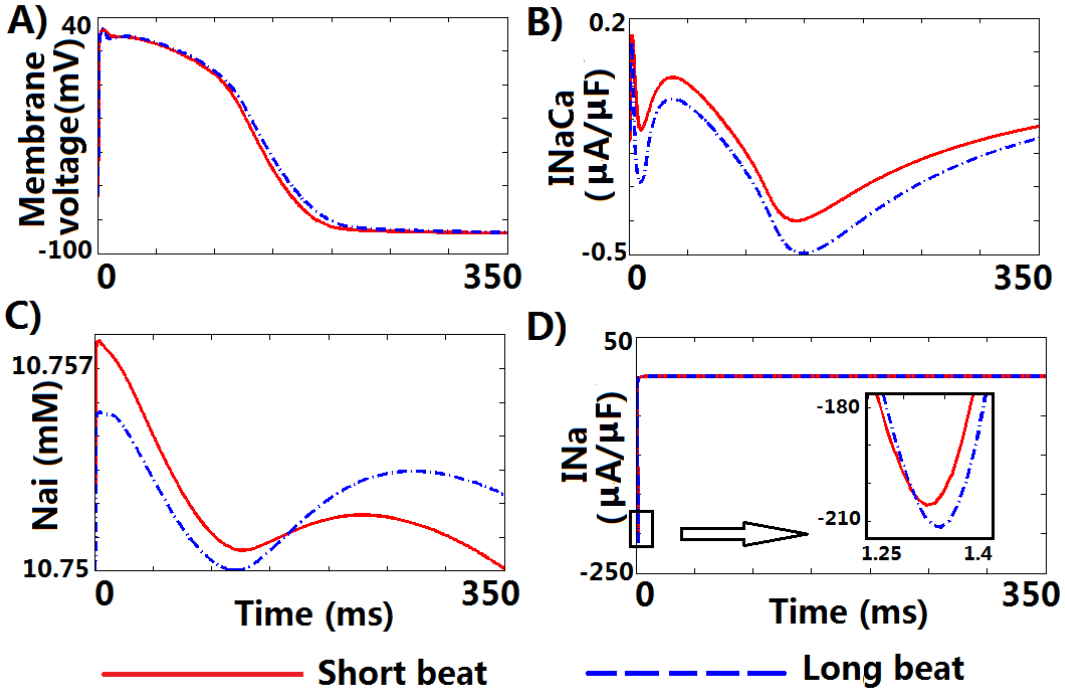


Figure 6.9: Sodium currents fluctuation analysis between long/short alternating beats in a representative model of cardiac alternans. A) transmembrane voltage. B) Na^+/Ca^{2+} exchanger current (I_{NaCa}). C) Intracellular Na^+ concentration (Na_i). D) Fast Na^+ current (I_{Na}).

Finally, stronger I_{Kr} conductance was also observed in the alternans models (Figure 6.1B). The stronger I_{Kr} can compensate the APD prolongation caused by the stronger I_{CaL}, which helped to maintain the physiological APD in the Eye-type alternans models. In addition, I_{Kr} can also affect the calcium fluctuation through the voltage-dependent regulation of I_{NaCa}. Figure 6.10 showed that modulation of I_{Kr} cannot significantly affect CaT levels. But as a repolarising current, stronger I_{Kr} can promote the depolarising forward-mode activity of I_{NaCa}; while weaker I_{Kr} had the opposite effect. Therefore, I_{Kr} can also affect the translation from calcium alternans to APD alternans through voltage-dependent regulation to I_{NaCa}.

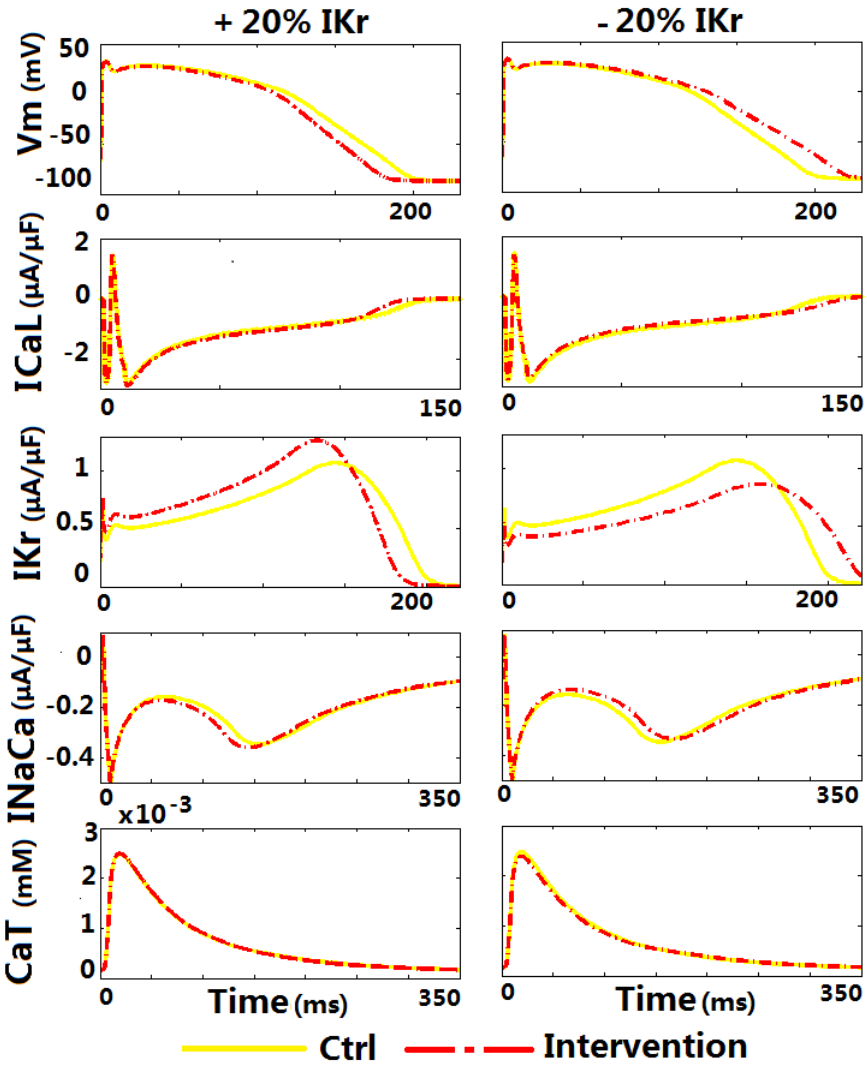


Figure 6.10: Effects of I_{Kr} modulation in the original ORd model.

6.4 Discussion and conclusions

In this study, we unravelled the mechanisms and network of events leading to the occurrence of two types of APD alternans identified in novel human ventricular *in vivo* and *in silico* electrophysiological data. Variability in ionic conductances and permeabilities is shown to determine how human membrane kinetics translates calcium fluctuations into APD alternans. This study presents two main methodological novelties including the focus on human both *in vivo* and *in silico*, and the investigation of mechanisms of APD alternans considering physiological variability. Our main findings are:

1) Both *in vivo* and *in silico* human ventricular cardiomyocytes display two types of APD alternans with Eye-type (closed bifurcation curve) and Fork-type restitution (open bifurcation curve). Similarities between human *in vivo* and *in silico* alternans lend credibility to the computational investigations on the underlying mechanisms. Both types of APD alternans are observed for long diastolic intervals (>270ms) and with normal (rather than prolonged) APD.
2) APD alternans in the *in silico* human cardiomyocyte population are consistently associated with fluctuations in SR Ca^{2+} content due to weak SERCA and strong RyR release, and translated into fluctuations in sarcolemmal Ca^{2+} balance and APD through a strong I_{NaCa}. Therefore, variability in ionic conductances and fluctuations do not explain alternative sources of Ca^{2+} alternans (such as RyR refractoriness), which still remain to be shown in human ventricular myocytes.
3) At increasingly fast frequencies, APD alternans disappear in Eye-type cardiomyocytes due to a strong I_{CaL}, which leads to a frequency-induced increase in intracellular calcium levels that promotes SERCA and restores SR content balance.
4) I_{CaL} conductance determines the effect of alterations in I_{CaL} inactivation kinetics in APD alternans, as it determines the balance between I_{CaL} effects directly on SCB and indirectly in SRCB through intracellular Ca^{2+} content and J_{rel}.

6.4.1 Fluctuations in SR Ca^{2+} content as a primary cause of APD alternans in human ventricular cardiomyocytes

Recent studies have reported that although there is bi-directional coupling between membrane voltage and CaT, APD alternans tend to be the secondary consequence of Ca^{2+} cycling disturbance (Kanaporis and Blatter, 2014). The relationship between SR

Ca^{2+} load and Ca^{2+} release on calcium alternans was proposed by Eisner *et al.* (Eisner *et al*., 2000). A steep Ca^{2+} release-SR Ca^{2+} load relationship was used to explain the generation of calcium alternans (Eisner *et al*., 2000). Our *in silico* analysis also revealed weaker Ca^{2+} re-uptake and stronger Ca^{2+} release in all types of Alternans models (Figure 6.3), even considering variability in ionic conductances and permeabilities in the simulations. The role of SR Ca^{2+} re-uptake in our results in human is consistent with the experimental observation that overexpression of SERCA2a suppresses alternans (Cutler *et al*., 2012, 2009; Xie *et al*., 2008), whereas the suppression of SR Ca^{2+} release has also been shown to inhibit APD alternans in rabbit myocytes (Kanaporis and Blatter, 2014).

In our human ventricular Alternans models, fluctuations in SR Ca^{2+} content can lead to Ca^{2+} and APD alternans, and this is in agreement with recordings in rat and rabbit isolated cell experiments (Díaz *et al*., 2004; Picht *et al*., 2006). Recordings in rabbit myocytes and intact hearts (Picht *et al*., 2006; Wang *et al*., 2014) have shown that in some cardiomyocytes, Ca^{2+} alternans can occur in the absence of SR Ca^{2+} content fluctuations due to RyR refractoriness during fast pacing. This was not observed in our human population triggering the following thoughts. Firstly, the human population study explored variability in ionic conductances and permeabilities, and SR Ca^{2+} content fluctuations were consistently observed during APD alternans. This suggests that differences in the mechanisms of Ca^{2+} alternans (SR Ca^{2+} fluctuations *versus* RyR refractoriness) are likely not to be explained simply by differences in ionic protein expression. Secondly, new experiments are required to evaluate the potential contribution of RyR refractoriness to alternans in human ventricular myocytes. The ORd model used to construct the population is able to reproduce key properties of Ca^{2+} cycling rate dependence as measured in human experiments, including frequency modulation of SR Ca^{2+} release, uptake and content, modulated by Ca^{2+}/calmodulin-dependent protein kinase II. Future experimental and theoretical studies are required to evaluate the need for updates in the complex calcium cycling framework, such as the calcium release units, to address the contributions of the '3R'

theory from calcium alternans to APD alternans (Qu *et al*., 2013; Rovetti *et al*., 2010).

6.4.2 Sarcolemmal calcium balance translates Ca^{2+} fluctuations into APD alternans in human ventricular cardiomyocytes

Our human ventricular population showed that I_{NaCa} was larger in Alternans than in Normal models. Furthermore, we found that the increase of CaT amplitude and long APD beats were in-phase for 95% of the models (Figure 6.7), as was shown by Wang *et al.* in intact rabbit hearts (Wang *et al*., 2014). An increase in CaT levels can induce both calcium-induced I_{CaL} inactivation (decrease inward current and shortening of APD) and increase of forward-mode I_{NaCa} (increase in inward current and prolongation of APD). Therefore, higher CaT corresponding to longer APD in our human models suggests that the forward-mode I_{NaCa} plays a more dominant role in prolonging APD for high calcium levels in the human ventricular myocytes, as in (Escobar and Valdivia, 2014).

Furthermore, interventions that promote the forward mode of I_{NaCa} may promote APD alternans. This can also be caused through its sensitivity to Na^+ shown in Figure 6.9. Another theoretical study using canine models also showed that suppressing I_{Na} can produce larger APD alternans (Fox *et al*., 2002). In our simulation results, fluctuations in I_{Na} and Na^+ concentration were tightly linked with the alternation of I_{NaCa} during APD alternans, supporting the additional sensitivity of APD alternans to sodium content.

Even though peak I_{CaL} does not fluctuate during APD alternans in the human ventricular models (Merchant and Armoundas, 2012), we show that both conductance and kinetics of I_{CaL} modulate APD alternans in human ventricular myocytes both through the direct electrogenic effect of I_{CaL} on membrane potential,

and through indirect effects on intracellular Ca^{2+} content (that determines SR release and uptake). Strong I_{CaL} as in Eye-type models results in larger Ca^{2+} accumulation at fast pacing rates, which promotes SERCA and leads to re-stabilisation of SR content and disappearance of APD alternans. Alterations in I_{CaL} inactivation kinetics can also modulate APD alternans, and their effect is different depending on the overall conductance of I_{CaL}, as shown in Figure 6.8.

6.4.3 Limitations

Rather than a single *in silico* model, the present study is built on a population-based *in silico* and *in vivo* approach, allowing the investigation of different alternans types in human ventricular cells and their common underlying mechanisms. Still, there are several limitations in this work: 1) *in vivo* information from AVR or CABG patients were used in this study, and we did not attempt to specifically model the pathologies of each patient. Instead, we varied the ionic properties of the ORd model in a wide range to investigate the contribution of variability in ionic conductances and permeabilities to explaining different APD alternans regimes. The *in silico* human models did predict similar alternans patterns at similar CLs to the *in vivo* data, supporting the validity of the methodology used. While we believe that ORd is currently the best model for the purposes of this study, the findings might be model specific. 2) Only epicardial models and recordings were considered in the study due to the difficulties in acquiring simultaneous epicardial and endocardial recordings *in vivo* in human. 3) Although ARI is widely accepted as a surrogate for APD, as all indirect measurements it may be affected by a bias. 4) In this study, we only considered the variability in ionic conductances and permeabilities. However, variability may also exist in current kinetics as a result of differences in protein structure and conformation (especially in the presence of genetic mutations). It is possible that alternans can also emerge from the kinetics of some currents, and for example RyR refractoriness as was shown in some rabbit ventricular cardiomycoytes

(Picht *et al*., 2006; Qu *et al*., 2013; Wang *et al*., 2014). Further experiments would need to confirm the contribution of RyR mechanisms in human. 5) Alternans in whole-ventricles are caused and modulated by a variety of factors, including gap junctional coupling, tissue heterogeneity and conduction velocity restitution (through for example I_{Na} recovery from inactivation). Further studies could focus on determining the interaction of the calcium-driven mechanisms of Eye-type and Fork-type alternans unravelled in our study with those additional factors in tissue.

Chapter 7

Effects of current interventions on the stability of different types of alternans models

7.1 Introduction

In the previous chapter, we investigated the mechanisms underlying the initiation and maintenance of alternans in the absence of APD prolongation. We also reported two types of APD alternans observed in both *in vivo* and *in silico* conditions. The generation of alternans is a complex process that involves an intricate network of multiple factors. The initiation of both Eye-type and Fork-type APD alternans in human ventricular cardiomyocytes is due to the disruption of SR Ca^{2+} balance (SRCB) and SR Ca^{2+} fluctuations caused by strong SR Ca^{2+} release (J_{rel}) and weak Ca^{2+} re-uptake (J_{up}). The sodium-calcium exchanger current (I_{NaCa}) acts as the main translator between Ca^{2+} alternans and APD alternans, and the sarcolemmal Ca^{2+} balance (SCB) is a good indicator of APD alternans magnitude. The disappearance of the Eye-type alternans at fast pacing rates was due to the potentiation of J_{up} and the restoration of SRCB induced by stronger I_{CaL}. Based on the mechanisms underlying the different subtypes of alternans, further studies need to be conducted to explore potential pharmacological interventions that might be beneficial in alternans inhibition. The ionic differences between Normal and Alternans models provided a good starting point for the investigation of such anti-arrhythmic strategies.

In Chapter 6, differences in current conductances or permeabilities were found in six of the main currents and fluxes between Normal and Alternans groups. G_{Na} and P_{Jup} were found to be smaller in Alternans group than in Normal group, while G_{CaL}, G_{Kr}, G_{NaCa} and P_{Jrel} were found to be larger. Therefore, enhancing I_{Na} and J_{up} or inhibiting I_{CaL}, I_{Kr}, I_{NaCa} and J_{rel} constitute plausible targets for alternans suppression. Experimentally, stronger I_{Na} can be induced by sodium channel activators, such as batrachotoxin and veratridine (Tikhonov and Zhorov, 2005), whereas stronger J_{up} can be achieved through SERCA2a genetic therapy (Hayward *et al*., 2015). The suppression of I_{CaL} and I_{Kr} can be achieved by applying Class IV (Ca^{2+} channels blockers) and Class III (K^{+} channel blockers) agents. Ryanodine and recently developed selective I_{NaCa} inhibitors (N. Jost et al., 2013) can be used to block the activity of RyR and the sodium-calcium exchanger, respectively.

The efficacy of these pharmacological targets can be investigated and compared using our experimentally-calibrated population of human *in silico* alternans models, as described in Chapter 6. Because of the ionic differences between different types of alternans models, their response to a same pharmacological intervention may be different; therefore, the population of alternans models also represents a suitable tool for the investigation of pharmacological action. Therefore, the aim of this part of the work is to further develop the use of the population of alternans models described in Chapter 6 to investigate the effects of different pharmacological treatments.

In this part of the work, we first compared the effects of all the above six interventions in alternans suppression. Inhibiting I_{NaCa}, I_{CaL} or enhancing J_{up} by 30% exhibited larger efficacy in alternans suppression than the rest of considered interventions. The effects of blocking I_{NaCa}, I_{CaL} and increasing J_{up} were then further explored and compared under different intervention levels.

7.2 Methods

The 87 models exhibiting alternans in Chapter 6 were used in this chapter to simulate the effect of different pharmacological interventions. The same simulation protocols and biomarker calculation algorithms were used as in Chapter 5 and Chapter 6. Different levels of interventions were achieved by introducing scaling factors to multiply the original current densities. This was equivalent to a single-pore block of drug action (Brennan *et al*., 2009).

7.3 Results

7.3.1 Comparison between the effects of different current interventions

Table 7.1 shows the comparison of median parameters between Normal and different subtypes of alternans. The differences with statistical significance ($p<0.05$) between alternans with respect to normal models are highlighted in bold. Eye-type models had stronger I_{CaL}, I_{Kr}, I_{NaCa} and J_{rel}, and weaker I_{Na} and J_{up} than the Normal models. Different from the Eye-type models, Fork-type models and CaT models had similar levels of G_{CaL} and G_{Kr} as normal. In addition, although showing differences in SR flux permeabilities, CaT models did not show a significant increase in G_{NaCa}, which explains the existence of Ca^{2+} alternans and small APD alternans in these models.

Median	GNa	GCaL	GKr	GNaCa	PJrel	PJup
Normal	100%	100%	100%	100%	100%	100%
Eye-type alternans	54%	167%	138%	140%	157%	53%
Fork-type alternans	76%	123%	104%	123%	140%	53%
CaT alternans	52%	119%	118%	113%	141%	64%

Table 7.1: Comparison of the medians of six current conductances and permeabilities between Normal, Eye-type alternans, Fork-type alternans and CaT alternans, relative to Normal models.

Figure 7.1 showed the resulting percentage of alternans types as well as the change of SCB and SRCB before and after the considered interventions. Initially, 54% of the alternans models were Fork-type, 16% of the alternans models were Eye-type, and 30% of the alternans models were CaT models (Figure 7.1A). Upon G_{Na} or PJ_{up} increase, or G_{CaL}, G_{Kr}, G_{NaCa} and P_{Jrel} decrease by 30%, the results showed that all of the six identified current interventions can convert different fractions of alternans models into non-alternating models (Figure 7.1B-G). The suppression of alternans was always accompanied by the recovery of SCB and SRCB, indicating the credibility of the mechanisms unraveled in Chapter 6.

Activating I_{Na} by 30% can inhibit 36% of the alternans models, with 7%, 44% and 14% of the models remaining Eye-type, Fork-type and CaT alternans models, respectively (Figure 7.1B). A modest decrease of SCB and SRCB magnitudes was observed after the intervention. Stronger I_{Na} can increase the intracellular Na^+ level, and therefore indirectly regulating SCB and SRCB by affecting I_{NaCa}.

Decreasing G_{CaL} by 30% successfully inhibited 63% of alternans models (Figure 7.1C). This was consistent with the results in Chapter 6. Decreasing I_{CaL} can suppress the calcium over-release in alternans models through calcium-induced calcium-release, and therefore can help to maintain both SRCB and SCB.

Blocking I_{Kr} by 30% suppressed 38% alternans models (Figure 7.1D). As shown in Chapter 6, modulating I_{Kr} had little effect on overall CaT levels, but can significantly affect I_{NaCa} through membrane voltage regulation. A weaker outward I_{Kr} can lead to slower inactivation of I_{CaL} and weaker inward forward-mode I_{NaCa}. Therefore, inhibiting I_{Kr} can affect alternans by indirectly regulating SCB and SRCB.

The strongest effect was observed when G_{NaCa} was decreased by 30% (Figure 7.1E), upon which 74% of alternans models were converted into non-alternating models. As a major translator between calcium alternans and APD alternans, I_{NaCa} directly affected SCB. By inhibiting the extrusion of the over-released Ca^{2+} from SR, I_{NaCa} also indirectly regulated SRCB by modulating intracellular calcium.

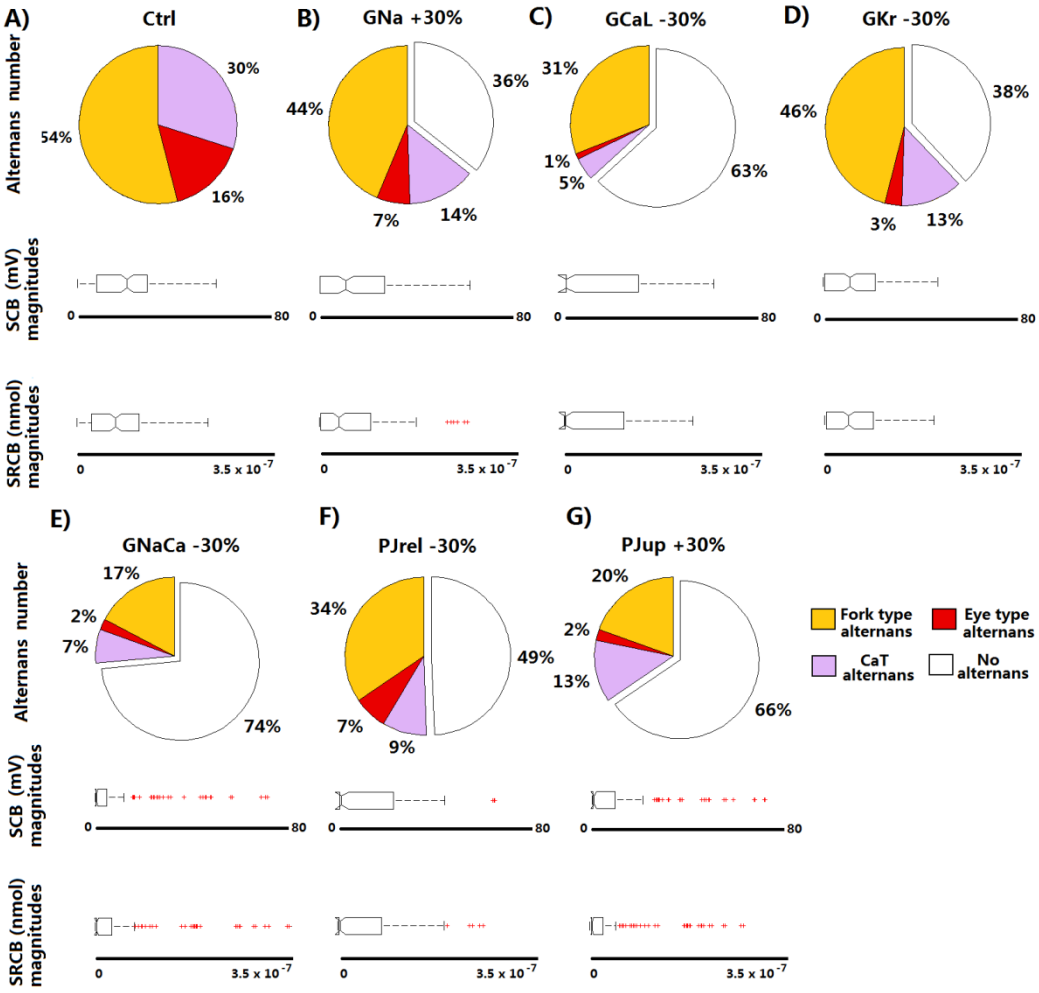


Figure 7.1: Effects of different current interventions on alternans models.

Blocking calcium release (P_{Jrel}) by 30% inhibited 49% alternans models (Figure 7.1F). As illustrated in Chapter 6, the disruption of SRCB and the fluctuation of SR Ca^{2+} was the initial event in alternans generation. Therefore, suppressing J_{rel} directly helped to maintain SRCB and eliminate Ca^{2+} fluctuations at fast pacing rates. Similar effects were observed in rabbits myocytes (Kanaporis and Blatter, 2014).

Increasing calcium re-uptake through SERCA (P_{Jup}) by 30% also effectively suppressed 66% alternans (Figure 7.1G), in agreement with previous experiments in guinea pigs targeting SERCA2a over-expression (Cutler *et al*., 2009). Similarly to P_{Jrel} inhibition, J_{up} enhancement helped to maintain SRCB and to abolish SR Ca^{2+} fluctuations.

In summary, the most effective interventions to inhibit alternans at 30% intervention levels were I_{CaL} block (63% alternans inhibited), I_{NaCa} block (74% alternans inhibited) and J_{up} enhancement (66% alternans inhibited). Therefore, we further investigated the effects of these three interventions in the following sections of this chapter.

7.3.2 Effects of I_{CaL} inhibition

Based on our previous results, I_{CaL} is an important regulator in alternans generation. The activity of I_{CaL} directly regulates J_{rel} through calcium-induced calcium-release, and the magnitude of I_{CaL} also directly affects the intracellular calcium level, which regulates a series of events such as calcium re-uptake and sarcolemmal calcium extrusion. Instead of using one single intervention level as in Figure 7.1, we further tested the effects of inhibiting I_{CaL} by 20%, 40% and 60%. 20% of I_{CaL} block converted 46% of the Alternans models into Normal models, and 60% of I_{CaL} inhibition completely eliminated all types of alternans (Figure 7.2A). This was due to the significant regulation effects of I_{CaL} on SCB and SRCB (Figure 7.2B-C).

However, the side effects of blocking I_{CaL} were also significant. Suppressing I_{CaL} by 60% led to more triangular and shorter APs (Figure 7.3A), and also severely decreased intracellular CaT level (Figure 7.3B), which may seriously compromise the inotropic response of cardiomyocytes.

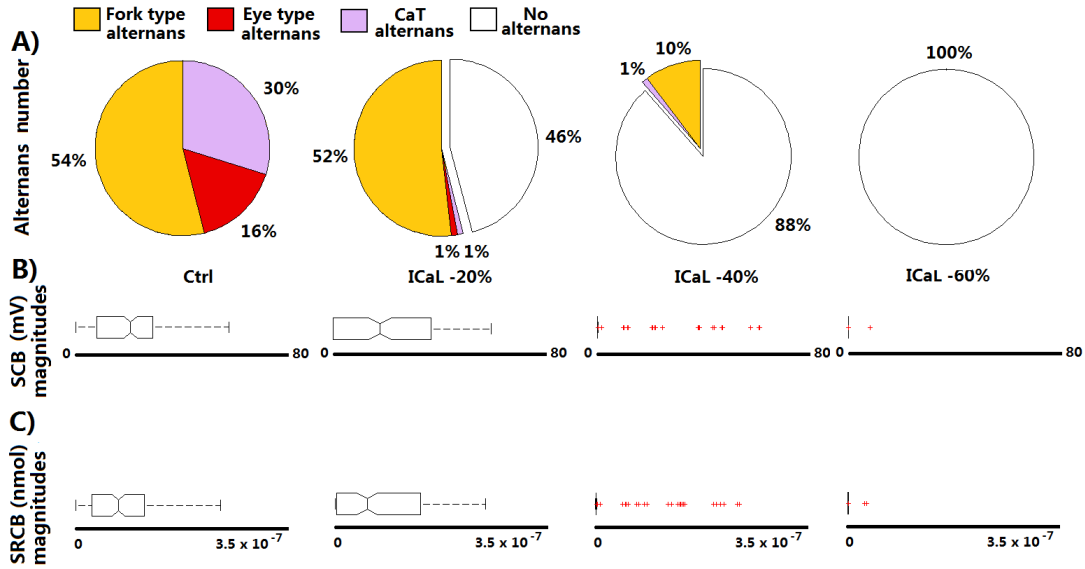


Figure 7.2: Suppression of APD alternans by I_{CaL} inhibition. A) Percentage of different types of alternans models under 20%, 40% and 60% I_{CaL} block. B, C) Effects of I_{CaL} inhibition on regulating the SCB and SRCB, respectively.

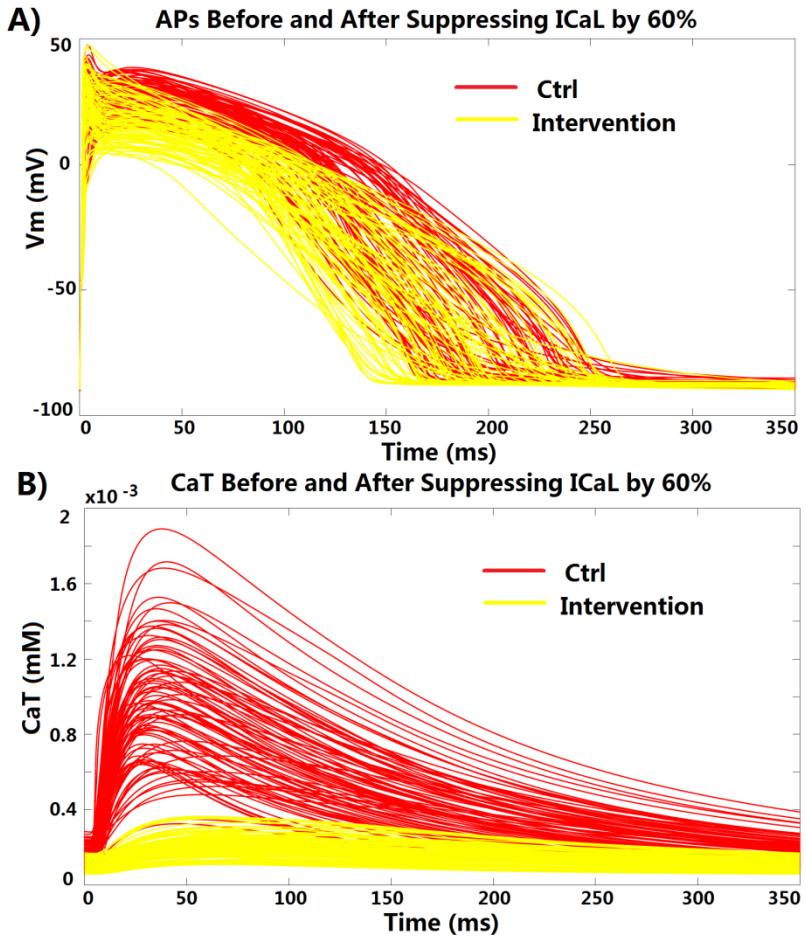


Figure 7.3: Effects of I_{CaL} down-regulation on AP and CaT.

7.3.3 Effects of I_{NaCa} inhibition

Based on our previous results, one of the fundamental events in the propagation of intracellular Ca^{2+} alternans to APD alternans is the extrusion of the over-released JSR calcium through I_{NaCa}, which is stronger in Alternans than in Normal models. In addition, I_{NaCa} is also a crucial regulator of SCB, which is a fundamental indicator of alternans even after introducing I_{CaL} kinetics variation. Having been identified as the most effective intervention to suppress alternans at 30% inhibition in Figure 7.1, we explored the effects of blocking the up-regulated I_{NaCa} by 20%, 40% and 60%. Reducing the increased I_{NaCa} in Alternans models by only 20% successfully converted 52% of the Alternans models into Normal models, whereas 60% I_{NaCa} reduction suppressed all the APD alternans (Figure 7.4A). I_{NaCa} modulation

eliminated APD alternans by reducing the fluctuation in both SCB and SRCB (Figure 7.4B-C). In fact, I_{NaCa} inhibition only moderately shortened APD and increased the magnitude of the intracellular Ca^{2+} transient (Figure 7.5A-B).

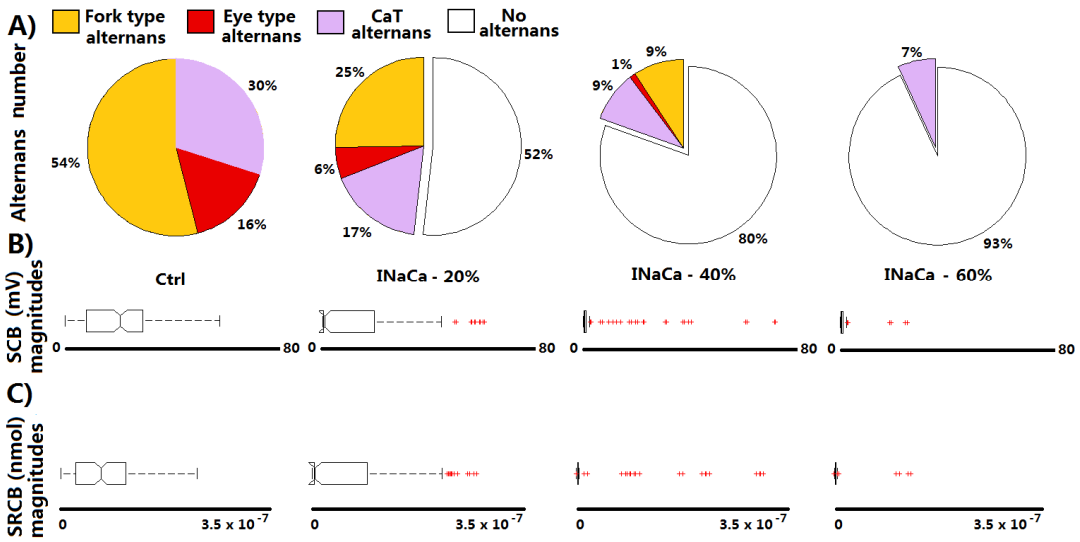


Figure 7.4: Suppression of APD alternans by I_{NaCa} inhibition. A) Percentage of different types of alternans models under 20%, 40% and 60% I_{NaCa} block. B, C) Effects of I_{NaCa} inhibition on regulating the SCB and SRCB, respectively.

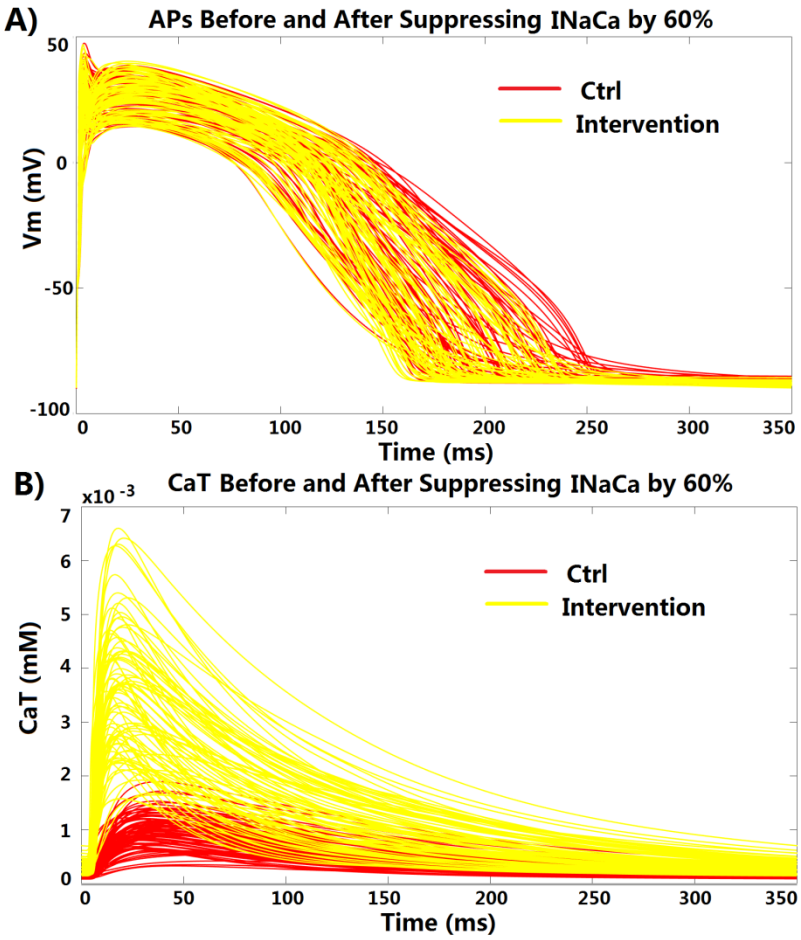


Figure 7.5: Effects of I_{NaCa} down-regulation on AP and CaT.

7.3.4 Effects of J_{up} enhancement

As demonstrated in Chapter 6, the initiation of alternans in our human ventricular cell models was due to the fluctuation of SR calcium level caused by the weak calcium re-uptake (J_{up}) and strong calcium release (J_{rel}). Enhancing calcium re-uptake has been shown to be able to suppress alternans generation, and is also regarded as a promising therapeutic target. Similar to I_{CaL} and I_{NaCa}, we also explored the effect of increasing J_{up} by 20%, 40% and 60% in the alternans models. Increasing J_{up} by 20% successfully converted 46% alternans models into non-alternating models, while 60% of the intervention eliminates 86% alternans models (Figure 7.6A). Enhancing J_{up} helped to maintain SRCB and therefore eliminated Ca^{2+} fluctuations and normalized SCB (Figure 7.6B-C). J_{up} modulation introduced minor changes to

the morphology and duration of APs, and only moderately increased CaT magnitudes (Figure 7.7). However, the effect of J_{up} enhancement was less significant compared to I_{CaL} or I_{NaCa} blockage: 10% of APD alternans remained persistent even upon 60% intervention (Figure 7.6A).

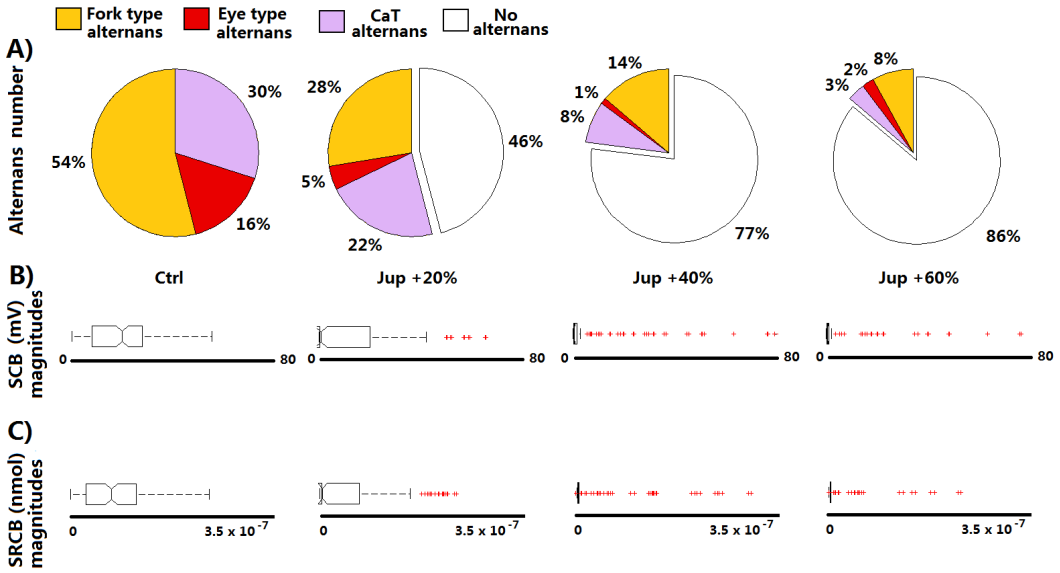


Figure 7.6: Suppression of APD alternans by increasing J_{up}. A) Percentage of different types of alternans models under 20%, 40% and 60% J_{up} enhancement. B, C) Effects of J_{up} enhancement on regulating the SCB and SRCB, respectively.

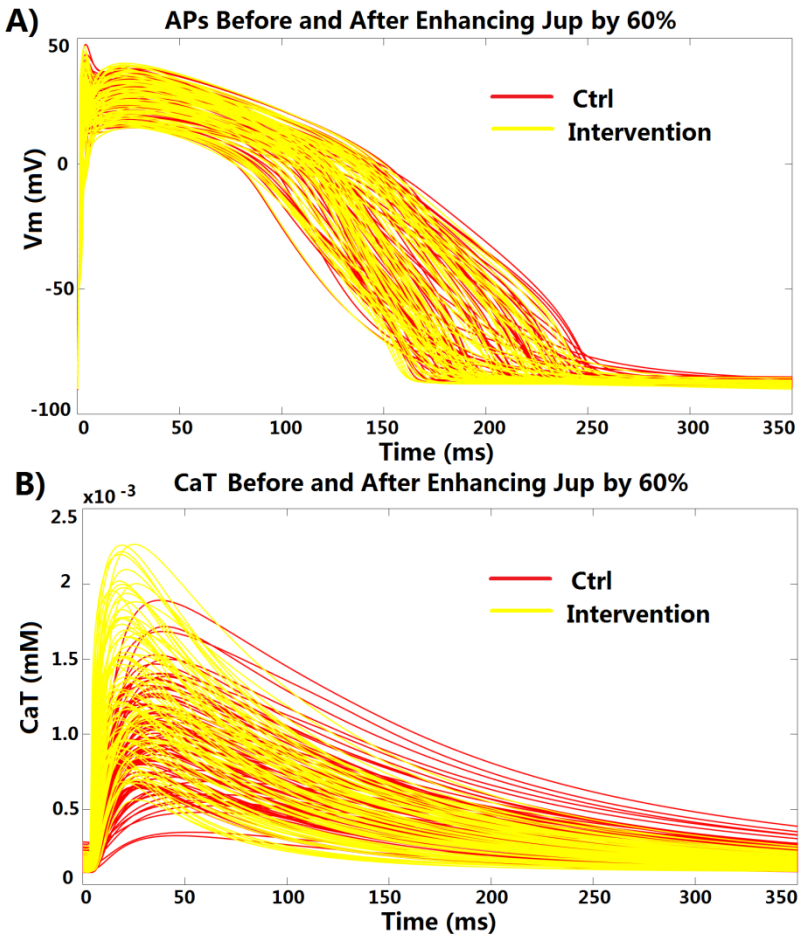


Figure 7.7: Effects of enhancing J_{up} on AP and CaT.

7.4 Discussion and conclusions

Based on the ionic differences between Normal and Alternans models, we analysed the effects of six different ionic interventions on the stability of alternans in our experimentally-calibrated population of human ventricular models. Our simulation study showed that enhancing I_{Na} or J_{up}, or inhibiting I_{CaL}, I_{Kr}, I_{NaCa} or J_{rel}, can suppress alternans generation. The inhibition of alternans after the interventions were all related to the regulation of SRCB and SCB. Further analysis was conducted to compare the effects of the three most effective interventions in alternans inhibition: inhibiting I_{CaL}, I_{NaCa} or enhancing J_{up}. Compared to other interventions, inhibiting I_{NaCa} emerges as the most effective anti-arrhythmic strategy for alternans suppression.

I_{NaCa} as an anti-arrhythmic target

I_{NaCa} is an important link between membrane voltage and the intracellular calcium transient. In Chapter 6, we discovered that I_{NaCa} was stronger in the alternans models, leading to smaller CaT amplitudes in alternans models when SR Ca^{2+} was over-released. In addition, I_{NaCa} plays a crucial role in the maintenance of SCB.

Compared with other currents or fluxes that were found to be different between normal and alternans models, I_{NaCa} may be the most promising anti-arrhythmic target for the following reasons:

1) I_{NaCa} suppression can effectively inhibit all types of alternans (eye type, fork type, and CaT alternans) due to its important role on the regulation of CaT level and SCB. As it was demonstrated in previous chapters, the initiation of alternans correlated with the over-release of SR calcium and the disruption of SRCB. Therefore in alternans models, if I_{NaCa} is strong, the over-released Ca^{2+} will be extruded from the cells, and it will be difficult for the SR Ca^{2+} level to recover, leading to persistent alternans. Under these conditions, if I_{NaCa} is inhibited, then the stronger J_{up} during the longer beat will be able to re-uptake the over-released SR Ca^{2+}, facilitating the recovery of JSR Ca^{2+} levels, ultimately yielding alternans suppression.

2) Smaller I_{Na} was found in our population of alternans models. The connection between I_{Na} and alternans was also found in other theoretical and experimental studies (Fox et al., 2002; Matthews et al., 2012). As it was demonstrated in Chapter 6, the fluctuation of intracellular Na^{+} was involved in the alternation process due to the key role of I_{NaCa} in alternans. Therefore, enhancing I_{Na} could be an indirect regulation to I_{NaCa} and SCB, but its effect on alternans suppression was the weakest among the studied interventions.

3) Decreasing I_{CaL} can also effectively inhibit alternans; however, it may also reduce the contractility of the myocytes due to reduced CaT levels, suggesting caution in the use of these therapies. In addition, as illustrated in Chapter 6, the disappearance of alternans at fast pacing rates in the Eye-type models was due to the stronger intracellular calcium accumulation induced by stronger I_{CaL}. The variation of I_{CaL} kinetics in Eye-type and Fork-type models also showed that the effect of modulating I_{CaL} can vary depending on baseline I_{CaL} levels.

4) Blocking I_{Kr} can promote alternans elimination through voltage-based regulation on I_{CaL} and I_{NaCa}. Nevertheless, the effects of this intervention on SCB and alternans are indirect, and I_{Kr} block can substantially prolong APD. As it was demonstrated in Chapter 4, the prolongation of APD can be another source of alternans generation.

5) Modulating the balance between J_{rel} and J_{up} fluxes can directly regulate SRCB, which is the key in alternans initiation. It has been reported that genetic SERCA2a over-expression in intact hearts can significantly increase the resistance to APD alternans and reduce alternans-mediated ventricular arrhythmias (Cutler *et al*., 2012). Although clinical trials on SERCA2a genetic therapies conferred several benefits (Sikkel *et al*., 2014), this anti-arrhythmic genetic strategy is still clinically challenging. One major obstacle is that the immune response of the patients can lead to the failure of gene delivery (Sikkel *et al*., 2014) (Hayward *et al*., 2015).

6) Although the population of models was derived from one single baseline formulation, most of the above results should not be model-specific, since they are consistent with many experimental observations in animals.

Therefore, our simulation results in the experimentally-calibrated population of human ventricular alternans models showed that, although enhancing I_{Na} or J_{up} or

reducing I_{CaL}, I_{Kr} or J_{up} can all suppress alternans generation to some extent, blocking I_{NaCa} was identified as the most feasible and effective strategy.

Chapter 8

Computational investigation of pro-arrhythmic mechanisms of LQT1 mutations in human ventricular cardiomyocytes

8.1 Introduction

In previous chapters, we have constructed a population of human ventricular models of cardiac electrophysiology, calibrated with *in vivo* human data to account for natural variability. Our main assumption underlying cardiac variability is that it is mainly caused by cell-to-cell variations of ionic conductances and permeabilities due to different protein expression level (Cummins et al., 2014; Devenyi and Sobie, 2015; Groenendaal et al., 2015; Sarkar et al., 2012; Sobie, 2009; Sobie and Sarkar, 2011; Yang and Clancy, 2012). However, when genetic mutations exist, the structure of a protein can be altered, and ionic channel kinetics may play additional important roles. Therefore, in this part of the thesis, we aim to explore the effects of genetic mutations into the population of models generated in previous chapters.

The hereditary long-QT syndrome (LQTS) is a type of cardiac pathological condition in which genetic mutations on ionic channels lead to the decrease of repolarisation currents or the increase of depolarisation currents, resulting in the prolongation of APD. Such an APD prolongation can be reflected as a longer interval between the Q wave and the T wave on the electrocardiogram.

The prevalence of LQTS is estimated to be from 1:2000 to 1:5000 (Barsheshet *et al*., 2013). However, the penetrance of the LQT mutation carriers is very low (about 25%) (Priori *et al*., 1999). According to (Priori, 2004), 32% of the LQT mutation carriers have normal QTc values, which suggests the existence of complex interactions and compensation effects between different ionic currents.

Mutations of the KCNQ1 gene that encodes the I_{Ks} channel subunit protein Kv7.1 (KvLQT1) is the most common type of LQTS (LQT1), with a frequency between 40-55% among all LQTS (Mizusawa *et al*., 2014). In an international study conducted by Moss *et al*., the effects of 77 different KCNQ1 mutations from 600 patients were investigated. Their results showed that patients with KCNQ1 mutations in the transmembrane region had a higher risk of syncope, aborted cardiac arrest and sudden cardiac death compared to mutations in the protein C-terminus (Moss *et al*., 2007). Similarly, patients with missense mutations (point mutations leading to the change of amino acid) are at higher risk for cardiac events than patients with other mutations (insertions, deletions, stop codon, *etc*) (Moss *et al*., 2007). Dominant negative mutations leading to the incorporation of defective subunits to membrane channels tend to be more dangerous than haploinsufficiency mutations, the latter producing subunits that fail to transport or incorporate to membrane proteins (Moss *et al*., 2007). In addition, patients with missense mutations in the cytoplasmic loops are more sensitive to β-adrenergic stimulation (Barsheshet *et al*., 2012).

To evaluate the risks of LQT mutations and to understand the mechanisms underlying the low penetrance of LQT, we aim to explore the interaction between one LQT mutation and cardiac variability. Firstly, we analysed LQT1 mutation patch clamp data for the construction of LQT1 mutation I_{Ks} models. The models for the mutant channels were built through the modification of a wild type I_{Ks} model by multi-objective fitting of experimental patch clamp data. The mutant channel models were then inserted into the population of human ventricular cell models constructed and calibrated in Chapter 4. The resulting population of LQT1 mutation human

ventricular cell models constituted a good platform to investigate the effect of LQT1 mutation on human ventricular electrophysiology, specifically focusing on evaluating the interactions between LQT1 mutant channels and the cardiac variability in other ionic currents.

8.2 Methods

8.2.1 Clinical identification of I_{Ks} mutations

Five different missense mutations were identified in the KCNQ1 gene from patients with prolonged QTc intervals (QT interval corrected with heart rate) at rest in the William Harvey Heart Centre at Queen Mary University of London. These were G229D (QTc 490ms), D242N (QTc data not available in clinical history), G325R (QTc 460ms), R518P (QTc 510ms) and Y662X (QTc 480ms).

8.2.2 I_{Ks} Mutants expression system for patch clamp experiments

To test the effects of the KCNQ1 mutations, the wild type (WT) KCNE1 gene was co-expressed with the KCNQ1 gene (WT or mutated) with a ratio of 1 to 1 to constitute complete I_{Ks} channels. For a same KCNQ1 mutation, two expression systems were constructed to simulate homozygous and heterozygous mutations: Single (KCNE1: KCNQ1_mutant=1:1) and Dominant Negative (DN) (KCNE1: KCNQ1_WT: KCNQ1_mutant=1:0.5:0.5). Full-length DNA sequences, encoding the above WT or mutated human genes, were cloned into expression vectors and then transiently transfected into Chinese hamster ovary (CHO) cells. This part of the experimental work was completed by Dr Stephen Harmer and Professor Andrew Tinker.

8.2.3 Patch clamp protocol

Currents produced by WT or mutated I_{Ks} channels were recorded from 8-12 transfected CHO cells, 2 days after transfection. Whole-cell patch clamp experiments were carried out at room temperature using an Axopatch 200B amplifier (Axon Instruments). For each depolarisation voltage stepped from −80 to +80 mV (in 10-mV increments), currents were recorded by holding the cell at a voltage of −80 mV for 3 s, followed by the depolarisation voltage for 2 s, followed by a repolarisation pulse back to −40 mV for 2 s (to measure tail currents) and then back to −80 mV for 3 s. This part of the wet lab experimental work was completed by Dr Stephen Harmer and Professor Andrew Tinker. The same protocol was replicated in the computational simulations (Figure 8.1A).

8.2.4 Biomarker calculation

The following biomarkers were calculated from the above described experimental patch clamp protocol:

- Current density (CD) was calculated from the last values of the activation current traces (Figure 8.1B).
- Peak tail current density (PTCD) was calculated from the largest values of the deactivation current traces (Figure 8.1C).
- Steady state of activation (SSA) was the relative ratio of PTCD against the largest PTCD values, and represented the voltage-dependence of channel activation (Figure 8.1C).
- Activation Thalf was calculated as the half activation time during depolarisation (Figure 8.1D).
- Activation Thalf-Inst was calculated as the half activation time during depolarisation after removing the instantaneous activation current (Figure 8.1E).
- Deactivation Tau was the time constant of the deactivation trace after fitting the

standard exponential equation (Figure 8.1F).

- Deactivation steady state (DSS) was calculated from the last value of the deactivation current trace (Figure 8.1G).

The experimental patch clamp biomarkers were calculated by Dr Stephen Harmer, and the corresponding *in silico* biomarkers were calculated after our simulation.

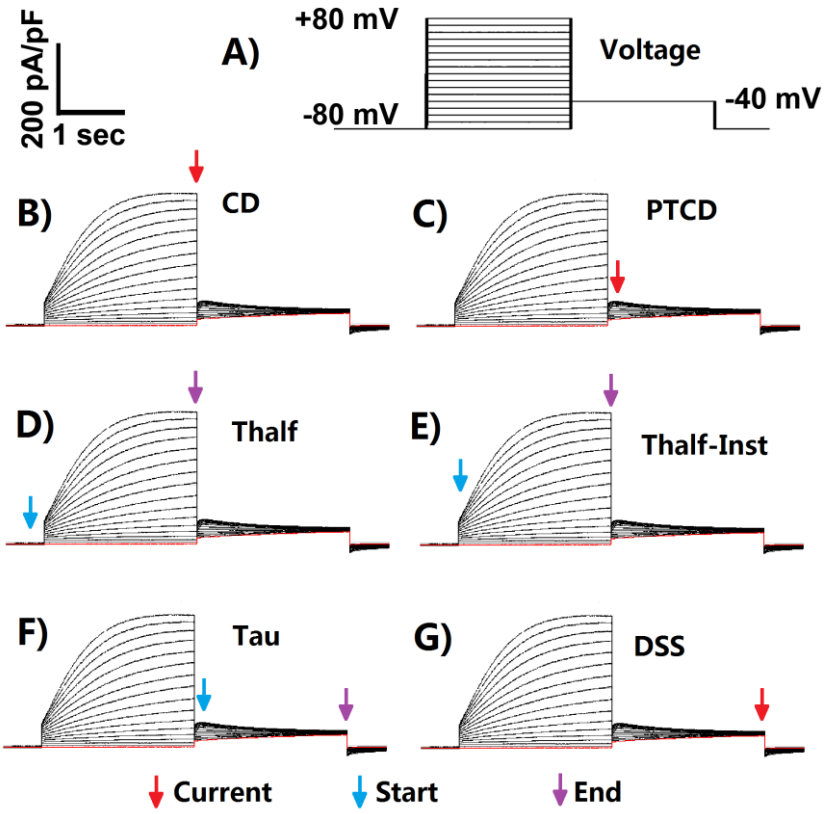


Figure 8.1: Patch clamp protocol and biomarkers calculation. A) voltage protocol described in 8.2.3; B) current density (CD); C) peak tail current density (PTCD); D) activation thalf (Thalf); E) activation thalf-inst (Thalf-Inst); F) deactivation tau (Tau); G) deactivation steady state (DSS).

8.2.5 Parameters related to mutations

The Hodgkin-Huxley I_{Ks} model from the O'Hara *et al.* model was used in the fitting of the experimental patch clamp biomarkers for the full range of holding potentials. In this model, the I_{Ks} current is mainly determined by the ion channel conductance (G_{Ks}), the state of activation gate (xs1) and the state of deactivation gate (xs2). Our

initial hypothesis was that the mutations that affect I_{Ks} channel expression levels can be simulated by varying G_{Ks}, and the mutations related to kinetic changes can be reproduced by varying the channel gating properties through modifications in xs1 and xs2.

In the O'Hara *et al*. model, the activation gate xs1 and the deactivation gate xs2 share a same steady state (Xss), but their time constants (Tau1 and Tau2) are different:

$$\mathrm{Xss} = \frac{\mathrm{A}}{1 + \mathrm{e}^{\frac{-(\mathrm{v}+\mathrm{B})}{\mathrm{C}}}} \tag{8.1}$$

$$\mathrm{Tau1} = \mathrm{a} + \frac{1}{\mathrm{b} \cdot \exp^{\frac{\mathrm{v}+\mathrm{c}}{\mathrm{d}}} + \mathrm{e} \cdot \exp^{\frac{-(\mathrm{v}+\mathrm{f})}{\mathrm{g}}}} \tag{8.2}$$

$$\mathrm{Tau2} = \frac{1}{\mathrm{h} \cdot \exp^{\frac{\mathrm{v}-\mathrm{i}}{\mathrm{j}}} + \mathrm{k} \cdot \exp^{\frac{-(\mathrm{v}+\mathrm{l})}{\mathrm{m}}}} \tag{8.3}$$

$$\frac{\mathrm{dxs1}}{\mathrm{dt}} = \frac{\mathrm{Xss} - \mathrm{xs1}}{\mathrm{Tau1}} \tag{8.4}$$

$$\frac{\mathrm{dxs2}}{\mathrm{dt}} = \frac{\mathrm{Xss} - \mathrm{xs2}}{\mathrm{Tau2}} \tag{8.5}$$

$$\mathrm{IKs} = \mathrm{GKs} \cdot \mathrm{xs1} \cdot \mathrm{xs2} \cdot (\mathrm{Vm} - \mathrm{EKs}). \tag{8.6}$$

In our estimation of mutant channel kinetics, parameters A-C in Xss, a-g in Tau1 and h-m in Tau2 were varied to fit the model output with the mutant I_{Ks} patch clamp data.

8.2.6 Preprocessing of CHO patch clamp data

CD values from CHO patch clamp experiments were much larger than those in cardiomyocytes and mathematical models, since I_{Ks} channels were over-expressed in the CHO cells. To normalise the large magnitude of CDs in CHO cells into physiological bounds, we assumed (given the same expression level) the correspondence between CDs of WT I_{Ks} in experiments and those in the ORd model. A good linear correlation was found between the WT CHO CDs and the WT ORd

model CDs. Therefore, CD signals were rescaled before used in the fitting of the ORd model, according to:

ORd model CD= 0.0019*CHO CD+0.0026. (r^2=0.9914) (Figure 8.2)

Similarly, PTCD and DSS from CHO cells were rescaled using the above formula. In addition, the rescaling can also remove the potential effect of experimental temperature on biomarkers.

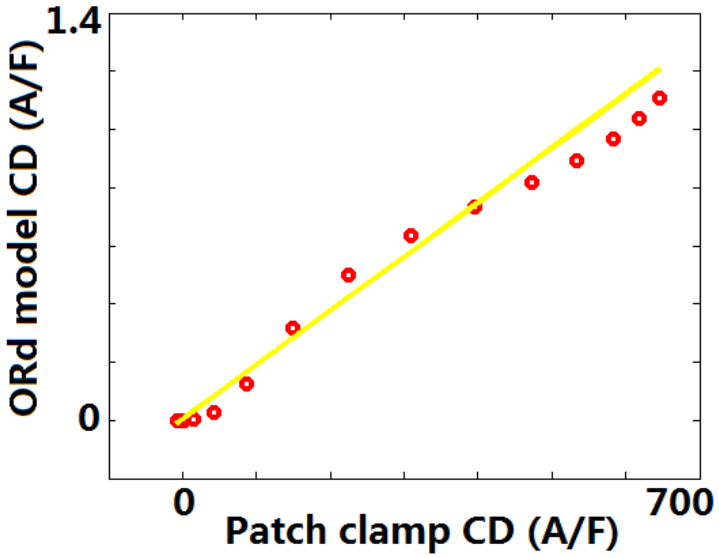


Figure 8.2: Linear correlation between WT patch clamp data (CD) and ORd model output (CD) after using the same patch clamp protocol.

8.2.7 Multi-start least square fitting

Least square curve fitting (lsqcurvefit) was combined with the Multi-Start algorithm in Matlab to find the global best fit values for the above parameters, so the new model can reproduce the similar patch clamp biomarkers as the mutated I_{Ks} channels.

8.3 Results

8.3.1 Patch clamp current traces of WT I_{Ks} and LQT1 mutants

I_{Ks} traces with the aforementioned LQT1 mutations (G229D, D242N, G325R, R518P,

Y662X) were compared as the first step of our analysis. When the LQT1 mutants were co-expressed with WT KCNE1 protein with a ratio of 1:1 (Single mutation, Figure 8.3A):

- I_{Ks} with G229D Single mutation exhibited an extremely fast activation process, but the steady state activation CDs were smaller compared with WT under high potentials. In addition, there was almost no deactivation.
- In D242N Single mutation, CDs were also much smaller, and the deactivation was very fast.
- There was no significant current when G325R and R518P mutated KCNQ1 were co-expressed with KCNE1. Further analysis showed that there was no membrane localisation of these mutated protein (data not shown), which suggested these mutations may have affected the structure and trafficking of the KCNQ1 protein.
- The effect of Y662X mutation seemed to be milder compared with other mutants. The activation process of Y662X tended to be slightly faster than WT.

When the LQT1 mutants were co-expressed with WT KCNQ1 protein and WT KCNE1 protein with a ratio of 0.5:0.5:1 (DN mutation, Figure 8.3B):

- The activation of DN G229D mutation was still faster than normal, and there was a significant instantaneous part of the activation process. The DSS of the deactivation process was considerably higher than WT.
- The CD of D242N DN mutation was higher than its Single mutation counterpart, and the deactivation process was still faster than WT.
- The current shapes of G325R and R518P DN mutations were similar as WT, but exhibiting weaker magnitudes, which suggested the current signals were produced by the WT KCNQ1/KCNE1channel co-expressed with the mutants.
- The DN Y662X mutant can produce a similar current trace as WT ion channels.

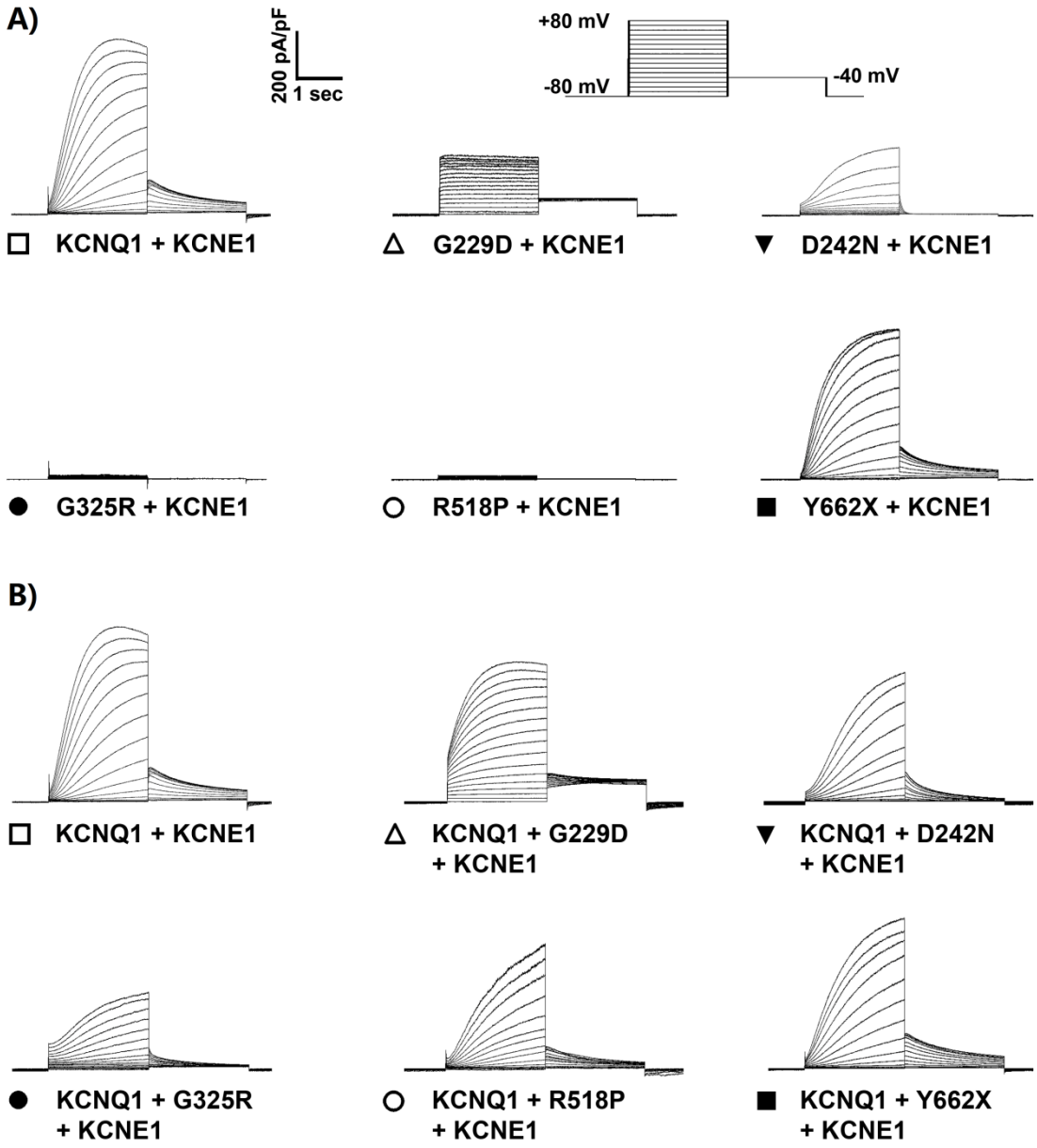


Figure 8.3: Representative traces of the currents produced by the LQT1 mutations G229D, D242N, G325R, R518P and Y662X. A) Example traces of Single mutations (KCNQ1/mutant channels co-expressed with KCNE1); B) Example traces of DN mutations (LQT1 mutations expressed in heterozygous fashion with the wild-type KCNQ1 and KCNE1). This figure was kindly provided by Dr Stephen Harmer and Professor Andrew Tinker at the William Harvey Heart Centre, Queen Mary University of London.

From the above analysis, we can see that the effect of Y662X was milder than the other mutants, G325R and R518P mainly affected the normal trafficking of KCNQ1 proteins, D242N produced a weaker I_{Ks} current probably related to a faster deactivation process, whereas the effects of G229D mutation were the most intricate

among the five considered mutations. Therefore, we chose G229D mutation as the simulation target.

8.3.2 The analysis of the KCNQ1 G229D mutation patch clamp biomarkers

The seven patch clamp biomarkers described above were compared between WT, G229D Single mutation and G229D DN mutation.

Compared with WT, the Single mutation of G229D showed larger CDs under low membrane potentials, but was weaker under high potentials (Figure 8.4A). Unlike the S-shape of WT I_{Ks} CDs, the CDs of G229D Single mutation exhibited linear growth while increasing membrane potentials (Figure 8.4A). The CDs of G229D DN mutation showed the mixed property of WT and G229D Single mutation (Figure 8.4A).

Similar to CD, the PTCD and SSA of WT I_{Ks} maintained around baseline under negative membrane potentials, and then gradually increased during positive potentials (Figure 8.4 B, C). After G229D Single mutation, baseline PTCD and SSA were considerably larger at low potentials, exhibiting a milder increase with the increase of membrane potentials (Figure 8.4 B, C). The G229D DN mutation caused higher baseline and a milder increase of PTCD and SSA. These phenomena suggested a change of I_{Ks} voltage sensitivity as a result of G229D mutation (Figure 8.4B, C).

The WT activation thalf gradually decreased as membrane voltage rose, which implied a faster activation process under larger membrane potentials (Figure 8.4D). The activation thalf of the G229D Single mutation was approximately zero at all potentials, and the thalf of the G229D DN mutation was practically constant around

140ms (Figure 8.4D). These data illustrated that the G229D mutation led to an instantaneous activation current. If the instantaneous component of activation current was removed, activation thalf-inst of the G229D Single mutation was higher than WT, while thalf-inst of the G229D DN mutation was still lower than WT (Figure 8.4E).

Since there was barely no decay in the deactivation traces of G229D Single mutation, deactivation tau was only analysed in the WT and G229D DN mutation. When the membrane voltage increased, the time constant of deactivation gradually decreased in WT whereas increased in the G229D DN mutation (Figure 8.4F). The DSS was abnormally larger in G229D mutations than in WT (Figure 8.4G).

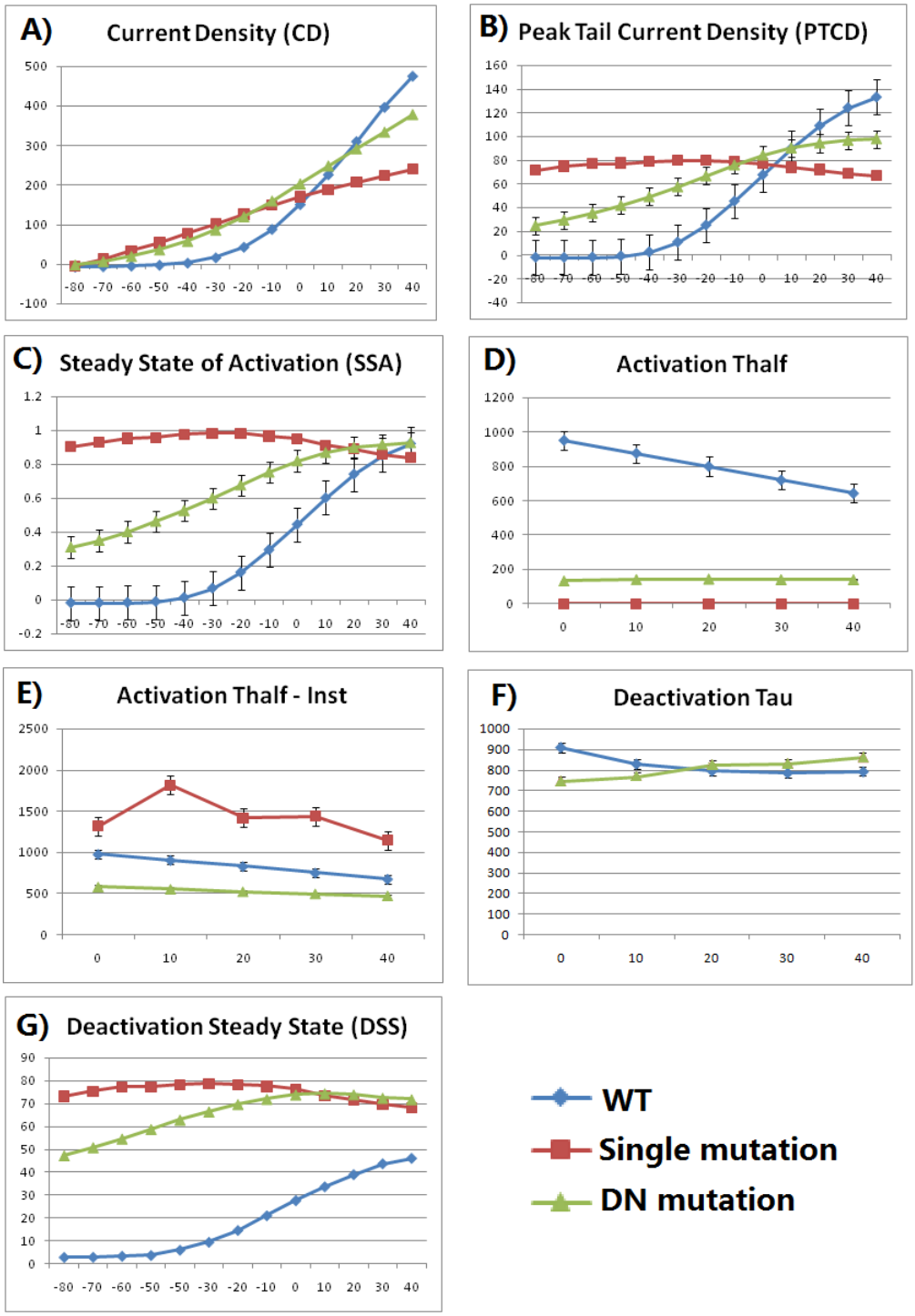


Figure 8.4: Comparison between I_{Ks} current biomarkers of WT, Single and DN G229D mutations from patch clamp experiments. A) Current density (CD) (pA/pF); B) Peak tail current density (PTCD) (pA/pF); C) Steady state of activation (SSA); D) Activation Thalf (ms); E) Activation Thalf-Inst (ms); F) Deactivation Tau (ms); G) Deactivation steady state (DSS) (pA/pF). Data provided by Dr Stephen Harmer and Professor Andrew Tinker.

8.3.3 Modification of WT ORd I_{Ks} model to fit WT and G229D mutated I_{Ks} patch clamp data

We subsequently modified the original ORd model to fit the patch clamp data of WT and G229D mutations. In this process, the average biomarkers from different cell groups were used in the fitting of different models for G229D Single and DN mutations, respectively. The best fit parameter sets for G229D Single and DN mutations were inserted into the I_{Ks} current formulation of the O'Hara *et al* model as shown below:

Dominant negative mutation:

$$\mathrm{Xss}_{\mathrm{G229D_{DN}}} = \frac{0.9465}{1 + \mathrm{e}^{\frac{-(\mathrm{v}+71.1239)}{27.4914}}} \tag{8.7}$$

$$\mathrm{Tau1}_{\mathrm{G229D_{DN}}} = 376.3354 + \frac{1}{0.000041329 \cdot \exp^{\frac{\mathrm{v}+70.7755}{11.4172}} + 0.000098594 \cdot \exp^{\frac{-(\mathrm{v}+202.6051)}{97.8909}}} \tag{8.8}$$

$$\mathrm{Tau2_G229D_DN} = \frac{1}{0.0019 \cdot \exp^{\frac{\mathrm{v}-87.0654}{106.6171}} + 0.000031856 \cdot \exp^{\frac{-(\mathrm{v}+355.0597)}{157.0970}}} \tag{8.9}$$

Single mutation:

$$\mathrm{Xss}_{\mathrm{G229D_{Single}}} = \frac{0.7029}{1 + \mathrm{e}^{\frac{-(\mathrm{v}+226.8211)}{38.7274}}} \tag{8.10}$$

$$\mathrm{Tau1}_{\mathrm{G229D_{Single}}} = 196.0892 + \frac{1}{67.7032 \cdot \exp^{\frac{\mathrm{v}+157.7247}{14.8435}} + 94.1943 \cdot \exp^{\frac{-(\mathrm{v}+458.5436)}{169.4608}}} \tag{8.11}$$

$$\mathrm{Tau2}_{\mathrm{G229D}_{\mathrm{Single}}} = \frac{1}{3.7679\mathrm{e}(-14)\cdot \exp^{\frac{\mathrm{v}-201.2472}{126.1263}} + 0.00062011\cdot \exp^{\frac{-(\mathrm{v}+34.5247)}{91.2525}}} \quad (8.12)$$

The fitting results for G229D DN and single mutations patch clamp biomarkers are shown in Figure 8.5 and Figure 8.6, respectively. The above KCNQ1 G229D mutation models can accurately reproduce the CD, PTCD, activation Thalf, deactivation Tau and DSS from the patch clamp experiments.

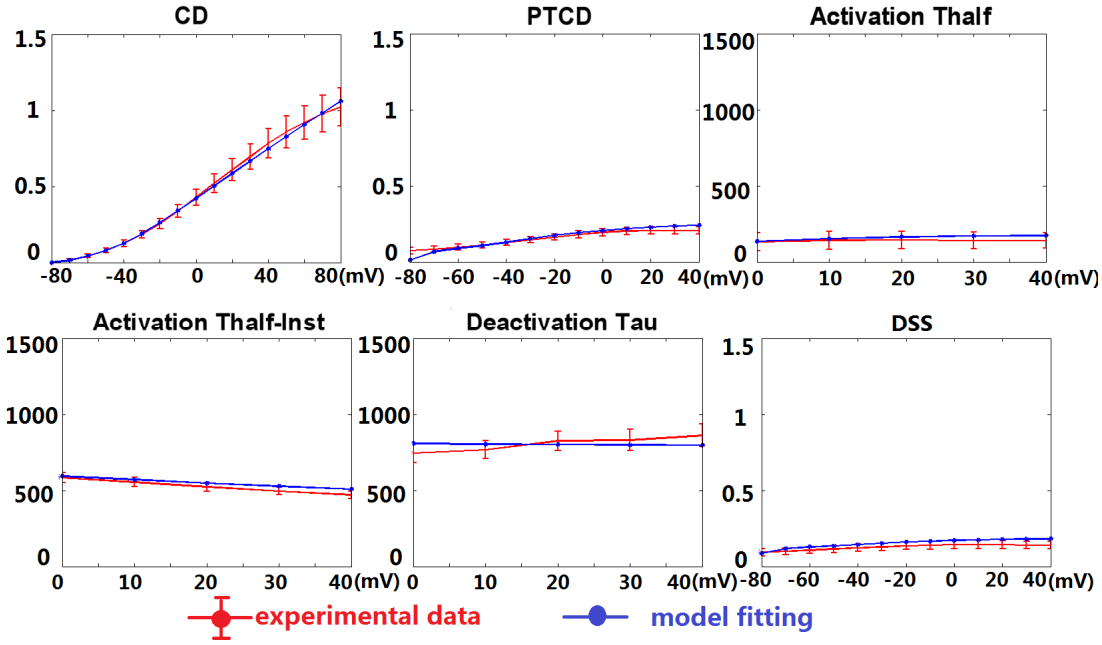


Figure 8.5: Multi-start best fitting results for KCNQ1 G229D DN mutation patch clamp biomarkers. Current density (CD) (μA/μF), Peak tail current density (PTCD) (μA/μF), Activation Thalf (ms), Activation Thalf-Inst (ms), Deactivation Tau (ms), and Deactivation steady state (DSS) (μA/μF).

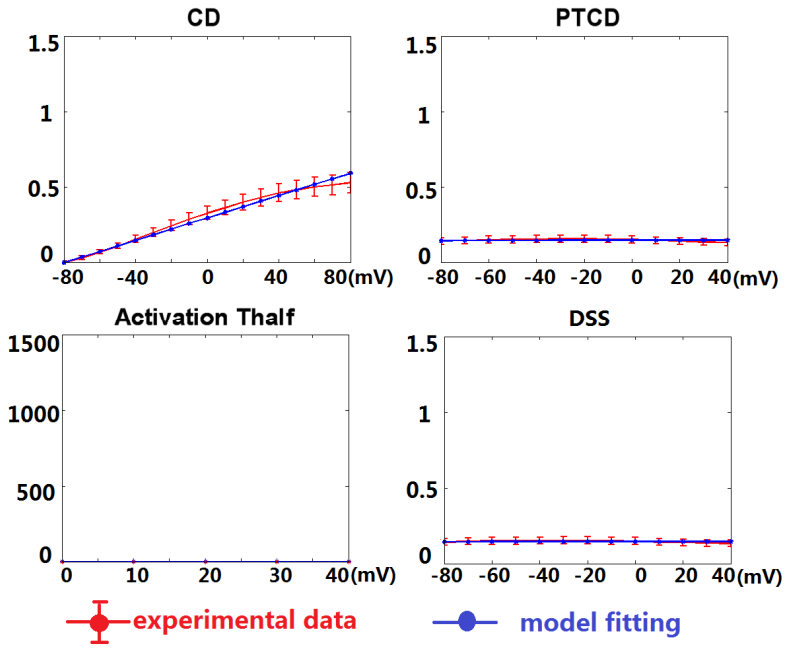


Figure 8.6: Multi-start best fitting results for KCNQ1 G229D Single mutation patch clamp biomarkers. Current density (CD) (μA/μF), Peak tail current density (PTCD) (μA/μF), Activation Thalf (ms), and Deactivation steady state (DSS) (μA/μF).

Simulated patch clamp experiments for G229D mutated I_{Ks} models accurately replicated I_{Ks} current traces as observed in experiments (Figure 8.7). The optimised parameter set for G229D Single mutation was not unique: except for the best fitting shown in Figure 8.6, another 18 parameter sets can produce similar fitting results. This was due to the fact that in G229D Single mutation, I_{Ks} current was nearly constant during activation and deactivation, and the complex formulations in equations 8.2 and 8.3 were almost unnecessary.

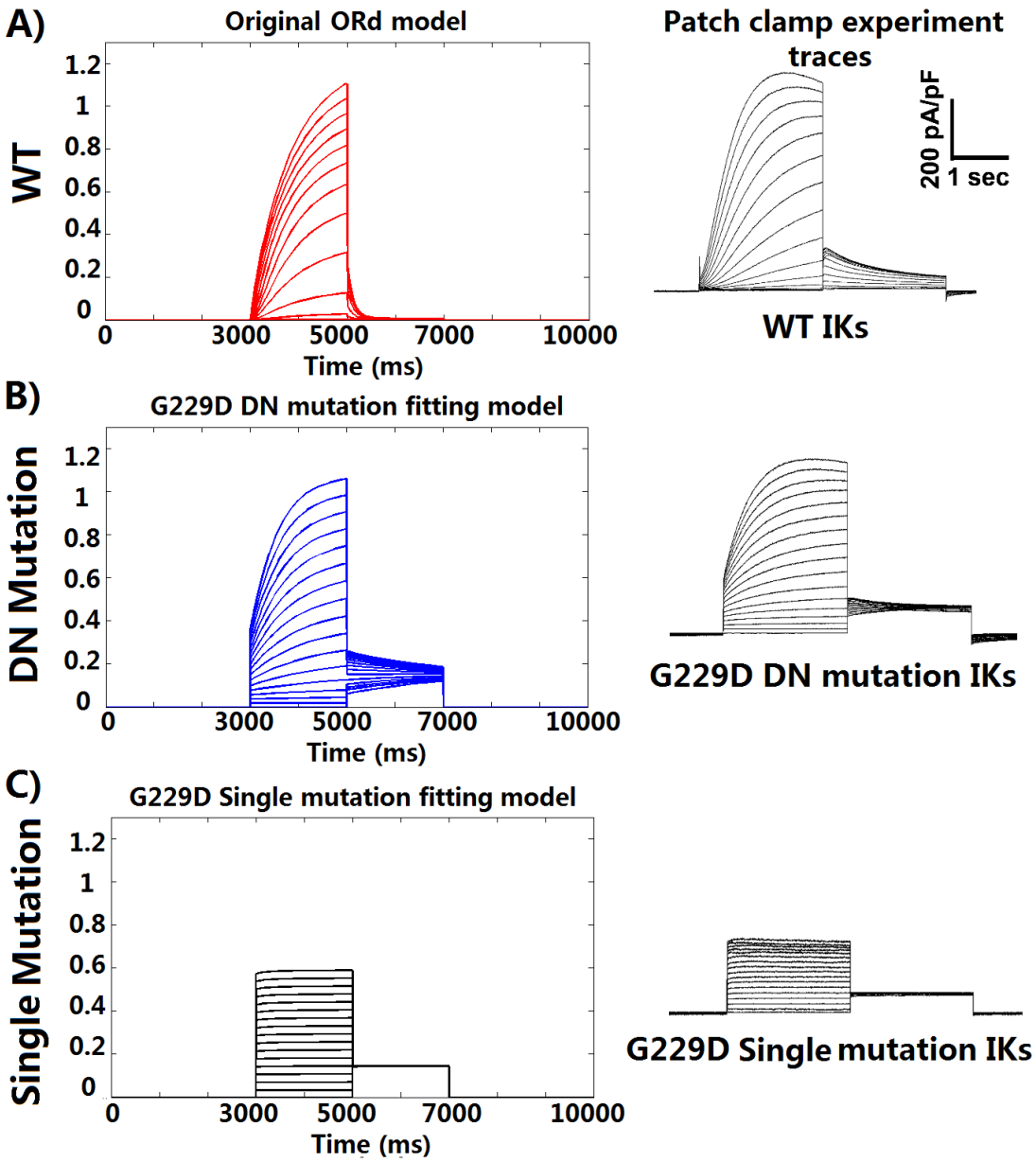


Figure 8.7: Comparison of I_{Ks} patch clamp traces between model (μA/μF) and experiments. A) WT I_{Ks}; B) KCNQ1 G229D DN mutation; C) KCNQ1 G229D Single mutation.

To explore the role of KCNQ1 G229D mutations in human cardiomyocytes, we firstly inserted the G229D mutated I_{Ks} formulation into the standard ORd model. A shortening of APD was observed in the KCNQ1 G229D mutated human ventricular cell model (Figure 8.8), due to a stronger I_{Ks} caused by the instantaneous activation, which closely follows the AP waveform. Despite the 19 possible parameter sets for the G229D Single mutation, they all produced similar APD shortening compared to the original WT ORd model (Figure 8.9). Therefore, the global best fitting parameter

set for the G229D Single mutation was used in further analysis.

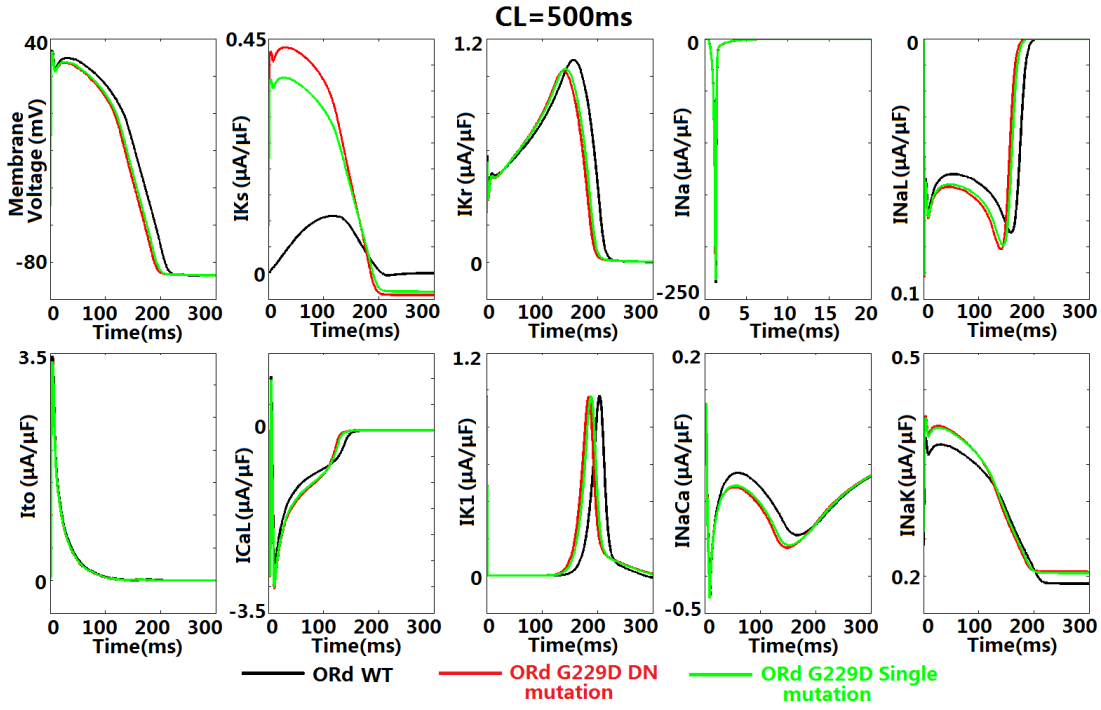


Figure 8.8: Effects of KCNQ1 G229D mutation on the baseline ORd model.

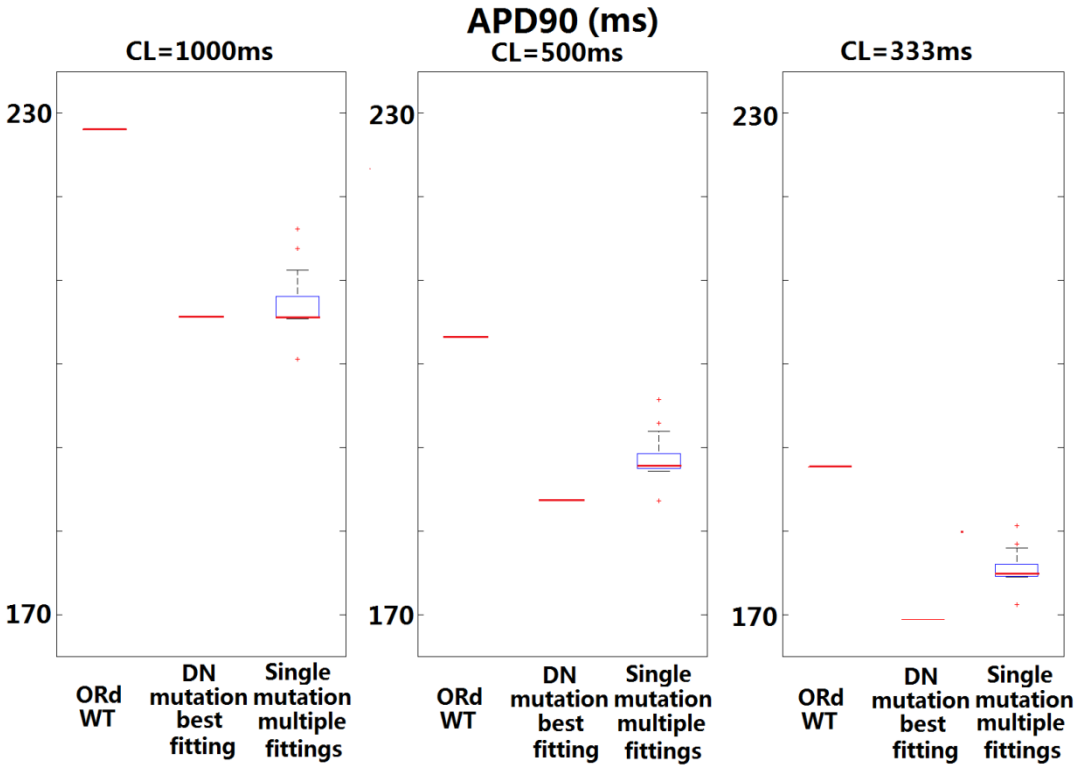


Figure 8.9 : Different G229D Single mutation fittings produced similar APD shortening.

8.3.4 Generation of the population of KCNQ1 G229D mutated human ventricular cell models

The I_{Ks} models with Single or DN G229D mutations were then inserted into the population of human ventricular cell models constructed in Chapter 5 to examine the interaction between G229D mutation and other ionic currents considering the possible natural variability in current conductances/permeabilities. In this population of human epicardial ventricular cell models constructed and calibrated in previous chapters, although there was obvious overlap in APDs between the WT population and the two mutant populations, the main effect of KCNQ1 G229D mutation for 3 testing pacing CLs (1000ms, 500ms, 333ms) was the shortening of APD (Figure 8.10).

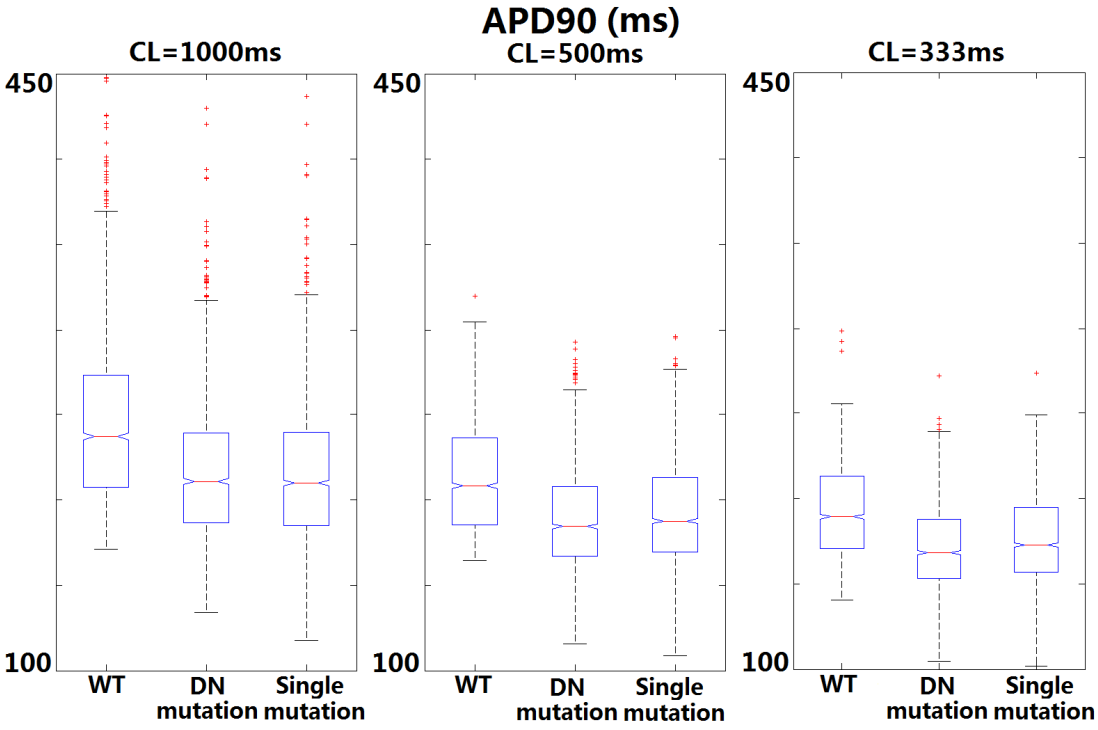


Figure 8.10: Effects of KCNQ1 G229D mutations on APD in the experimentally-calibrated population of human epicardial ventricular cell models.

8.3.5 Effects of KCNQ1 G229D mutation in the population of models

8.3.5.1 KCNQ1 G229D mutation can lead to different responses in the population of models

For each model in the population, we also compared the APD before and after introducing the G229D DN mutation (Figure 8.11). Although there were some cases where the KCNQ1 G229D mutation caused obvious APD shortening, there were many cases where the introduction of the mutation caused little change in APD. Only a very small proportion of models exhibited APD prolongation after introducing KCNQ1 G229D mutation.

To further explore the different responses of the models to this mutation, two subgroups were categorised from the original population: Stable Sensitive (1069/2326, **46%**) or Stable Not Sensitive (1037/2326, **44%**), according to the absolute difference $|APD_{G229D}- APD_{WT}|$ being greater or smaller to 10% of the respective APD_{WT} for all the considered CLs.

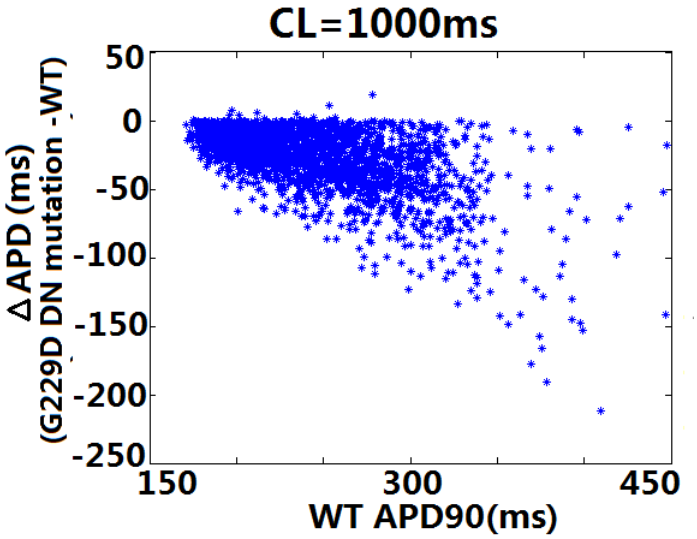


Figure 8.11: Effects of KCNQ1 G229D DN mutation on APD in the population, comparing with WT.

Compared to the Not Sensitive group, the Sensitive group tended to have longer WT APD_{90}, longer WT APD_{30}, smaller WT APD_{tri} and bigger WT APA (Figure 8.12). These phenomena could also be explained by the stronger G_{Na}, smaller G_{to} and G_{CaL}, weaker G_{Kr}, and stronger G_{Ks} and G_{K1} found in the Sensitive group (Figure 8.13).

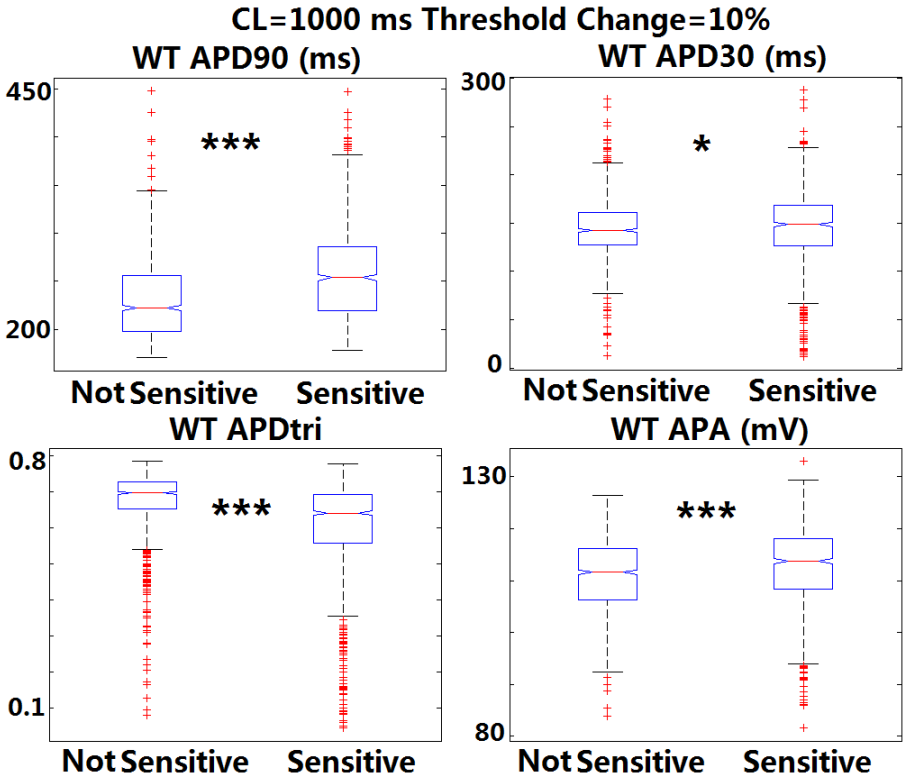


Figure 8.12: Comparison of the WT biomarkers between the Not Sensitive group and Sensitive group.

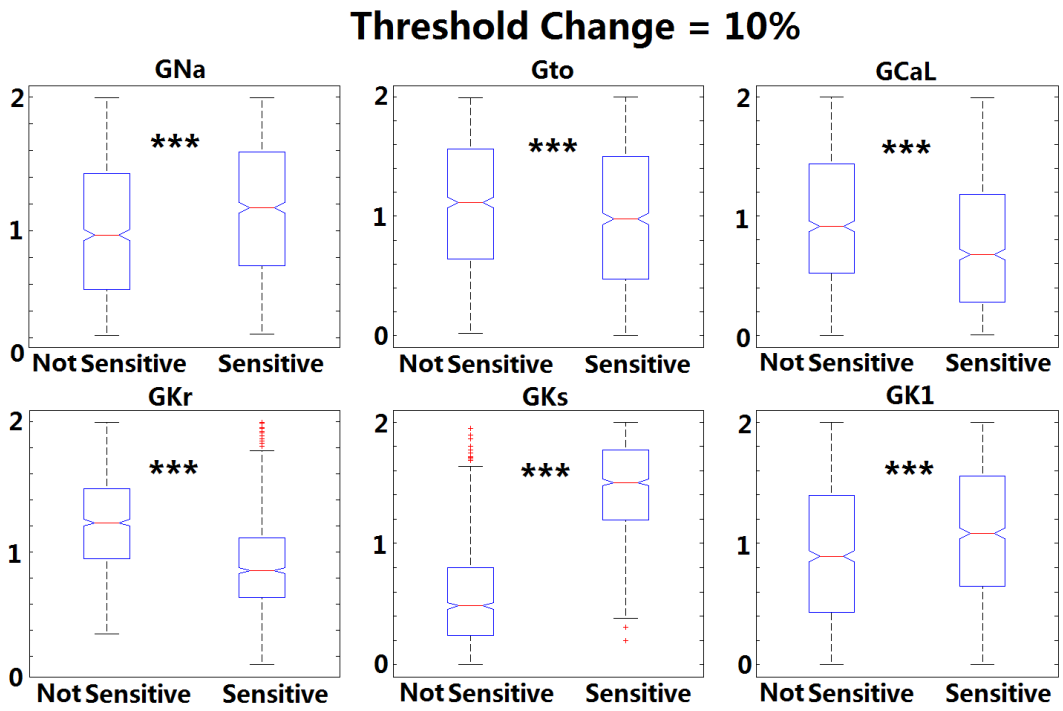


Figure 8.13: Comparison of current conductance scaling factors between the Not Sensitive and Sensitive groups.

8.3.5.2 Baseline levels of I_{Kr}, I_{Ks} and I_{CaL} are the main determinants for the extent of APD shortening after KCNQ1 G229D mutation

A partial correlation analysis was also used to explain the response of the models to the KCNQ1 G229D mutation (Figure 8.14), and the baseline conductances of I_{CaL}, I_{Kr} and I_{Ks} were identified as the most important determinants for the response of a model to this I_{Ks} mutation. I_{Kr} and I_{CaL} were positively correlated to the change of APD after the G229D mutation, meaning that if a model had a stronger I_{Kr} and I_{CaL}, APD of the mutants would be relatively longer compared to WT. On the other hand, I_{Ks} was negatively correlated to the change of APD induced by the mutation; therefore, a stronger I_{Ks} in a model tended to produce a shorter APD after KCNQ1 G229D mutation.

The above results were corroborated by Figure 8.15, which illustrated the relationship between I_{Ks}, I_{Kr}, I_{CaL} and the change of APD after KCNQ1 G229D mutation. Models with weak baseline I_{CaL} and I_{Kr} and strong baseline I_{Ks} exhibited

the most significant APD shortening after introducing the mutation, while models with strong I_{Kr} and I_{CaL} and weak I_{Ks} were less sensitive to the mutation (Figure 8.15).

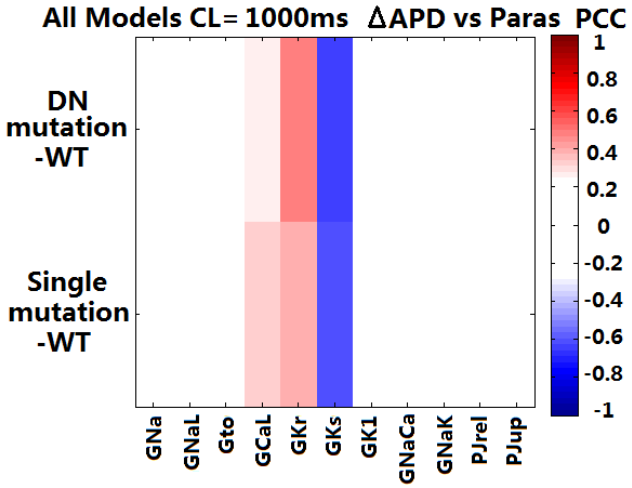


Figure 8.14: Partial correlation analysis of models' response in APD to the introduction of KCNQ1 G229D mutation.

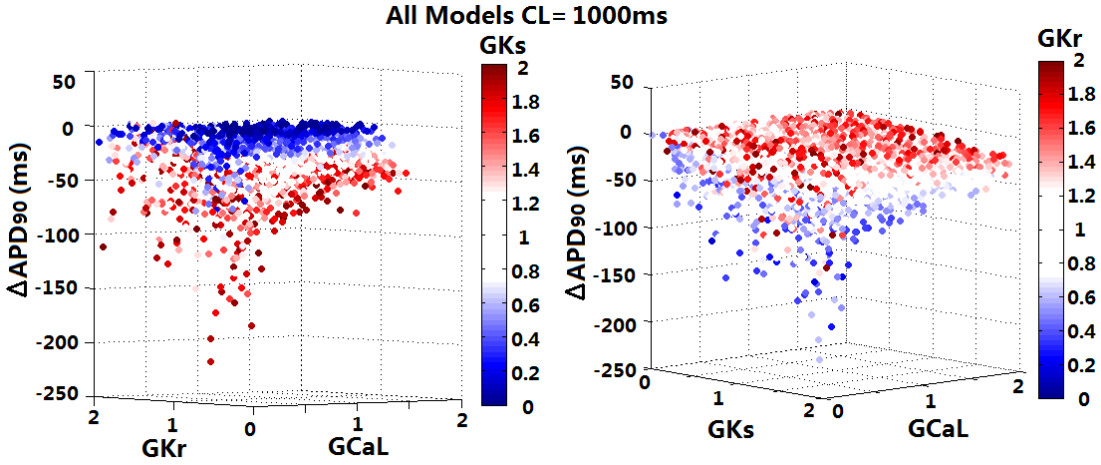


Figure 8.15: The response of APD_{90} to KCNQ1 G229D mutation was related to the baseline level of G_{CaL}, G_{Kr} and G_{Ks}. $\Delta APD = APD_{G229D_DNmutation} - APD_{WT}$.

8.3.5.3 The subtle interplay between the change of I_{Kr} and I_{Ks} after KCNQ1 G229D mutation can lead to APD prolongation

Although the majority of models tended to display shorter APDs after introducing KCNQ1 G229D mutation, 17 models showed APD prolongation to different extents at a CL of 1000ms (Figure 8.11). To understand the ionic mechanisms underlying APD prolongation and APD shortening, we analysed the change of individual

currents induced by the mutation. As illustrated in Figure 8.16, both models yielding either APD prolongation or APD shortening exhibited a smaller phase 2 AP plateau in mutants than in WT, due to the instantaneous activated KCNQ1 G229D I_{Ks} current caused from the early phases of the AP. The biggest differences in ionic currents were the increase of I_{Ks} (directly caused by the mutation) and the secondary decrease of I_{Kr}.

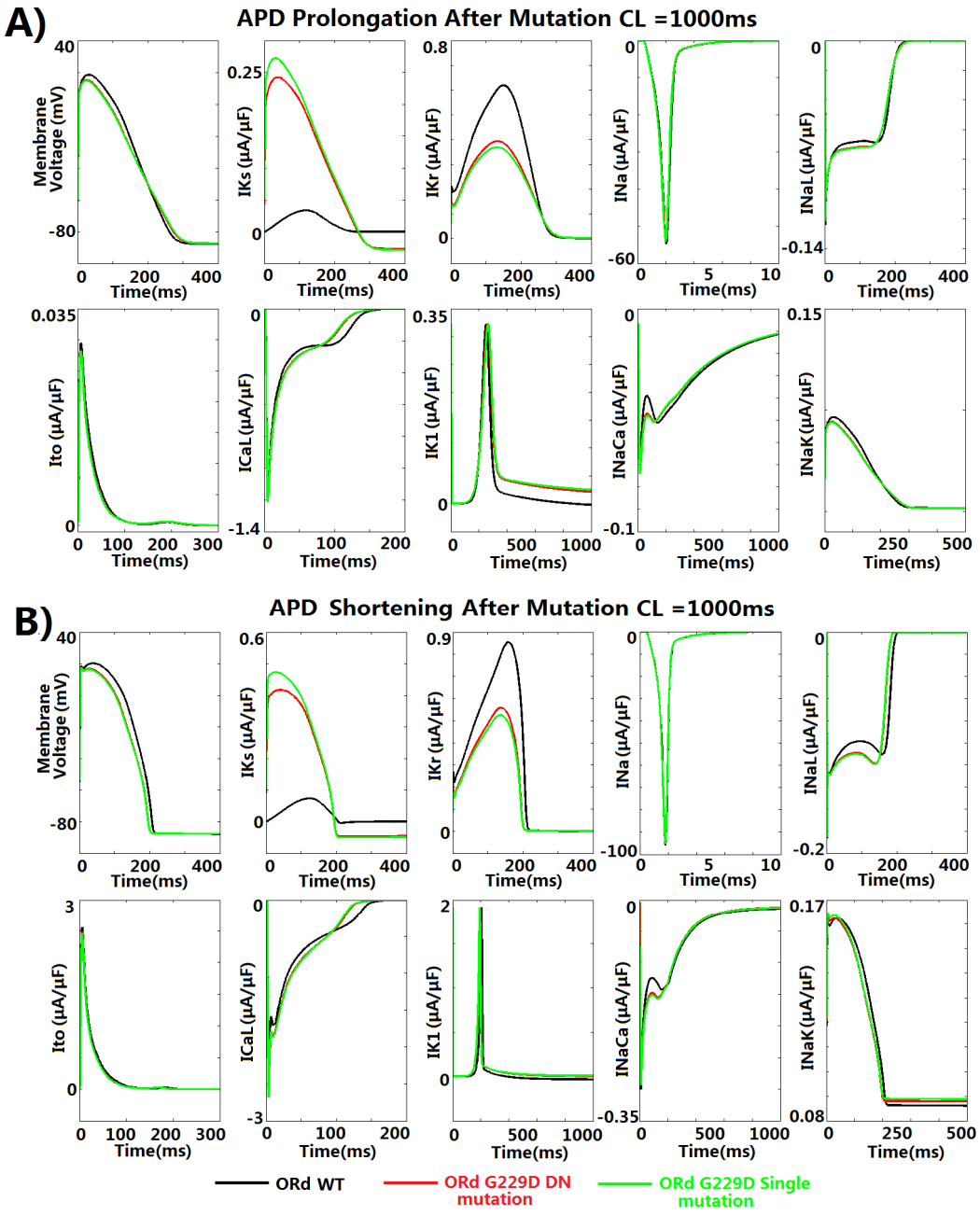


Figure 8.16: Effects of KCNQ1 G229D mutation on different ionic currents in representative models displaying (A) APD prolongation and (B) APD shortening, at CL=1000ms.

The reduction of I_{Kr} magnitude after KCNQ1 G229D mutation was caused by the smaller AP plateau (Figure 8.16 A and B, first panels in their first rows). As it was shown in Figure 8.17A, the activity of I_{Kr} was regulated dynamically with the change of membrane voltage. During the phase 2 plateau of the AP, a reduction in membrane voltage can lead to significant reduction in I_{Kr} activity, which explained the smaller I_{Kr} amplitudes after the mutation (Figure 8.16 A and B, third panels in their first rows). This highlighted the subtle interplay between the increase of I_{Ks} amplitude and the decrease of I_{Kr} amplitude after KCNQ1 G229D mutation. If the increase of I_{Ks} amplitude was predominant, APD would be shorter; otherwise, APD would remain constant or may be prolonged.

Using the sum of I_{Kr} and I_{Ks} amplitudes as a coarse estimate of repolarisation strength, the change of repolarisation strength after introducing the KCNQ1 G229D mutation can be estimated in the whole population of models. As shown in Figure 8.17B, the 17 G229D mutation models displaying APD prolongations tended to have weaker repolarisation strength than the WT (points at the upper left corner). For the majority mutation models displaying shorter APD, their repolarisation strength after the mutation tended to be stronger than in WT.

We also noticed that the 17 models displaying APD prolongations after introducing the KCNQ1 G229D mutation only showed prolongations at a pacing CL of 1000ms, which suggested that the rate-dependence of ionic currents can also play a role in the regulation process. Figure 8.17C showed the rate dependent changes of I_{Kr} and I_{Ks}. From this figure, it was clear that for longer pacing CLs the magnitude of I_{Ks} will decrease, whereas I_{Kr} would become stronger. Therefore, slow pacing conditions could facilitate for the change of I_{Kr} to be dominant under the existence of KCNQ1 G229D mutation. To test this hypothesis, we simulated the whole population of models at CL=2000ms. As shown in Figure 8.17D, at a slower pacing CL of 2000ms, more models displayed APD prolongations compared to WT after introducing the

mutation. These 75 models showing AP prolongations also had weaker repolarisation strength after introducing the mutation.

For long pacing CL, current kinetics at resting potentials plays more important roles for the rate dependency of the current. Figure 8.17E-F showed the activation and deactivation time constants for both WT and DN mutation at multiple potentials. Currently, there was a lack of experimental human I_{Ks} deactivation kinetics data at the resting potential for both WT and G229D mutation, and the accuracy of the Figure 8.17D may be affected if deactivation kinetics is faster at resting potentials. However, both WT and G229D DN mutation models can reproduce the similar trend of I_{Ks} rate dependency observed experimentally (Rocchetti et al., 2001), therefore the phenomena in Figure 8.17D should not be affected qualitatively.

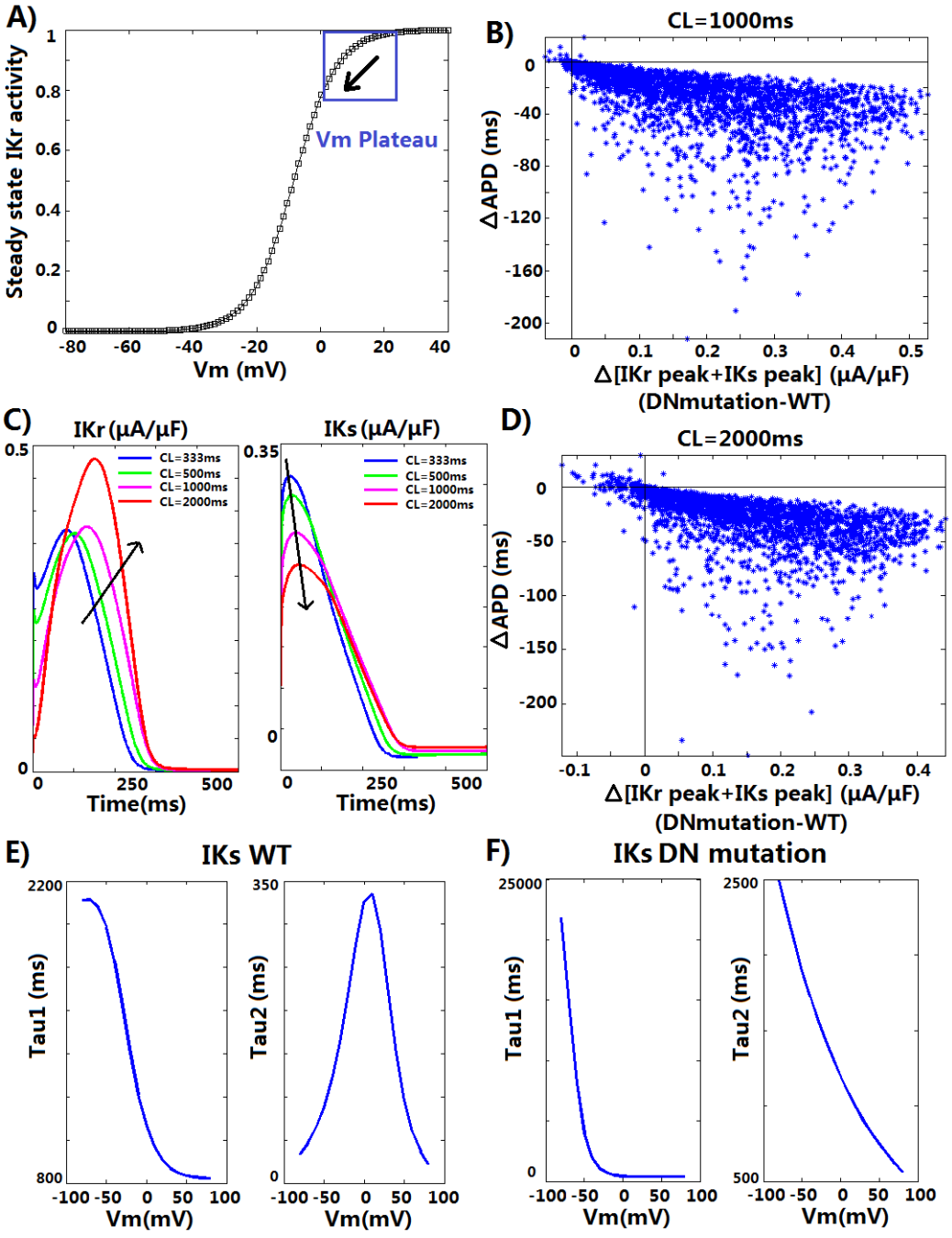


Figure 8.17: The subtle balance between I_{Kr} decrease and I_{Ks} increase after KCNQ1 G229D mutation regulates APD. A) Dependence of steady state I_{Kr} activation with the change of membrane voltage (Vm) in ORd model. B) Relationship between the change of repolarisation strength (estimated using the sum of peak I_{Ks} and peak I_{Kr}) and the change of APD after KCNQ1 G229D mutation at CL=1000ms. C) Rate dependence of I_{Kr} and I_{Ks} with the change of pacing CLs for G229D DN mutation. Arrows indicate the increase of CLs. D) The relationship between the change of repolarisation strength and the change of APD after KCNQ1 G229D mutation at CL=2000ms. ΔAPD= $APD_{G229D_DNmutation}$- $APD_{WT.}$ Activation time constants (Tau1) and deactivation time constants (Tau2) of the WT (E) and G229D DN mutation (F) IKs model with the change of Vm.

8.4 Discussion and conclusions

In this chapter, we developed I_{Ks} mutation models for KCNQ1 G229D single and DN mutations. By varying the current kinetics parameters in the ORd I_{Ks} formulation, the effects of the KCNQ1 G229D mutation can be reproduced without modifying the structure of the equations. The effects of the KCNQ1 G229D mutation were explored both in the standard ORd model and in the population of human ventricular cell models developed in Chapter 5. The main findings are the following:

1) The primary effect of this mutation was APD shortening; however, about 44% of the models were not sensitive to the introduction of KCNQ1 G229D mutation. Further comparison between the sensitive and non-sensitive models revealed that the baseline level of multiple currents, such as I_{Na}, I_{to}, I_{CaL}, I_{Kr}, I_{Ks} and I_{K1} can affect the sensitivity of a model to the KCNQ1 G229D mutation.
2) Partial correlation analysis on the population of models revealed that the most important determinants for the extent of APD shortening after KCNQ1 G229D mutation were I_{CaL}, I_{Kr} and I_{Ks}. If the baseline levels of I_{CaL} and I_{Kr} were weak and the baseline level of I_{Ks} was strong, the KCNQ1 G229D mutation could result in more significant APD shortening.
3) Although the majority of models displayed shorter APD after the introduction of the KCNQ1 G229D mutation, a small fraction of models showed APD prolongation. These phenomena were due to the subtle interplay between the decrease of I_{Kr} activity and the increased I_{Ks} activity, as a result of KCNQ1 G229D-induced changes in the AP plateau potential. If the reduction of I_{Kr} was dominant compared to the enhancement of I_{Ks}, the overall repolarisation strength would decrease, leading to longer APDs. Under longer pacing CLs, I_{Kr} activity will increase whereas the I_{Ks} activity decreases; therefore, slower pacing facilitates a predominant role for changes in I_{Kr} magnitude induced by the KCNQ1 G229D mutation.

Gain-of-function KCNQ1 mutations: atrial fibrillation and LQT?

The KCNQ1 G229D mutation has been previously related to the onset of atrial fibrillation (AF) (Hasegawa *et al*., 2014), commonly associated with APD shortening. Similar KCNQ1 gain-of-function gene mutations have been also reported, S140G (Y.-H. Chen et al., 2003), V141M (Hong *et al*., 2005), Q147R (Lundby *et al*., 2007), S209P (Das *et al*., 2009), R231C (Bartos *et al*., 2011), R231H (Bartos *et al*., 2013), V241F (Ki *et al*., 2014). All these studies reported akin connections between the different gain-of-function KCNQ1 mutations and the onset of AF (Bartos et al., 2013, 2011; Y.-H. Chen et al., 2003; Das et al., 2009; Ki et al., 2014; Lundby et al., 2007), or short QT syndrome (Hong *et al*., 2005).

Intriguingly, borderline QT prolongation has been also reported as related to some gain-of-function KCNQ1 mutations (Bartos et al., 2013, 2011; Y.-H. Chen et al., 2003; Hasegawa et al., 2014; Lundby et al., 2007). For example, according to (Y.-H. Chen et al., 2003), several individuals affected by S140G displayed prolonged QTc (9 of 16 patients, range 0.45 to 0.53 s). Similarly, R231C mutation in KCNQ1 was found as well to be related to both AF and LQT1 (Bartos *et al*., 2011). According to (Hasegawa *et al*., 2014), a borderline level of QT prolongation was also observed in their KCNQ1 G229D mutation patient after undergoing radiofrequency catheter ablation therapy, and this borderline criteria of QT prolongation was also shared by his asymptomatic mother (Hasegawa *et al*., 2014). Therefore, the effects of KCNQ1 gain-of-function mutations can be highly complex, involving the interaction between multiple electrophysiological factors in each individual.

In this study, a population of experimentally-calibrated human ventricular cell models was used as a platform to investigate the complex interactions between different currents after KCNQ1 G229D mutation, accounting for natural variability in the expression of ionic currents. Our simulation results show the possibility of both APD prolongation and APD shortening as a result of KCNQ1 G229D mutation.

Slower pacing rates tended to favour APD prolongation after the mutation, which also suggested the potential proarrhythmic risk at rest or during sleeping. Indeed, asleep episodes of sudden cardiac arrest have been previously reported under similar gain-of-function KCNQ1 mutations (Bartos *et al*., 2013). Although our population of models were able to predict APD prolongation after the KCNQ1 G229D mutation, the probability for the AP prolongation was low compared to AP shortening under normal pacing rates (CL=1000ms). Since the AP prolongation after G229D mutation involves a delicate voltage-dependent current regulation and a subtle balance between the change of I_{Kr} and I_{Ks}, more research can be conducted in future work to explore the effects of I_{Kr} kinetics variability.

β-adrenergic stimulation on I_{Ks}

The β-adrenergic stimulation pathway has been identified as a main trigger of arrhythmic events for LQT1 patients (Barsheshet *et al*., 2012). It is known that cytoplasmic loops (C-loops) are important in the sympathetic regulation of the KCNQ1 channel (Matavel *et al*., 2010). In a recent study of LQT1 mutations, 860 patients were categorized into carriers of missense mutations located in the C-loops, transmembrane region, and C/N terminus. The mutation carriers of KCNQ1 C-loop had the highest risk for aborted cardiac arrest and sudden cardiac death, and the effect of β-blocker therapy was most significant in this cohort of patients (Barsheshet *et al*., 2012). G229D is located in the fourth transmembrane segment of Kv7.1, known as the voltage sensor (Hasegawa *et al*., 2014). Although not located in the C-loops, it is still likely that the β-adrenergic stimulation alters the function of the mutated I_{Ks} channel. For example, according to (Bartos *et al*., 2013), R231H mutation of KCNQ1 was found to be resistant to PKA stimulation. Therefore, further experiments can be designed to investigate the response of the KCNQ1 G229D mutation under adrenergic stimulation.

Risk stratification for LQTS mutation carriers

According to the latest research of (Ghouse *et al*., 2015) based on Human Gene

Mutation Database, 26 variants previously reported to be LQTS-associated did not show significant effects on the QTc intervals and the overall mortality. Therefore, although statistical analysis based on human genome data can provide abundant information regarding the potential risk of many genetic variations, functional analysis using electrophysiological experimental techniques is still needed to confirm the electrophysiological effect of an individual mutation. Even for a mutation that is proven to be able to alter the function of an ion channel, it is very likely that the carrier of this mutation is asymptomatic under normal conditions, but may be more sensitive to pharmacological side effects than non-carriers (Campbell *et al*., 2013). Therefore, to improve the risk stratification of genetic mutation carriers, further research is still needed to achieve the genotype-specific treatment of heritable arrhythmia (Campbell *et al*., 2013).

Computational cardiac models can be a very useful tool to explore the effects of ion channel mutations and to investigate proarrhythmic risk. For instance, 1-dimensional transmural simulations were used to investigate the effects of 34 loss-of function LQT mutations, and their simulated results suggested that prolongation in transmural repolarisation can significantly affect the patients with mild QTc durations (Hoefen *et al*., 2012). The proarrhythmic effects of the gain-of-function mutations S140G and V241F were also simulated computationally in human atria models (Imaniastuti et al., 2014; Kharche et al., 2012), and re-entrant waves exhibited increased sustainability under the presence of the mutations. Therefore, it will be interesting to extend the KCNQ1 G229D mutated I_{Ks} model into human ventricular tissue modelling in future work.

Conclusions

In this Chapter, we investigated the effect of KCNQ1 G229D mutation. Although APD prolongation in a gain-of-function I_{Ks} mutation is very counterintuitive, our simulations show that it is possible, even if it only occurred as small prolongations in a very small proportion of the population. This effect was due to the interplay

between the mutated I_{Ks} and variable I_{Kr}, and other factors are needed to explain the prolongation observed in the patient (QTc=490 ms), with the most likely factor being the impact of the adrenergic modulation which needs to be further investigated.

Chapter 9

Conclusions and discussions

9.1 Summary

Sudden cardiac death caused by cardiac arrhythmias is one of the most common causes of mortality. The generation of arrhythmias is difficult to predict in advance due to the complexity of the cardiac electrophysiological system and incomplete understanding of a variety of proarrhythmic mechanisms. The existence of inter-subject and intra-subject variability can increase the complexity of the cardiac system, and can therefore significantly affect the development and understanding of life-threatening cardiac abnormalities in different individuals. Therefore, more research is needed to explore the effect of cardiac variability, especially for human *in vivo* conditions.

However, the study of cardiac variability is usually very difficult. In wet lab experiments, recordings are nearly always averaged to describe the typical behaviour of cardiac cells and tissue. Thus, the variability between cardiac cells is generally neglected in experimental research. Biophysically detailed computational cardiac models have been playing an increasingly important role in cardiac research. However, these computational models are normally developed based on averaged experimental data, and the effect of variability has often been neglected in *in silico* research, until recently.

In addition, due to the inherent ethical limitations in human cardiac research, most

cardiac research uses animals as experimental resources. The proarrhythmic ionic mechanisms for human *in vivo* conditions are much less known.

Therefore, the goal of this thesis is to use biophysically detailed human cell models to investigate proarrhythmic ionic mechanisms and to explore the effect of ionic variability in human ventricular electrophysiology. In this thesis, we have investigated three pro-arrhythmic conditions: post myocardial infarction epicardial border zone, cardiac alternans and ionic channel mutation.

We began in Chapter 2 by introducing the basic function and structure of the heart. Then we introduced the basic electrophysiological characteristics of cardiomyocytes, such as ion channel gating, action potential, and excitation-contraction coupling. Following this we reviewed relevant electrophysiological techniques used in *in vitro* and *in vivo* experiments. Mechanisms affecting cardiac variability were then reviewed, such as circardian rhythms, drug exposure, and sympathetic neural stimulation. We then described several proarrhythmic conditions that are relevant to this thesis: myocardial infarction, cardiac alternans and LQT syndrome. We finished this chapter by reviewing antiarrhythmic drugs and the inter-species difference between human and animals.

In Chapter 3, we reviewed computational modelling in cardiac cellular electrophysiology. We began with the basic concept underlying the Hodgkin-Huxley formulation and the Markov chain formulation of ionic currents. We then briefly reviewed the development of cardiac modelling since the 1962 Noble model, followed by recently published human ventricular cell models, a comparison between a human ventricular cell model and a canine ventricular cell model to illustrate the inter-species similarities and differences. Following this was a brief introduction to the modelling of diseased cardiomyocytes and drug effects. Different approaches for the modelling of cardiac variability were then introduced and compared.

In Chapter 4 we presented the first results of this thesis. In this part of the study, we modified a standard healthy human model (O'Hara *et al*., 2011) into a post infarction epicardial border zone cell model by introducing analogous current remodelling as that observed in canine. The increase of APD and the generation of cardiac alternans were observed after the introduction of the remodelling. The application of I_{Kr} block can further increase the dispersion between NZ and EBZ cells, and facilitate the development of alternans in the EBZ. The remodelling of current conductances is proved as sufficient to cause the proarrhythmic properties in the EBZ cell, and further modification to current kinetics only affected the sensitivity of the EBZ to faster CLs.

In Chapter 5 we constructed and calibrated a population of human epicardial ventricular cell models. Based on the results of chapter 4, the variability of current conductances was sufficient to induce proarrhythmic conditions. Therefore, we generated an initial population of human ventricular cell models sharing the same kinetics equations, but with different conductance values. To exclude nonphysiological models in the initial population, we applied several electrophysiology filters in the calibration to select the models whose outputs were in range with the experimental human data. The most pivotal filter was the human *in vivo* ARI at multiple pacing frequencies, as a surrogate of APD. The calibrated human ventricular cell models were then used in the following chapters as a platform to include the effect of cardiac variability in human ventricular cell modelling.

In Chapter 6 we investigated the mechanisms underlying different types of alternans using the population of human ventricular cell models developed in Chapter 5. Six ionic currents and fluxes were found to be related to the generation of alternans, and two types of APD alternans were observed in the models. Similar types of APD alternans were also observed in the *in vivo* ARI data. Then we focused on the investigation of the ionic current mechanisms for the initiation of calcium alternans

and the transition from CaT alternans to APD alternans. The fluctuation of SR calcium was identified as the primary mechanism underlying calcium alternans in the population of human ventricular cell models, and I_{NaCa} was the main translator between calcium alternans and APD alternans. The difference between the two types of APD alternans was due to the rate-dependence of I_{CaL} and CaT. The net balance of sarcolemmal calcium inflow and outflow was identified to be a good indicator of alternans magnitudes.

In Chapter 7 we further simulated the effects of potential pharmacological interventions on the alternans models. Based on the simulation results in Chapter 6, the pharmacological interventions on six currents or ionic fluxes were explored, and decreasing I_{CaL} or I_{NaCa} and increasing J_{up} were found to be the most effective strategies to inhibit alternans generation. Further comparison of these three interventions revealed that decreasing I_{CaL} or I_{NaCa} was more effective than the upregulation of SERCA in alternans suppression. However, I_{CaL} inhibition can also seriously affect the contractility of cardiac myocytes by decreasing the amplitude of the calcium transient. Therefore, the modulation of I_{NaCa} was accounted as the most promising and feasible anti-arrhythmic target against cardiac alternans.

The population of human ventricular cell models developed and calibrated in Chapter 5 was then used to investigate the interaction between a I_{Ks} mutation and natural cardiac variability. The characteristics of the KCNQ1 G229D mutation were reproduced in the I_{Ks} model by changing current kinetics to fit KCNQ1 G229D mutation patch clamp data. Incorporating the G229D mutated I_{Ks} model into the population of human ventricular cell models revealed that the effect of I_{Ks} mutation on the overall behaviour of a cardiomyocyte strongly depended on the interactions between I_{Ks}, I_{Kr} and I_{CaL}.

9.2 Key contributions and main findings

The first key contribution of this thesis is the development of a cellular model of the human post-infarcted EBZ. As an important source of spatio-temporal dispersion, the EBZ has been previously studied, but most of these studies were conducted using animals due to ethical difficulties in human. Our human model of EBZ cell predicted similar APD prolongation as observed in canine, and also suggested the potential risk of cardiac alternans due to longer APDs. This human EBZ cell model might serve as a useful tool to evaluate the effects of anti-arrhythmic drugs in post MI patients.

The second major contribution of this thesis is the generation of a human population of ventricular cell models calibrated based on *in vivo* human data. Inter-subject variability is a crucial factor that determines the different phenotype of the same genetic mutation carriers, and is also responsible for the diverse responses of different individuals to same pharmacological interventions. Intra-subject variability also affects multiple factors determining the spatio-temporal synchronization of cardiac tissue. Therefore, this population of human ventricular cell models provides a suitable platform for the investigation of cardiac proarrhythmic mechanisms given the numerous possible combinations of current variations.

The third key contribution of the thesis is the study of the ionic mechanisms underlying cardiac alternans under physiological human APDs. Cardiac alternans are generally believed to be related to fast pacing rates and long APDs. However, multiple studies have reported the existence of alternans in the absence of APD prolongation, indicating the plausibility of additional mechanisms beyond cellular restitution properties. In this study, we have unraveled the fact that human ventricular APD alternans can generate under normal physiological APDs due to the fluctuation of the calcium subsystem. This means that apart from APD prolongation, calcium fluctuation is an independent source of alternans initiation.

Although calcium alternans have been frequently studied in animal experiments, the key mechanisms of human cardiac alternans are much less understood. In addition, the transfer from calcium alternans to APD alternans still remained unclear, especially for human ventricular alternans. Another major result of this thesis is that I_{NaCa} functions as the key translator between calcium alternans and APD alternans in human cardiomyocytes. The simulation results of pharmacological interventions also suggest I_{NaCa} as a promising anti-arrhythmic target for alternans inhibition.

Finally another major contribution of the thesis is the study of the interaction between ionic channel mutations and cardiac variability. The low penetrance of genetic mutation carriers, especially I_{Ks} mutation carriers, has been reported previously. Using the population of human ventricular cell models, we revealed that the effect of an ion channel gene mutation strongly depends on the electrical balance of the whole cell.

9.3 Future directions

9.3.1 Incorporating post-MI EBZ information from human

In Chapter 4, we have generated a cellular human model for post-MI EBZ. Although the original healthy human ventricular cell model was constructed based on experimental data from over 100 human hearts (O'Hara *et al*., 2011), the post-MI electrophysiological remodelling we incorporated into the model was transformed from canine data. Thus, some inter-species differences between the human and canine EBZ could affect the accuracy of the human EBZ model. Therefore, even though our study in the modelling of the human EBZ single cell yet constitutes a first step in the iteration between computational, experimental and clinical work, it can still provide a useful tool for the investigation of proarrhythmic conditions in post-MI patients.

One potential approach to address this problem is to obtain human EBZ data from patients. In recent research by Taggart *et al.* (Taggart *et al*., 2014), biopsies were taken from specific sites from patients during cardiac surgery, and then analysed using mRNA profiling and Western blot. If a similar approach could be applied to post-MI conditions, it would enable the comparison of ion channel expression profiles between NZ and EBZ, allowing for a more direct and accurate incorporation of the post-MI human EBZ remodelling *in silico*.

9.3.2 Variation of current conductances based on experimental data

In this thesis, we have generated an initial population of 10000 models by randomly varying the strength of 11 key currents and fluxes. The main assumption underlying the cell-to-cell variability is that it primarily stems from different levels of ion channel densities regulated by protein expression(Cummins et al., 2014; Devenyi and Sobie, 2015; Groenendaal et al., 2015; Sarkar et al., 2012; Sobie, 2009; Sobie and Sarkar, 2011; Yang and Clancy, 2012), while the ion channel kinetics should be relatively stable in the absence of genetic mutations. When we introduced variations of current conductance parameters to capture a broad range of physiological responses, we assumed initial uniform distributions within ±100% of their default strength, due to the difficulties in getting real conductance ranges in human cardiomyocytes.

Although it is possible to measure the conductance of an individual cell using voltage clamp experiments, the isolation procedure causes severe damage to the cells, which then alters the current conductances values (Yue *et al*., 1996). If this experimental challenge could be resolved, future studies might incorporate natural variability ranges as observed in a particular type of cells from specific species. Then the current conductance parameter sampling range and density could be determined

directly from the experimental data.

9.3.3 Ryanodine receptor refractoriness and calcium alternans in human cardiomyocytes

In Chapter 6, we have investigated the mechanisms underlying cardiac alternans generation using the population of human ventricular cell model constructed and calibrated in Chapter 5. The initiation of alternans in our human ventricular cell models was found to be due to the fluctuation of SR calcium levels caused by the over-release of SR calcium. This was in agreement with previous observations in rabbit and rat isolated cells (Díaz et al., 2004; Picht et al., 2006). However, recent results in rabbit myocytes and intact hearts have revealed that calcium alternans can initiate before the development of SR calcium fluctuation (Picht et al., 2006; Wang et al., 2014), and the refractoriness of RyR can be the source of alternans initiation. Therefore, future experiments are needed to evaluate the contributions of RyR mechanisms in human. If calcium alternans caused by RyR refractoriness can happen before the fluctuation of SR calcium levels in human cardiomyocytes, then this implies the calcium subsystem in the O'Hara *et al.* model needs to be updated. A more complex calcium cycling framework, such as calcium release units (Nivala and Qu, 2012), might need to be incorporated into the model.

9.3.4 Repolarisation strength and β-adrenergic stimulation

In Chapter 8, we developed a mutated I_{Ks} model with the G229D mutation in the KCNQ1 subunit, and we also investigated the interaction between I_{Ks} G229D mutation and variability in 11 key currents and fluxes. The mutated I_{Ks} model reproduced the instantaneous activation of I_{Ks} observed in experiments, and predicted the shortening of APD in both the standard O'Hara *et al.* model and the

majority of population of human ventricular cell models. The shortening of APDs was consistent with the AP shortening associated to juvenile-onset of atrial fibrillation reported by Hasegawa *et al.* (Hasegawa *et al*., 2014). However, the borderline LQT observed by Hasegawa *et al.* and our collaborators was only consistent with a small fraction of our population of human ventricular models incorporating variability of currents and fluxes. Since the voltage-dependent regulation of I_{Kr} was identified to be a crucial factor in the development of AP prolongation, future study can be designed to explore the variations in I_{Kr} kinetics and their effect on overall repolarisation strength.

The β-adrenergic stimulation cascade is a natural regulator of repolarisation strength in cardiac electrophysiological system, and previous research have identified the augmentation of I_{Ks} current under β-adrenergic stimulation (Marx *et al*., 2002). β-adrenergic stimulation might also have an influence on the mutant phenotype. According to (Bartos *et al*., 2013), a similar gain-of-function KCNQ1 mutation R231H was found to be resistant to PKA stimulation. It will be very interesting to investigate the electrophysiological response of KCNQ1 G229D mutation to β-adrenergic stimulation. In addition, β-adrenergic stimulations can also affect the effect of I_{Ks} channel mutations by regulating the current densities of other relevant currents, such as I_{Na} (Wang *et al*., 2009) and I_{CaL} (Ganesan *et al*., 2006).

9.3.5 Risk stratification for different subgroups and individuals

To investigate the effect of natural variability in proarrhythmic mechanisms, a population of human ventricular cell models was developed and calibrated based on *in vivo* human data from 41 patients in this study. A potential future direction can be the development of population of models for a subgroup of patients and even for different individuals.

For instance, instead of using the ARI data from all patients to select the models with physiological behaviour, the ARI range of male or female patients can be used as a calibration filter to select the models that match the properties of the subgroups. Then the ionic differences between male and female patients could be compared using the corresponding subpopulation of models.

Another application of subpopulations of models could be the risk stratification of pharmacological drugs. Once a population of models is constructed and calibrated for a specific group of patients, the effects of different ionic interventions could be tested for the subgroup.

9.3.6 The effects of tissue coupling

In this thesis, we used single cell simulations to explore the proarrhythmic ionic mechanisms in human ventricular cell models. However, cardiac arrhythmias occur at the tissue level, and the effect of gap junction coupling and 3-D tissue structure can also affect the origin of arrhythmias. For example, it has been reported that the intercellular electrical coupling between myocytes can decrease the probability of alternans generation, but also stabilise alternans once initiated (Hammer *et al*., 2015). Some proarrhythmic conditions, such as re-entry, can only be studied in 2-D or 3-D simulations. Therefore, a promising line of future investigations would be the extension of this thesis results to tissue modeling.

The major challenge is that the computational cost increases vastly even for a simple 1-D or 2-D simulation. Performing a single 3-D tissue simulation for a biophysically-detailed model can require supercomputing resources, and performing tissue simulation studies for a population of thousands of models is currently unfeasible. Therefore, the next research step can start from simple 1-D simulations for the 87 alternans models. It would be interesting to explore the stability of

Eye-type and Fork-type alternans, and their development into concordant or discordant alternas, after introducing tissue coupling.

9.4 Conclusions

Considerable research has been conducted to study proarrhythmic mechanisms using animal assays; therefore, the translation from research to human is usually compromised due to significant inter-species differences. The large costs of human testing and ethical limitations also create barriers between basic science and clinical applications. In addition, the existence of inter-subject and intra-subject variability largely increases the complexity of human cardiac electrophysiological studies.

In this thesis, we used human ventricular cell models developed based on human data to investigate proarrhythmic mechanisms in three pathological conditions: the post-MI EBZ, cardiac alternans under normal APDs and ion channel genetic mutation. Initially in Chapter 4, we introduced the post-MI remodelling reported in canine EBZ into the healthy human ventricular epicardial cell models. We observed the development of alternans due to the prolongation of APD after electrical remodelling. We also found that the modification of current conductances was sufficient to reproduce the similar changes in AP morphology as observed in canine, and that further modifications of current kinetics did not fundamentally alter the characteristics of the EBZ. Therefore we conclude that the variation of current conductances plays a key role in determining the development of pathological conditions.

Thus in the next part of our study, we included the effect of current density variations to generate a large initial population of models in Chapter 5. The *in vivo* human ARIs were used to select the models with physiological APDs from the initial population. Then the mechanisms underlying cardiac alternans with normal APDs were

investigated in Chapter 6. Our population of human ventricular cell alternans models was able to reproduce two types of APD alternans behaviours observed in patients: the Eye-type and Fork-type alternans. We found that in our population of human ventricular cell models, the initiation of alternans was due to the fluctuation of SR calcium level caused by the loss of SRCB between calcium release and calcium re-uptake. The I_{NaCa} was the main link to convert calcium fluctuations into APD alternans. The magnitude of APD alternans was strongly correlated to the fluctuation of SCB, which is the overall calcium flow balance on cell membrane. Due to the potential role of I_{CaL} kinetics in alternans, we also explored the effect of varying I_{CaL} kinetics. The results showed that variations to I_{CaL} kinetics can affect the stability of alternans, but it is still through the regulation of SRCB and SCB.

We also explored the effect of potential pharmacological interventions on the alternans models in Chapter 7. Suppressing I_{CaL} or I_{NaCa} and up-regulating SERCA activity tended to be the most effective strategy to inhibit alternans generation. According to the simulation results, inhibiting I_{CaL} can impair the contractility of myocytes by severely decreasing the amplitude of the intracellular calcium transient. Up-regulating SERCA is pharmacologically challenging, and it also appeared to be less effective than blocking the sodium-calcium exchanger. Therefore, we support the conclusion that using sodium-calcium exchanger blockers tends to be the most promising strategy to inhibit alternans.

Finally, in Chapter 8, we explored the effect of G229D mutation in the I_{Ks} subunit KCNQ1. We developed a G229D mutant model for I_{Ks} which reproduced the instantaneous activation observed in patch clamp experiments. The I_{Ks} KCNQ1 G229D mutation tended to induce the shortening of the APD in the standard ORd model, and its effect in the population of models revealed that the effect of I_{Ks} gene mutation can be significantly affected by the channel density itself and its interaction with other ionic currents, such as I_{Kr} and I_{CaL}. The most significant APD shortening were observed when baseline I_{Kr} and I_{CaL} were weak and baseline I_{Ks} was strong. In

addition, the decrease of I_{Kr} density caused by the instantaneous I_{Ks} activation can sometimes overcome the effect of G229D mutation and lead to AP prolongation due to a weaker overall repolarisation strength.

To conclude, we hope that the work presented in this thesis provides a valuable contribution to the understanding of ionic current interactions with the existence of variability in human cardiac electrophysiology. We hope the new technique developed in this thesis to integrate mathematical modeling and *in vivo* human cardiac electrophysiological variability can be a useful platform for the future investigation of other pathological conditions. We also hope that our work can be potentially informative for the development and risk stratification of anti-arrhythmic drugs.

References

Abe, S., Nagamoto, Y., Fukuchi, Y., Hayakawa, T., Kuroiwa, A., 1989. Relationship of alternans of monophasic action potential and conduction delay inside the ischemic border zone to serious ventricular arrhythmia during acute myocardial ischemia in dogs. Am. Heart J. 117, 1223–1233. doi:10.1016/0002-8703(89)90400-6

Abrams, D.J., Macrae, C.A., 2014. Long QT syndrome. Circulation 129, 1524–1529. doi:10.1161/CIRCULATIONAHA.113.003985

Aggarwal, R., Boyden, P.A., 1995. Diminished Ca2+ and Ba2+ currents in myocytes surviving in the epicardial border zone of the 5-day infarcted canine heart. Circ. Res. 77, 1180–1191.

Aggarwal, R., Pu, J., Boyden, P.A., 1997. Ca(2+)-dependent outward currents in myocytes from epicardial border zone of 5-day infarcted canine heart. Am. J. Physiol. 273, H1386–1394.

Akar, F.G., Wu, R.C., Deschenes, I., Armoundas, A.A., Piacentino, V., Houser, S.R., Tomaselli, G.F., 2004. Phenotypic differences in transient outward K+ current of human and canine ventricular myocytes: insights into molecular composition of ventricular Ito. Am. J. Physiol. Heart Circ. Physiol. 286, H602–609. doi:10.1152/ajpheart.00673.2003

Alvarez-Lacalle, E., Cantalapiedra, I.R., Peñaranda, A., Cinca, J., Hove-Madsen, L., Echebarria, B., 2013. Dependency of Calcium Alternans on Ryanodine Receptor Refractoriness. PLoS ONE 8, e55042. doi:10.1371/journal.pone.0055042

Arevalo, H., Plank, G., Helm, P., Halperin, H., Trayanova, N., 2013. Tachycardia in Post-Infarction Hearts: Insights from 3D Image-Based Ventricular Models. PLoS ONE 8, e68872. doi:10.1371/journal.pone.0068872

Armoundas, A.A., Hohnloser, S.H., Ikeda, T., Cohen, R.J., 2005. Can microvolt T-wave alternans testing reduce unnecessary defibrillator implantation? Nat. Clin. Pract. Cardiovasc. Med. 2, 522–528. doi:10.1038/ncpcardio0323

Armoundas, A.A., Tomaselli, G.F., Esperer, H.D., 2002. Pathophysiological basis and clinical application of T-wave alternans. J. Am. Coll. Cardiol. 40, 207–217. doi:10.1016/S0735-1097(02)01960-5

Aziz, E.F., Javed, F., Pratap, B., Herzog, E., 2010. Strategies for the prevention and treatment of sudden cardiac death. Open Access Emerg. Med. OAEM 2010, 99–114. doi:10.2147/OAEM.S6869

Baba, S., Dun, W., Cabo, C., Boyden, P.A., 2005. Remodeling in cells from different regions of the reentrant circuit during ventricular tachycardia. Circulation 112, 2386–2396. doi:10.1161/CIRCULATIONAHA.105.534784

Barsheshet, A., Dotsenko, O., Goldenberg, I., 2013. Genotype-Specific Risk Stratification and Management of Patients with Long QT Syndrome. Ann. Noninvasive Electrocardiol. 18, 499–509. doi:10.1111/anec.12117

Barsheshet, A., Goldenberg, I., O-Uchi, J., Moss, A.J., Jons, C., Shimizu, W., Wilde,

A.A., McNitt, S., Peterson, D.R., Zareba, W., Robinson, J.L., Ackerman, M.J., Cypress, M., Gray, D.A., Hofman, N., Kanters, J.K., Kaufman, E.S., Platonov, P.G., Qi, M., Towbin, J.A., Vincent, G.M., Lopes, C.M., 2012. Mutations in cytoplasmic loops of the KCNQ1 channel and the risk of life-threatening events: implications for mutation-specific response to β-blocker therapy in type 1 long-QT syndrome. Circulation 125, 1988–1996. doi:10.1161/CIRCULATIONAHA.111.048041

Bartos, D.C., Anderson, J.B., Bastiaenen, R., Johnson, J.N., Gollob, M.H., Tester, D.J., Burgess, D.E., Homfray, T., Behr, E.R., Ackerman, M.J., Guicheney, P., Delisle, B.P., 2013. A KCNQ1 mutation causes a high penetrance for familial atrial fibrillation. J. Cardiovasc. Electrophysiol. 24, 562–569. doi:10.1111/jce.12068

Bartos, D.C., Duchatelet, S., Burgess, D.E., Klug, D., Denjoy, I., Peat, R., Lupoglazoff, J.-M., Fressart, V., Berthet, M., Ackerman, M.J., January, C.T., Guicheney, P., Delisle, B.P., 2011. R231C mutation in KCNQ1 causes long QT syndrome type 1 and familial atrial fibrillation. Heart Rhythm Off. J. Heart Rhythm Soc. 8, 48–55. doi:10.1016/j.hrthm.2010.09.010

Beadle, R., Williams, L., Lim, H.S., 2010. Drug-implantable cardioverter-defibrillator interactions. Expert Rev. Cardiovasc. Ther. 8, 1267–1273. doi:10.1586/erc.10.114

Beeler, G.W., Reuter, H., 1977. Reconstruction of the action potential of ventricular myocardial fibres. J. Physiol. 268, 177–210.

Bernus, O., Wilders, R., Zemlin, C.W., Verschelde, H., Panfilov, A.V., 2002. A computationally efficient electrophysiological model of human ventricular cells. Am. J. Physiol. Heart Circ. Physiol. 282, H2296–2308. doi:10.1152/ajpheart.00731.2001

Boukens, B.J., Sulkin, M.S., Gloschat, C.R., Ng, F.S., Vigmond, E., Efimov, I.R., 2015. Transmural APD gradient synchronizes repolarization in the human left ventricular wall. Cardiovasc. Res. doi:10.1093/cvr/cvv202

Brennan, T., Fink, M., Rodriguez, B., 2009. Multiscale modelling of drug-induced effects on cardiac electrophysiological activity. Eur. J. Pharm. Sci. Off. J. Eur. Fed. Pharm. Sci. 36, 62–77. doi:10.1016/j.ejps.2008.09.013

Britton, O.J., Bueno-Orovio, A., Ammel, K.V., Lu, H.R., Towart, R., Gallacher, D.J., Rodriguez, B., 2013. Experimentally calibrated population of models predicts and explains intersubject variability in cardiac cellular electrophysiology. Proc. Natl. Acad. Sci. 110, E2098–E2105. doi:10.1073/pnas.1304382110

Bueno-Orovio, A., Cherry, E.M., Fenton, F.H., 2008. Minimal model for human ventricular action potentials in tissue. J. Theor. Biol. 253, 544–560. doi:10.1016/j.jtbi.2008.03.029

Bueno-Orovio, A., Hanson, B.M., Gill, J.S., Taggart, P., Rodriguez, B., 2012. In Vivo Human Left-to-Right Ventricular Differences in Rate Adaptation Transiently Increase Pro-Arrhythmic Risk following Rate Acceleration. PLoS ONE 7, e52234. doi:10.1371/journal.pone.0052234

Campbell, C.M., Campbell, J.D., Thompson, C.H., Galimberti, E.S., Darbar, D.,

Vanoye, C.G., George, A.L., 2013. Selective targeting of gain-of-function KCNQ1 mutations predisposing to atrial fibrillation. Circ. Arrhythm. Electrophysiol. 6, 960–966. doi:10.1161/CIRCEP.113.000439

Carro, J., Rodríguez, J.F., Laguna, P., Pueyo, E., 2011. A human ventricular cell model for investigation of cardiac arrhythmias under hyperkalaemic conditions. Philos. Transact. A Math. Phys. Eng. Sci. 369, 4205–4232. doi:10.1098/rsta.2011.0127

Chen, H., Kim, L.A., Rajan, S., Xu, S., Goldstein, S.A.N., 2003. Charybdotoxin binding in the I(Ks) pore demonstrates two MinK subunits in each channel complex. Neuron 40, 15–23.

Chen, Y.-H., Xu, S.-J., Bendahhou, S., Wang, X.-L., Wang, Y., Xu, W.-Y., Jin, H.-W., Sun, H., Su, X.-Y., Zhuang, Q.-N., Yang, Y.-Q., Li, Y.-B., Liu, Y., Xu, H.-J., Li, X.-F., Ma, N., Mou, C.-P., Chen, Z., Barhanin, J., Huang, W., 2003. KCNQ1 gain-of-function mutation in familial atrial fibrillation. Science 299, 251–254. doi:10.1126/science.1077771

Chou, C.-C., Zhou, S., Hayashi, H., Nihei, M., Liu, Y.-B., Wen, M.-S., Yeh, S.-J., Fishbein, M.C., Weiss, J.N., Lin, S.-F., Wu, D., Chen, P.-S., 2007. Remodelling of action potential and intracellular calcium cycling dynamics during subacute myocardial infarction promotes ventricular arrhythmias in Langendorff-perfused rabbit hearts. J. Physiol. 580, 895–906. doi:10.1113/jphysiol.2006.120659

Clancy, C.E., Rudy, Y., 1999. Linking a genetic defect to its cellular phenotype in a cardiac arrhythmia. Nature 400, 566–569. doi:10.1038/23034

Clancy, Sato, D., 2013. Cardiac Electrophysiological Dynamics From the Cellular Level to the Organ Level. Biomed. Eng. Comput. Biol. 69. doi:10.4137/BECB.S10960

Coronel, R., de Bakker, J.M.T., Wilms-Schopman, F.J.G., Opthof, T., Linnenbank, A.C., Belterman, C.N., Janse, M.J., 2006. Monophasic action potentials and activation recovery intervals as measures of ventricular action potential duration: experimental evidence to resolve some controversies. Heart Rhythm Off. J. Heart Rhythm Soc. 3, 1043–1050. doi:10.1016/j.hrthm.2006.05.027

Coronel, R., Opthof, T., Taggart, P., Tytgat, J., Veldkamp, M., 1997. Differential electrophysiology of repolarisation from clone to clinic. Cardiovasc. Res. 33, 503–517.

Crumb, W.J., Pigott, J.D., Clarkson, C.W., 1995. Comparison of Ito in young and adult human atrial myocytes: evidence for developmental changes. Am. J. Physiol. 268, H1335–1342.

Cummins, M.A., Dalal, P.J., Bugana, M., Severi, S., Sobie, E.A., 2014. Comprehensive analyses of ventricular myocyte models identify targets exhibiting favorable rate dependence. PLoS Comput. Biol. 10, e1003543. doi:10.1371/journal.pcbi.1003543

Cutler, M.J., Rosenbaum, D.S., 2009. Risk stratification for sudden cardiac death: is there a clinical role for T wave alternans? Heart Rhythm Off. J. Heart

Rhythm Soc. 6, S56–61. doi:10.1016/j.hrthm.2009.05.025
Cutler, M.J., Wan, X., Laurita, K.R., Hajjar, R.J., Rosenbaum, D.S., 2009. Targeted SERCA2a gene expression identifies molecular mechanism and therapeutic target for arrhythmogenic cardiac alternans. Circ. Arrhythm. Electrophysiol. 2, 686–694. doi:10.1161/CIRCEP.109.863118
Cutler, M.J., Wan, X., Plummer, B.N., Liu, H., Deschenes, I., Laurita, K.R., Hajjar, R.J., Rosenbaum, D.S., 2012. Targeted Sarcoplasmic Reticulum Ca2+ ATPase 2a Gene Delivery to Restore Electrical Stability in the Failing Heart. Circulation 126, 2095–2104. doi:10.1161/CIRCULATIONAHA.111.071480
Das, S., Makino, S., Melman, Y.F., Shea, M.A., Goyal, S.B., Rosenzweig, A., Macrae, C.A., Ellinor, P.T., 2009. Mutation in the S3 segment of KCNQ1 results in familial lone atrial fibrillation. Heart Rhythm Off. J. Heart Rhythm Soc. 6, 1146–1153. doi:10.1016/j.hrthm.2009.04.015
Davies, M.R., Mistry, H.B., Hussein, L., Pollard, C.E., Valentin, J.-P., Swinton, J., Abi-Gerges, N., 2012. An in silico canine cardiac midmyocardial action potential duration model as a tool for early drug safety assessment. Am. J. Physiol. Heart Circ. Physiol. 302, H1466–1480. doi:10.1152/ajpheart.00808.2011
Decker, K.F., Heijman, J., Silva, J.R., Hund, T.J., Rudy, Y., 2009. Properties and ionic mechanisms of action potential adaptation, restitution, and accommodation in canine epicardium. Am. J. Physiol. Heart Circ. Physiol. 296, H1017–1026. doi:10.1152/ajpheart.01216.2008
Decker, K.F., Rudy, Y., 2010. Ionic mechanisms of electrophysiological heterogeneity and conduction block in the infarct border zone. Am. J. Physiol. Heart Circ. Physiol. 299, H1588–1597. doi:10.1152/ajpheart.00362.2010
Devenyi, R.A., Sobie, E.A., 2015. There and back again: Iterating between population-based modeling and experiments reveals surprising regulation of calcium transients in rat cardiac myocytes. J. Mol. Cell. Cardiol. doi:10.1016/j.yjmcc.2015.07.016
Díaz, M.E., O'Neill, S.C., Eisner, D.A., 2004. Sarcoplasmic Reticulum Calcium Content Fluctuation Is the Key to Cardiac Alternans. Circ. Res. 94, 650–656. doi:10.1161/01.RES.0000119923.64774.72
DiFrancesco, D., Noble, D., 1985. A model of cardiac electrical activity incorporating ionic pumps and concentration changes. Philos. Trans. R. Soc. Lond. B. Biol. Sci. 307, 353–398.
Dun, W., Baba, S., Yagi, T., Boyden, P.A., 2004. Dynamic remodeling of K+ and Ca2+ currents in cells that survived in the epicardial border zone of canine healed infarcted heart. Am. J. Physiol. Heart Circ. Physiol. 287, H1046–1054. doi:10.1152/ajpheart.00082.2004
Dun, W., Boyden, P.A., 2005. Diverse phenotypes of outward currents in cells that have survived in the 5-day-infarcted heart. Am. J. Physiol. Heart Circ. Physiol. 289, H667–673. doi:10.1152/ajpheart.00180.2005
Durgan, D.J., Young, M.E., 2010. The cardiomyocyte circadian clock: emerging roles in health and disease. Circ. Res. 106, 647–658.

doi:10.1161/CIRCRESAHA.109.209957

Echt, D.S., Liebson, P.R., Mitchell, L.B., Peters, R.W., Obias-Manno, D., Barker, A.H., Arensberg, D., Baker, A., Friedman, L., Greene, H.L., 1991. Mortality and morbidity in patients receiving encainide, flecainide, or placebo. The Cardiac Arrhythmia Suppression Trial. N. Engl. J. Med. 324, 781–788. doi:10.1056/NEJM199103213241201

Eisner, D.A., Choi, H.S., Díaz, M.E., O'Neill, S.C., Trafford, A.W., 2000. Integrative Analysis of Calcium Cycling in Cardiac Muscle. Circ. Res. 87, 1087–1094. doi:10.1161/01.RES.87.12.1087

El-Sherif, N., Scherlag, B.J., Lazzara, R., Hope, R.R., 1977. Re-entrant ventricular arrhythmias in the late myocardial infarction period. 1. Conduction characteristics in the infarction zone. Circulation 55, 686–702.

Escobar, A.L., Valdivia, H.H., 2014. Cardiac alternans and ventricular fibrillation: a bad case of ryanodine receptors reneging on their duty. Circ. Res. 114, 1369–1371. doi:10.1161/CIRCRESAHA.114.303823

Estner, H.L., Zviman, M.M., Herzka, D., Miller, F., Castro, V., Nazarian, S., Ashikaga, H., Dori, Y., Berger, R.D., Calkins, H., Lardo, A.C., Halperin, H.R., 2011. The critical isthmus sites of ischemic ventricular tachycardia are in zones of tissue heterogeneity, visualized by magnetic resonance imaging. Heart Rhythm Off. J. Heart Rhythm Soc. 8, 1942–1949. doi:10.1016/j.hrthm.2011.07.027

Fabiato, A., 1983. Calcium-induced release of calcium from the cardiac sarcoplasmic reticulum. Am. J. Physiol. 245, C1–14.

Feng, J., Yue, L., Wang, Z., Nattel, S., 1998. Ionic mechanisms of regional action potential heterogeneity in the canine right atrium. Circ. Res. 83, 541–551.

Fink, M., Noble, D., Virag, L., Varro, A., Giles, W.R., 2008. Contributions of HERG K+ current to repolarization of the human ventricular action potential. Prog. Biophys. Mol. Biol. 96, 357–376. doi:10.1016/j.pbiomolbio.2007.07.011

Fishman, G.I., Chugh, S.S., Dimarco, J.P., Albert, C.M., Anderson, M.E., Bonow, R.O., Buxton, A.E., Chen, P.-S., Estes, M., Jouven, X., Kwong, R., Lathrop, D.A., Mascette, A.M., Nerbonne, J.M., O'Rourke, B., Page, R.L., Roden, D.M., Rosenbaum, D.S., Sotoodehnia, N., Trayanova, N.A., Zheng, Z.-J., 2010. Sudden cardiac death prediction and prevention: report from a National Heart, Lung, and Blood Institute and Heart Rhythm Society Workshop. Circulation 122, 2335–2348. doi:10.1161/CIRCULATIONAHA.110.976092

Fletcher, K., Shah, R.R., Thomas, A., Tobin, F., Rodriguez, B., Mirams, G.R., Saiz, J., Noble, D., 2011. Novel approaches to assessing cardiac safety--proceedings of a workshop: regulators, industry and academia discuss the future of in silico cardiac modelling to predict the proarrhythmic safety of drugs. Drug Saf. 34, 439–443. doi:10.2165/11591950-000000000-00000

Fossa, A.A., Wisialowski, T., Wolfgang, E., Wang, E., Avery, M., Raunig, D.L., Fermini, B., 2004. Differential effect of HERG blocking agents on cardiac electrical alternans in the guinea pig. Eur. J. Pharmacol. 486, 209–221. doi:10.1016/j.ejphar.2003.12.028

Fox, J.J., McHarg, J.L., Gilmour, R.F., 2002. Ionic mechanism of electrical alternans. Am. J. Physiol. Heart Circ. Physiol. 282, H516–530. doi:10.1152/ajpheart.00612.2001

Franz, M.R., 1999. Current status of monophasic action potential recording: theories, measurements and interpretations. Cardiovasc. Res. 41, 25–40.

Franz, M.R., Burkhoff, D., Spurgeon, H., Weisfeldt, M.L., Lakatta, E.G., 1986. In vitro validation of a new cardiac catheter technique for recording monophasic action potentials. Eur. Heart J. 7, 34–41.

Gaborit, N., Le Bouter, S., Szuts, V., Varro, A., Escande, D., Nattel, S., Demolombe, S., 2007. Regional and tissue specific transcript signatures of ion channel genes in the non-diseased human heart. J. Physiol. 582, 675–693. doi:10.1113/jphysiol.2006.126714

Ganesan, A.N., Maack, C., Johns, D.C., Sidor, A., O'Rourke, B., 2006. Beta-adrenergic stimulation of L-type Ca2+ channels in cardiac myocytes requires the distal carboxyl terminus of alpha1C but not serine 1928. Circ. Res. 98, e11–18. doi:10.1161/01.RES.0000202692.23001.e2

Ghouse, J., Have, C.T., Weeke, P., Bille Nielsen, J., Ahlberg, G., Balslev-Harder, M., Appel, E.V., Skaaby, T., Olesen, S.-P., Grarup, N., Linneberg, A., Pedersen, O., Haunsø, S., Hastrup Svendsen, J., Hansen, T., Kanters, J.K., Salling Olesen, M., 2015. Rare genetic variants previously associated with congenital forms of long QT syndrome have little or no effect on the QT interval. Eur. Heart J. doi:10.1093/eurheartj/ehv297

Glukhov, A.V., Fedorov, V.V., Kalish, P.W., Ravikumar, V.K., Lou, Q., Janks, D., Schuessler, R.B., Moazami, N., Efimov, I.R., 2012. Conduction remodeling in human end-stage nonischemic left ventricular cardiomyopathy. Circulation 125, 1835–1847. doi:10.1161/CIRCULATIONAHA.111.047274

Glukhov, A.V., Fedorov, V.V., Lou, Q., Ravikumar, V.K., Kalish, P.W., Schuessler, R.B., Moazami, N., Efimov, I.R., 2010. Transmural dispersion of repolarization in failing and nonfailing human ventricle. Circ. Res. 106, 981–991. doi:10.1161/CIRCRESAHA.109.204891

Goldberger, J.J., Buxton, A.E., Cain, M., Costantini, O., Exner, D.V., Knight, B.P., Lloyd-Jones, D., Kadish, A.H., Lee, B., Moss, A., Myerburg, R., Olgin, J., Passman, R., Rosenbaum, D., Stevenson, W., Zareba, W., Zipes, D.P., 2011. Risk Stratification for Arrhythmic Sudden Cardiac Death Identifying the Roadblocks. Circulation 123, 2423–2430. doi:10.1161/CIRCULATIONAHA.110.959734

Goldhaber, J.I., Xie, L.-H., Duong, T., Motter, C., Khuu, K., Weiss, J.N., 2005. Action Potential Duration Restitution and Alternans in Rabbit Ventricular Myocytes The Key Role of Intracellular Calcium Cycling. Circ. Res. 96, 459–466. doi:10.1161/01.RES.0000156891.66893.83

Gönczi, M., Birinyi, P., Balázs, B., Szentandrássy, N., Harmati, G., Könczei, Z., Csernoch, L., Nánási, P.P., 2012. Age-dependent changes in ion channel mRNA expression in canine cardiac tissues. Gen. Physiol. Biophys. 31, 153–162. doi:10.4149/gpb_2012_017

Grandi, E., Pasqualini, F.S., Bers, D.M., 2010. A novel computational model of the human ventricular action potential and Ca transient. J. Mol. Cell. Cardiol. 48, 112–121. doi:10.1016/j.yjmcc.2009.09.019

Groenendaal, W., Ortega, F.A., Kherlopian, A.R., Zygmunt, A.C., Krogh-Madsen, T., Christini, D.J., 2015. Cell-Specific Cardiac Electrophysiology Models. PLoS Comput Biol 11, e1004242. doi:10.1371/journal.pcbi.1004242

Hammer, K.P., Ljubojevic, S., Ripplinger, C.M., Pieske, B.M., Bers, D.M., 2015. Cardiac myocyte alternans in intact heart: Influence of cell-cell coupling and β-adrenergic stimulation. J. Mol. Cell. Cardiol. 84, 1–9. doi:10.1016/j.yjmcc.2015.03.012

Hasegawa, K., Ohno, S., Ashihara, T., Itoh, H., Ding, W.-G., Toyoda, F., Makiyama, T., Aoki, H., Nakamura, Y., Delisle, B.P., Matsuura, H., Horie, M., 2014. A novel KCNQ1 missense mutation identified in a patient with juvenile-onset atrial fibrillation causes constitutively open IKs channels. Heart Rhythm Off. J. Heart Rhythm Soc. 11, 67–75. doi:10.1016/j.hrthm.2013.09.073

Haws, C.W., Lux, R.L., 1990. Correlation between in vivo transmembrane action potential durations and activation-recovery intervals from electrograms. Effects of interventions that alter repolarization time. Circulation 81, 281–288.

Hayward, C., Banner, N.R., Morley-Smith, A., Lyon, A.R., Harding, S.E., 2015. The Current and Future Landscape of SERCA Gene Therapy for Heart Failure: A Clinical Perspective. Hum. Gene Ther. 26, 293–304. doi:10.1089/hum.2015.018

Hodgkin, A.L., Huxley, A.F., 1952a. Currents carried by sodium and potassium ions through the membrane of the giant axon of Loligo. J. Physiol. 116, 449–472.

Hodgkin, A.L., Huxley, A.F., 1952b. The components of membrane conductance in the giant axon of Loligo. J. Physiol. 116, 473–496. doi:10.1113/jphysiol.1952.sp004718

Hodgkin, A.L., Huxley, A.F., 1952c. The dual effect of membrane potential on sodium conductance in the giant axon of Loligo. J. Physiol. 116, 497–506.

Hodgkin, A.L., Huxley, A.F., 1952d. A quantitative description of membrane current and its application to conduction and excitation in nerve. J. Physiol. 117, 500–544.

Hoefen, R., Reumann, M., Goldenberg, I., Moss, A.J., O-Uchi, J., Gu, Y., McNitt, S., Zareba, W., Jons, C., Kanters, J.K., Platonov, P.G., Shimizu, W., Wilde, A.A.M., Rice, J.J., Lopes, C.M., 2012. In silico cardiac risk assessment in patients with long QT syndrome: type 1: clinical predictability of cardiac models. J. Am. Coll. Cardiol. 60, 2182–2191. doi:10.1016/j.jacc.2012.07.053

Hoffman, B.F., Cranefield, P.F., Lepeschkin, E., Surawicz, B., Herrlich, H.C., 1959. Comparison of cardiac monophasic action potentials recorded by intracellular and suction electrodes. Am. J. Physiol. 196, 1297–1301.

Hong, K., Piper, D.R., Diaz-Valdecantos, A., Brugada, J., Oliva, A., Burashnikov, E., Santos-de-Soto, J., Grueso-Montero, J., Diaz-Enfante, E., Brugada, P., Sachse, F., Sanguinetti, M.C., Brugada, R., 2005. De novo KCNQ1 mutation

responsible for atrial fibrillation and short QT syndrome in utero. Cardiovasc. Res. 68, 433–440. doi:10.1016/j.cardiores.2005.06.023

Hund, T.J., Rudy, Y., 2004. Rate Dependence and Regulation of Action Potential and Calcium Transient in a Canine Cardiac Ventricular Cell Model. Circulation 110, 3168–3174. doi:10.1161/01.CIR.0000147231.69595.D3

Imaniastuti, R., Lee, H.S., Kim, N., Youm, J.B., Shim, E.B., Lim, K.M., 2014. Computational prediction of proarrhythmogenic effect of the V241F KCNQ1 mutation in human atrium. Prog. Biophys. Mol. Biol. 116, 70–75. doi:10.1016/j.pbiomolbio.2014.09.001

Iyer, V., Mazhari, R., Winslow, R.L., 2004. A Computational Model of the Human Left-Ventricular Epicardial Myocyte. Biophys. J. 87, 1507–1525. doi:10.1529/biophysj.104.043299

Janse, M.J., Wit, A.L., 1989. Electrophysiological mechanisms of ventricular arrhythmias resulting from myocardial ischemia and infarction. Physiol. Rev. 69, 1049–1169.

Jeyaraj, D., Haldar, S.M., Wan, X., McCauley, M.D., Ripperger, J.A., Hu, K., Lu, Y., Eapen, B.L., Sharma, N., Ficker, E., Cutler, M.J., Gulick, J., Sanbe, A., Robbins, J., Demolombe, S., Kondratov, R.V., Shea, S.A., Albrecht, U., Wehrens, X.H.T., Rosenbaum, D.S., Jain, M.K., 2012. Circadian rhythms govern cardiac repolarization and arrhythmogenesis. Nature 483, 96–99. doi:10.1038/nature10852

Jiang, M., Cabo, C., Yao, J., Boyden, P.A., Tseng, G., 2000. Delayed rectifier K currents have reduced amplitudes and altered kinetics in myocytes from infarcted canine ventricle. Cardiovasc. Res. 48, 34–43.

John, R.M., Tedrow, U.B., Koplan, B.A., Albert, C.M., Epstein, L.M., Sweeney, M.O., Miller, A.L., Michaud, G.F., Stevenson, W.G., 2012. Ventricular arrhythmias and sudden cardiac death. The Lancet 380, 1520–1529. doi:10.1016/S0140-6736(12)61413-5

Jost, N., Nagy, N., Corici, C., Kohajda, Z., Horváth, A., Acsai, K., Biliczki, P., Levijoki, J., Pollesello, P., Koskelainen, T., Otsomaa, L., Tóth, A., Papp, J.G., Varró, A., Virág, L., 2013. ORM-10103, a novel specific inhibitor of the Na+/Ca2+ exchanger, decreases early and delayed afterdepolarizations in the canine heart. Br. J. Pharmacol. 170, 768–778. doi:10.1111/bph.12228

Jost, N., Virág, L., Comtois, P., Ordög, B., Szuts, V., Seprényi, G., Bitay, M., Kohajda, Z., Koncz, I., Nagy, N., Szél, T., Magyar, J., Kovács, M., Puskás, L.G., Lengyel, C., Wettwer, E., Ravens, U., Nánási, P.P., Papp, J.G., Varró, A., Nattel, S., 2013. Ionic mechanisms limiting cardiac repolarization reserve in humans compared to dogs. J. Physiol. 591, 4189–4206. doi:10.1113/jphysiol.2013.261198

Kanaporis, G., Blatter, L.A., 2014. The Mechanisms of Calcium Cycling and Action Potential Dynamics in Cardiac Alternans. Circ. Res. CIRCRESAHA.114.305404. doi:10.1161/CIRCRESAHA.116.305404

Kharche, S., Adeniran, I., Stott, J., Law, P., Boyett, M.R., Hancox, J.C., Zhang, H., 2012. Pro-arrhythmogenic effects of the S140G KCNQ1 mutation in human

atrial fibrillation - insights from modelling. J. Physiol. 590, 4501–4514. doi:10.1113/jphysiol.2012.229146

Ki, C.-S., Jung, C.L., Kim, H., Baek, K.-H., Park, S.J., On, Y.K., Kim, K.-S., Noh, S.J., Youm, J.B., Kim, J.S., Cho, H., 2014. A KCNQ1 mutation causes age-dependant bradycardia and persistent atrial fibrillation. Pflüg. Arch. Eur. J. Physiol. 466, 529–540. doi:10.1007/s00424-013-1337-6

Koller, M.L., Maier, S.K.G., Gelzer, A.R., Bauer, W.R., Meesmann, M., Gilmour, R.F., 2005. Altered dynamics of action potential restitution and alternans in humans with structural heart disease. Circulation 112, 1542–1548. doi:10.1161/CIRCULATIONAHA.104.502831

Koller, M.L., Riccio, M.L., Gilmour, R.F., 1998. Dynamic restitution of action potential duration during electrical alternans and ventricular fibrillation. Am. J. Physiol. 275, H1635–1642.

Kowey PR, 1998. Pharmacological effects of antiarrhythmic drugs: Review and update. Arch. Intern. Med. 158, 325–332. doi:10.1001/archinte.158.4.325

Kramer, J.B., Saffitz, J.E., Witkowski, F.X., Corr, P.B., 1985. Intramural reentry as a mechanism of ventricular tachycardia during evolving canine myocardial infarction. Circ. Res. 56, 736–754.

Le Bouter, S., El Harchi, A., Marionneau, C., Bellocq, C., Chambellan, A., van Veen, T., Boixel, C., Gavillet, B., Abriel, H., Le Quang, K., Chevalier, J.-C., Lande, G., Léger, J.J., Charpentier, F., Escande, D., Demolombe, S., 2004. Long-term amiodarone administration remodels expression of ion channel transcripts in the mouse heart. Circulation 110, 3028–3035. doi:10.1161/01.CIR.0000147187.78162.AC

Li, G.-R., Lau, C.-P., Leung, T.-K., Nattel, S., 2004. Ionic current abnormalities associated with prolonged action potentials in cardiomyocytes from diseased human right ventricles. Heart Rhythm 1, 460–468. doi:10.1016/j.hrthm.2004.06.003

Linz, K.W., Meyer, R., 2000. Profile and kinetics of L-type calcium current during the cardiac ventricular action potential compared in guinea-pigs, rats and rabbits. Pflüg. Arch. Eur. J. Physiol. 439, 588–599.

Lou, Q., Fedorov, V.V., Glukhov, A.V., Moazami, N., Fast, V.G., Efimov, I.R., 2011. Transmural heterogeneity and remodeling of ventricular excitation-contraction coupling in human heart failure. Circulation 123, 1881–1890. doi:10.1161/CIRCULATIONAHA.110.989707

Lue, W.M., Boyden, P.A., 1992. Abnormal electrical properties of myocytes from chronically infarcted canine heart. Alterations in Vmax and the transient outward current. Circulation 85, 1175–1188.

Lundby, A., Ravn, L.S., Svendsen, J.H., Olesen, S.-P., Schmitt, N., 2007. KCNQ1 mutation Q147R is associated with atrial fibrillation and prolonged QT interval. Heart Rhythm Off. J. Heart Rhythm Soc. 4, 1532–1541. doi:10.1016/j.hrthm.2007.07.022

Luo, C.H., Rudy, Y., 1994a. A dynamic model of the cardiac ventricular action potential. I. Simulations of ionic currents and concentration changes. Circ.

Res. 74, 1071–1096.
Luo, C.H., Rudy, Y., 1994b. A dynamic model of the cardiac ventricular action potential. II. Afterdepolarizations, triggered activity, and potentiation. Circ. Res. 74, 1097–1113.
Macia, E., Dolmatova, E., Cabo, C., Sosinsky, A.Z., Dun, W., Coromilas, J., Ciaccio, E.J., Boyden, P.A., Wit, A.L., Duffy, H.S., 2011. Characterization of gap junction remodeling in epicardial border zone of healing canine infarcts and electrophysiological effects of partial reversal by rotigaptide. Circ. Arrhythm. Electrophysiol. 4, 344–351. doi:10.1161/CIRCEP.110.959312
Maltsev, V.A., Kyle, J.W., Mishra, S., Undrovinas, A., 2008a. Molecular identity of the late sodium current in adult dog cardiomyocytes identified by Nav1.5 antisense inhibition. Am. J. Physiol. Heart Circ. Physiol. 295, H667–676. doi:10.1152/ajpheart.00111.2008
Maltsev, V.A., Reznikov, V., Undrovinas, N.A., Sabbah, H.N., Undrovinas, A., 2008b. Modulation of late sodium current by Ca2+, calmodulin, and CaMKII in normal and failing dog cardiomyocytes: similarities and differences. Am. J. Physiol. Heart Circ. Physiol. 294, H1597–1608. doi:10.1152/ajpheart.00484.2007
Maltsev, V.A., Sabbah, H.N., Higgins, R.S., Silverman, N., Lesch, M., Undrovinas, A.I., 1998. Novel, ultraslow inactivating sodium current in human ventricular cardiomyocytes. Circulation 98, 2545–2552.
Maltsev, V.A., Undrovinas, A.I., 2006. A multi-modal composition of the late Na+ current in human ventricular cardiomyocytes. Cardiovasc. Res. 69, 116–127. doi:10.1016/j.cardiores.2005.08.015
Mansourati, J., Le Grand, B., 1993. Transient outward current in young and adult diseased human atria. Am. J. Physiol. 265, H1466–1470.
Marder, E., Taylor, A.L., 2011. Multiple models to capture the variability in biological neurons and networks. Nat. Neurosci. 14, 133–138. doi:10.1038/nn.2735
Marino, S., Hogue, I.B., Ray, C.J., Kirschner, D.E., 2008. A methodology for performing global uncertainty and sensitivity analysis in systems biology. J. Theor. Biol. 254, 178–196. doi:10.1016/j.jtbi.2008.04.011
Marx, S.O., Kurokawa, J., Reiken, S., Motoike, H., D'Armiento, J., Marks, A.R., Kass, R.S., 2002. Requirement of a macromolecular signaling complex for beta adrenergic receptor modulation of the KCNQ1-KCNE1 potassium channel. Science 295, 496–499. doi:10.1126/science.1066843
Matavel, A., Medei, E., Lopes, C.M.B., 2010. PKA and PKC partially rescue long QT type 1 phenotype by restoring channel-PIP2 interactions. Channels Austin Tex 4, 3–11.
Matthews, G.D.K., Guzadhur, L., Grace, A., Huang, C.L.-H., 2012. Nonlinearity between action potential alternans and restitution, which both predict ventricular arrhythmic properties in Scn5a+/- and wild-type murine hearts. J. Appl. Physiol. Bethesda Md 1985 112, 1847–1863. doi:10.1152/japplphysiol.00039.2012

McKay, M.D., Beckman, R.J., Conover, W.J., 1979. A Comparison of Three Methods for Selecting Values of Input Variables in the Analysis of Output from a Computer Code. Technometrics 21, 239–245. doi:10.2307/1268522

Merchant, F.M., Armoundas, A.A., 2012. Role of Substrate and Triggers in the Genesis of Cardiac Alternans, From the Myocyte to the Whole Heart: Implications for Therapy. Circulation 125, 539–549. doi:10.1161/CIRCULATIONAHA.111.033563

Mizusawa, Y., Horie, M., Wilde, A.A.M., 2014. Genetic and clinical advances in congenital long QT syndrome. Circ. J. Off. J. Jpn. Circ. Soc. 78, 2827–2833.

Moore, H.J., Franz, M.R., 2007. Monophasic action potential recordings in humans. J. Cardiovasc. Electrophysiol. 18, 787–790. doi:10.1111/j.1540-8167.2006.00756.x

Moss, A.J., Robinson, J.L., 2002. The Long-QT Syndrome. Circulation 105, 784–786. doi:10.1161/hc0702.105125

Moss, A.J., Shimizu, W., Wilde, A.A.M., Towbin, J.A., Zareba, W., Robinson, J.L., Qi, M., Vincent, G.M., Ackerman, M.J., Kaufman, E.S., Hofman, N., Seth, R., Kamakura, S., Miyamoto, Y., Goldenberg, I., Andrews, M.L., McNitt, S., 2007. Clinical aspects of type-1 long-QT syndrome by location, coding type, and biophysical function of mutations involving the KCNQ1 gene. Circulation 115, 2481–2489. doi:10.1161/CIRCULATIONAHA.106.665406

Muller, J.E., Ludmer, P.L., Willich, S.N., Tofler, G.H., Aylmer, G., Klangos, I., Stone, P.H., 1987. Circadian variation in the frequency of sudden cardiac death. Circulation 75, 131–138.

Muller, J.E., Stone, P.H., Turi, Z.G., Rutherford, J.D., Czeisler, C.A., Parker, C., Poole, W.K., Passamani, E., Roberts, R., Robertson, T., 1985. Circadian variation in the frequency of onset of acute myocardial infarction. N. Engl. J. Med. 313, 1315–1322. doi:10.1056/NEJM198511213132103

Näbauer, M., Beuckelmann, D.J., Uberfuhr, P., Steinbeck, G., 1996. Regional differences in current density and rate-dependent properties of the transient outward current in subepicardial and subendocardial myocytes of human left ventricle. Circulation 93, 168–177.

Narayan, S.M., Franz, M.R., Lalani, G., Kim, J., Sastry, A., 2007. T-wave alternans, restitution of human action potential duration, and outcome. J. Am. Coll. Cardiol. 50, 2385–2392. doi:10.1016/j.jacc.2007.10.011

Nash, M.P., Bradley, C.P., Paterson, D.J., 2003. Imaging electrocardiographic dispersion of depolarization and repolarization during ischemia: simultaneous body surface and epicardial mapping. Circulation 107, 2257–2263. doi:10.1161/01.CIR.0000065602.78328.B5

Nash, M.P., Mourad, A., Clayton, R.H., Sutton, P.M., Bradley, C.P., Hayward, M., Paterson, D.J., Taggart, P., 2006. Evidence for Multiple Mechanisms in Human Ventricular Fibrillation. Circulation 114, 536–542. doi:10.1161/CIRCULATIONAHA.105.602870

Nassif, G., Dillon, S.M., Rayhill, S., Wit, A.L., 1993. Reentrant circuits and the effects of heptanol in a rabbit model of infarction with a uniform anisotropic

epicardial border zone. J. Cardiovasc. Electrophysiol. 4, 112–133.
Neher, E., Sakmann, B., 1976. Single-channel currents recorded from membrane of denervated frog muscle fibres. Nature 260, 799–802. doi:10.1038/260799a0
Nichol, G., Thomas, E., Callaway, C.W., Hedges, J., Powell, J.L., Aufderheide, T.P., Rea, T., Lowe, R., Brown, T., Dreyer, J., Davis, D., Idris, A., Stiell, I., Resuscitation Outcomes Consortium Investigators, 2008. Regional variation in out-of-hospital cardiac arrest incidence and outcome. JAMA 300, 1423–1431. doi:10.1001/jama.300.12.1423
Nivala, M., Qu, Z., 2012. Calcium alternans in a couplon network model of ventricular myocytes: role of sarcoplasmic reticulum load. Am. J. Physiol. Heart Circ. Physiol. 303, H341–352. doi:10.1152/ajpheart.00302.2012
Noble, D., 2002. Modeling the heart--from genes to cells to the whole organ. Science 295, 1678–1682. doi:10.1126/science.1069881
Noble, D., 1962. A modification of the Hodgkin--Huxley equations applicable to Purkinje fibre action and pace-maker potentials. J. Physiol. 160, 317–352.
Noble, D., Garny, A., Noble, P.J., 2012. How the Hodgkin–Huxley equations inspired the Cardiac Physiome Project. J. Physiol. 590, 2613–2628. doi:10.1113/jphysiol.2011.224238
O'Hara, T., Virág, L., Varró, A., Rudy, Y., 2011. Simulation of the Undiseased Human Cardiac Ventricular Action Potential: Model Formulation and Experimental Validation. PLoS Comput Biol 7, e1002061. doi:10.1371/journal.pcbi.1002061
Olsson, B., Varnauskas, E., Korsgren, M., 1971. Further improved method for measuring monophasic action potentials of the intact human heart. J. Electrocardiol. 4, 19–23.
Panfilov, A.V., 2006. Is heart size a factor in ventricular fibrillation? Or how close are rabbit and human hearts? Heart Rhythm Off. J. Heart Rhythm Soc. 3, 862–864. doi:10.1016/j.hrthm.2005.12.022
Passini, E., Mincholé, A., Coppini, R., Cerbai, E., Rodriguez, B., Severi, S., Bueno-Orovio, A., n.d. Mechanisms of pro-arrhythmic abnormalities in ventricular repolarisation and anti-arrhythmic therapies in human hypertrophic cardiomyopathy. J. Mol. Cell. Cardiol. 0. doi:10.1016/j.yjmcc.2015.09.003
Perchenet, L., Hinde, A.K., Patel, K.C., Hancox, J.C., Levi, A.J., 2000. Stimulation of Na/Ca exchange by the beta-adrenergic/protein kinase A pathway in guinea-pig ventricular myocytes at 37 degrees C. Pflüg. Arch. Eur. J. Physiol. 439, 822–828.
Péréon, Y., Demolombe, S., Baró, I., Drouin, E., Charpentier, F., Escande, D., 2000. Differential expression of KvLQT1 isoforms across the human ventricular wall. Am. J. Physiol. Heart Circ. Physiol. 278, H1908–1915.
Piacentino, V., Weber, C.R., Chen, X., Weisser-Thomas, J., Margulies, K.B., Bers, D.M., Houser, S.R., 2003. Cellular basis of abnormal calcium transients of failing human ventricular myocytes. Circ. Res. 92, 651–658. doi:10.1161/01.RES.0000062469.83985.9B

Picht, E., DeSantiago, J., Blatter, L.A., Bers, D.M., 2006. Cardiac alternans do not rely on diastolic sarcoplasmic reticulum calcium content fluctuations. Circ. Res. 99, 740–748. doi:10.1161/01.RES.0000244002.88813.91

Pinto, J.M., Boyden, P.A., 1999. Electrical remodeling in ischemia and infarction. Cardiovasc. Res. 42, 284–297.

Pitt-Francis, J., Pathmanathan, P., Bernabeu, M.O., Bordas, R., Cooper, J., Fletcher, A.G., Mirams, G.R., Murray, P., Osborne, J.M., Walter, A., Chapman, S.J., Garny, A., van Leeuwen, I.M.M., Maini, P.K., Rodríguez, B., Waters, S.L., Whiteley, J.P., Byrne, H.M., Gavaghan, D.J., 2009. Chaste: A test-driven approach to software development for biological modelling. Comput. Phys. Commun., 40 YEARS OF CPC: A celebratory issue focused on quality software for high performance, grid and novel computing architectures 180, 2452–2471. doi:10.1016/j.cpc.2009.07.019

Potse, M., Vinet, A., Opthof, T., Coronel, R., 2009. Validation of a simple model for the morphology of the T wave in unipolar electrograms. Am. J. Physiol. Heart Circ. Physiol. 297, H792–801. doi:10.1152/ajpheart.00064.2009

Priebe, L., Beuckelmann, D.J., 1998. Simulation study of cellular electric properties in heart failure. Circ. Res. 82, 1206–1223.

Priori, S.G., 2004. Inherited arrhythmogenic diseases: the complexity beyond monogenic disorders. Circ. Res. 94, 140–145. doi:10.1161/01.RES.0000115750.12807.7E

Priori, S.G., Napolitano, C., Schwartz, P.J., 1999. Low penetrance in the long-QT syndrome: clinical impact. Circulation 99, 529–533.

Priori, S.G., Schwartz, P.J., Napolitano, C., Bloise, R., Ronchetti, E., Grillo, M., Vicentini, A., Spazzolini, C., Nastoli, J., Bottelli, G., Folli, R., Cappelletti, D., 2003. Risk stratification in the long-QT syndrome. N. Engl. J. Med. 348, 1866–1874. doi:10.1056/NEJMoa022147

Pruvot, E.J., Katra, R.P., Rosenbaum, D.S., Laurita, K.R., 2004. Role of calcium cycling versus restitution in the mechanism of repolarization alternans. Circ. Res. 94, 1083–1090. doi:10.1161/01.RES.0000125629.72053.95

Pueyo, E., Corrias, A., Virág, L., Jost, N., Szél, T., Varró, A., Szentandrássy, N., Nánási, P.P., Burrage, K., Rodríguez, B., 2011. A Multiscale Investigation of Repolarization Variability and Its Role in Cardiac Arrhythmogenesis. Biophys. J. 101, 2892–2902. doi:10.1016/j.bpj.2011.09.060

Pu, J., Boyden, P.A., 1997. Alterations of Na+ currents in myocytes from epicardial border zone of the infarcted heart. A possible ionic mechanism for reduced excitability and postrepolarization refractoriness. Circ. Res. 81, 110–119.

Qi, X.Y., Yeh, Y.-H., Xiao, L., Burstein, B., Maguy, A., Chartier, D., Villeneuve, L.R., Brundel, B.J.J.M., Dobrev, D., Nattel, S., 2008. Cellular signaling underlying atrial tachycardia remodeling of L-type calcium current. Circ. Res. 103, 845–854. doi:10.1161/CIRCRESAHA.108.175463

Qu, Z., Nivala, M., Weiss, J.N., 2013. Calcium alternans in cardiac myocytes: order from disorder. J. Mol. Cell. Cardiol. 58, 100–109. doi:10.1016/j.yjmcc.2012.10.007

Qu, Z., Xie, Y., Garfinkel, A., Weiss, J.N., 2010. T-wave alternans and arrhythmogenesis in cardiac diseases. Front. Physiol. 1, 154. doi:10.3389/fphys.2010.00154

Ramirez-Correa, G.A., Murphy, A.M., 2007. Is phospholamban or troponin I the "prima donna" in beta-adrenergic induced lusitropy? Circ. Res. 101, 326–327. doi:10.1161/CIRCRESAHA.107.158873

Ren, L., Fang, X., Wang, Y., Qi, G., 2011. T-wave alternans and heart rate variability: a comparison in patients with myocardial infarction with or without diabetes mellitus. Ann. Noninvasive Electrocardiol. Off. J. Int. Soc. Holter Noninvasive Electrocardiol. Inc 16, 232–238. doi:10.1111/j.1542-474X.2011.00437.x

Rocchetti, M., Besana, A., Gurrola, G.B., Possani, L.D., Zaza, A., 2001. Rate dependency of delayed rectifier currents during the guinea-pig ventricular action potential. J. Physiol. 534, 721–732. doi:10.1111/j.1469-7793.2001.00721.x

Romero, L., Pueyo, E., Fink, M., Rodríguez, B., 2009. Impact of ionic current variability on human ventricular cellular electrophysiology. Am. J. Physiol. Heart Circ. Physiol. 297, H1436–1445. doi:10.1152/ajpheart.00263.2009

Rosenbaum, D.S., Jackson, L.E., Smith, J.M., Garan, H., Ruskin, J.N., Cohen, R.J., 1994. Electrical alternans and vulnerability to ventricular arrhythmias. N. Engl. J. Med. 330, 235–241. doi:10.1056/NEJM199401273300402

Rovetti, R., Cui, X., Garfinkel, A., Weiss, J.N., Qu, Z., 2010. Spark-Induced Sparks As a Mechanism of Intracellular Calcium Alternans in Cardiac Myocytes. Circ. Res. 106, 1582–1591. doi:10.1161/CIRCRESAHA.109.213975

Rudy, Y., 2006. Modelling and imaging cardiac repolarization abnormalities. J. Intern. Med. 259, 91–106. doi:10.1111/j.1365-2796.2005.01586.x

Sakmann, B., Neher, E., 1984. Patch clamp techniques for studying ionic channels in excitable membranes. Annu. Rev. Physiol. 46, 455–472. doi:10.1146/annurev.ph.46.030184.002323

Sarkar, A.X., Christini, D.J., Sobie, E.A., 2012. Exploiting mathematical models to illuminate electrophysiological variability between individuals. J. Physiol. 590, 2555–2567. doi:10.1113/jphysiol.2011.223313

Schwartz, P.J., Stramba-Badiale, M., Crotti, L., Pedrazzini, M., Besana, A., Bosi, G., Gabbarini, F., Goulene, K., Insolia, R., Mannarino, S., Mosca, F., Nespoli, L., Rimini, A., Rosati, E., Salice, P., Spazzolini, C., 2009. Prevalence of the congenital long-QT syndrome. Circulation 120, 1761–1767. doi:10.1161/CIRCULATIONAHA.109.863209

Seemann, G., Sachse, F.B., Weiss, D.L., Dössel, O., 2003. Quantitative reconstruction of cardiac electromechanics in human myocardium: regional heterogeneity. J. Cardiovasc. Electrophysiol. 14, S219–228.

Shan, J., Kushnir, A., Betzenhauser, M.J., Reiken, S., Li, J., Lehnart, S.E., Lindegger, N., Mongillo, M., Mohler, P.J., Marks, A.R., 2010. Phosphorylation of the ryanodine receptor mediates the cardiac fight or flight response in mice. J. Clin. Invest. 120, 4388–4398. doi:10.1172/JCI32726

Shannon, T.R., Wang, F., Puglisi, J., Weber, C., Bers, D.M., 2004. A mathematical treatment of integrated Ca dynamics within the ventricular myocyte. Biophys. J. 87, 3351–3371. doi:10.1529/biophysj.104.047449

Shkryl, V.M., Maxwell, J.T., Domeier, T.L., Blatter, L.A., 2012. Refractoriness of sarcoplasmic reticulum Ca2+ release determines Ca2+ alternans in atrial myocytes. Am. J. Physiol. Heart Circ. Physiol. 302, H2310–2320. doi:10.1152/ajpheart.00079.2012

Sikkel, M.B., Hayward, C., MacLeod, K.T., Harding, S.E., Lyon, A.R., 2014. SERCA2a gene therapy in heart failure: an anti-arrhythmic positive inotrope. Br. J. Pharmacol. 171, 38–54. doi:10.1111/bph.12472

Silva, J., Rudy, Y., 2005. Subunit Interaction Determines IKs Participation in Cardiac Repolarization and Repolarization Reserve. Circulation 112, 1384–1391. doi:10.1161/CIRCULATIONAHA.105.543306

Silverman, W.R., Roux, B., Papazian, D.M., 2003. Structural basis of two-stage voltage-dependent activation in K+ channels. Proc. Natl. Acad. Sci. U. S. A. 100, 2935–2940. doi:10.1073/pnas.0636603100

Sobie, E.A., 2009. Parameter sensitivity analysis in electrophysiological models using multivariable regression. Biophys. J. 96, 1264–1274. doi:10.1016/j.bpj.2008.10.056

Sobie, E.A., Sarkar, A.X., 2011. Regression methods for parameter sensitivity analysis: applications to cardiac arrhythmia mechanisms. Conf. Proc. Annu. Int. Conf. IEEE Eng. Med. Biol. Soc. IEEE Eng. Med. Biol. Soc. Annu. Conf. 2011, 4657–4660. doi:10.1109/IEMBS.2011.6091153

Soltysinska, E., Olesen, S.-P., Christ, T., Wettwer, E., Varró, A., Grunnet, M., Jespersen, T., 2009. Transmural expression of ion channels and transporters in human nondiseased and end-stage failing hearts. Pflüg. Arch. Eur. J. Physiol. 459, 11–23. doi:10.1007/s00424-009-0718-3

Steinhaus, B.M., 1989. Estimating cardiac transmembrane activation and recovery times from unipolar and bipolar extracellular electrograms: a simulation study. Circ. Res. 64, 449–462.

Syed, Z., Vigmond, E., Nattel, S., Leon, L.J., 2005. Atrial cell action potential parameter fitting using genetic algorithms. Med. Biol. Eng. Comput. 43, 561–571.

Szabó, G., Szentandrássy, N., Bíró, T., Tóth, B.I., Czifra, G., Magyar, J., Bányász, T., Varró, A., Kovács, L., Nánási, P.P., 2005. Asymmetrical distribution of ion channels in canine and human left-ventricular wall: epicardium versus midmyocardium. Pflüg. Arch. Eur. J. Physiol. 450, 307–316. doi:10.1007/s00424-005-1445-z

Szentadrassy, N., Banyasz, T., Biro, T., Szabo, G., Toth, B.I., Magyar, J., Lazar, J., Varro, A., Kovacs, L., Nanasi, P.P., 2005. Apico–basal inhomogeneity in distribution of ion channels in canine and human ventricular myocardium. Cardiovasc. Res. 65, 851–860. doi:10.1016/j.cardiores.2004.11.022

Szentandrássy, N., Kistamás, K., Hegyi, B., Horváth, B., Ruzsnavszky, F., Váczi, K., Magyar, J., Bányász, T., Varró, A., Nánási, P.P., 2015. Contribution of ion

currents to beat-to-beat variability of action potential duration in canine ventricular myocytes. Pflüg. Arch. Eur. J. Physiol. 467, 1431–1443. doi:10.1007/s00424-014-1581-4

Taggart, N.W., Haglund, C.M., Tester, D.J., Ackerman, M.J., 2007. Diagnostic miscues in congenital long-QT syndrome. Circulation 115, 2613–2620. doi:10.1161/CIRCULATIONAHA.106.661082

Taggart, P., Boyett, M.R., Logantha, S., Lambiase, P.D., 2011. Anger, emotion, and arrhythmias: from brain to heart. Front. Physiol. 2, 67. doi:10.3389/fphys.2011.00067

Taggart, P., Orini, M., Hanson, B., Hayward, M., Clayton, R., Dobrzynski, H., Yanni, J., Boyett, M., Lambiase, P.D., 2014. Developing a novel comprehensive framework for the investigation of cellular and whole heart electrophysiology in the in situ human heart: Historical perspectives, current progress and future prospects. Prog. Biophys. Mol. Biol. 115, 252–260. doi:10.1016/j.pbiomolbio.2014.06.004

ten Tusscher, K.H.W.J., Noble, D., Noble, P.J., Panfilov, A.V., 2004. A model for human ventricular tissue. Am. J. Physiol. Heart Circ. Physiol. 286, H1573–1589. doi:10.1152/ajpheart.00794.2003

Ten Tusscher, K.H.W.J., Panfilov, A.V., 2006. Cell model for efficient simulation of wave propagation in human ventricular tissue under normal and pathological conditions. Phys. Med. Biol. 51, 6141–6156. doi:10.1088/0031-9155/51/23/014

ten Tusscher, K.H.W.J., Panfilov, A.V., 2006. Alternans and spiral breakup in a human ventricular tissue model. Am. J. Physiol. Heart Circ. Physiol. 291, H1088–1100. doi:10.1152/ajpheart.00109.2006

Teodorescu, C., Reinier, K., Dervan, C., Uy-Evanado, A., Samara, M., Mariani, R., Gunson, K., Jui, J., Chugh, S.S., 2010. Factors associated with pulseless electric activity versus ventricular fibrillation: the Oregon sudden unexpected death study. Circulation 122, 2116–2122. doi:10.1161/CIRCULATIONAHA.110.966333

Tikhonov, D.B., Zhorov, B.S., 2005. Sodium channel activators: model of binding inside the pore and a possible mechanism of action. FEBS Lett. 579, 4207–4212. doi:10.1016/j.febslet.2005.07.017

Tsuji, Y., Zicha, S., Qi, X.-Y., Kodama, I., Nattel, S., 2006. Potassium channel subunit remodeling in rabbits exposed to long-term bradycardia or tachycardia: discrete arrhythmogenic consequences related to differential delayed-rectifier changes. Circulation 113, 345–355. doi:10.1161/CIRCULATIONAHA.105.552968

Valdivia, H.H., 2015. Mechanisms of Cardiac Alternans in Atrial Cells Intracellular Ca2+ Disturbances Lead the Way. Circ. Res. 116, 778–780. doi:10.1161/CIRCRESAHA.115.305923

Valentin, J.-P., Bialecki, R., Ewart, L., Hammond, T., Leishmann, D., Lindgren, S., Martinez, V., Pollard, C., Redfern, W., Wallis, R., 2009. A framework to assess the translation of safety pharmacology data to humans. J. Pharmacol.

Toxicol. Methods 60, 152–158. doi:10.1016/j.vascn.2009.05.011
Vaughan Williams, E.M., 1970. The experimental basis for the choice of an anti-arrhythmic drug. Adv. Cardiol. 4, 275–289.
Verkhratsky, A., Krishtal, O.A., Petersen, O.H., 2006. From Galvani to patch clamp: the development of electrophysiology. Pflüg. Arch. Eur. J. Physiol. 453, 233–247. doi:10.1007/s00424-006-0169-z
Viswanathan, P.C., Shaw, R.M., Rudy, Y., 1999. Effects of IKr and IKs Heterogeneity on Action Potential Duration and Its Rate Dependence A Simulation Study. Circulation 99, 2466–2474. doi:10.1161/01.CIR.99.18.2466
Walmsley, J., Rodriguez, J.F., Mirams, G.R., Burrage, K., Efimov, I.R., Rodriguez, B., 2013. mRNA expression levels in failing human hearts predict cellular electrophysiological remodeling: a population-based simulation study. PloS One 8, e56359. doi:10.1371/journal.pone.0056359
Wang, H., Yang, Z., Zhang, Y., Yang, J., Liu, Y., Li, C., 2009. Beta-receptor activation increases sodium current in guinea pig heart. Acta Pharmacol. Sin. 30, 1115–1122. doi:10.1038/aps.2009.96
Wang, L., Myles, R.C., De Jesus, N.M., Ohlendorf, A.K.P., Bers, D.M., Ripplinger, C.M., 2014. Optical mapping of sarcoplasmic reticulum Ca2+ in the intact heart: ryanodine receptor refractoriness during alternans and fibrillation. Circ. Res. 114, 1410–1421. doi:10.1161/CIRCRESAHA.114.302505
Wan, X., Cutler, M., Song, Z., Karma, A., Matsuda, T., Baba, A., Rosenbaum, D.S., 2012. New experimental evidence for mechanism of arrhythmogenic membrane potential alternans based on balance of electrogenic INCX / ICa currents. Heart Rhythm Off. J. Heart Rhythm Soc. 9, 1698–1705. doi:10.1016/j.hrthm.2012.06.031
Watanabe, M.A., Fenton, F.H., Evans, S.J., Hastings, H.M., Karma, A., 2001. Mechanisms for discordant alternans. J. Cardiovasc. Electrophysiol. 12, 196–206.
Wenk, J.F., Klepach, D., Lee, L.C., Zhang, Z., Ge, L., Tseng, E.E., Martin, A., Kozerke, S., Gorman, J.H., Gorman, R.C., Guccione, J.M., 2012. First evidence of depressed contractility in the border zone of a human myocardial infarction. Ann. Thorac. Surg. 93, 1188–1193. doi:10.1016/j.athoracsur.2011.12.066
Wyatt, R., 1980. Comparison of estimates of activation and recovery times from bipolar and unipolar electrograms to in vivo transmembrane APDs. Proc IEEE Eng Med Biol Soc 2nd ann conf, 22–25.
Xiao, L., Xiao, J., Luo, X., Lin, H., Wang, Z., Nattel, S., 2008. Feedback remodeling of cardiac potassium current expression: a novel potential mechanism for control of repolarization reserve. Circulation 118, 983–992. doi:10.1161/CIRCULATIONAHA.107.758672
Xie, L.-H., Sato, D., Garfinkel, A., Qu, Z., Weiss, J.N., 2008. Intracellular Ca alternans: coordinated regulation by sarcoplasmic reticulum release, uptake, and leak. Biophys. J. 95, 3100–3110. doi:10.1529/biophysj.108.130955

Xin Zhou, Bueno-Orovio, A., Orini, M., Hanson, B., Hayward, M., Taggart, P., Lambiase, P.D., Burrage, K., Rodriguez, B., 2013. Population of human ventricular cell models calibrated with in vivo measurements unravels ionic mechanisms of cardiac alternans, in: Computing in Cardiology Conference (CinC), 2013. Presented at the Computing in Cardiology Conference (CinC), 2013, pp. 855–858.

Yang, P.-C., Clancy, C.E., 2012. In silico Prediction of Sex-Based Differences in Human Susceptibility to Cardiac Ventricular Tachyarrhythmias. Front. Physiol. 3, 360. doi:10.3389/fphys.2012.00360

Yap, Y.G., Duong, T., Bland, M., Malik, M., Torp-Pedersen, C., Køber, L., Connolly, S.J., Marchant, B., Camm, J., 2005. Temporal trends on the risk of arrhythmic vs. non-arrhythmic deaths in high-risk patients after myocardial infarction: a combined analysis from multicentre trials. Eur. Heart J. 26, 1385–1393. doi:10.1093/eurheartj/ehi268

Yue, A.M., Paisey, J.R., Robinson, S., Betts, T.R., Roberts, P.R., Morgan, J.M., 2004. Determination of human ventricular repolarization by noncontact mapping: validation with monophasic action potential recordings. Circulation 110, 1343–1350. doi:10.1161/01.CIR.0000141734.43393.BE

Yue, L., Feng, J., Li, G.R., Nattel, S., 1996. Transient outward and delayed rectifier currents in canine atrium: properties and role of isolation methods. Am. J. Physiol. 270, H2157–2168.

Zagotta, W.N., Hoshi, T., Aldrich, R.W., 1994. Shaker potassium channel gating. III: Evaluation of kinetic models for activation. J. Gen. Physiol. 103, 321–362.

Zaza, A., Belardinelli, L., Shryock, J.C., 2008. Pathophysiology and pharmacology of the cardiac "late sodium current." Pharmacol. Ther. 119, 326–339. doi:10.1016/j.pharmthera.2008.06.001

Zicha, S., Moss, I., Allen, B., Varro, A., Papp, J., Dumaine, R., Antzelevich, C., Nattel, S., 2003. Molecular basis of species-specific expression of repolarizing K+ currents in the heart. Am. J. Physiol. Heart Circ. Physiol. 285, H1641–1649. doi:10.1152/ajpheart.00346.2003

Zimetbaum, P., 2012. Antiarrhythmic Drug Therapy for Atrial Fibrillation. Circulation 125, 381–389. doi:10.1161/CIRCULATIONAHA.111.019927

Zygmunt, A.C., Eddlestone, G.T., Thomas, G.P., Nesterenko, V.V., Antzelevitch, C., 2001. Larger late sodium conductance in M cells contributes to electrical heterogeneity in canine ventricle. Am. J. Physiol. Heart Circ. Physiol. 281, H689–697.